AKADEMIE DER WISSENSCHAFTEN DER DDR

ZfK

ZENTRALINSTITUT FÜR KERNFORSCHUNG
ROSSENDORF BEI DRESDEN

ZfK – 646

Proceedings of the XVIIth International Symposium on Nuclear Physics

– Nuclear Reactions –

organized by
Technical University of Dresden
November 9 – 13, 1987 in Gaussig (GDR)

edited by
D. Seeliger and H. Kalka

May 1988

ISSN 0138-2950

Postanschrift: Akademie der Wissenschaften der DDR
Zentralinstitut für Kernforschung Rossendorf
Postschließfach 19
Dresden
8051
Deutsche Demokratische Republik

Diese Publikation wurde in der Abteilung Information des Zentralinstitutes für Kernforschung hergestellt

III-12-12 I 1525/88

AKADEMIE DER WISSENSCHAFTEN DER DDR

Z E N T R A L I N S T I T U T F Ü R K E R N F O R S C H U N G

R O S S E N D O R F B E I D R E S D E N

ZfK - 646

PROCEEDINGS

of the XVIIth International Symposium

on Nuclear Physics

- Nuclear Reactions -

organized by

Technical University of Dresden

November 9 - 13, 1987 in Gaussig (GDR)

edited by

D. Seeliger and H. Kalka

May 1988

Editorial Note

In preparing this material for press, the editors have compiled and paginated the original manuscripts as submitted by the authors. Some of the papers which didn't meet the requirements stated in the 2nd announcement have been accepted after re-typing and editor proof.
Authors are themselves responsible for obtaining necessary permissions to reproduce copyright material from other sources.

Dear Colleagues,

On the behalf of the Rector of the Technical University Dresden and as the chairman of the Organizing Committee I welcome you at the

XVIIth International Symposium on Nuclear Physics

in the castle Gaussig.

In this year our Symposium is mainly dealing with different aspects of the nuclear reaction mechanism including the mechanism of nuclear fission.
Nuclear reaction mechanism was the main topic of our Gaussig meetings also 17 years ago, when we started the first small symposia of this series here in the same building. Especially, pre-equilibrium reactions have been discussed in Gaussig since the very beginning of this specific topic with great enthusiasm. And, as the present meeting will show, there is no end of this interesting subject. The same holds for the physics of nuclear fission, which seems to have a renaissance during the last years - but not only at Gaussig. There are many other new aspects and directions in the investigations of nuclear reactions. A few of them are mentioned here: The influence of weak interactions on nuclear processes, the quark structure of nucleons inside the nuclei and the use of heavy-ion and high-energy electron beams for experimental investigations. Altogether, this results in a continuing interest of many laboratories in the world to this field, as it is demonstrated by the participation of so many distinguished scientists at the present meeting.

I hope you will have an interesting scientific event within the old castle of Gaussig and a pleasant stay in the surroundings of Dresden.

D. Seeliger

LIST OF PARTICIPANTS

I. Angeli	Debrecen University	HUNGARIA
E. Augustyniak	INS Warsaw	POLAND
V.V. Balashov	Moscow University	USSR
O.V. Bochkarev	Kurchatov Inst. Moscow	USSR
R. Capote	Habana University	CUBA
T. Elfruth	TU Dresden	GDR
V.I. Furman	JINR Dubna	USSR
S. Gmuca	IP Bratislava	CSR
F. Gönnenwein	Tübingen Iniversity	FRG
T. Hehl	TU Dresden	GDR
H. Helfer	TU Dresden	GDR
C.M. Herbach	TU Dresden	GDR
H. Kalka	TU Dresden	GDR
E.V. Korolev	RI Leningrad	USSR
A. Lajtai	Budapest University	HUNGARIA
R. Lopez	Habana University	CUBA
V.P. Lunev	FEI Obninsk	USSR
Z. Mate	INR Debrecen	HUNGARIA
H. Märten	TU Dresden	GDR
A. Meister	TU Dresden	GDR
A. Mondragon	Mexico University	MEXICO
W. Neubert	CINR Rossendorf	GDR
J. Oravec	MFFUK Bratislava	CSR
W. Pilz	CINR Rossendorf	GDR
S.G. Popov	INP Novosibirsk	USSR
B.S. Ratner	INR Moscow	USSR
D. Richter	TU Dresden	GDR
I. Rotter	CINR Rossendorf	GDR
A. Ruben	TU Dresden	GDR
D. Seeliger	TU Dresden	GDR
K. Seidel	TU Dresden	GDR
S.P. Simakov	FEI Obninsk	USSR
K. Sistemich	KFA Jülich	FRG
G. Staudt	Tübingen University	FRG
K. Takada	Kyushu University	JAPAN
J. Theobald	TH Darmstadt	FRG
N.V. Titov	INR Moscow	USSR
M. Torjman	TU Dresden	GDR/SYRIA
J. Turkiewicz	INS Warsaw	POLAND
S. Unholzer	TU Dresden	GDR
V.G. Zelevinsky	INP Novosibirsk	USSR
H. Al Obiesi	TU Dresden	GDR/SYRIA

TABLE OF CONTENTS

o

SEARCH FOR P-ODD AND P-EVEN CORRELATIONS IN NUCLEAR REACTIONS

N.A. Titov

Institute for Nuclear Research, Academy of Sciences of the USSR

The paper reviews the main results of researches of spacial parity violation effects in nuclear reactions performed by the INR - LINP[+] group.

I. Introduction

The spacial parity violation nuclear systems is due to interference of strong and weak nucleon-nucleon interaction /1,2/. The spacial parity violation effects serve as a test for existing models of strong interaction in elementary particle physics as well as in nuclear physics. Over the past ten years there were found the P-odd escape asymmetry of the heavy nuclei fission fragments /3/ and the spacial parity-violating rotation of a neutron polarization upon their passage through ^{117}Sn /4/. Our investigations of them resulted in finding the P-even left-right asymmetry in heavy nuclei fission and the P-odd difference in total cross-sections of interaction of longitudinally polarized neutrons with some nuclei. The analysis of these and some other results makes it possible to clarify the mechanism of neutron reactions, structure of highly excited nuclear states, fission physics in more detail.

II. Heavy nuclei fission

In 1977 the group led by G.V. Danelyan found the spacial parity nonconservation in heavy nuclear fission by polarized thermal neutrons. The fragment escape probability depended on correlation:

$$W \sim 1 + a_p(\vec{S}, \vec{P}) \quad ,$$

$\vec{S}$ and $\vec{P}$ being the unit vectors in the direction of neutron polarization and light fragment momentum.

The magnitude of light (heavy) fragment escape asymmetry with respect to captured neutrons spin appeared to be of the order of 10^{-4}, which is essentially greater than the characteristic value $F = (2 \div 6) \cdot 10^{-7}$. Such a magnitude of asymmetry was inconsistent with the existing knowledge according to which it was supposed that at great ($10^6 \div 10^8$) number of final states the asymmetry which could exist for a single final state would have to be mutually compensated on detecting the whole spectrum of light (or heavy) fragments. It was not clear how a weak interaction which affects on the state of one nucleon can define the movement of a fragment consisting of 100 + 140 nucleons. So it was decided to examine a new phenomenon in detail to study its nature and search for possible false effects. It was interesting to compare the nuclear fission with α-decay of polarized nuclei - another process in which one can observe P-odd escape asymmetry of a heavy charged particle. In light nuclei the magnitude of P-odd asymmetry can be calculated in detail and serve as a source of information of a weak opposite parity state mixing matrix-element as well a nuclear enhancement factor. The experiment with light polarized nuclei is analogous if they are produced through the capture of polarized neutrons. But a small size of the expected effects became a barrier to performance of such investigations. Storage of a large amount of events to get statistically significant results is possible only at a counting rate of 10^6 - 10^8 events per second. So the recording facilities with a necessary operating rate were to be developed.

The task was to determine the change in number of particles produced during reactions examined in the direction towards the detector while the neutron beam polarization pointing towards the detector, was reversed. In reations (n,p), (n,a), (n,f) on polarized thermal neutrons the produced particles have fixed energies (in (n,f) on ^{233}U, ^{235}U, in spite of energy fluctuations both fragments can be identified) and are emitted in opposite directions. The latter means that desired asymmetry has an opposite sign for light and

[+] Leningrad Institute of Nuclear Physics

heavy fragments and so they have to be registrated separately, otherwise the desired asymmetry will be mutually compoensated. This task is usually realized ba means of the amplitude analysis of detectors signal but here restrictions arise on a count rate, i.e. on sensitivity, obtained in the experiment. The integral method is used to overcome these restrictions /5/. To detect reaction products in integrating mode the gas proportional chamber was used with separation of light products from heavy ones based on the difference in their ranges.

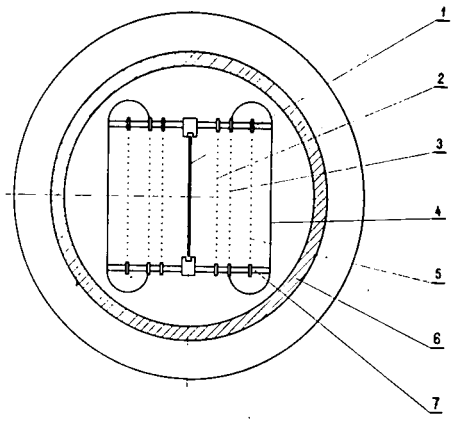

Fig. 1 shows the transversal cross-section of the chamber. Target (1) and detectors are put in the same frame (6). The high potential solid (4) and wire (3) electrodes are located around the signal one (5). The gas pressure inside the chamber is chosen in a such way so as to allow the heavy products having less range to stop in gas out of the sensitive volume, and the light ones to pass through the wire electrode (3). The shielding action of this electrode and purifying field produced by the earth electrode (2) make the detector insensitive to ionization, isolated outside the sensitive volume between electrodes (3) and (4).

A current tapped off from the signal electrode is only produced by light reaction products. On reversing the neutron polarization direction towards the detector, the current varies in proportion to corresponding change of a number of particles detected. Detectors current variation was measured by the synchronous detection method with using analog integration, conversion to numerical code and further digital processing.

To choose proper pressure of a gas mixture in the chamber there was examined either dependence of a relative fraction of coinciding in time pulses in two symmetrically placed detectors pn pressure (see Fig. 1) or a sign correlation of their current signals. Since for thin targets on detecting a heavy fragment the twin light one, which has a longer range, had to be registrated by the second detector, time coincidence disappearance meant that such a pressure was obtained a which a heavy fragment was not detected.

The experiments were carried out at the B.P. Konstantinov Institute of Nuclear Physics, using a polarized thermal-neutron beam with an intensity of $6 \cdot 10^7$ neutrons/sec of the VVR-M reactor, a degree of polarization being 95 ÷ 97 %. The neutron spin was flipped with respect to the guiding magnetic field direction by a high frequency adiabatic spin flipper.

The sign of the sought-for effect changed independently on reversing the direction of a guiding magnetic field in the target region. The use of two different methods for changing the sign of the effect enabled us to control and cancel a possible false effect and to obtain a result with an accuracy that was twice as greater as that in the case of measurements with depolarized beam as a control one.

To suppress the effect of neutron beam intensity fluctuations caused by that of the reactor power a so-called "differential method" was used: the power fluctuations contribution to the difference of signals from two opposite detectors canceled, and the sought-for effect wassummarized. Substraction was made either in analog form at the differential amplifier or numerically while processing the independently recorded signals of both detectors.

The first measurements performed with a ^{235}U-target corroborated the occurance of the effect and its dependence neither on chemical composition of the target (U_3O_8) nor on substrate influence. The fragment β-decay background influence has also been estimated /6/.

Table 1

Target (mg/cm^2)	Detection conditions	(a_p), 10^{-4}
0.3 U_3O_8 - 140 Al - 0.3 U_3O_8	$\langle(\vec{S},\vec{P})\rangle$ = 0.91	0.62 ± 0.14
- " -	-background, I/I_f 0.05	0.07 ± 0.14
0.2 U_3O_8 - 0.15 Ti - 0.2 U_3O_8	$\langle(\vec{S},\vec{P})\rangle$ = 0.88	0.93 ± 0.26
0.25 Ti - 0.5 UF_4 - 0.25 Ti	$\langle(\vec{S},\vec{P})\rangle$ = 0.88	0.83 ± 0.14
- " -	$\langle(\vec{S},\vec{P})\rangle$ = 0.88 intensity being increased	0.84 ± 0.11

Note: The magnitude $\langle(\vec{S},\vec{P})\rangle$ is determined by a solid angle in which fragments are detected and dependence of their energy release within this solid angle on an angle between $\vec{S}$ and $\vec{P}$.

In the subsequent paper /7/ a new phenomenon was observed - the P-even left right fission fragment escape asymmetry due to interference of the S- and P-wave neutron capture states. Addition of P-odd asymmetry with a coefficient a_p and P-even one with a coefficient a_{RL} gives the same kind of total asymmetry, but it is directed along the axis $\vec{n}$:

$$W \sim 1 + a_p(\vec{S},\vec{P}) + a_{RL}\,\vec{S}(\vec{P}_n,\vec{P}) = 1 + (\vec{n},\vec{P})$$

where $\vec{n} = a_p\vec{S} + a_{RL}[\vec{S},\vec{P}_n]$, $\vec{S}$, $\vec{P}_n$, $\vec{P}$ being the unit vectors in direction of neutron polarization, momenta of a neutron and a light fragment, respectively.

Projection of the total asymmetry on the plane perpendicular to the beam axis is given in Fig. 2 for the ^{235}U fission.

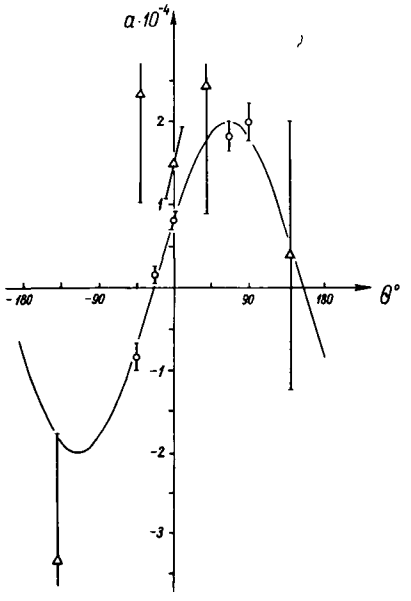

Fig. 2 Circles denote the results of our paper /7/, triangles - the data obtained by the Danielyan group in their previous work when the left--right asymmetry was not found.

Here angles 0° and 180° correspond to P-odd asymmetry, 90° and 270° - to P-even one.

As a result of data processing presented in Fig.2, the following values of the asymmetry coefficients have been obtained:

$$a_p = (0.78 \pm 0.10) \cdot 10^{-4} ;$$

$$a_{RL} = (1.75 \pm 0.10) \cdot 10^{-4} .$$

It was shown that the observed phenomenon of the left-right asymmetry is not connected with the instrumental distorsion of the P-odd asymmetry which can arise due to a misaligment of the polarization axis or the displacement of the center of mass of the "glowing region" of the target relative to its geometrical center; and depends neither on external magnetic field at the target nor on chemical composition of this target (see Table 2). The left-right asymmetry has also been found in the ^{233}U fission, instrumental errors and magnetic field influence being absent.

The group led by G.A. Petrov, which also performed investigations of P-parity violating effects in fission at the VVR-M reactor, confirmed the occurance of left-right asymmetry in the ^{233}U-fission and found it in the ^{239}Pu-one /8/.

$$a_{RL}\,(^{233}U) = -(6.43 \pm 0.51) \cdot 10^{-4}$$

$$a_{RL}\,(^{239}Pu) = (1.25 \pm 0.29) \cdot 10^{-4} .$$

In 1982 the same group made the difficult experiment on studying the dependence of a_{RL} on neutron energy within the region 0.025 + 0.29 eV /9/ and did not find any resonance enhancement effect for thermal neutrons. Thus, the experimental data show that the left--right asymmetry is a typical phenomenon for nuclear fission with a characteristic value $\sim 1 \cdot 10^{-4}$.

Table 2

Target	$a_p \langle(S,P)\rangle P_n$, 10^{-4}	$a_{RL} \langle(S,P)\rangle P_n$, 10^{-4}	arctg (a_p/a_{RL})	Notes
$^{235}UF_4$	0.65 ± 0.11	1.55 ± 0.14	22.9° ± 3.3°	detector I
$^{235}UF_4$	0.63 ± 0.10	1.35 ± 0.12	25.0° ± 3.3°	detector II
$^{235}UF_4$	0.65 ± 0.07	1.46 ± 0.08	24.1° ± 2.1°	detector I + II
$^{235}U_3O_8$	0.33 ± 0.11	1.01 ± 0.09	18.0° ± 5.5°	detector I
$^{235}U_3O_8$	0.56 ± 0.10	0.96 ± 0.10	30.2° ± 5.6°	detector II
$^{235}U_3O_8$	0.41 ± 0.08	0.97 ± 0.07	22.9° ± 3.8°	detector I + II
$^{235}U_3O_8$		1.04 ± 0.08		mag. field 2.3 times greater
$^{233}UF_4$	2.38 ± 0.35	-2.88 ± 0.36	-39.6° ± 4.9°	detector I
$^{233}UF_4$	3.10 ± 0.28	-2.48 ± 0.27	-51.3° ± 4.4°	detector II
$^{233}UF_4$	2.81 ± 0.25	-2.67 ± 0.25	-46.5° ± 3.3°	detector I + II
$^{233}UF_4$	2.50 ± 0.49	-3.10 ± 0.43	-38.9° ± 6.7°	detector I + II mag. field 2.3 times greater

The magnitude of the left-right asymmetry depends on three factors: the relative value of the P-wave capture amplitude, the degree of "surviving" during cooling of a compound nucleus and the degree of averaging after summation over final states. Since the experiment showed that the values observed were practically equal to the first factor, the second and third ones have to be of about 1. Thus, the O.P. Sushkov - V.V. Flambaum hypothesis was substantiated which supposed the connection between the P-odd fragment emission asymmetry and the "dynamical" mixing of hot compound nucleus states, produced through the neutron capture. In this model /10,11/ at the fixed nucleus energy ($\Delta E \ll D$) the mixture of states of opposite parity, which are preserved during cooling, determines the state mixing of a cold severely deformed nucleus at the saddle point, where angular distribution of fragments is formed. To get an interference of the opposite parity states it is necessary for fission channels of different parity and moment to belong to the rotation band arising from one and the same intrinsic state of a cold pear-shaped necleus, which is fixed by K.

The left-right asymmetry in the O.P. Sushkov - V.V. Flambaum model is described analogously.

III. Spacial parity violation in the light nuclei

The search for a P-odd escape asymmetry of a-particles in the reactions $^6Li(n,a)^3H$ and $^{10}B(n,a)^7Li$, which were proposed in Ref. /12/ as well as protons in the reaction $^3He(n,p)^3H$ was carried out at the installation described above. The results are given in Table 3.

Only the difference signal of both detectors was monitored, because the level of statistical fluctuations was 2 - 3 times lower than that, associated with neutron flux intensity variations. The left-right asymmetry was found in the reaction $^6Li(n,a)^3H$. The additional experiment showed its dependence on neutron momentum, which confirms that it can be interpreted as the interference of the S-P-wave neutron capture.

Table 3

Reaction	Target (mg/cm^2)	a_{RL}, 10^{-5}	a_p, 10^{-5}	Notes
$^6Li(n,a)^3H$	0.1Ti-0.88+0.29^{6}Li-0.1Ti	-10.6 ± 0.4	+0.30 ±0.51	λ_n = 2.7 A
- " -	1.5Al-2.6^{6}LiF-1.5Al	- 8.9 ± 0.3	0.16 ±0.23	λ_n = 2.7 A
- " -	- " -	- 5.6 ± 0.4	- " -	λ_n = 4.7 A
$^{10}B(n,a_0+a_1)^7Li$	0.1Ti-0.3^{10}B(81%)-0.1Ti	- 0.40± 0.60	-0.13 ±0.24	λ_n = 2.7 A
$^{10}B(n,a_0)^7Li$	0.1Ti-0.5^{10}B(81%)-0.1Ti	7.7 ± 0.6	<1.8 (90 %)	λ_n = 2.7 A
$^{10}B(n,a_1)^7Li^+$	- " -	< 1.2(90% c.l.)	<0.37(90 %)	- " -
$^3He(n,p)^3H$	^{3}He + 2 % CO_2	0.06± 0.080	0.038±0.048	- " -
$^6Li(n,a)^3H$	1.5Al-3.5^{6}LiF-1.5Al	-	0.007±0.080	$\vec{S} \parallel \vec{P}_n \parallel \vec{P}$
$^{10}B(n,a_0)^7Li$	0.2Ti-0.32^{10}B(81%)-0.2Ti	-	0.21 ±0.34	- " -
$^{10}B(n,a_1)^7Li^+$	- " -	-	0.035±0.068	- " -

The reaction $^{10}B(n,a)^7Li$ has two channels, which correspond to the ^{7}Li-nucleus production in the ground and the first excited (0.48 MeV) states. In the first experiments the mixture of both lines of a-particles was detected. In the second one a-particles of the a_0-line were detected separately in the additional sensitive volume, what yielded simutaneous measurement of the effects at both lines. The left-right asymmetry was found at the a_0-line.

The percularity of the experiment with the reaction $^3He(n,p)^3H$ was using as a target a part of the chamber volume filled with a mixture ^{3}He + 2 % CO_2 which was intersected by the beam.

The beam in these experiments was transverely polarized. If the polarization axis deviates from the direction toward the detector, the projection of a left-right asymmetry could imitate a P-odd asymmetry. The uncertainty in the orientation of the polarization axis, $\lesssim 3^o$, places a limit on the order of 10^{-5} on the sensitivity to a P-odd asymmetry. In Ref. /14/ the left-right asymmetry background was suppressed further by taking the measurements with a longitudinally polarized beam, with 10 targets and 40 detectors along the beam axis (see Fig. 3). In this geometry ($\vec{S} \parallel \vec{P}n \parallel \vec{P}$) the detectors are relatively insensitive to a left-right asymmetry, and the magnitude of this asymmetry was suppressed by orientin the polarization axis parallel to the beam axis within an angle of less than 1°.

As in the earlier experiments, the detectors were gas-folled proportional chambers with wire electrodes. The detectors, operated in an integrating regime detected only the light reaction products. The sensitive volume of each detector was divided into two parts, the outer part detected (in the study of the reaction ^{10}B + n) only the a_0-line. The analogous results for a_p were obtained in Ref. /15/.

These results are quite close to the lower limit of the estimate $a_p \sim 10^{-5} - 10^{-6}$ found in Ref. /12/. The further increase in accuracy was limited by the intensity of the neutron beam. It is worth mentioning that a value $a_p^o = (0.8 \div 3.8) \cdot 10^{-6}$ was predicted in Ref. /16/.

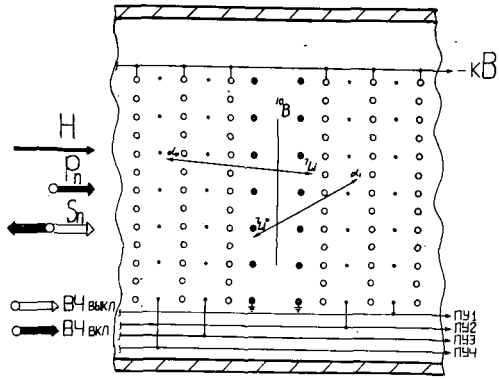

Fig. 3. One of the ten detecting modules in a common housing. The ^{10}B target is at the center. Open circles - high-voltage electrodes defining the sensitive volumes; points - signal electrodes (the corresponding electrodes are connected in parallel, and the resultant signal is fed to a single preamplifier (ПУ); filled circles - electrodes of the purifying field. Shown at the left is the direction along which tne neutron beam is incident and the neutron polarization direction with the ef field of the flipper turned on for the indicated direction of the guiding magnetic field H.

IV. Spacial parity violation in neutron optics

The amplitude of the neutron scattering on nucleus f(0) determined the neutron wave refractive index in medium n:

$$n = 1 + \frac{2\pi}{k^2} \varrho f(0)$$

ϱ being a number of nuclei per 1 cm^3, k - a wave number.

A P-odd component of the f(0) proportional correlation $(\vec{S}\cdot\vec{P}_n)$ results in rotation of the neutron polarization plane in the medium ($\sim$Ren) and in difference of total interaction cross-sections for longitudinally polarized neutrons ($\sim$ Im n). In some papers it was suggested to search for the first effect as a source of information about a weak odd--neutron - nucleus interaction (a parameter X_N^n from Ref. /1/). To enhance the effect it was proposed to use resonances in the neutron - point nucleus system (refere to /4/).

The experiment carried out at the Laue-Langevin Institute, revealed the unexpectedly large value of the effect for the ^{117}Sn sample /4/. In the references /17,19/ the effect enhancement was ascribed to the vicinity of the p-wave resonance. To explain the magnitude of the P-odd mixing a new weak interaction with a constant $\sim$100 G was supposed to occur /17/. It was shown in Ref. /18/ that a weak mixing of opposite parity states is determined by a virtual excitation of a compound nucleus (e.g. ^{118}Sn) where this mixing (as for the P-odd effects in fission, $^{113}Cd(n, \gamma_0)$ is "dynamically" enhanced. The same authors suggested searching for analogous effects in nuclei with low-lying compound p-resonances: ^{139}La, ^{93}Nb. For thermal neutrons such effects ($\sim$Im n) were predicted to be of the order of 10^{-5} - 10^{-6}.

In Ref. /4/ the effect Im n $\sim A_t = (N^+ - N^-)/P_n(N^+ + N^-) = -(9.8 \pm 4.0) \cdot 10^{-6}$ was measured for the ^{117}Sn sample with $A_{tot}^{dep} = -(3.0 \pm 5.3) \cdot 10^{-6}$ as a "zero" experiment. The results obtained did not allow to make the definite conclusions because the precision of measurements performed was small due to large contribution of the neutron beam intensity fluctuations to an error.

A "differential" method was used at the installation which is described in Fig. 4 to cancel out the fluctuations in the intensity of the neutron beam.

After passage through the adiabatic high frequency flipper the beam was split into two parts with a ^6LiF-collimator. The beams entered adiabatically the solenoids which produced longitudinal magnetic fields in opposite directions. Two identical samples were placed into the solenoids. Both beams were adjusted with a high accuracy. The scattered ne neutrons were absorbed with additional collimators.

The neutrons which were transmitted through the sample, were detected by two multiwire proportional chambers filled with a mixture ^3He(o.35 kg/cm^2 of partial pressure) CO_2 (0.5 kg/cm^2) Ar (1.45 kg/cm^2), which were placed in the same gas volume. The neutron detection efficiency of the chambers appeared to be about 80 %.

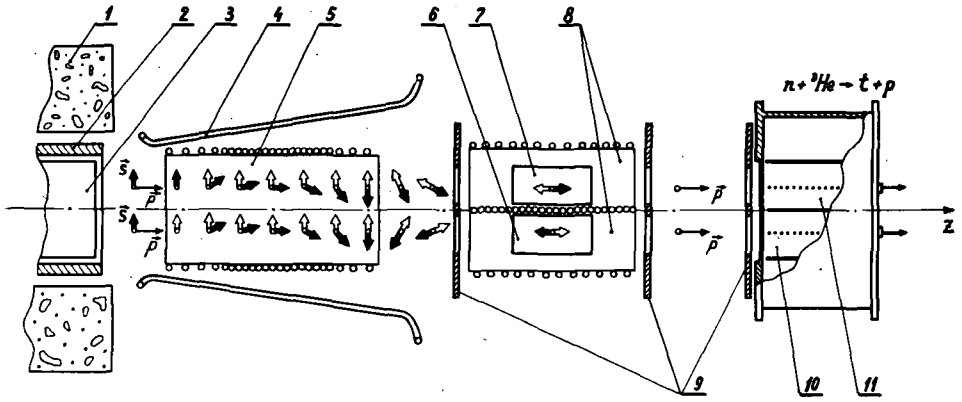

Fig. 4. Experimental set-up: 1 - neutron guide tube shielding; 2 - permanent magnet; 3 - neutron guide tube; 4 - flipper magnetic fields coils; 5 - flipper HF coil; 6, 7 8 samples; 8 - reversed magnetic field solenoids; 9 - LiF diaphragms - 10, 11 - detectors; ↕ - high frequency on, ⇕ - HF-off.

Thus, the parity violation effect, as in previous investigations, had an opposite sign in both detectors. A differential signal included a double parity nonconservation effect, all fluctuations of the beam intensity except statistical ones being substracted. Such an approach made it possible to increase the senstivity of the experiment by 52 - 5 times in comparison with a case when only one beam was used for measurements and ensured monitoring of the majority of spurious effects. The test experiments and signal processing procedure were similar to that described above.

The results of measurements of the P-parity nonconservation effects taken in the transmittance experiment are listed in the Table 4. The measured variable is $A_{tot,\gamma} = \frac{1}{P_n}(N^+ - N^-)/(N^+ + N^-)$, where P_n is the degree of beam polarization, N^+ and N^- are intensities of the detected neutrons or γ-quanta, corresponding to parallel (+) and antiparallel (-) directions of the spin and neutron momentum. The experimental data show the neutron helicity dependent effects for ^{117}Sn, ^{139}La, ^{nat}Br.

Table 4

Nucleus	σ_{tot}	σ_γ	L/L_{rel}	$A_{tot}(10^{-6})$	$\frac{\Delta\sigma_t}{2\sigma_t}(10^{-6})$	$A_\gamma(10^{-6})$	$\frac{\Delta\sigma_\gamma}{2\sigma_\gamma}(10^{-6})$	Ref.
^{nat}Sn	2.9	1..	0.9	- 0.6±1.0	-	-	-	20
^{117}Sn	3.7	1.2	1.1	- 6.8±0.8	6.2 ± 0.7	19.8±1.9	22.6±1.9	20
^{139}La	19.6	9.4	1.0	- 9.0±1.4	9.0 ± 1.4	12.2±1.9	16.1±2.0	20
^{nat}Br	15.5	9.8	1.27	-12.5±1.2	9.8 ± 1.0	10.5±1.4	15.5±1.5	21
^{27}Al	1.65	0.24	1.55	- 1.1±2.3	0.7 ± 1.5	3.1±4.2	3.5±5.1	-
^{93}Nb	7.5	1.15	1.05	- 0.3±1.9	0.3 ± 1.8	1.2±2.6	1.3±3.4	-

The experiment for studing the dependence of the radiative capture cross-section on neutron helicity was as follows. The neutron beam passed through a sample placed in the single solenoid with a longitudinal field, two scintillation detectors with NaJ(Tl) crystals Ø 150 x 100 mm and photomultiplier ФЭУ-49 were located on both sides of the sample at the distance of about 50 mm from the neutron beam.

The auxiliary integral current signal was recorded which was proportional to the reactor power, that is to the neutron beam intensity. Substraction of this signal from the sum of signals of γ-detectors permitted to cancel out the neutron intensity fluctuations and to keep the measurement error on the level of counting statistics.

The measurements were taken like in previous experiments. To the observable variable A_γ there were made the measured corrections for γ-background in the detectors and the calculated corrections for the background induced by the process of scattered neutron capture in the sample.

The results are presented in Table 4. When measuring in the depolarized beam, no effects were observed.

Therefore we can make a conclusion that both the total cross-section and the radiative capture one depend on an neutron hecility. The values of $\sigma_\gamma/\sigma_{tot}$ make one assume that the P-parity nonconservation in the total cross-section within the experiment errors is due to that which occurs through radiation capture.

The existence of a large P-odd effect in the total interaction cross-section of neutrons with ^{117}Sn, ^{139}La, ^{nat}Br corroborated the resonance nature of its enhancement. Only the presence of a resonance factor $[(E-E_o) + i\Gamma/2]^{-1}$ in the parity-violating scattering amplitude besides a purely real vertex of the weak mixing of states with opposite parity /17-19/ gives us an imaginary part of the neutron scattering amplitude, which is responsible for the effects observed. It is very easy to explain the equation $\Delta\sigma_{tot} \simeq \Delta\sigma_\gamma$ within the scope of the resonance model but in Ref. /22/ it is shown to be a general consequence of a threshold behaviour of the elastic scattering amplitudes and exothermic reaction.

The resonance nature of observable effects were exhibited in the experiments performed by the JINR. The magnitude A_{tot} was measured for resonance neutrons and its resonance behaviour was studied in the vicinity of P-wave resonances 1.33 eV (^{117}Sn), 0.75 eV (^{139}La), 0.88 eV (^{81}Br) /23/. Comparing the results /20,21,23/ one can see, that energy behaviour of the effect is in good agreement with the Breit-Wigner formula at $\Delta E \sim 10\Gamma$ (except a slight discrepancy for ^{117}Sn), which is a surprising fact.

The observation of the spacial parity violation in neutron optics opens a new field for studying the weak interaction in atomic nuclei because, in principle, it allows to examine a wide range of nuclei and various states of the same nuclei. Investigation of a phenomenon known as "the dynamical enhancement" is of greate interest which, as shown in Ref. /24/, has universal nature and can enhance any weak, for example, Coriolis, effects in highly excited states of nuclei.

V. Perspectives

Revelation of a resonance nature of the P-parity nonconservation stimulated the development of some proposals on studing the effects in neutron resonances with 10 - 100 eV--energy, These are, for example, researches of a difference in total interaction cross--sections /18/, the P-odd asymmetries in neutron scattering /17/ and nuclei fission (analogously to /3/), asymmetry of captured γ-quanta.

Another important lead for further research is associated with search for P- and T-odd effects, which also have to undergo resonance enhancement /17,25,26/. It is proposed to search for rotation of a polarization plane of neutrons during their passage through a polarized target (correlation being $\vec{P}[\vec{S}_n \times \vec{S}_t]$, where $\vec{S}$, $\vec{P}$ are spin and momentum of a neutron, $\vec{S}_t$ is spin of a nucleus of the target) /17,26/ as well as in backward scattering /25/.

It will be possible to realize all these proposals only by means of a new generation of neutron spallation sources based on the intermediate- and high-energy proton accelerators. A pulsed neutron source being developed at the Moscow Meson Factory of the Institute for Nuclear Research of the Academy of Sciences of the USSR falls into this category. The beams under construction will surpass the ones used at the JINR in quality by $10^3 + 10^5$ times. Today a polarized proton target - a neutron polarizer is under construction.

There is a problem which can be examined before starting a polarized beam - a search for correlations $(\vec{P}_n, \vec{P}_f)$ in heavy nuclear fission /28/. It was shown that the effect can be observed at some resonances up to 30 - 50 eV even without using the proton compressing

storage ring /29/.

In conclusion I would like to thank V.M. Lobashev who is the leader of the works presented in this review and all the co-workers for the great pleasure received from our collaboration, T.E. Grebenjkova for the help in preparing this manuscript, as well as Dr. D. Seeliger and Dresden Technical University for the invitation to participate in the Symposium.

References

1 B. Desplauques. Nucl.Phys. 1980. v. A335, p. 147
2 V.M. Dubovik, S.V. Zenkin, et al. Annals of Physics (N.Y.), 1986
3 G.V. Danilyan, B.D. Vodennikov et al. "Physics and Chemistry of Fission 1979; 1980, v. 1, p. 111
4 M. Forte et al. Phys.Rev.Lett. 1980, v. 45, p. 2088
5 V.M. Lobashev, Yadernaya Fizika 1965, v. 2, issue 5, p. 957
6 Borovikova et al. Pis'ma JETF 1979, v. 30, p. 527
7 V.A. Vesna et al. Pis'ma JETF 1980, v. 31, p. 704
8 A.K. Petukhov et al. Pis'ma JETF 1980, v. 32, p. 324
9 G.V. Valjski et al, Yadernaya Fizika 1984, V. 39, p. 276
10. V.V. Flambaum, O.P. Sushkov. Phys. Lett., 1980, v. 94B, p. 277
11. O.P. Sushkov, V.V. Flambaum, Yad. Fiz. 1981, v. 33, p. 1749
12 G.A. Lobov, G.V. Danilyan. Izvestiya AN SSSR (ser.fiz.) 1977, v. 41, p. 1548
13 V.A. Vesna et al. Pis'ma JETF 1981, v. 33, p. 429
14 V.A. Vesna et al. Pis'ma JETF 1983, v. 38, p. 265
15 P.A. Krupchitski et al. Yad. Fiz. 1986, v. 43, p. 1359
16 E.S. Rzhevski. Preprint ITEP - 152, Moscow, 1983
17 L. Stodolsky. Phys.Lett. 1980, v. 96B, p. 127
18 O.P. Sushkov, V.V. Flambaum. Pis'ma JETF 1980, v. 32, p. 377
19 V.E. Bunakov, V.P. Gudkov. Preprint LINP N661, Leningrad, 1981
20. E.A.K. Lomensky et al. Phys. Lett. 1981, v. 107B, p. 322
21 V.A. Vesna et al. Pis'ma JETF 1982, v. 35, p. 351
22 L. Stodolsky. Nuclear Physics 1982, v. 197B, p. 213
23 V.P. Alfimenkov et al. Nucl. Phys. 1983, v. A398, p. 93
24 O.P. Sushkov, V.V. Flambaum. Nucl. Phys. 1984, v. A412, p. 13
25 G.A. Lobov. Yadernaya Fisika 1982, v. 35, p. 1408
26 Kabir P.K. Physical Review D, 1982, v. 25, p. 2013
27 Yu. Ya. Stavinsky. Proceedings of the IV All-Union seminar "The programme of experimental researches at the INR meson factory", Moscow, 1986, p. 7
28 V.V. Flambaum. Yadernaya Fisika, 1985, v. 42, p. 578
29 N.A. Titov. Proceedings of the V All-Union seminar "The programme of experimental researches at the INR meson factory", Moscow, 1987.

MULTISTEP COMPOUND PROCESSES IN NUCLEAR REACTIONS

P.E. Hodgson

Nuclear Physics Laboratory, Oxford

Abstract

The quantum-mechanical theory of multistep compound reactions due to Feshbach, Kerman and Koonin is reviewed and applied to the analysis of reactions of neutrons with ^{59}Co, ^{93}Nb and ^{209}Bi. A detailed study is made of reactions at 14 MeV, and in addition the total cross-sections in several reaction channels are presented in the range 10 - 20 MeV. Conclusions are drawn concerning the energy variations of the contributions of direct, pre--equilibrium and compound nucleus reactions.

1. Introduction

During the ninteen sixties, evidence accumulated indicating that it is possible for particles to be emitted after the first stage of a nucleat interaction but long before the attainment of statistical equilibrium; these are the pre-equilibrium particles. Many attempts have been made to understand such reactions in terms of a series of nucleon-nucleon interactions within the target nucleus. Starting with the pioneer work of Griffin /1/, a series of semi-classical or exciton models of varying complexity has been developed, and with appropriate choice of parameters these are often able to fit the observed energy and angular distributions of the emitted particles. More recently, several quantum--mechanical theories have been proposed, and these provide in principle a way of calculating the cross-sections of pre-equilibrium processes without the uncertainties of the semi-classical approximations. This makes it possible to analyse in a unified way the cross-sections in all the contributing reaction channels at moderate energies.

Pre-equilibrium processes make substantial and in some cases dominant contributions to the cross-sections of reactions initiated by neutrons from 10 to 20 MeV. The multistep compound (MSC) theory of Feshbach, Kerman and Koonin /2/ is described in section 2, and applied to some neutron reactions on ^{59}Co and ^{93}Nb in section 3. The semi-classical and quantum-mechanical theories of multistep processes are discussed in section 4.

This review includes some of the materials already presented at the International Symposium on Physics at Tandem (Beijing 1986) and then describes in more detail the work completed since then. This new work includes a study of the energy variations of the cross-sections in several reaction channels for the interactions of reactions with ^{93}Nb and ^{209}Bi. This shows the contributions of the multistep processes to the cross-sections as a function of neutron energy. Particular attention has been given to the cross-sections of alpha-emitting reactions, and some new results are presented.

2. The quantum-mechanical theory of Feshbach, Kerman and Koonin

The basic physical picture underlying the quantum-mechanical multistep theory is the same as for the exciton model. It is assumed that the interaction between the incident nucleon and the target nucleus takes place in a number of stages of increasing complexity. To evaluate the probability of emission after the first stage but before the attainment of statistical equilibrium it is necessary to consider the mechanism of nuclear excitation in detail. The nucleus is excited by a series of nucleon-nucleon collisions between the projectile and the target nucleons. These take place in stages, or doorway states of increasing complexity beginning with the projectile in the continuum. The first interaction creates a particle-hole pair, giving a 2-particle 1-hole (2p1h) state. There are a large number of possible 2p1h states. Subsequent interactions create additional particle-

-hole pairs, giving 3p2h states and once again there are very many 3p-2h states for each 2p1h state. This process continues until the excitation is spread through the nucleus to produce a fully-equilibrated nucleus which then decays statistically.

At each stage it is useful to consider separately the states with at least one particle in the continuum and the states with all particles bound; these states may be formally described by the projections P and Q acting on the total waveform Ψ, with $P + Q = 1$. The set of states $P\Psi$ contribute to the multistep direct process and the complementary set of states $Q\Psi$ to the multistep compound process. These states are shown in Figure 1, with the arrows indicating transitions from one configuration to another. Of only two-body interactions are present these transitions can only take place between neighbouring stages; this is the chaining hypothesis.

At each stage there are three possibilities: excitation of an additional particle-hole pair, de-excitation of a particle-hole pair, and emission into the continuum. The transition matrix for the de-excitation of a particle-hole pair is the same as the corresponding matrix for its excitation, but because the density of final states is so much greater for the states with more particle-hole pairs the probability of excitation of an additional particle-hole pair is much greater than of de-excitation. Thus transitions to states of greater complexity are much more probable than transitions to states of lesser complexity. It is therefore good approximation to neglect the transitions going to states of lower exciton number; this is the never-come-back assumption.

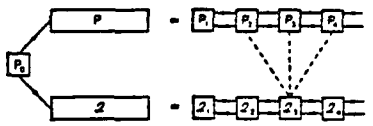

Figure 1 Multistep description of a nuclear reaction

The pre-equilibrium emission can take place directly at each stage from the P-chain, or indirectly from the Q chain. In the latter case the emission process goes through states in the P-chain; this can happen in three different ways as shown in Fig. 1. The more energetic particles come from the early stages of the chain and the less energetic from the later stages.

The time structure of the interactions is more complicated. The multistep direct reactions take place down the P-chain, and these direct processes take place rapidly. The transitions down the Q-chain, on the other hand, take place much more slowly, and indeed a state of quasi-equilibrium is attained at each stage so that the emission is compound in character with a symmetric angular distribution. A large number of individual interactions take place at each stage, but nearly all of them leave the number of particles and holes unchanged. It is only very occasionally that a collision results in a transition to a state of greater complexity or to the P-chain and hence to the continuum. To obtain the emission probabilities only these escape probabilities need be calculated, together with the probabilities for exciting a further particle-hole pair. The vastly greater number of interactions taking place within each stage in the Q-chain without changing the exciton number are only important for their role in ensuring statistical equilibrium at each stage.

The relative reaction fluxes passing down the P and Q chains depends strongly on the incident energy. At low energies the Q-chain interactions dominate, giving symmetric multistep compound angular distributions. As the energy increases the P chain interactions become increasing important until finally they are responsible for almost all the cross--section giving forward-peaked multistep direct angular distributions. The transitions between the P and Q chains are small and average out, so that the contributions of the P and Q chains can be evaluated separately, and their sum compared with experiment.

To describe the multistep compound process mathematically, let $\Gamma_n\downarrow$ be the damping width corresponding to the transition from the nth to the $n + 1^{th}$ state, and $\Gamma_n\uparrow$ the escape width for the transition from the nth state into the continuum. The total width for the decay of the nth state is therefore

$$\Gamma_n = \Gamma_n^{\downarrow} + \Gamma_n^{\uparrow} \tag{2.1}$$

The total probability for emission into the continuum from the nth state is then the product of three factors for each value of the total angular momentum J:

a) the probability of formation of the compound system, which is given by the optical model expression

$$\sigma_C^{\ell J} = \pi\lambda^2 \frac{2\pi < \Gamma_{\ell J}^{in} >}{< D_{\ell J} >} \tag{2.2}$$

where the last factor is the strength function.

b) the probability of the system arriving to the Nth stage without particle emission. This is given by the product of the probabilities of surviving the mth stage,

$$\prod_{m=1}^{N-1} W_{m+1,m} = \prod_{m=1}^{N-1} \frac{< \Gamma_{mJ}^{\downarrow} >}{< \Gamma_{mJ} >} \tag{2.3}$$

where $\langle \Gamma_{mJ}^{\downarrow} \rangle$ is the damping width for the transition to a stage of higher exciton number and $\langle \Gamma_{mJ} \rangle$ is the total width.

c) the probability that a particle will be emitted into the continuum from the Nth stage. This is given by a sum over all possible emission processes divided by the sum over all processes. Emission can take place in three ways, so the emission probability is given by the sum of products of emission widths $\Gamma_{NJ}^{\ell s \nu \uparrow}(U)$ and the level densities $\rho_J^N(U)$ of the final states of the residual nucleus at excitation energy U. This gives the factor

$$\frac{\left\langle \Gamma_{NJ}^{\ell s \nu}(U) \rho_J^N(U) \right\rangle}{< \Gamma_{NJ} >} \tag{2.4}$$

Collecting these factors together gives for the double differential-section for pre--equilibrium emission by the multistep compound process

$$\frac{d^2\sigma}{d\Omega d\epsilon} = \pi\lambda^2 \sum_J (2J+1) \left[\sum_{N=1}^{r} \sum_{\ell s \lambda \nu} C_{\ell s J}^{\lambda} P_\lambda(\cos\theta) \sum_\nu \frac{< \Gamma_{NJ}^{\ell s \nu}(U) \rho_J^N(U) >}{< \Gamma_{NJ} >} \right] \times$$
$$\times \left(\prod_{m=1}^{N-1} \frac{< \Gamma_{mJ}^{\downarrow} >}{< \Gamma_{mJ} >} \right) \frac{2\pi < \Gamma_{\ell J}^{in} >}{< D_{\ell J} >} \tag{2.5}$$

All the factors in the above expressions are calculated quantum-mechanically or, as in the case of the level density function, obtained from the known systematics of nuclear properties. The measured cross-section for the formation of the compound nucleus is used, and if it is not available it can be obtained from the optical model.

The particle-hole level densities are calculated using Ericson's expression based on the equidistant spacing model, with an additional factor giving the spin distribution

$$\rho_J^N(E) = \rho_N(E) S_J^N \equiv \rho_n(E) S_J^n \tag{2.6}$$

where n = 2N + 1 and

$$\rho_n(E) = \frac{g(gE)^{(n-1}}{p!h!(n-1)!} \tag{2.7}$$

in which g is the total single-particle density and p, h the numbers of particles and holes (n = p + h).

The spin-dependent factor S_J^n is given by

$$S_J^n = \frac{2J+1}{\sqrt{\pi}\, n^{3/2} \sigma^3} \exp\left[-\frac{(J+\frac{1}{2})^2}{n\sigma^2} \right] \tag{2.8}$$

The spin cut-off parameter σ^2 is related to the nuclear temperatur τ by the expression

$$\sigma^2 = 2C\tau \tag{2.9}$$

where $C \sim A^{2/3}/90$ (MeV^{-1}) and

$$E = a\tau^2 - \tau \tag{2.10}$$

and $a = \pi^2 g/6$.

Each of the widths corresponding to the three emission processes may be expressed as a product of three factors, the first depending on the level densities, the second on angular momentum coupling and the third on the wavefunctions of the interacting particles:

$$< \Gamma_{NJ}^{\ell s \nu}(U)\rho_s^\nu(U) >= X_{NJ}^{\ell s \nu}(U)A_N^\nu(U)\theta_N^\nu(U). \tag{2.11}$$

The full expressions for the first two of these functions are given by FKK and the third is

$$\theta(U) = V_0\left(\frac{4\pi}{3}r_0^3\right)\frac{1}{4\pi}\int_0^\infty u_{j1}(r)u_{j2}(r)u_{j\ell}(r)u_{j3}(r)dr/r^2 \tag{2.12}$$

where V_o is the strength of the residual two-body interaction and the radial wave functions $u_{j1}(r)$ and $u_{j2}(r)$ refer to the bound particles before the interaction, $u_{j3}(r)$ to the bound particle after the interaction and $u_{j1}(r)$ to the particle emitted into the continuum.

At lower energies where there are few contributing channels it is possible to fix the strength of the effective interaction V_o directly and accurately by normalising the sum of the cross-sections in all the reaction channels to the total reaction cross-section σ_R obtained from the optical model potential or from experiment. Thus, at a particular energy

$$\sum_i V_0^2 f_i(E) + \sum_j \sigma_j(E) = \sigma_R \tag{2.13}$$

where i, j label the reaction channels. $V_o^2 f_i(E)$ is the total reaction cross-section in the ith channel and $\sigma_j(E)$ that in the jth channel. In this expression the cross-sections in the first i channels are calculated using the multistep theory, and those in the remaining j channels are either calculated by the Weisskopf-Ewing theory or taken from experimental data.

In the calculations reported here we evaluate the matrix elements using constant wavefunctions inside the nucleus and a two-body interaction of zero range as originally suggested by FKK. This of course overestimates the cross-sections and so thus requires small values of the effective interaction V_o. In a subsequent calculation Bonetti and Colombo /3/ repeated the calculation with realistic wavefuntions and a density-dependent Yukawa interaction and showed that the corresponding V_o is consistent with that found in other analysis. The main effect of using these approximate wavefuntions is thus absorbed by the renormalisation of the effective interaction; the effect on the energy spectra is small. Making the calculations in this way substantially reduced the computation time.

Feshbach, Kerman and Koonin also derived an expression for the double differential cross-section for pre-equilibrium emission by the multistep direct process.

3. Multistep analysis of neutron-induced reactions

The Milan group has already made many calculations using the multistep compound and multistep direct theories /3/. More recently, the multistep compound theory has been used to calculate the inelastic spectrum of neutrons emitted when 14 MeV neutrons interact with ^{59}Co, ^{93}Nb and ^{209}Bi /4,5/. These reactions are particularly suitable to test the theory as much data are available, and they are also of practical importance.

At these energies, there are rather few open reaction channels and so it is possible to make a relatively complete analysis. In particular, the effective interaction strength can be fixed by the requirement that the sum of all the non-elastic cross-sections is the

reaction cross-section.

Preliminary calculations of the total cross-sections in the various channels were made using the Weisskopf-Ewing /7/ theory, and the results are shown in Fig. 2. The optical potentials used are given in Ref. 4. At energies less than 9 MeV only the (n,n'), (n,γ), (n,p) and (n,α) cross-sections are appreciable, and of these (n,n') accounts for about 97 % of the total. The value of the effective interaction V_0 may therefore be determined accurately from equation (2.13) using the Weisskopf-Ewing values for the three smaller cross-sections. The main uncertainty comes from the calculated total

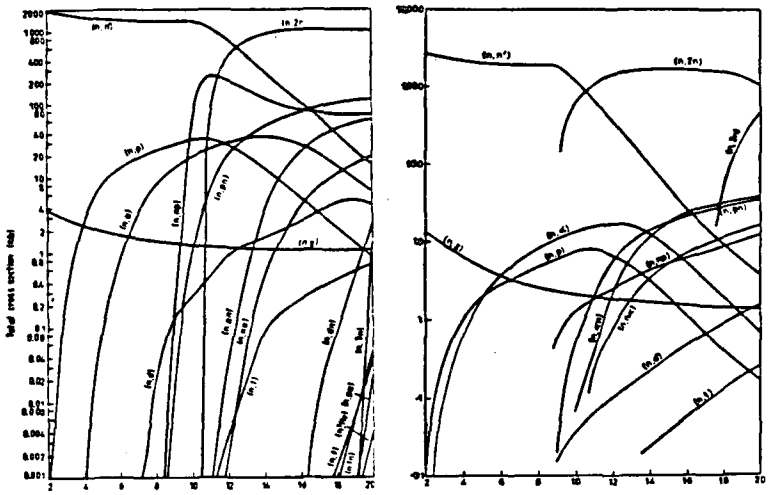

Incident neutron energy in MeV

Figure 2 Total cross-sections of all reactions of neutrons on ^{59}Co and ^{93}Nb as a function of neutron energy calculated with the Weisskopf-Ewing theory.

reaction cross-section. At 14 MeV the situation is quite different; the (n,2n) cross-section dominates, (n,n') is still large and (n,np) and (n,pn) are quite important. The measured neutron inelatic cross-section includes the neutrons from all these reactions, whereas the calculated neutron inelastic cross-section refers only to the neutrons emitted first, i.e. it gives the (n,n') cross-section together with half the (n,np) and (n,2n) cross-sections but not those of the neutrons from (n,pn) or the second neutrons from (n,2n).

Examination of the angular distributions of the emitted neutrons and protons show that they are almost symmetric, with a slight forward excess. This indicates that the reaction mechanism is predominantly compound, with a small direct contribution that for ^{59}Co can be estimated from the forward excess to be about 100mb for neutrons and about 20mb for protons. This direct contribution has now been calculated, and is included in the 30° distribution in Fig. 3.

The total reaction cross-section for 14 MeV neutrons on ^{59}Co is 1370 ± 30mb (MacGregor et al /6/) and allowing 120 ± 40mb for direct processes leaves 1250 ± 50mb for compound nucleus processes. This is therefore the sum of the cross-sections of the compound nucleus contributions to the contributing reactions, provided there are no direct contributions to the alpha emission reactions. This latter qualification can be tested when the corresponding angular distributions are available but since the total cross-sections in the alpha channels are small this will not significantly affect the analysis.

The multistep compound theory was used to evaluate the neutron and proton emission cross-sections, and the alpha-emission cross-sections were taken to have the value of 45mb given by the Weisskopf-Ewing /7/ theory. Using the level-density parameters of Brancazio and Cameron /8/, and taking the total compound nucleus cross-section to be 1250mb the value of V_0 was determined to be 0.90.

The emission of the first particle leaves the residual nucleus in a spectral distribution of excitation energies, and the theory may now be used to calculate the cross-section corresponding to the emission of a proton, neutron or alpha particle as second particle.

This gives the (n,2n), (n,np), (n,pn) and n,α) cross-sections, and also the (n,n') and (n,p) in cases where there is no second particle emitted. The cross-sections of the two--particle emission reactions obtained in this way are appreciable smaller than the values obtained from the Weisskopf-Ewing theory alone because the possibility of pre-equilibrium emission of the first particle implies a lower excitation energy in the residual nucleus and hence reduced probability for the emission of a second particle. These cross-sections are given in Table 1 and compared with the experimental values. This is only possible for the total (n,2n), (n,p) and (n,α) cross-sections obtained from radiochemical analyses; in other cases cross-sections obtained must be combined before such comparisons are made. Thus only the total of the (n,np), (n,pn) and (n,d) reactions is obtainable radiochemically, and particle emission cross-sections, that can be measured as energy and angular distribution, refer to the sum of several separate reactions. Thus the total neutron emission cross-section is the sum of the cross-section for the emission of a neutron as first particle and that for the emission of a neutron as second particle (i.e. the sum of (n,2n), (n,pn) and (n,αn)). Using the values from Table 1 gives 1758mb as the total compound nucleus neutron emission cross-section. Adding the direct component of 100mb gives 1858mb, which may be compared with the value 1780 ± 100mb obtained from the experimental data of Sal'nikov et al. /9/.

The calculations also give the double differential cross-section for neutron emission, and this is compared with the experimental data of Sal'nikov et al. in Fig. 3.

In a similar way the proton emission cross-section may be obtained as the sum of the cross-section for the emission of a proton as first particle and that for the emission of a proton as second particle (i.e. (n,np)). This gives 149mb as the total compound nucleus proton emission cross-section, which may be compared with the value 97 ± 12mb obtained from the experimental data of Colli et al. /1/. The double differential cross-section for proton emission is compared with the data in Fig. 4.

A similar analysis was made of the reactions of 14 MeV neutrons on ^{93}Nb, and the calculated neutron emission spectrum is compared with the experimental data in Fig. 5 and the total cross-sections in Table 2. The calculated neutron emission spectrum for ^{209}Bi is compared with the data in Fig. 6.

The calculation have now been made over a range of energies and compared with the experimental excitation functions for the (n,2n), (n,3n), (n,p) and (n,α) cross sections.

Table 1

Total cross-sections of neutron reactions on ^{59}Co at 14 MeV

Reaction	Theory	Experiment	Reaction	Theory	Experiment
(n,n')	475	–	Neutron Emission	1858 ± 90	$1780 \pm 100^{(9)}$
$(n,2n)$	592	$640 \pm 0^{(15)}$	Proton Emission	149	$97 \pm 12^{(10)}$; $108 \pm 22^{(11)}$
(n,pn)	72	$\gtrsim 35^{(11)}$	Total Reaction	–	$1370 \pm 30^{(6)}$
(n,np)	25				
(n,p)	52	$81 \pm 10^{(12)}$; $75 \pm 15^{(13)}$; $29 \pm 4^{(14)}$			
(n,α)	43	$30 \pm 4^{(15)}$			
$(n,\alpha n)$	2	–			

Table 2
Total cross-sections of neutron reactions on ^{93}Nb at 14 MeV

Reaction	Theory	Experiment	Reaction	Theory	Experiment
(n,n')	347		Neutron Emission	2321	$2500 \pm 120^{(9)}$
$(n,2n)$	1283	$1279 \pm 88^{(16)}$	Proton Emission	76	$44 \pm 2^{(11)}$; $51 \pm 8^{(22)}$
(n,pn)	35		Deuteron Emission	0.2*	$8 \pm 3^{(22)}$†
(n,np)	3		Alpha Emission	26*	$14 \pm 3^{(22)}$†
(n,p)	73		Total Reaction	–	1731 ± 30
(n,α)	–	$11.1 \pm 2.7^{(17)}$; $9 \pm 2^{(18)}$; $9.5 \pm 0.5^{(19)}$, $9.3 \pm 3^{(20)}$			
$(n,\alpha n)$	2	–			

* Weisskopf-Ewing Theory † At 15 MeV.

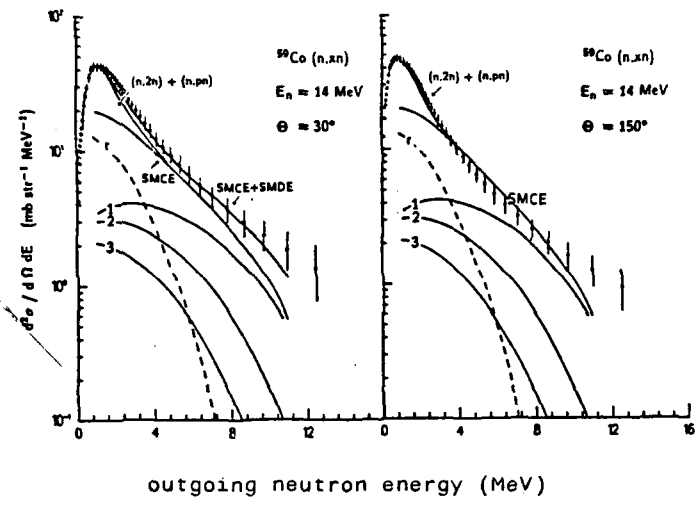

Figure 3 Energy spectra of neutrons emitted at 30° and 150° from ^{59}Co at an incident neutron energy of 14 MeV. The experimental data of Sal'nikov /9/ are compared with statistical multistep compound (SMC) calculations. The curves labelled with the value of N show the contributions of N-step processes and the broken and dotted curves show those due to the residual r-stage processes for the (n,n') and the (n,2n) + (n,pn) reactions respectively. The full curve gives the sum of these processes (Field /4/).

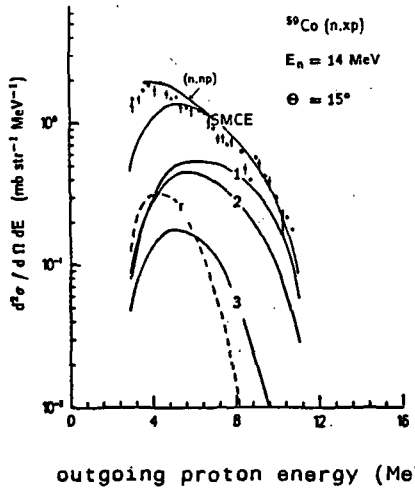

Figure 4 Energy spectrum of protons emitted at 15° from ^{59}Co at an incident energy of 14 MeV. The experimental data /10/ are compared with the statistical multistep compound (SMC) calculations. The curves labelled with the values of N show the contributions of N-step processes and the broken and dotted curves those due to the residual r-stage processes for the (n,np) reactions respectively. The full curve gives the sum of these processes (Field /4/).

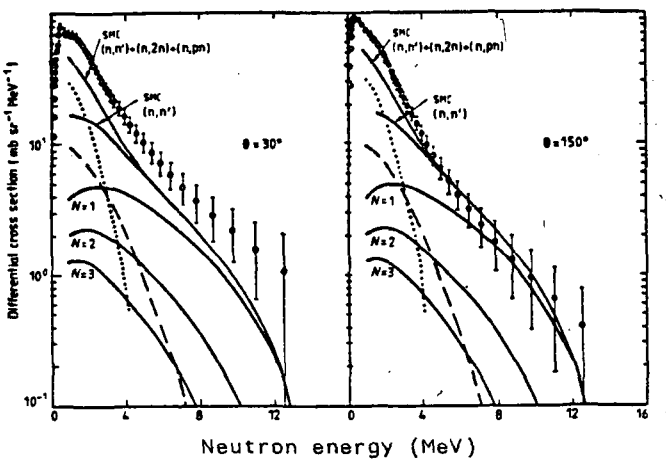

Figure 5 Energy spectra of neutrons emitted at 30° and 150° from ^{93}Nb at an incident neutron energy of 14 MeV. The experimental data of Sal'nikov /9/ are compared with statistical multistep compound (SMC) calculations. The curves labelled with the value of N show the contributions of N-step processes and the broken and dotted curves show those due to the residual r-stage processes for the (n,n') and the (n,2n) + (n,pn) reactions respectively. The full curve gives the sum of these processes.

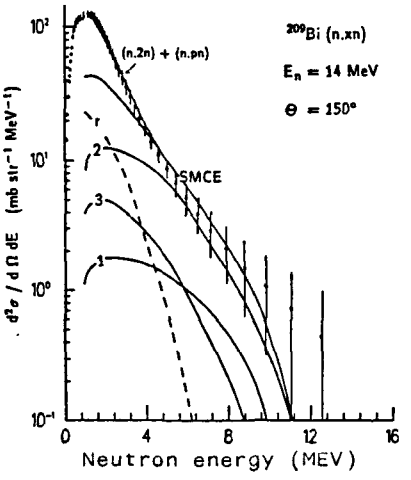

Figure 6 Energy spectrum of neutrons emitted at 150° from ^{209}Bi at an incident neutron energy of 14 MeV. The experimental data of Sal'nikov /9/ are compared with statistical multistep compound (SMC) calculations. The curves labelled with the values of N show the contributions of N-step processes and the broken curve that due to the residual r-stage process. The full curve gives the sum of these processes (Field /4/).

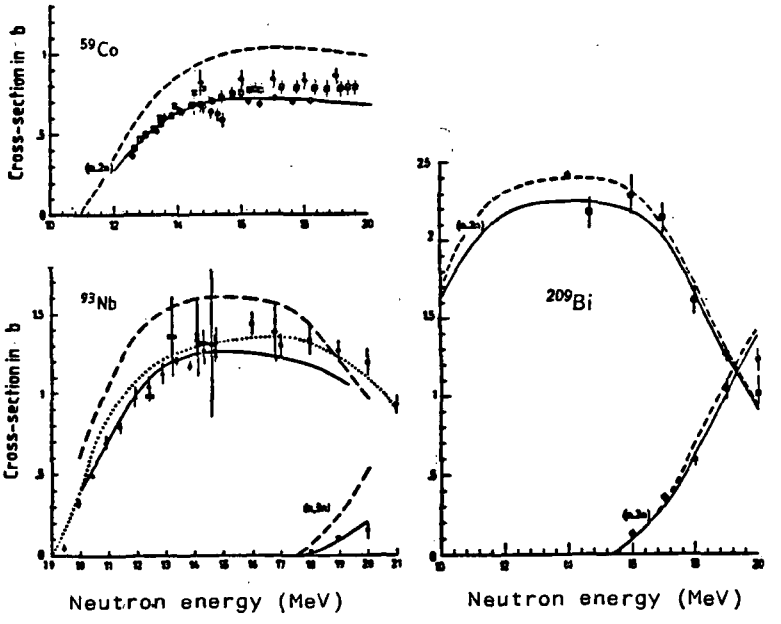

Figure 7 Excitation functions for the (n,2n) and (n,3n) reactions on ^{59}Co, ^{93}Nb and ^{209}Bi. The solid curves were calculated using the SMCE results as input for the second stage and the dashed curves using the Weisskopf-Ewing theory for both stages. References to the data on ^{59}Co may be found in Wilmore and Hodgson /15/ and Hasan et al. /16/, those on ^{93}Nb in Strohmaier /24/, and those on ^{209}Bi in Veeser et al. /16/. The dotted curve for ^{93}Nb shows the result of exciton model calculations by Strohmaier /24/ (Field /4/).

The (n,2n) and (n,3n) cross-sections

The Weisskopf-Ewing calculation gives (n,2n) cross sections that are up to 30 % greater than the measured values in the energy range from threshold to 20 MeV (Holub et al. /23/. This difference is attributable to pre-equilibrium emission, which gives more neutrons of higher energy, which in turn reduces the energy of the residual nucleus and with it the probability of the emission of a second neutron, thus reducing the (n,2n) cross-section. The magnitude of this reduction was calculated using the statistical multistep compound theory and the results are compared with experimental data in Fig. 7.

The (n,p) and (n,px) cross sections

The measurements of proton emission by the activation method gives only the (n,p) cross-section whereas techniques detecting the emitted protons give the (n,px) cross-section, where x indicates the inclusion of all other proton-emitting reactions like (n,pn) and (n,np). The cross-sections of these reactions obtained by the Weisskopf-Ewing and statistical multistep compound theories are compared with some activation data in Fig. 8.

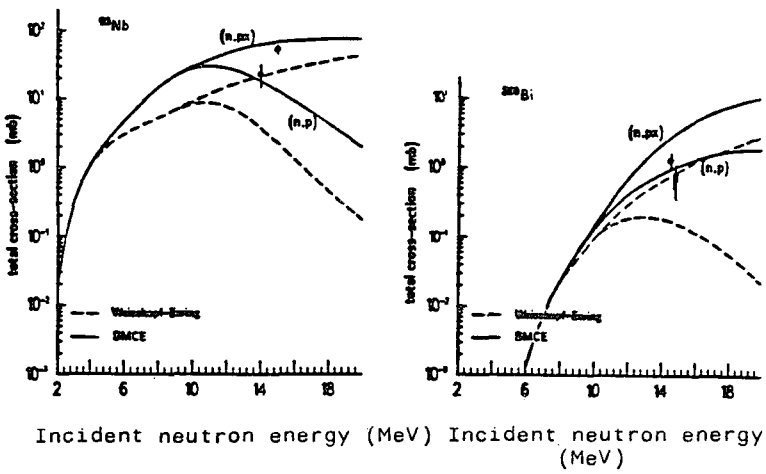

Figure 8 Excitation functions for the (n,p) reaction on ^{93}Nb and ^{209}Bi. The solid curves were calculated using the SMCE results as input for the second stage and the dotted curves using the Weisskopf-Ewing theory for both stages. References to the data on ^{59}Co may be found in Wilmore and Hodgson /15/ and Hasan et al. /26/, those on ^{93}Nb in Strohmaier /24/, and those on ^{209}Bi in Mukherjee et al. /27/. (Field /4/).

The (n,α) and (n,αx) cross-sections

The same considerations as those mentioned in the previous section apply to (n,α) and (n,αx) reactions. Weisskopf-Ewing /7/ calculations are compared with the experimental data for the excitation function in Figs. 9 and 10 and for the energy spectrum of the emitted alpha-particles for an incident energy of 14 MeV in Fig. 11. The excitation function for the (n,α) reaction calculated with the Weisskopf-Ewing theory was normalised to the data at low energies and falls substantially below the data for energies above 10 MeV. This is attributable to the pre-equilibrium component, and the exciton model calculations of Strohmaier /24/ do indeed fit the data well. Measurements of the angular distribution of the emitted alpha-particles by Bormann et al. /25/ show a marked forward peaking, so the pre-equilibrium emission takes place by the multistep direct process. It is not surprising that the (n,α) pre-equilibrium cross-section is much greater than the Weisskopf-Ewing /7/ cross-section because if the alpha-particle is not emitted with high energy the residual nucleus has enough energy to evaporate a neutron. The alpha-particle emission spectrum in Fig. 11 is the sum of the (n,α), (n,αn) and(n,nα) cross-sections and for comparison with the data the Weisskopf-Ewing calculations are normalised to the total alpha-emission cross-section of 10mb. This comparison shows an excess of high-energy particles that is characteristic of pre-equilibrium emission, and this is confirmed by the exciton model calculations of Strohmaier /24/. Calculations of alpha-emission using the Feshbach-Kerman--Koonin theory are in progress.

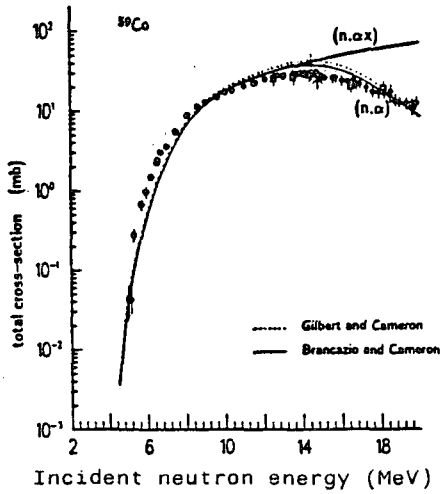

Figure 9 Excitation functions for the (n,α) reaction on ^{59}Co compared with the Weisskopf--Ewing calculations. The solid curves were calculated using the level density parameters of Brancazio and Cameron /8/ and the dotted curves using those of Gilbert and Cameron /28/. References to the data may be found in Wilmore and Hodgson /15/ (Field /4/).

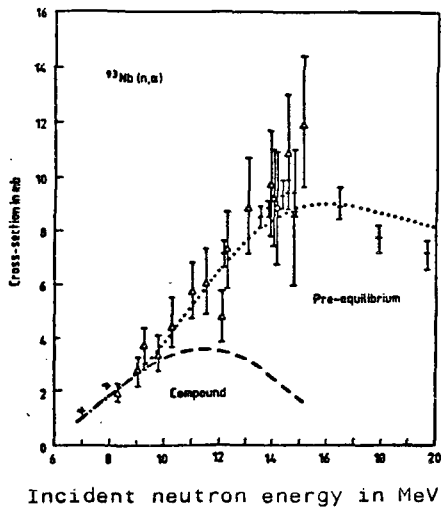

Figure 10 Total cross-section for the (n,α) reaction on ^{93}Nb compared with Weisskopf--Ewing calculations (dashed curves) and the exciton model calculations of Strohmaier /24/ (dotted curve). The data are from Bramlitt and Fink /17/ (x), Blosser et al. /18/ (o), Prestwood and Bayhurst /19/ (+) and Tewes et al. /29/ (◊) (Strohmaier /24/.

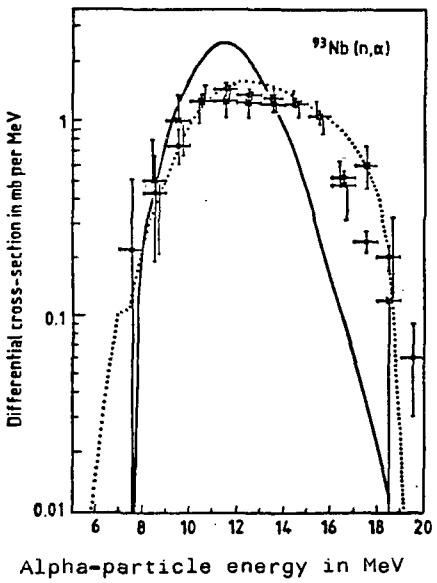

Figure 11 Energy spectrum of alpha-particles emitted from ^{93}Nb at an incident neutron energy of 14 MeV compared with normalised Weisskopf-Ewing calculations for the sum of the (n,α) and (n,nα) reactions (full curve) and exciton model calculations of Strohmaier /24/ (dotted curve).

These calculations of the pre-equilibrium cross-sections as a function of incident energy allow the changing contributions of the various reaction processes to be determined, and the results are shown in Fig. 12. It will be noticed that the compound nucleus cross-section falls with increasing energy, while the direct cross-section rises. Within the compound nucleus cross-section, the contribution of the multistep compound process at first rises with energy, attains a maximum and then falls. The energy at which the multistep compound cross-section is maximal increases with target mass.

The present understanding of the cross-sections in the weaker channels such a (n,t) is unsatisfactory. There is very little experimental data and these cross-sections are generally much greater than those given by the statistical theories. It is likely that they are predominantly direct or multistep direct, but this will not be known until pre-equilibrium calculations are compared with accurate experimental data.

4. Discussion

The various pre-equilibrium theories differ appreciably in their flexibility, in several different respects. The semi-classical theories have been applied to a much wider range of reactions that the quantum-mechanical theories, in particular to those initiated by complex particles and those leading to the emission of many particles. By contrast, the quantum-mechanical theories have so far been confined to nucleon interaction with not more than two emergent particles. In the next few years the quantum-mechanical theories will certainly be applied to a wider range of reactions, but a present the semi-classical theories are the only ones that can be used for many of the more complicated reactions.

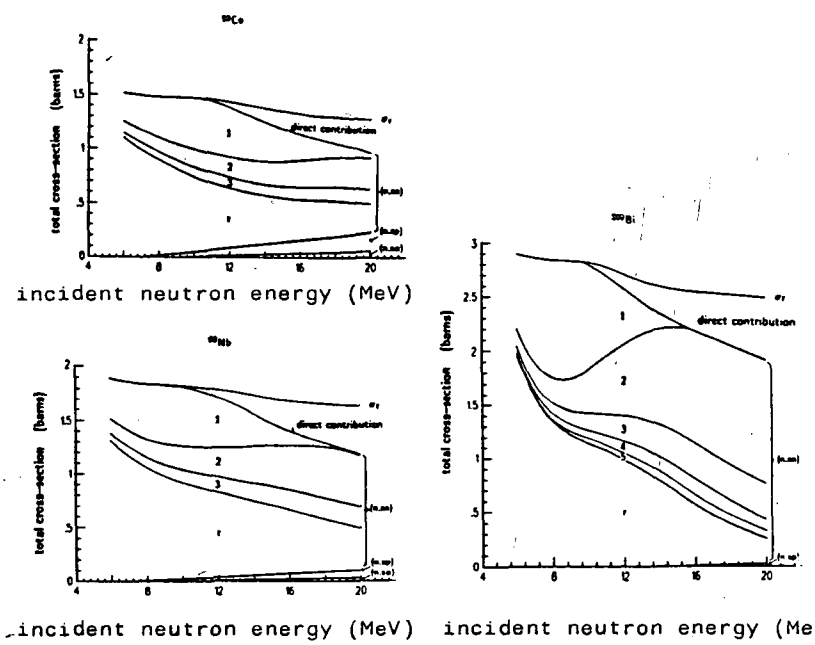

Figure 12 The total cross-sections as a function of incident neutron energy for ^{59}Co, ^{93}Nb and ^{209}Bi. The SMCE calculations are restricted to bound states and include the finite depth of the potential well.

The semi-classical theories are also more flexible in that they have more model parameters than the quantum-mechanical theories. Here one must distinguish between internal parameters that are special to the particular theory and those that are fixed by some external constraint. As an example of the former we may mention the parametrisation of the residual matrix element in the exciton model which at present cannot be calculated from a more fundamental theory. In the latter category are the optical model and level density parameters. Here there is a further distinction that is important for the predictive power of these theories: reliable global optical potentials are now available for nucleons so that the cross-sections can be calculated from them for any nucleons with good accuracy.

The particle-hole level density parameters, on the other hand, cannot be represented with sufficient accuracy by global formulae and only the total level density can be fitted to the experimental data for each nucleus. Therefore there is a strong need to obtain reliable expressions for these particle-hole level densities, in particular for the lowest stages. These considerations apply both to the semi-classical and to the quantum mechanical theories.

If all that is required is a fit to a particular data set, this can be achieved by both the semi-classical and the quantum-mechanical theories for the energy distributions of the emerging particles. The semi-classical calculation may require some adjustment of an 'internal' parameter, and both types are subject to the above remarks about 'external' parameters, particularly those relating to particle-hole level densities. In practice the range of applicability of the semi-classical models is often well known and it is not necessary to adjust "internal" model parameters in each computation. The differences between the results are therefore quite small and further calculations are needed to detect deviations in other energy and mass ranges.

With respect to angular distributions the quantum-mechanical effects may be more important. The most recent semi-classical models are based upon the scattering in infinite nuclear matter with quasi-classical descriptions of refraction and/or finite-size effects. Conceptually the quantum mechanical theories are of course superior. In particular, there are difficulties in the description of back-angle cross sections with the semi-classical theories that do not exist in quantum-mechanical theories. This was illustrated recently by Holler et al. /30/ in an comparison of semi-classical and quantum-mechanical pre-equilibrium calculations for the $^{65}Cu(p,\alpha n)$ reaction at 26.7 MeV. The hybrid model of Blann and Vonach /31/ gives a good overall fit to the energy distribution of the emitted neutrons but is unable to fit the angular distribution in the very forward and backward directions. As shown in Figure 13(a) the back-angle discrepancy persists when refraction and finite-size effects are included in the calculations. Similar calculations have been made by Gruppelaar /32/ using the PRANG code, giving the dotted curve in Figure 13(a). The differences are due to a truncation of the Legendre polynomial expansion to $l_{max} = 6$ and to an adjustment of f_2 by 20 % just to avoid negative values of the scattering kernel. The resulting curve is still below the data a backward angles. Quantum-mechanical calculations with the FKK theory are however able to fit the data over the whole angular range, as shown in Figure 13(b). This shows tat the quantum-mechanical theories are able to evaluate interference effects that are beyond the scope of the semi-classical theories. In addition, the description of finite-size effects leads to serious difficulties in the semi-classical models, which perhaps could be solved in a pragmatic way by utilizing the results for a systematic study of precompound angular distribution using quantum-mechanical theories.

Acknowledgements

This work is part of programme of quantum-mechanical studies of pre-equilibrium reactions that is being carried out in collaboration with Prof. R. Bonetti (Milan), Dr. D. Wilmore and Dr. G.M. Field (Oxford) and I am grateful to them for permitting me to present their results. Some of these results have been presented, together with a survay of semi--classical theories by Dr. H. Gruppelaar (Petten) and Dr. P. Nagel (NEA Data Bank), to the International Conference on Nuclear Data for Basic and Applied Science held in Santa Fé, New Mexico in May 1985. A fuller account of this work was published in Revista del Nuovo Cimento /33/.

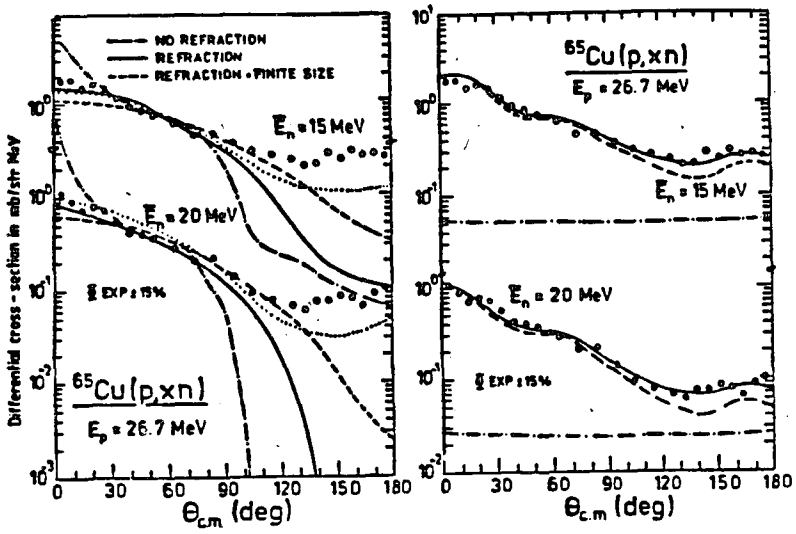

Figure 13

a) Angular distributions for the ^{65}Cu(p,xn) reaction at 26.7 MeV compared with geometry--dependent hybrid model calculations. The data are plotted in E_n = 1 MeV bins centred at energies E_n. The calculations are shown for pure NN-scattering (dot-dash), NN-scattering with entrance channel refraction (solid) and with refraction plus finite-size correction (dashed) /30/, the dotted curve has been added and shows the results of using the same model (PRANG). It refraction effects are not included and a very large number of Legendre coefficients are used the dot-dash curve is reproduced. Introduction of entrance and exit refraction and truncation of l_{max} = 6 gives slightly better results as the dashed curve. Correcting for the negative values of the scattering kernel by increasing f_2 by 20 % gives the dotted curve. A further increase of f_2 would fit the data.

b) Angular distributions for the ^{65}Cu(p,xn) reaction at 26.7 MeV compared with FKK quantum-mechanical calculations. The statistical multistep direct contributions are shown by the dashed line, the statistical multistep compound by the dash-dot line and their sum by the solid line /30/.

References

1 J.J. Griffin, Phys.Rev.Lett. 17, 478 (1966)

2 H. Feshbach, Proceeding of International Conference on Nuclear Reaction Mechanism Varenna (1977)
H. Feshbach, A. Kerman and S. Koonin, Ann.Phys. (New York), 125, 429 (1980)
H. Feshbach, Ann. Phys. (New York), 159, 150 (1985)

3 L. Avaldi, R. Bonetti and L. Colli-Milazzo, Phys.Lett. 94B, 463 (1980)
R. Bonetti, M. Camnasio, L. Colli-Milazzo,and P.E. Hodgson, Phys.Rev. C24, 71 (1981)
R. Bonetti, L. Colli-Milazzo, I. Doda and P.E. Hodgson, Phys.Rev. C26, 2417 (1982)
R. Bonetti and L. Colombo, Phys.Rev. C28, 980 (1983)
R. Bonetti, L. Colli-Milazzo and M. Melanotte, Phys.Rev. C27, 1003 (1983)
R. Bonetti, L. Colli-Milazzo, A.De Rosa, G. Inglima, E. Perillo, M. Sandoli and F. Shahin, Phys.Rev. C21, 816 (1980)
R. Bonetti, L. Colli-Milazzo, M. Melanotte, A. De Rosa, G. Inglima, E. Perillo, M. Sandoli, V. Russo, N. Saurier and F. Shahin, Phys.Rev. C25, 717 (1982)

4 G.M. Field, R. Bonetti and P.E. Hodgson, J. Phys. G12, 93 (1986)
G.M. Field, Thesis Oxford (1987)

5 M. Herman, A. Marcinkowski and K. Stankiewicz, Nucl.Phys. A430, 69 (1984)
K. Stankiewicz, A. Marcinkowski and M. Herman, Nucl.Phys. A435, 67 (1985)

6. M.H. MacGregor, W.P. Ball and R. Booth, Phys.Rev. 108, 726 (1957)
7 V.F. Weisskopf and D.H. Ewing, Phys.Rev. 57, 472 (1940)
8 P.J. Brancazio and A.G.W. Cameron, Can. J. Phys. 47, 1029 (1969)
9 O.A. Sal'nikov, G.N. Lovchikova, G.V. Kotelnikova, A.M. Trufanov and N.I. Fetisov, Yad. Fiz. 12, 1132 (1970; Sov. J. Nuc. Phys. 122, 620 (1971)
10 L. Colli, S. Micheletti and M. Pignanelli, Nuovo Cim. 21, 966 (1961)
11 K.R. Alvar, Nucl. Phys. A195, 289 (1972)
12 D.L. Allan, Nucl. Phys. 24, 274 (1961)
13 R.S. Storey, W. Jack and A. Ward, Proc. Phys. Soc. 75, 526 (1960)
14 F.L. Hassler and R.A. Peck, Phys. Rev. 125, 1011 (1962)
15 D. Wilmore and P.E. Hodgson, J. Phys. G11, 1007 (1985)
16 L.R. Veeser, E.D. Arthur and P.G. Young, Phys. Rev. C16, 1792 (1977)
17 E.T. Bramlitt and R.W. Fink, Phys. Rev. 131, 2649 (1963)
18 H.G. Blosser, G.D. Goodman and T.H. Handley, Phys.Rev. 110, 531 (1958)
19 R.J. Prestwood and B.P. Bayhurst, Los Alamos Report La-2493, TID-4500 (1961)
20 P. Kulisic, V. Adjacic, N. Cindro, B. Lalovic and B. Strohal, Nucl. Phys. 54, 17 (1964)
21 G. Traxler, R. Chalupka, R. Fischer, B. Strohmaier, M. Uhl and H. Vonach, Nucl. Sci. Eng. 90, 174 (1985)
22 S.M. Grimes, R.C. Haight and J.D. Anderson, Phys. Rev. C17, 508 (1978)
23 E. Holub, N. Cindro, O. Bersillon and J. Jary, Z. Phys. A 289, 421 (1979)
24 B. Strohmaier, Ann. Nucl. Energy 9, 397 (1982)
25 M. Bormann, W. Schmidt, V. Schröder, W. Scobel and U. Seabeck, Nucl. Phys. A186, 65 (1972)
26 S.J. Hasan, A. Pavlik, G. Winkler, M. Uhl and M. Kaba, J. Phys. G12, 397 (1986)
27 S.K. Mukherjee, A.K. Ganguly and N.K. Majumder, Proc.Phys.Soc. (Lond) 77, 508 (1961)
28 A. Gilbert and A.G.W. Cameron, Can. J. Phys. 43, 1446 (1968)
29 H.A. Tewes, A.A. Caretto, A.E. Miller and D.R. Nethaway, University of California Radiation Laboratory Report 6028-T (1960)
30 Y. Holler, A. Kaminsky, R. Langkau, W. Scobel, M. Trabandt and R. Bonetti, Nucl. Phys A442, 79 (1985)
31 M. Blann and H.K. Vonach, Phys. Rev. C28, 1475 (1983)
32 P.E. Hodgson, G.M. Field, H. Gruppelaar and P. Nagel, International Conference on Nuclear Data for Basic and Applied Science, (Santa Fé) (1985); Radiation Effects 95, 27 (1986)
33. H. Gruppelaar, P. Nagel and P.E. Hodgson, Revista del Nuovo Cimento 9 No. 7.1 (1986)

SMD/SMC-MODEL FOR PRACTICAL APPLICATIONS

H. Kalka
Technische Universität Dresden, Sektion Physik, Mommsenstr. 13, Dresden, DDR-8027
German Democratic Republic

For many years nuclear reaction mechanism has been investigated within the theoretical concepts of statistical multistep compound (SMC) /1-6/ and statistical multistep direct (SMD) processes /2,3,7,8/. Till now a lot of experimental data are compared either within a pure SMC-model /1,9,10/ or within a pure SMD-approach /11,12/. But in nucleon-nucleus reactions at bombarding energies between 5 and 30 MeV (which is of interest for nuclear technology) both SMD and SMC processes are important. Therefore we present a simple SMD/SMC-model for practical applications, firstly proposed in /13/, which calculates energy and angular distributions of neutrons and protons. In this model besides the excitation of particle-hole states (excitons) also the direct excitation of collective modes (phonons) are considered.

The SMD/SMC-model will be derived from first principles (Green's function formalism; Gaussian Ensembles). Even this general approach allows a classification of the most current multistep theories. The interplay between these theories as well as the role of the phenomenological exciton model (EM) /14-16/ becomes obvious.
Finally, within the SMD/SMC-model (which differ from EM) numerical calculations are performed without any free parameter for different nuclei and incidence energies.

1. Green's function formalism

A very direct and general approach to nuclear reactions is obtained by the Green's function (GF) formalism /3/. Within this formalism the T-matrix for the reaction A+a → B+b is given by

$$T_{fi}(E) = \int d^3x_{[B^*+b+a]}\, \tilde{\varphi}^{(-)*}_{bB}(x_{[b+B^*]})\, T(B^*+b,a)\, \tilde{\varphi}^{(+)}_{a}(x_{[a]}) \equiv \langle f^{(-)} | T | i^{(+)} \rangle \qquad (1.1)$$

where B^* symbolizes the number of excited quasiparticles plus holes (excitons) of the residual nucleus B, i.e., the exciton number of the composite system, n=p+h, is equivalent to $(b+B^*)$. The explicit form of the distored waves $\tilde{\varphi}_a^{(+)}$, $\tilde{\varphi}_{bB}^{(-)}$ is presented in /3/.

In many-body theory /17,18/ the transition operator entering the l.h.s. of (1.1) can be expanded (graphically) in powers of a so-called irreducible interaction I,

$$T = I + IG^{o}T. \qquad (1.2)$$

The (ph-line irreducible) effective interaction I is a sum of different Feynman graphs, which can not be cut into two parts by just cutting ap, (a+1) p1h ,..., $(b+p_B)ph_Bh$ lines. The GF $G^o(n,n)$ is a product of n single-particle GF's, and has the following spectral representation

$$G^{o}(n,n) = \sum_{\nu} \frac{\varphi_{n\nu}(x_{[n]})\,\varphi^{*}_{n\nu}(x'_{[n]})}{E - e_{n\nu}} + \sum_{c\varrho} \frac{\tilde{\varphi}^{(-)}_{n\varrho c}(x_{[n]})\,\tilde{\varphi}^{(-)*}_{n\varrho c}(x'_{[n]})}{E - E_{n\varrho c} - i\eta} \equiv G_b(n,n) + G_u(n,n) \qquad (1.3)$$

where $\varphi_{n\nu}$, $\tilde{\varphi}^{(-)}_{n\varrho c}$ are bound and unbound eigenfunctions in exciton class n. It is especially convenient for the further treatment to have equations in which the pole part of G^o occures rather than (1.2). Therefore G^o is splitted into a pole part G' (at $E = e_{n\nu}$ and $E = E_{n\varrho c}$) and a smooth energy dependent regular part G_R (principle value integral). Then the regular part of G^o will be used to define a new effective interaction /17/

$$I' = I + I\, G_R\, I' \tag{1.4}$$

which yields the renormalized iterative equation

$$T = I' + I'\,(G'_u + G'_b)\,T \tag{1.5}$$

instead of (1.2). But for simplicity, in using (1.5) we omit the prime henceforth.

Usually, in nuclear physics the general expression (1.5) is decomposed into two parts,

$$T = T^u + T^u G_b T \equiv T^u + T^b \tag{1.6}$$

where the so-called multistep direct part is given by

$$T^u = I + IG_u T^u = I \sum_{s=o}^{\infty} (G_u I)^s, \tag{1.7}$$

and the multistep compound part has the form

$$T^b = T^u G_b T^u + T^u G_b T^u G_b T^u + \ldots = T^u \sum_{s=1}^{\infty} (G_b T^u)^s. \tag{1.8}$$

In contrast to the multistep direct processes (1.7) the multistep compound series (1.8) describes processes in which the nuclear system undergoes at least one transition to stages in which all particles are in bound states, characterized by G_b. Thus there is no one single-step term within the multistep compound series (1.8) which quite naturally occure in (1.7).

Eqs. (1.6) to (1.8) are of exact character and can be applied to reactions with composite particles. Similar (approximate) expressions were derived either within a shell-model approach /1/ or projection operator formalism /2/. Then the cross section is obtained after inserting (1.6) into (1.1) and taking the absolute square of it. But for complex nuclides, and high incidence energies this problem can not be solved exactly because of too many (overlapping) nuclear states, and the lack of information about it. Analytical expressions can be obtained only for energy averaged cross sections

$$\sigma_{if} = (4\pi^3/k^2)\ \overline{|T_{fi}|^2} \tag{1.9}$$

by using statistical assumptions. In this manner the (microsopical) multistep processes become statistical multistep processes. Since the statistical assumptions are chosen so that all interference terms between T^u and T^b vanish, $\overline{T^u_{fi}\, T^{b*}_{fi}} = 0 = \overline{T^b_{fi}\, T^{u*}_{fi}}$ for $i \neq f$, the average cross section splits into a pure SMD and SMC contribution,

$$\sigma_{if} = (4\pi^3/k^2)\ \left\{ \overline{|T^u_{fi}|^2} + \overline{|T^b_{fi}|^2} \right\} \equiv \sigma^{SMD}_{if} + \sigma^{SMC}_{if}. \tag{1.10}$$

After defining the statistical assumptions (Sect. 2) we derive from (1.10) analytical expressions for the SMC (Sect. 4) and SMD cross section (Sect. 5). In the following we restrict ourselves to nucleon-nucleus reactions.

2. Statistical assumptions (Gaussian Ensembles)

Over the years several different statistical methods and techniques are introduced for carrying out the average cross section (1.10). First of all, according to the separate definitions /18/ of GF's at finite ($\theta \neq 0$) and zero temperature ($\theta = 0$) we distinguish between thermodynamical approaches, and the usual (zero temperature) approaches. In the first case there is the approach of Mädler and Reif /6/ basing on non-equilibrium statistical operator. In the second case, which are more common, we can distinguish between two formulations:

i) On one hand, there is the unified theory /2,3/ where the relative phases of certain matrix elements (of different operators and products of operators) are assumed to become random within an "optical-background representation" /19/. This method was improved by Adhikari /4/.

ii) Otherwise, following the pioneer work of Agassi e.a. /1/ there are many approaches /5,20,21/ which are based on random-matrix ensembles (GOE,GUE) /22/. Here the equivalence between energy and ensemble averages is postulated.

Comparing i) and ii) the last one is proved to be the more fundamental concept /5/ since the final result of the SMC-approach of Feshbach e.a. /2/ can be obtained by further approximations (never-come back assumption) immediately from the random-matrix approach. In other respects, even the Gaussian Ensembles (GOE,GUE) are used for description of stochastic (chaotic) behaviour which is observed in both nuclear spectroscopy and nuclear reactions /23/.

Despite the fact that the statistical methods are very different, the final result of all SMC-theories are similar to each other, and can be fairly approximated /21/ by the phenomenological EM.

Because of the general position of the random-matrix method even this method will be used in our further treatment. Before defining the statistical assumptions, i.e., the Gaussian Orthogonal and Unitary Ensembles (GOE,GUE) we have to distinguish between different types of matrix elements of the (renormalized) effective interaction I. According to the decomposition (1.6) of G^0 into a bound and unbound part we have to separate between bound-bound, bound-unbound, unbound-bound, and unbound-unbound matrix elements, I_b, I_{bu}, I_{ub}, I_u. In practical cases it is often possible to choose I_b, I_{bu}, and I_{ub} as real quantities. Then each of them should form a GOE, whereas the complex unbound-unbound element I_u should be a member of GUE.

According to GOE,GUE the first moments (mean value) of all elements vanish, $\overline{I} \equiv 0$, and the second moments are given by /1,24/

$$\overline{I_{n'\nu'n\nu}\, I_{m'\mu'm\mu}} = \left(\delta_{n'm'}\delta_{\nu'\mu'}\delta_{nm}\delta_{\nu\mu} + \delta_{n'm}\delta_{\nu'\mu}\delta_{nm'}\delta_{\nu\mu'}\right)\, \overline{I^2}(n,n') \tag{2.1}$$

$$\overline{I_{n'\varsigma'c',n\nu}\, I_{n_1'\varsigma_1'c_1',n_1\nu_1}} = \delta_{n'n_1'}\delta_{\varsigma'\varsigma_1'}\delta_{c'c_1'}\delta_{nn_1}\delta_{\nu\nu_1}\, \overline{I^2}(n,n'c') \tag{2.2}$$

$$\overline{I_{n'\varsigma'c',n\varsigma c}\, I_{n_1'\varsigma_1'c_1',n_1\varsigma_1c_1}} = \delta_{n'n_1'}\delta_{\varsigma'\varsigma_1'}\delta_{c'c_1'}\delta_{nn_1}\delta_{\varsigma\varsigma_1}\delta_{cc_1}\, \overline{I^2}(nc,n'c') \tag{2.3}$$

for I_b, I_{bu} and I_u. A relation analogous to (2.2) holds for I_{ub}, and its second moment $\overline{I^2}(cn,n')$. Here, the average lines are depicted as contraction lines. Further, different types of matrix elements are assumed to be statistical independent, for example, $\overline{I_u I_b} = 0 = \overline{I_{ub} I_b}$ etc.

The channel index $c = (\varepsilon\Omega,\gamma)$ will be chosen as energy, direction, and particle type $\gamma = \nu$ or π (neutron or proton) of the particle in the continuum. For this reason δ_{cc}, changes to $\delta_{\gamma\gamma}$, $\delta(\varepsilon-\varepsilon')\,\delta(\Omega-\Omega')$. Thus all continuum states are normalized per energy unit.

3. Parametrization of mean square matrix elements

Before deriving the general expressions for SMC and SMD processes there remains now the interesting question of how to relate all unbound mean square matrix elements, (2.2) and (2.3), to the bound-bound ones (2.1). As it will be explained in the Appendix, this can be done (for the angle-integrated case) by simple transformations,

$$\overline{I^2}(n\varepsilon,n') \simeq \overline{I^2}(n,n')\,\varrho(\varepsilon) \quad , \qquad \overline{I^2}(n,n'\varepsilon') \simeq \overline{I^2}(n,n')\,\varrho(\varepsilon) \tag{3.1}$$

$$\overline{I^2}(n\varepsilon,n'\varepsilon') \simeq \overline{I^2}(n,n')\,\varrho(\varepsilon)\,\varrho(\varepsilon')/4\pi \tag{3.2}$$

where

$$\varrho(\varepsilon)\,d\varepsilon = V_N\, d^3p/(2\pi\hbar)^3 = 4\pi V_N\, m\,(2m\varepsilon)^{1/2}\, d\varepsilon/(2\pi\hbar)^3 \tag{3.3}$$

is the single-particle state density in the nuclear volume $V_N = 4\pi r_0^3\, A/3$. Similar unbound/bound transformations are proposed in /2/ (see eq. (5.34) therein).

Referring back to the more general case of angular distributions $\overline{I_u^2}$ can be factorized /24,25/ into an angle-independent part (3.2), and an angular part,

$$\overline{I^2}(n\varepsilon\Omega,n'\varepsilon'\Omega') = (4\pi)^{-1}\,\overline{I^2}(n\varepsilon,n'\varepsilon')\sum_L (2L+1)\,\mu_L(n\varepsilon,n'\varepsilon')\,P_L(\cos\vartheta) \tag{3.4}$$

where $P_L(\cos\vartheta) = P_L(\cos\theta)\,P_L(\cos\theta')$, and $\mu_{L=0} = 1$.

The dependence of $\overline{I^2}$ on particle type γ (neutron or proton) will be considered in a quite phenomenological way

$$\overline{I^2}(n\varepsilon\alpha,n'\varepsilon'\beta) = \overline{I^2}(n\varepsilon,n'\varepsilon')\,P_\alpha(\varepsilon)\,P_\beta(\varepsilon') \tag{3.5}$$

by introduction of penetration factors

$$P_\gamma(\varepsilon) = \delta_{\gamma\nu} + [\sigma_\pi(\varepsilon)/\sigma_\nu(\varepsilon)] \tag{3.6}$$

which are 1 for neutrons, and which simulate a threshold behaviour for protons. $\sigma_\gamma(\varepsilon)$ is the OM reaction cross section for particle type γ at incidence energy ε. Similar expressions for $\overline{I_{bu}^2}$ and $\overline{I_{ub}^2}$ are obtained by ignoring P_α or P_β, respectively.

4. SMC processes

According to (1.10) the SMC cross section will be obtained from (1.8). By some authors /1,3/ this problem was not solved exactly but was solved to a good approximation by inserting $T^u \equiv I$ in (1.8). Following /2/ we extend this approximation by an additional term IG_uI which yields for the born series (1.8)

$$T_{fi}^b = I_{ub} G_b \sum_{s=0}^{\infty} \left(I_b G_b + I_{bu} G_u I_{ub} G_b \right)^s I_{bu} = I_{ub} \left[G_b^{-1} - I_b - I_{bu} G_u I_{ub} \right]^{-1} I_{bu} \tag{4.1}$$

It turns out below that even the term IG_uI in (4.1) is responsible for the escape widths $\Gamma\uparrow$ in the Pauli master eq. (4.11).

Now the (ensemble) average $\overline{T_{fi}^b T_{fi}^{b*}}$ is carried out /1/ by breaking up the power-series expansion of $T_{fi}^b T_{fi}^{b*}$ into a sum of all possible ways of averaging products of pairs (contractions) of the random matrix elements defined in (2.1) and (2.2). In proceeding this we restrict ourselves to (lowest-order) contractions that leads to analytical expressions (for damping and escape widths) which are of first order in $\overline{I^2}$, i.e., contractions that are not intersect each other.

Formally, the contraction procedure is treated in two steps /1,21/. In the first step all internal contractions within the power series (4.1) are considered. After summing up they are included in the so-called optical propagator

$$\tilde{G}_b^{-1} = G_b^{-1} - \overline{I_b G_b I_b} - \overline{I_{bu} G_u I_{ub}} \tag{4.2}$$

which has the spectral representation

$$(\tilde{G}_b^{-1})_{n\nu n'\nu'} = \delta_{nn'} \delta_{\nu\nu'} \left[E - e_{n\nu} + \frac{i}{2} \left(\Gamma_n\downarrow + \Gamma_n\uparrow \right) \right]. \tag{4.3}$$

The damping and escape widths are given by

$$\Gamma_n\downarrow = \sum_{n'} \Gamma_{nn'}\downarrow \,, \qquad \Gamma_{nn'}\downarrow = 2\pi \overline{I^2}(n,n') S_{n'} \tag{4.4a}$$

$$\Gamma_n\uparrow = \sum_{n'\gamma} \int d\varepsilon' \, \Gamma_{n,n'\gamma}(\varepsilon')\uparrow \,, \qquad \Gamma_{n,n'\gamma}(\varepsilon')\uparrow = 2\pi (2s+1) \overline{I^2}(n,n'\varepsilon'\gamma) S_{n'\gamma}(U) \tag{4.4b}$$

where $S_{n'}$ and $S_{n',\gamma}(U)$ are state densities of bound configurations in exciton class n' at excitation energy E, and in exciton class (n'-1) at residual energy $U=E-\varepsilon'-B_\gamma$. B_γ is the binding energy of particle type γ.

In the second step, after replacing all G_b in (4.1) by $\tilde{G}_b$, cross contractions between T_{fi}^b and T_{fi}^{b*} are performed. Symbolically this can be written as

$$\sigma_{fi}^{SMC} = \frac{4\pi^3}{k^2} \, I_{ub} \left[\tilde{G}_b^{-1} - I_b \right]^{-1} I_{bu} \; I_{ub} \left[-I_b + \tilde{G}_b^{*-1} \right]^{-1} I_{bu} \tag{4.5}$$

$$= \frac{4\pi^3}{k^2} \sum_{mn} \overline{I^2}(1\varepsilon,m) S_m (A^{-1})_{mn} \sum_k \Gamma_{n,k\beta}(\varepsilon')\uparrow \tag{4.6}$$

with the dynamical matrix

$$A_{nn'} = (\Gamma_n\downarrow + \Gamma_n\uparrow)\,\delta_{nn'} - \Gamma_{nn'}\downarrow . \tag{4.7}$$

Here, the short-hand definition /21/ for the propagator contraction,

$$\widetilde{G}_b\widetilde{G}_b^* = \sum_\nu (\widetilde{G}_b\widetilde{G}_b^*)_{n\nu n\nu} = 2\pi\varrho_n / (\Gamma_n\downarrow + \Gamma_n\uparrow) \tag{4.8}$$

was used. The sum over k in (4.6) runs over the exit modes of the final state $\widetilde{\Phi}_f^{(-)}$.

Eq. (4.6) is derived for the most general case where the effective interaction I changes the exciton number without any restriction. Therefore, in (4.6) the sum over m occurs. It displays the fact that starting at the initial single-particle state 1p different exciton states (2p1h, 3p2h, ...) can be excited by a single step (multi-doorway model). However, in nuclear physics it is quite reasonable to choose I as a two-body interaction which cannot change n by more than 2 ($\Delta n = n'-n = 2,0,-2$). Therefore we specify all damping and escape widths (4.4) henceforth by the superscripts (+), (0), and (-). However, the damping widths $\Gamma_n^{(0)}\downarrow$ do not occure because they cancel in (4.7) automatically.

The two-body assumption simplifies the SMC model (4.6) essentially. Thus the dynamical matrix $A_{nn'}$ becomes three-diagonal. Otherwise, the sum over m disappear, and the multi-doorway model reduces /5/ to an 1-entrance doorway model with the initial exciton number $m = n_o$.

Mathematically, the two-body assumption is connected with a transition from GOE to a Two-Body Random Ensemble (as a special case of an Embodded GOE) /22/. This transformation can be performed by a manipulation of the state densities ϱ_n adjoining $\overline{I^2}$ in (4.4). Intuitively, this problem was firstly solved by Williams /26/ who has introduced the density of accessible final states $\varrho_n^{(\Delta n)}$ for damping widths. The final state densities for escape widths are also obtained by combinatorical methods from appropriate diagrams /2,13/. This procedure contains the assumption that the two-body interaction is independend of exciton number, $\overline{I^2}(n,n') \equiv \overline{I^2}$.

The inverse of the three-diagonal dynamical matrix in (4.6) is easily solved by the iterative relation,

$$-\hbar\delta_{nn_o} = \Gamma_{n-2}^{(+)}\downarrow \tau_{n-2} + \Gamma_{n+2}^{(-)}\downarrow \tau_{n+2} - \Gamma_n\tau_n \tag{4.9}$$

where $\Gamma_n = \Gamma_n\downarrow + \Gamma_n\uparrow$ is the total width. Relation (4.9) which was obtained here by contraction technique is well-known as the time-integrated master equation. Mathematically, this can be understood from the definition of the mean life time

$$\tau_n = \int_0^\infty P_n(t)\,dt = (A^{-1})_{n_o n} \tag{4.10}$$

where the occupation probability $P_n(t)$ satisfies the Pauli mater equation

$$dP_n/dt = -\sum_m P_m A_{mn} \tag{4.11}$$

and the conditions $P_n(t=0) = \delta_{nn_o}$, and $P_n(t=\infty) = 0$.

Assuming, $\Gamma_n^{(-)}\downarrow \equiv 0$ (never-come back assumption) eq. (4.9) reduces immediately to the result of Feshbach e.a. /2/,

$$\tau_n = \frac{1}{\hbar\Gamma_n} \prod_{k=1}^{n-1} \left(\frac{\Gamma_k\downarrow}{\Gamma_k} \right) \tag{4.12}$$

where the value in round brackets is interpreted as depletion factor. But the never-come back assumption fails in the description of emissions from complex states $n > n_0$, especially at $n = \bar{n} \equiv (2gE)^{1/2}$, where $\Gamma_n^{(+)}\downarrow \simeq \Gamma_n^{(-)}\downarrow$ holds. Here, $g = A/13$ is the single-particle state density of the composite system (in MeV^{-1}). Thus, in contrast to the master-eq. approach, (4.10) together with (4.9), which describes both preequilibrium and equilibrium emission in an unified manner the approach (4.12) is applicable to preequilibrium emission only. In the last case, the compound-nucleus emission has to be calculated separately within an evaporation model or Hauser-Feshbach theory. This was done in /9,10/.

Returning to the SMC cross section the two-body assumption reduces (4.6) to the familiar form

$$\frac{d\sigma_{\alpha\beta}^{SMC}(\varepsilon)}{d\varepsilon'} = \sigma_\alpha^{SMC}(\varepsilon) \sum_{n=n_0}^{\bar{n}} \tau_n \left(\Gamma_{n\beta}^{(+)}(\varepsilon')\uparrow + \Gamma_{n\beta}^{(0)}(\varepsilon')\uparrow + \Gamma_{n\beta}^{(-)}(\varepsilon')\uparrow \right) / \hbar \tag{4.13}$$

where the absorption cross section (into bound configurations)

$$\sigma_\alpha^{SMC}(\varepsilon) \equiv \sum_{\beta=\pi,\nu} \int d\varepsilon' \frac{d\sigma_{\alpha\beta}^{SMC}(\varepsilon)}{d\varepsilon'} = \frac{2\pi V_N}{\hbar v_\alpha} \overline{I^2}\, \rho_{n=1}^{(+)} = \frac{V_N}{\hbar v_\alpha} \Gamma_{n=1}^{(+)}\downarrow \tag{4.14}$$

acts in (4.13) as a normalization constant.

If now the unbound/bound reduction (3.1) is used the SMC-model becomes free of matrix elements throughout. This is, because $\Gamma_{n\beta}(\varepsilon')\uparrow$, and τ_n^{-1} are both proportional to $\overline{I_b^2}$, and all $\overline{I_b^2}$ cancel exactly within the sum of (4.13). The only mean square matrix element that survives is that in (4.14) which defines the normalization constant. In this way the s h a p e of the SMC emission cross section becomes independent of $\overline{I^2}$.

For the sake of completeness we have to mention in which sense the SMC-model (4.13) differ from the phenomenological EM. The only difference lies in the definitions of escape widths. Within the EM the emission rates (for simplicity we ignore neutron/proton distinction)

$$W_n(\varepsilon') = \frac{2s+1}{\pi^2\hbar^3}\, m\varepsilon'\, \sigma^{inv}(\varepsilon')\, \frac{p(n-1)}{gE} \left(\frac{U}{E}\right)^{n-2} \tag{4.15}$$

are obtained from Detailed Balance principle, and σ^{inv} is approximated by the OM reaction cross section. However, the phenomenological formula (4.15) can be derived immediately from $\Gamma_n^{(0)}(\varepsilon')\uparrow/h$ defined in (4.4b) if the final state density is taken from (5.16) of refs. /2/, and if we use the straight-forward definition

$$\sigma^{inv}(\varepsilon') \equiv (4\pi^3/k'^2)\, \overline{I^2}(n,n'\varepsilon')\, \rho_n^{(0)} \qquad \text{for} \quad n=n'. \tag{4.16}$$

In (4.16) the final state density for $\Delta n = 0$ transitions /27/

$$\rho_n^{(0)} = g(gE)\left\{ p(p-1) + 4ph + h(h-1) \right\} / (2n) \tag{4.17}$$

should be used.

In summary, it has been shown that in contrast to the SMC-model (4.13) the EM contains the escape width for $\Delta n = 0$ transition only, i.e., $\Gamma^{(+)}_{n\beta}(\varepsilon')\uparrow = 0 = \Gamma^{(-)}_{n\beta}(\varepsilon')\uparrow$. Furthermore, since in EM the entire inverse cross section (4.16) rather than $I^2(n,n'\varepsilon')$ enters the emission rates the matrix elements cannot cancel within the EM.

5. SMD-processes

Originally, the random-matrix approach /1,5/ was formulated as a pure SMC theory. But there are several different attempts to include afterwards direct reactions into this approach:

i) The S-matrix in the presence of direct reactions is reduced to the one without direct reactions by an unitary Engelbrecht-Weidenmüller transformation U, so that all informations on the direct reactions are contained in U /28,29/.

ii) First of all, the statistical assumptions (2.3) are introduced within the leading-particle concept /24/ formulated for description of angular distributions in fast processes.

iii) After discretization of the continuum by a Hernandez-Montragon transformation /30/ direct interactions are replaced by interactions between resonant states. These are incorporated into a Generalized random-matrix model /21/ for both SMC and SMD processes based on GOE and GUE. The obtained model which is the microscopical counterpart of the phenomenological EM can be applied for excitation energies below 20 MeV only.

Besides the above approaches we present now a rigorous derivation within the essential framework of random matrices (GUE). Starting at (1.7), and using the statistical assumptions (2.3) the SMD cross section in (1.10) splits into a sum over s-step contributions

$$G^{SMD}_{if} = \frac{4\pi^3}{k^2} \sum_{s=0} \left(I_u G_u \right)^s I_{(\pm)} \; I^*_{(\pm)} \sum_{t=0} \left(G^*_u I^*_u \right)^t = \sum_{s=1} G^{(s)}_{if} \tag{5.1}$$

Here we ignore all internal contractions, i.e., in contrast to the SMC-case (4.2) we have $\tilde{G}_u = G_u$. It leads to the propagator contraction

$$\overline{G_u \; G_u^*} \equiv \sum_{\varrho} (G_u \; G_u^*)_{n\varrho c, n\varrho c} = 2\pi^2 \varrho_{n\gamma}(U) \tag{5.2}$$

which differ essentially from (4.8). In (5.1) we have to distinguish between two kinds of unbound matrix elements, where $I_u \equiv \langle - | I | - \rangle$ is defined between outgoing waves $\tilde{\rho}^{(-)}$, and otherwise $I_{(\pm)} \equiv \langle - | I | + \rangle$ is defined between one incomming and one outgoing wave. But following Feshbach /31/ we take

$$\overline{I_{(\pm)} \; I^*_{(\pm)}} \simeq \overline{I_u \; I^*_u} \equiv \overline{I^2_u}. \tag{5.3}$$

After performing all (first-order) cross-contractions in (5.1) we obtain for the single-, and s-step contribution

$$\frac{d^2 \sigma^{(1)}_{\alpha\beta}(\varepsilon)}{d\varepsilon' d\Omega'} = \frac{4\pi^3}{k^2} \; \frac{1}{2\pi^2} \; W^{(1)}_{\alpha\beta}(\varepsilon, \varepsilon'\Omega') \tag{5.4a}$$

$$\frac{d^2\sigma^{(s)}_{\alpha\beta}(\varepsilon)}{d\varepsilon' d\Omega'} = \frac{4\pi^3}{k^2}\frac{1}{2\pi^2}\sum_{\gamma_1\cdots\gamma_{s-1}}\int d\varepsilon_1 d\Omega_1 d\varepsilon_2 d\Omega_2 \cdots d\varepsilon_{s-1} d\Omega_{s-1} W^{(1)}_{\alpha\gamma_1}(\varepsilon,\varepsilon_1,\Omega_1) W^{(2)}_{\gamma_1\gamma_2}(\varepsilon_1,\Omega_1,\varepsilon_2,\Omega_2)\cdots W^{(s)}_{\gamma_{s-1}\beta}(\varepsilon_{s-1},\Omega_{s-1},\varepsilon',\Omega') \quad (5.4b)$$

with the transition probability (for particle-hole excitations)

$$W^{(s)}_{\alpha\beta}(\varepsilon\Omega,\varepsilon'\Omega') = 2\pi^2\,\overline{I_u^2}(\varepsilon\Omega\alpha,\varepsilon'\Omega'\beta)\,\rho^{(+)}_{n\beta}(U) \quad (5.5)$$

where n = 2s+1. For the mean square matrix element the parametrization (3.2) and (3.4) should be used. Expressions (5.4) were obtained already by Feshbach e.a. /2/ by different methods. Notice, that the definitions of the transition probability (5.5) differ from that in /2/ by a factor $\rho(\varepsilon)\rho(\varepsilon')/4\pi$, and from that in /13/ by a factor $\rho(\varepsilon)/4\pi$.

The excitation of collective modes can be introduced easily into this concept by replacing the particle-hole matrix element by a simple ansatz,

$$I_u \longrightarrow I_u + I_{vib} + I_{rot} \quad (5.6)$$

where I_{vib} and I_{rot} describe the excitation of vibrations (phonons) and rotations. Assuming statistical independence between all different types of matrix elements ($\overline{I_u I_{vib}} \equiv 0$, etc.) the transition probability (5.5) splits into three components,

$$W^{(s)}_{\alpha\beta} = W^{(s)\,ex}_{\alpha\beta} + W^{(s)\,vib}_{\alpha\beta} + W^{(s)\,rot}_{\alpha\beta}\,. \quad (5.7)$$

Here, the label (ex) denotes the non-collective particle-hole (exciton) transition probability.

For the angular distributions we obtain from (3.4) together with the oversimplified assumption that $\mu_L(\varepsilon,\varepsilon')$ is independent of both ε and ε' a simple expression for each s-step process

$$\frac{d^2\sigma^{(s)}_{\alpha\beta}(\varepsilon)}{d\varepsilon'\,d\Omega'} = \frac{1}{4\pi}\frac{d\sigma^{(s)}_{\alpha\beta}(\varepsilon)}{d\varepsilon'}\sum_L (2L+1)\,\mu_L^s\,P_L(\cos\theta'). \quad (5.8)$$

6. SMD/SMC-model

The aim of this Sect. is to connect the obtained SMC and SMD results according to (1.10) into a simple model available for numerical calculations in the incidence energy region between 5 and 30 MeV. For this reason our model bases on the assumption that the single-step and two-step contributions are of pure direct type (5.4), whereas all next following steps (beginning at exciton number n_o = 5) are pure SMC-processes (4.13). The double-differential x-section will be written as

$$\frac{d^2\sigma_{\alpha\beta}(\varepsilon)}{d\varepsilon'\,d\Omega'} = \frac{1}{4\pi}\left[\frac{d\sigma^{SMD}_{\alpha\beta}(\varepsilon)}{d\varepsilon'}\sum_L (2L+1)\,a_L(\varepsilon')P_L(\cos\theta') + \frac{d\sigma^{SMC}_{\alpha\beta}(\varepsilon)}{d\varepsilon'}\right] \quad (6.1)$$

In (6.1) the angular distribution of the SMC-emission is assumed to be isotropic while for the SMD-processes the empirical systematics of Kalbach and Mann /32/ rather than (5.9) is used.

The SMC x-section in (6.1) is defined by (4.13) and (4.9). For the appropriate final state densities of escape and damping widths (4.4) we refer to /13/. The normalization constant in (4.13) is chosen as

$$\sigma_\alpha^{SMC}(\varepsilon) = \sigma_\alpha(\varepsilon) - \sum_{\beta=\nu,\pi} \sigma_{\alpha\beta}^{SMD}(\varepsilon) \tag{6.2}$$

where σ_α is the optical model reaction cross section (Wilmore-Hodgson for neutrons, and Becchetti-Greenlees for protons).

Within the SMD-description we restrict ourselves to the excitation of non-collective particle-hole states and surface vibrations, i.e., the first two terms in (5.6). For the explicit expressions of the (angle-integrated) transition probability (5.5) we take the ansatz

$$W_{\alpha\beta}^{ex}(\varepsilon,\varepsilon') = 2\pi^2(2s+1)\, R_{\alpha\beta}\, P_\alpha(\varepsilon) P_\beta(\varepsilon')\, \overline{I^2}\, \rho(\varepsilon)\rho(\varepsilon')\, (g/2)^2 (\varepsilon-\varepsilon'+B_\alpha-B_\beta) \tag{6.3}$$

$$W_{\alpha\beta}^{vib}(\varepsilon,\varepsilon') = 2\pi^2\, \delta_{\alpha\beta}\, P_\alpha(\varepsilon) P_\beta(\varepsilon') \sum_\lambda \overline{I_\lambda^2}\, \rho(\varepsilon)\rho(\varepsilon')\, \delta(\varepsilon-\varepsilon'-\omega_\lambda). \tag{6.4}$$

The label (s) on $W_{\alpha\beta}^{(s)}$ is omitted in (6.3) and (6.4) since we assume an adiabatic behaviour of the target nucleus in which the excited particle-hole pair or phonon does not influence (the final state density of) the next following collision. Through the combinatorical factor /13/

$$R_{\alpha\beta} = \delta_{\alpha\beta} + (1 - \delta_{\alpha\beta})\,(N\delta_{\beta\nu} + Z\delta_{\beta\pi})/A \tag{6.5}$$

in (6.3) the statistical weight of the creation of particle-hole pairs of neutrons and protons as well as exchange processes (non-diagonal part) is considered. A,N,Z refer to the mass, neutron, and proton number of the target nucleus. After inserting (6.3) in (5.4a) we obtain, for example, for the (neutron inelastic) single-step process the familiar form

$$\frac{d\sigma^{(1)}(\varepsilon)}{d\varepsilon'} = \left(\frac{m V_N}{2\pi\hbar^2}\right)^2 4\pi\,(2s+1)\,\overline{I^2}\left(\frac{g}{2}\right)^2(\varepsilon-\varepsilon')\sqrt{\frac{\varepsilon'}{\varepsilon}} \tag{6.6}$$

The exact value of $\overline{I^2}$ in (6.3) and (6.6) will be estimated below.

Expression (6.4) describes the excitation of phonons of multi-polarity λ at energy ω_λ, and with deformation parameter β_λ. For the mean square matrix element $\overline{I^2}$ the simple ansatz /33/

$$\overline{I_\lambda^2} = (3a/R)^2\, \beta_\lambda^2\, V_o^2\, /(16\pi) \tag{6.7}$$

is done, where $V_o = (52 - 0.3\varepsilon)$ MeV is the (OM) real well depth of the nucleus. The square of $(3a/R) \simeq V_{surf}/V_N$ in (6.7) is introduced since we restrict ourselves to processes

which take place on the nuclear surface (surface vibrations). In this way V_N which enter both $\varrho(\varepsilon)$ and $\varrho(\varepsilon')$ in (6.4) will be replaced by $V_{surf} \simeq 4\pi a R^2$, where a = 0.65 is the diffusness parameter, and $R = 1.2\ A^{1/3}$ fm. In contrast to the particle-hole excitation (6.3) there is no spin factor (2s+1) in (6.4). It is dropped since in phonon excitations spin-flip processes are negligible /33/.

Besides the parameters β_λ and ω_λ which can be taken from nuclear data tables /33,34/ the phonon-excitation ansatz (6.4) is parameter-free. It differ from the oversimplified assumption in /13/ where $\overline{I_\lambda^2} \propto \varkappa \overline{I^2}$, and $\varkappa \gg 1$.

There remains now the important question of how to determine the precise value of $\overline{I^2}$ which enters (6.3). This will be done starting from the known OM reaction cross-section (for neutrons) which can be decomposed into a (energy-integrated) single-step and one multistep component,

$$\sigma_\alpha(\varepsilon) = \sum_{\beta=\pi,\nu} \sigma_{\alpha\beta}^{(1)}(\varepsilon) + \sigma_\alpha^{(M)}(\varepsilon) . \tag{6.8}$$

The multistep contribution

$$\sigma_\alpha^{(M)}(\varepsilon) = \frac{2\pi V_N}{\hbar v} \left(\frac{A + Z\delta_{\alpha\nu} + N\delta_{\alpha\pi}}{2A} \right) \overline{I^2} \left(\frac{g}{2}\right)^3 \frac{E^2}{2} \tag{6.9}$$

includes all processes in which the ingoing particle produces a composite system that decay by further collisions into more complex states. Ignoring unbound/bound restrictions in the final state density all multistep processes (without SMD/SMC-distinction) are considered in (6.9) immediately. Using (6.8) and (6.9) we obtain the value of $\overline{I^2}$ from the OM reaction cross-section. In solving this problem it turns out that $\overline{I^2}$ depends on incidence energy and can fairly be approximated by

$$\overline{I^2} = \overline{I^2}(\varepsilon) \simeq 1800\ A^{-3}\ \varepsilon^{-1} \qquad \text{for} \qquad A \lesssim 100 , \tag{6.10}$$

and $\varepsilon \gtrsim 5$ MeV. Formally, it looks very similar to the Kalbach-Cline parametrization /35/, however, in (6.10) there is an incidence-energy dependence rather than a dependence on excitation energy E. Even the parametrization (6.10) provides to obtain simple analytical expressions for the direct two-step processes similar to those given in Appendix B of /13/.

7. Results and Summary

Calculations of (n,n') and (n,p) emission spectra within the SMD/SMC-model (code EXIFON /36/) were performed for four nuclides at different incidence energies ε. The following input data are used:

	B_ν/MeV	B_π/MeV	ω_2/MeV	β_2	ω_3/MeV	β_3
52 - Cr	7.80	11.04	1.42	0.22	4.60	0.18
56 - Fe	7.64	9.09	0.85	0.24	4.52	0.18
65 - Cu	6.95	8.37	1.35	0.18	3.70	0.16
93 - Nb	7.26	6.57	0.93	0.10	2.30	0.13

The binding energies are taken from /37/ (linear -shell-term formula). In the calculations we have restricted ourselves to the lowest 2^+, and 3^- phonon excitations only. The values ω_2, β_2 are taken from /34/, while ω_3 is taken from the systematic given in /33/.

The β_3-parameter was approximated by $(0.007\omega_3)^{1/2}$. All delta functions in (6.4) are replaced by Gaussians of width 1 MeV for $\varepsilon \lesssim 20$ MeV, and 2 MeV for $\varepsilon = 25.7$ MeV. In using $g = A/13$ we ignore shell- and pairing-effects till now. Finally, we use $r_0 = 1.2$ fm in (3.3).

Results are depicted in Fgs. 1. to 9. The meaning of the curves: SMC-contribution (dotted line), SMD-contribution (dashed - dotted line), the sum of SMC and SMD (full line). Further, the individual single- and two-step contributions (broken lines) are denoted by the appropriate label.
At $\varepsilon = 14$ MeV the discrepancy in the low energy part is due-to the neglection of (n,2n)-processes in our calculations. For $\varepsilon = 25.7$ MeV also the Legendre-coefficients of the double-differential cross-section $f_L(\varepsilon,\varepsilon') = \{d_\sigma^{SMD}(\varepsilon)/d\varepsilon')/(d\sigma(\varepsilon)/d\varepsilon')\}a_L(\varepsilon')$ are shown. Finally, for 93-Nb also (n,p) energy- and angular distributions are depicted for $\varepsilon = 14$ MeV. Experimental data are taken from /38-42/.

The incidence energy dependence of SMC and SMD processes, as well as the individual SMD-contributions (in mb) are summarized in the following table for 93-Nb.

ε/MeV	σ_ν	SMC	SMD	(ex)	(vib)	(exex)	(exvib)	(vibex)	(vibvib)	(vibvibvib)	$\sigma_{\nu\pi}$
5.2	2037	1861	176	68.0	104	0.5	0.7	1.3	1.2	0.0	0.4
14.0	1781	1410	335	184	112	9.1	7.9	15.7	5.9	0.2	36
25.7	1536	828	568	338	86.3	56.5	24.9	53.3	8.7	0.5	139

As we see, particle-hole excitation rises with increasing energy whereas the phonon-contribution is almost incidence energy independent. The direct three-phonon excitation which was also included in the calculations turns out to be negligible, and can thus be neglected.

In summary, the predicted SMD/SMC-model which was obtained from first principles is successful in reproducing of experimental data. Despite the fact that it includes besides the SMC-processes also the multistep direct excitation of non-collective and collective modes this model is extraordinary simple (computing time of micro-computer: a few seconds).

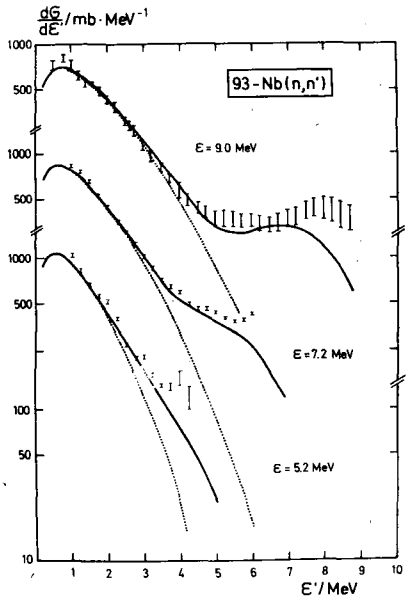

Fig. 1.

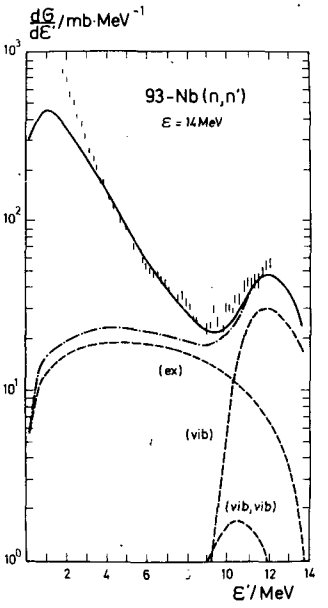

Fig. 2.

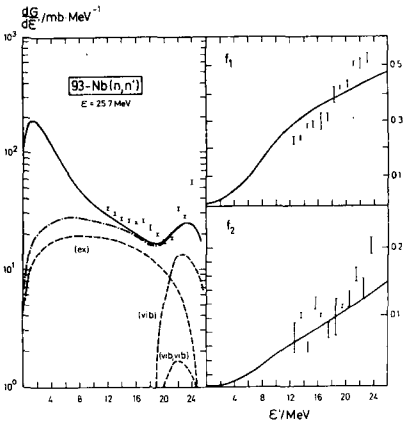

Fig. 3.

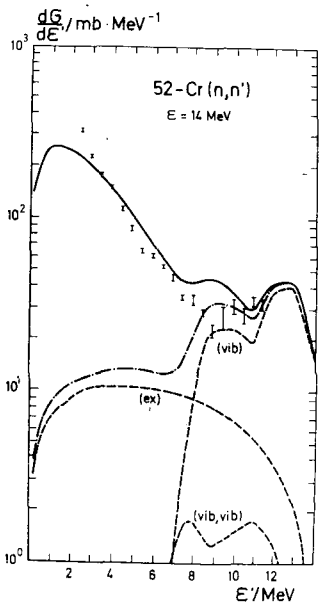

Fig. 4.

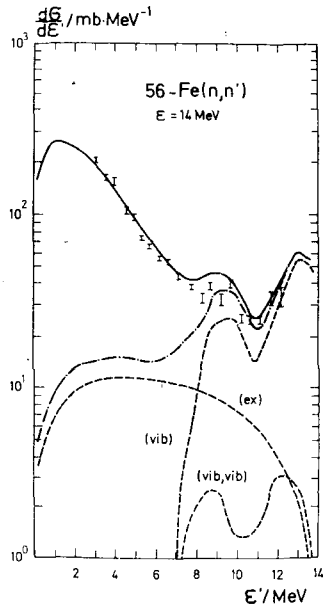

Fig. 5.

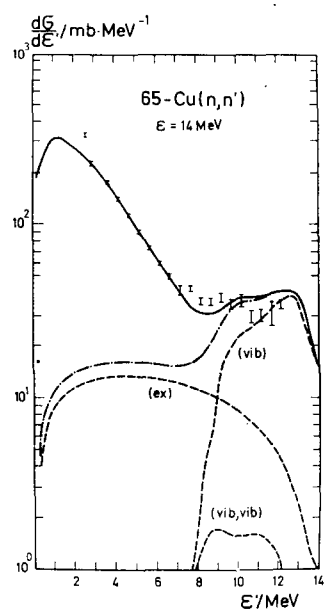

Fig. 6.

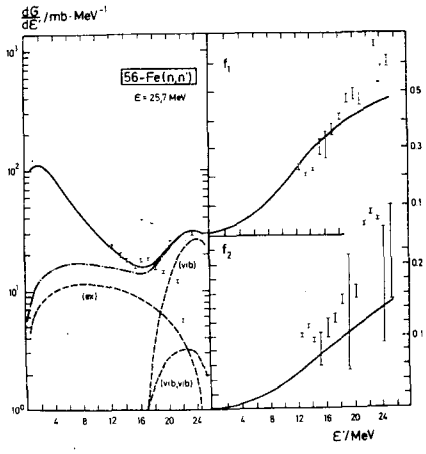

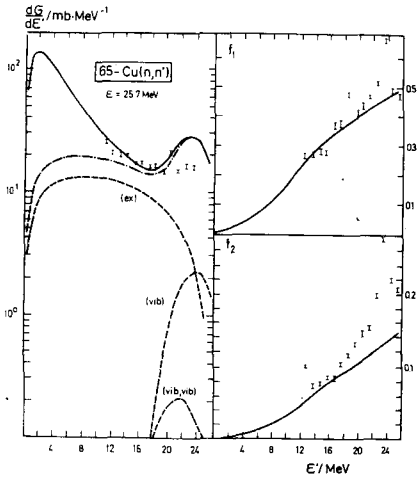

Fig. 7.

Fig. 8.

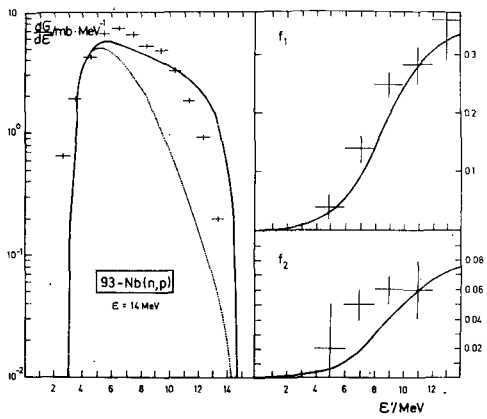

Fig. 9.

APPENDIX

In order to familiarize the reader with the unbound/bound transformations (3.1), (3.2) we look, for example, at the (angle-integrated) bound-unbound interaction

$$\overline{I^2}(n,n'\varepsilon') \equiv \int d\Omega' \, \overline{I^2}(n,n'\varepsilon'\Omega') = \sum_{l} (2l+1) \, \overline{I^2}(n,n'\varepsilon' l) \tag{A.1}$$

Consider now the single-particle (radial) wave function of the unbound state in $\overline{I^2}(n,n'\varepsilon' l)$, which has the form (for $kR > 1$) /43/

$$\varphi_l(\varepsilon') = \vartheta_l^{1/2}(\varepsilon') \, u_l(r) \qquad\qquad \vartheta_l \simeq (R/\pi)/(\hbar v) \tag{A.2}$$

inside the nucleus ($r \lesssim R$), whereas the smooth energy-dependent part $u_l(r)$ of type sin (kr) is normalized to unity. If we take $\Sigma(2l+1) \simeq 2(kR)^2/3$ we obtain immediately from (A1) and (A2) the final result (3.1). A similar explanation is presented in /3/.

References

/ 1/ Agassi, D., Weidenmüller, H.A., Mantzouranis, G.: Phys. Rep. 22C, 145 (1975)
/ 2/ Feshbach, H., Kerman, A., Koonin, S.: Ann. Phys. 125, 429 (1980)
/ 3/ Zhivopistsev, F.A., Sukharevsky, V.G.: Phys.Elem. Particle and Nucl., Dubna, 15, 1208 (1984)
/ 4/ Sadhan K. Adhikari: Phys. Rev. C31, 1220 (1985)
/ 5/ McVoy, K.W., Tang,X.T.: Phys. Rep. 94, 139 (1983)
/ 6/ Mädler, P., Reif, R.: Nucl. Phys. A373, 27 (1982)
/ 7/ Tamura, T., Udagawa, T., Lenske, H.: Phys. Rev. C26, 379 (1982)
/ 8/ Reif, R.: Acta Phys. Slovaca 25, 208 (1975)
/ 9/ Herman, M., Marcinkowski, A., Stankiewicz, K.: Nucl. Phys. A430, 69 (1984)
/10/ Field, G.M., Bonetti, R., Hodgson, P.E.: J. Phys. G12, 93 (1986)
/11/ Bonetti, R., Camnasio, M., Colli-Milazzo, L., Hodgson, P.E.: Phys. Rev. C24, 71 (1981)
/12/ Marcinkowski, A.: Proc. IAEA Advisory Group Meeting on Nuclear Theory for Fast Neutron Nuclear Data Evaluation, Beijing, 1987, in print
/13/ Kalka, H., Zhivopistsev, F.A., Seeliger, D.: will be published in Z. Phys. A
/14/ Griffin, J.J.: Phys. Rev. Lett.17, 478 (1966); Phys. Lett. 24B, 5 (1967)
/15/ Seidel, K., Seeliger, D., Reif, R., Toneev, V.D.: Phys. Elem. Particle and Nucl., Dubna, 7, 499 (1976)
/16/ Blann, M.: Ann. Rev. Nucl. Sci. 25, 123 (1975)
/17/ Migdal, A.B.: Theory of Finite Fermi Systems and Applications to Nuclei Wiley Interscience, New York (1967)
/18/ Abrikosov, A.A., Gorkov, L.P., Dzyaloshinski, I.E.: Methods of Quantum Theory in Statistical Physics. Prentice Hall (1963)
/19/ Kawai, M., Kerman, A.K., McVoy, K.W.: Ann. Phys. 75, 126 (1973)
/20/ Verbaarschot, J., Weidenmüller, H.A., Zirnbauer, M.R.: Phys. Rep. 129, 367 (1985)
/21/ Kalka, H.: thesis, TU Dresden (1986)
/22/ Brody, T.A., Flores, J., French, J.B., Mello, P.A., Pandey, A., Wong, S.S.W.: Rev. Mod. Phys. 53, 385 (1981)
/23/ Weidenmüller, H.A.: MPI - V10, Heidelberg (1985)
/24/ Mantzouranis, G., Agassi, D., Weidenmüller, H.A.: Phys. Lett. 57B, 220 (1975)
/25/ Akkermans, J.M., Gruppelaar, H.: Z. Phys. A300, 345 (1981)
/26/ Williams Jr., F.C.: Phys. Lett. 31B, 194 (1970)
/27/ Oblozinsky, P., Ribansky, I., Betak, E.: Nucl. Phys. A226, 347 (1974)

/28/ Engelbrecht, C.A., Weidenmüller, H.A.: Phys. Rev. C8, 859 (1973)
/29/ Nishioka, H., Weidenmüller, H.A.: Phys. Lett. 157B, 101 (1985)
/30/ Hernandez, E., Mondragon, A.: Phys. Rev. C29, 722 (1984)
/31/ Feshbach, H.: Ann. Phys. 159, 150 (1985)
/32/ Kalbach, C., Mann, F.M.: Phys. Rev. C23, 112 (1981)
/33/ Bohr, A., Mottelson, B.R.: Nuclear Structure, Vol II. Benjamin, New York (1975)
/34/ Raman, S., Malarkey, C.H., Milner, W.T., Nestor, C.W., Stelson, P.H.: At. Data and Nucl. Data Tabl., 36, 1 (1987)
/35/ Kalbach-Cline, C.: Nucl. Phys. A193, 417 (1972)
/36/ Kalka, H.: code EXIFON (1987), unpublished
/37/ Ando,Y., Uno, M., Yamada, M.: JAERI-M 83-025 (1983)
/38/ Takahashi, A., e.a.: OKTAVIAN report A 83-01 (1983)
/39/ Marcinkovski, A., e.a.: Nucl. Sci. and Eng. 83, 13 (1983)
/40/ Simakov, S.P., Lovchikova, G.N., Lunev, V.P., Salnikov, O.A., Titarenko, N.N.: Yad. Fiz. 37, 801 (1983)
/41/ Adel-Fawzy, M., Förtsch, H., Mittag, S., Schmidt, D., Seeliger, D., Streil, T.: EXFOR 32001, IAEA-NDS (1982)
/42/ Traxler, G., Chalupka, A., Fischer, R., Strohmaier, B., Uhl, M., Vonach, H.: Nucl. Sci. and Eng. 90, 174 (1985)
/43/ Lüders, G.: Zs.f.Naturforsch. 10a, 581 (1955)

Note added in proof:

The escape mode $\Gamma_{n\beta}^{(+)}(\varepsilon')\uparrow$ in (4.13) is energetically impossible and should be neglected in SMC-processes where all particles are in bound configurations. However, in additional calculations it was proved that even this mode has a small influence on the SMC-emission spectra for $n \geq 5$.

DOUBLE-DIFFERENTIAL NEUTRON EMISSION CROSS SECTIONS OF ^{238}U AT 14 MEV NEUTRON INCIDENCE ENERGY

T. Elfruth, T. Hehl, H. Kalka, H. Märten, M. Payrovan+, A. Ruben, D. Seeliger, K. Seidel and S. Unholzer
Technische Universität Dresden, Sektion Physik, Mommsenstr. 13, Dresden, DDR-8027, GDR

Abstract

Neutron emission cross sections have been measured with time-of-flight spectroscopy in a wide range of emission angles. The data obtained are compared with previous results.

The emission cross sections have been calculated without any parameter fit. Multiple chance fission, (n,inf) with i = 0,1,2, and (n,jn)-processes with j = 1,2,3 have been taken into account where in the pre-equilibrium stage of the compound system single-particle and collective excitations have been included.

1. Introduction

In fusion-fission hybrid reactor designs ^{238}U is a blanket component arranged at the plasma chamber wall for neutron multiplication, energy enhancement and plutonium breeding. Therefore, the cross sections of the total neutron production and of all partial processes at 14 MeV neutron incidence energy must be determined with high accuracy /1/. The investigation at 14 MeV is also of use for fission reactor data at other energies in the fast neutron range.

In experiments either the neutron emission is determined as sum of contributions from all open (n,xn)-reactions and from all fission channels or (if it is measured in coincidence with a fission chamber used as sample) as sum of fragment neutrons and pre-fission neutrons from all open fission channels. Theoretical calculations must be performed to decompose the measured data, where the energy and the angular distributions of the emitted neutrons can be used as information sources.

In the work presented, the double-differential cross sections of the total neutron emission are determined with the time-of-flight spectrometer at the pulsed neutron generator of TU Dresden. They are compared with data obtained by other groups /2-5/ and with the ENDF/B-IV evaluation.

In a second part of the work, the double-differential cross sections of all neutron producing reaction channels are calculated using statistical models of direct reactions, compound reactions and fission. The components are summed up and compared with the experimental results.

2. Measurement

The experimental arrangement is shown in Figs. 1 and 2. Ring geometry with flight path arranged at 90° to the deuteron beam direction is used, so that the average incidence neutron energy E_o is 14.1 - 14.2 MeV for all emission angles $15^o - \vartheta - 165^o$ (and symmetric to $\vartheta = 90^o$). The flight path is about 5 m. The neutron generator operated in a pulsed regime with deuteron pulses of 2 ns f.w.h.m. and 5 MHz repetition rate, produces $2 - 5 \times 10^9$ neutrons per s. The neutron production is determined by counting the α-particles.

The sample consisting of metallic uranium depleted in ^{235}U to 0.4 % has 8.0 cm inner diameter, 12.0 cm outer diameter and a thickness of 0.6 cm.

The neutron detector is a liquid scintillator NE 213 (12.7 cm Ø x 3.8 cm) coupled with a XP 2041 photomultiplier. It is biased at 2 MeV neutron energy. The neutron detection efficiency $\varepsilon(E)$ is determined by time-of-flight spectroscopy of neutrons scattered from H, of 14.1 MeV neutrons and of neutrons from a Cf-252 fission chamber. A Monte-Carlo code

+ from I.R. Iran, IAEA fellowship

is used to calculate $\varepsilon(E)$ too.

The microcomputer control of the spectrometer with free-programmable sample changing and shifting (ϑ) allows to subdivide the data acquisition in many short periods to inspect the data after each short-time run and to cover the chosen ϑ many times.

The data obtained are reduced to $\sigma_{nM}(E_o\ ;\ E,\vartheta)$ by

$$\sigma_{nM}(E_o;E,\vartheta) = \frac{N_n(t)/\Delta E \cdot \Delta\Omega_\alpha \cdot L^2 \cdot s^2 \cdot f_1(\vartheta)}{N_\alpha \cdot Z_N \cdot F_D \cdot \varepsilon(E)}$$

where $N_n(t)$ is the neutron time-of-flight spectrum corrected for background, dead time and differential non-linearity; N_α are the α-counts; $\Delta\Omega_\alpha$ is the solid angle of α-counting; f_1 is the number of α-particles/sr counted per 14 MeV neutrons/sr striking on the sample; s is the distance tritium target/sample; L is the distance sample/neutron detector; F_D is the neutron detector front-area; Z_N is the number of uranium nuclei in the sample; $\varepsilon(E)$ is the neutron detector efficiency.

More details of the date acquisition and reduction procedure can be found in Ref. /6/. The cross sections transformed into the center-of-mass system and integrated over ϑ are shown in Fig. 3. The error bars represent only the statistical uncertainties. The systematic uncertainty of the quantities in equ. (1) is altogether 10 % to 15 % /6/; but the σ_{nM} must be corrected for finite sample size yet.

The comparison of the $\sigma_{nM}(E)$ available in the literature, shows a spread larger than the required accuracy. The ENDF/B-IV evaluation underestimates at least the emission of high-energy neutrons. The angular distributions are in ENDF/B-IV assumed to be isotropic, with exception of those for the four pseudolevels. But, also in the middle-energy range they are forward-peaked as shown in Fig. 6 for E = 5.5 and 7.5 MeV and in Ref. /3,5/.

3. Calculation

The neutron producing reaction channels open at 14 MeV neutron incidence energy are shown in Fig. 4. At each stage of a compound-system cascade connected by neutron emission (n_j), the neutron emission competes with fission leading to fragment neutron evaporation (n_f), and with γ-deexcitation. The $\sigma_{n_j}(E,\vartheta)$ determines all following neutron emissions $\sigma_{n_{j+1}}$, ... and the number of fission events in the channels f_j, f_{j+1}, ... Contributions to n_1 arise not only from compound nucleus emissions but also from direct and other pre-compound processes. Therefore, especially the n_1-emission should be treated carefully.

The SMD/SMC model /7/ used to calculate the $\sigma_{n_j}(E,\vartheta)$, has the advantage that in the statistical multistep direct processes (MSD) besides particle-hole excitation (excitons) also direct collective vibrations (phonons) are included in a consistent way. The contribution of direct scattering from the ground-state rotational band is separately taken into account using a calculation of Lunev /8/. The statistical multistep compound (SMC) emission is calculated by solving the master equation for pre-compound and compound nucleus stages beginning with n = 5 exciton states.

The cross sections of the three fission channels are calculated by Maslov /9/ using double-humped fission barriers. The value obtained for $\sigma_{n,f} + \sigma_{n,n'f} + \sigma_{n,2nf}$, is in agreement with recent experimental data and is 5 % smaller than that of ENDF/B-IV.

The energy and angular distributions of the fission neutrons $\tilde{\nu}_{f_j}(E,\vartheta)$ are calculated with the GMNM-code /10/ that starts with neutron evaporation spectra (Maxwellian) in the system of the accelerated fragments which are assumed to be spheroids. The $(\tilde{\nu}_{n,f} + \tilde{\nu}_{n,n'f} + \tilde{\nu}_{n,2nf})$-value is as in ENDF/B-IV.

The sum of all neutron producing components is compared in Fig. 5 with experimental data of angle-integrated emission cross sections.

The altogether relatively good description of the E-dependence shows that the main reaction mechanism are met. The deviation for E ≥ 10 MeV may be caused by both experimental and calculation inaccuracies.

The angular distributions in the middle-energy range of the spectrum presented in

Fig. 6, demonstrate that the forward-peaking is determined by the n_1-emission whereas n_f are symmetrically to $\vartheta = 90^o$ (nearly isotropic) emitted. The ratio of these components seems also to be met by the calculations.

References

/ 1/ World Request List for Nuclear Data, INDC(SEC)-88/URSF, IAEA Vienna, 1983
/ 2/ J. Voignier et al., CEA-3503 (1968)
/ 3/ J.L. Kammerdiener, UCRL-51232 (1972)
/ 4/ A.P. Degtyarev et al., Yad. Fizika 34 (1981) 299
/ 5/ Shen Guanren et al., AGM on Nuclear Theory for Applications, Beijing, 1987
/ 6/ T. Elfruth et al., INDC(GDR)-044/GI, Vienna, 1986
/ 7/ H. Kalka, XVII. Int. Symp. on Nuclear Physics, Gaussig, 1987
/ 8/ V.P. Lunev, private communication, 1987
/ 9/ V.M. Maslov, private communication, 1987
/10/ H. Märten et al., Int. Conf. on Neutron Physics, Kiev, 1987

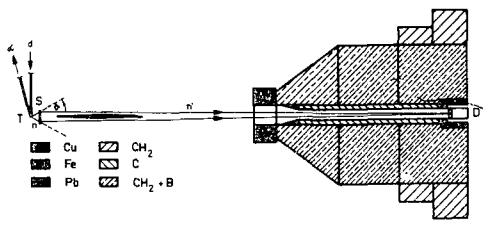

Fig. 1 Geometrical arrangement of the time-of-flight spectrometer.
T, tritium target; S, ring sample; D. neutron detector

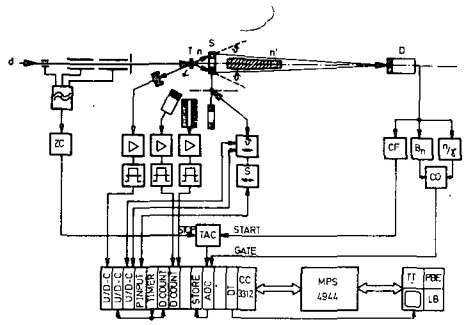

Fig. 2 Block scheme of the spectrometer.
ZC, zero-crossing trigger; CF, constant-fraction trigger; B_n, proton-recoil-energy discriminator; n/γ, neutron-gamma discriminator; CO, coincidence; ϑ ↔, sample shifter; S ↔ sample changer; TAC, time-to-amplitude converter; U/D-C, up-and-down counter; ADC, analog-to-digital converter; CC, controller of the CAMAC crate; MPS, microcomputer

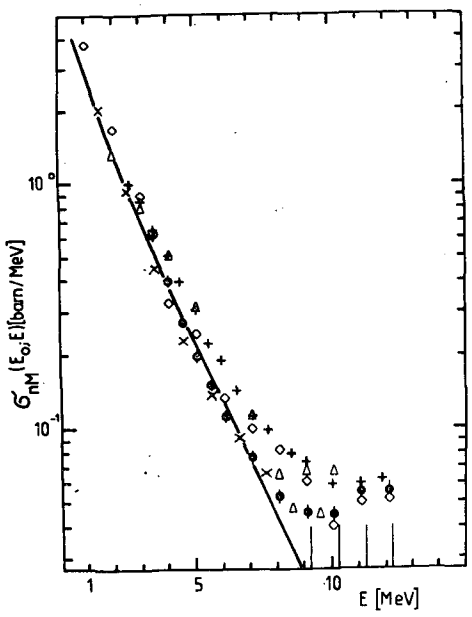

Fig. 3 Angle-integrated neutron emission cross sections of ^{238}U at E_o = 14.15 MeV.
ϕ, present work; x /2/, ◇ /3/, Δ /4/, + /5/;
——, ENDF/B-IV

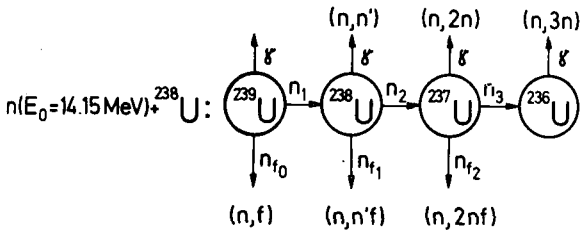

Fig. 4 Neutron producing reaction channels of ^{238}U bombarded with 14.15 MeV neutrons

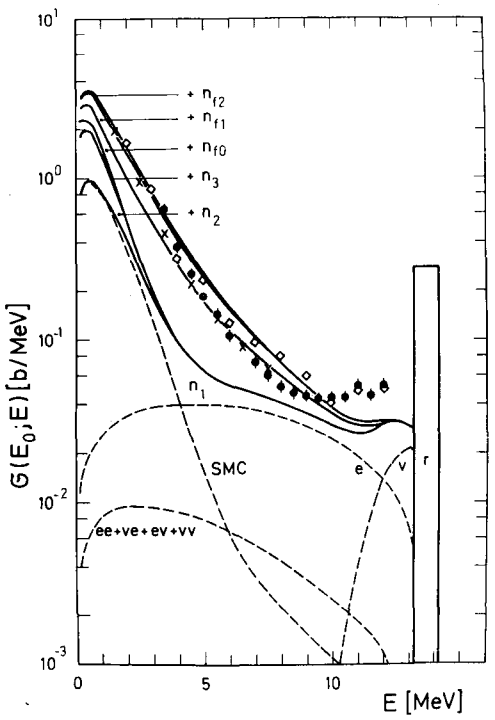

Fig. 5 Energy-differential neutron emission cross section calculated as sum of the components indicated in Fig. 4 (——), and compared with experimental data (x /2/, ◊ /3/; ♦, present work). The n_1-emission consists of (---) one-step direct scattering from rotational states (r) with excitation of vibrations (v) and with excitation of 1 particle- 1 hole states (e), of two-step direct scattering (ee + ve + ev + vv) and of statistical compound emissions (SMC) in the pre-compound and in the compound nucleus stage.

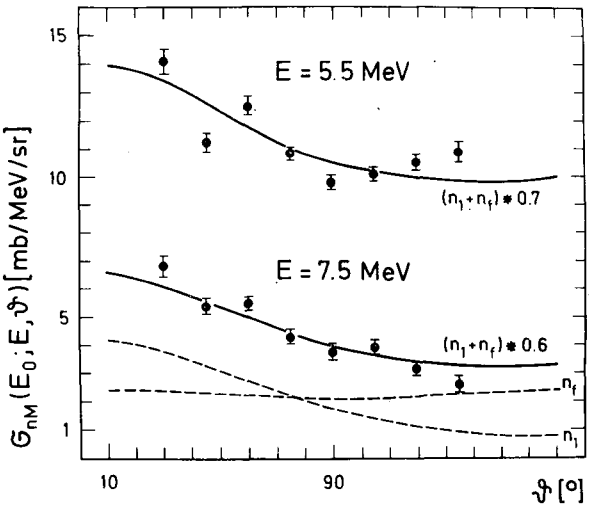

Fig. 6 Double-differential neutron emission cross sections at emission energies 5.5 MeV and 7.5 MeV calculated (——) as sum of the n_1 emissions (---) and all fragment neutrons ($n_{f_0} + n_{f_1} + n_{f_2} = n_f$, ---), and compared with the experimental data of the present work. To discuss the relative angular distributions, the calculated values are adapted to the experimental by the factors inserted.

A SEMIEMPIRICAL DESCRIPTION OF DOUBLE-DIFFERENTIAL NEUTRON EMISSION SPECTRA FOR 93-NIOBIUM

M. Torjman, H. Kalka, D. Hermsdorf, D. Seeliger
Technische Universität Dresden, Sektion Physik, Mommsenstr. 13, Dresden, DDR-8027, German Democratic Republic

Abstract

A simple procedure of semiempirical parametrization of the direct contributions in double-differential neutron emission cross sections is proposed. For the case ^{93}Nb + n in the broad incidence energy range from 5 MeV to 26 MeV this ansatz is proved. In addition to spectra calculations with the exciton model it provides a satisfactory description of the experimental behaviour in the full neutron incidence and emission energy range including angular distributions.

1. Introduction

The knowledge of accurate double-differential neutron emission cross sections in the whole incidence energy range up to 20 MeV is of crucial interest for fusion reactor blanket and shielding calculations /1/.
Theoretical predictions are needed, especially, to fill the gap of experimental data on double-differential neutron emission cross sections in the incidence energy range between 7 MeV and 14 MeV. One of the few cases, for which experimental double-differential neutron emission cross sections are available in the whole energy range, is ^{93}Nb+n.

Therefore, this case is a very suitable one for testing the applicability of different models and computer programmes along the energy scale /2, 3/. In this way, the most suitable theoretical approaches could be selected for the calculation of the main body of missing information on double-differential neutron emission cross sections. The present paper is one attempt in this direction mainly aiming a simple theoretical description of the highest part of emission spectra suitable for date evaluation

2. Exciton Model Calculation

During the last 20 years the exciton model and its later modifications was widely and succesfully used for calculations of neutron emission spectra /4-7/.

However, this simple statistical multistep reaction model does not describe single-step direct excitations of noncollective and especially of collective modes which are responsible for the highest part of experimental neutron emission spectra (It is well-known for many years, that the direct collective excitation of low-lying states by inelastic scattering of neutrons occurs with high probability).
An empirical ansatz for the average description of the direct part (DI) in the double-differential neutron emission cross sections is presented in sec. 3 which has to be added to the emission spectra calculated by the exciton model (EM), where the assumption is made, that the anisotropy of angular distributions is due-to the direct excitation only:

$$\frac{d^2\sigma(\varepsilon)}{d\varepsilon' d\Omega} = \frac{1}{4\pi}\left[\frac{d\sigma^{DI}(\varepsilon)}{d\varepsilon'}\sum_L (2L+1)\, a_L(\varepsilon')\, P_L(\cos\theta) + \frac{d\sigma^{EM}(\varepsilon)}{d\varepsilon'}\right] \qquad (1)$$

The expansion coefficients $a_L(\varepsilon')$ are taken from the Kalbach-Mann Systematics /8/.

The emission spectra of the exciton model

$$\frac{d\sigma^{EM}(\varepsilon)}{d\varepsilon'} = \sigma_{abs}(\varepsilon) \sum_{n=3}^{\bar{n}} \tau_n W_n(\varepsilon') \tag{2}$$

is calculated without fitting parameters by means of the code AMAPRE /9/. The life time τ_n is taken from (up to $t = \infty$) time integrated master equations including in this way also the compound nucleus neutron emission. For the emission rates $w_n(\varepsilon')$ from n-exciton states the well-known formula basing on the detailed balance principle is used. The transition rates λ_n^+ and λ_n^- which occur in the master equation are calculated by the Golden Rule using final state densities of Oblozinsky e.a. /10/.

The mean square matrix element is estimated from the imaginary part of the optical model. Nuclear structure influence (shell and pairing effects) on the exciton state density are taken into-account following /11,12/.
Further details of the exciton model calculations are reported elsewhere /9,13/.
As yet, calculations with the code AMAPRE do not include the emission of secondary neutrons. However, for investigations of the high-energy part of the spectra this is not necessary. The results of this calculations are shown by dotted lines in Fig. 1 - 3.

3. Parametrization of the direct Contribution

The usual way of calculating direct reaction contributions by DWBA or CC methods is well-known /14/. The task is more involved in the case of statistical multistep direct theory /15,16/. Special nuclear structure informations are needed in both cases for practical calculations which are usually both difficult and time-consuming.
On the other hand it was founded from comparisons with experiments, that the direct part in the spectra shows a simple systematical behaviour, suitable for crude empirical parametrization /17,18/.
Basing on this observations we propose the following empirical ansatz for the direct contribution to the differential cross section in (1):

$$\frac{d\sigma^{DI}(\varepsilon)}{d\varepsilon'} = \frac{C_1}{\varepsilon}\, g(\varepsilon,\varepsilon'). \tag{3}$$

With a normalization constant C_1 [mb] and the relative function

$$g(\varepsilon,\varepsilon') \equiv \frac{d\sigma^{DI}(\varepsilon)}{d\varepsilon'} \Big/ \frac{d\sigma(\varepsilon)}{d\varepsilon'} = \exp\left\{-\frac{(\varepsilon-\varepsilon')^2}{2D^2}\right\} H(\varepsilon,\varepsilon') \tag{4}$$

is given by a Gaussian having the width

$$D = \varepsilon / C_2 \tag{5}$$

and the Heavyside step function $H(\varepsilon-\varepsilon')$.

In the case of ^{93}Nb we found that using the constants C_1 = 600 mb and C_2 = 3 a reasonable description of the experiments is obtained, as shown at Figs. 1 - 3 by broken lines.
The parametrization of the direct part (3) leads to a constant energy-integrated value, independent of incidence energy,

$$\sigma^{DI}(\varepsilon) = \int d\varepsilon' \frac{d\sigma^{DI}(\varepsilon)}{d\varepsilon'} = \frac{C_1}{C_2} \left(\frac{\pi}{2}\right)^{1/2}. \tag{6}$$

The sum of both contributions (1) shown as full line is in satisfactory agreement with the experimental emission spectra in a very broad incidence energy range, except the lowest part of the spectra, where secondary neutrons from the (n,2n) reaction occur.
To compare the calculated angular distributions with experimental data we use the Legendre polynomial expansion

$$\frac{d^2\sigma(\varepsilon)}{d\varepsilon' d\Omega} = \frac{1}{4\pi} \frac{d\sigma(\varepsilon)}{d\varepsilon'} \sum_L (2L+1) f_L(\varepsilon,\varepsilon') P_L(\cos\Theta). \tag{7}$$

Comparing (7) with the model ansatz (1) and the definition (4) we get the relation between f_L and the Kalbach-Mann coefficients a_L as

$$f_L(\varepsilon,\varepsilon') = g(\varepsilon,\varepsilon')\, a_L(\varepsilon') \qquad \text{for} \quad L \geq 1. \tag{8}$$

Formula (8) can be interpreted as the reduction of Kalbach-Mann coefficients due-to the dominance of isotropic multistep compound emission at lowes emission energies (This is understandable, because the $a_L(\varepsilon')$ coefficients had been fixed at high incidence energies, where the direct process is dominant).
Both coefficients $a_L(\varepsilon')$ and $f_L(\varepsilon,\varepsilon')$ are shown on Figs. 4 - 6 for L = 1,2. It is evident, that the reduced coefficients $f_L(\varepsilon,\varepsilon')$ give a much better description of the experimental angular distributions than the $a_L(\varepsilon')$ coefficients.

4. Conclusions

In the case ^{93}Nb + n the simple parametrization of direct excitations introduced give a reasonable description of the experimental spectra over broad incident and emission energy ranges, including the highest part of the spectra.
Below 14 MeV the calculations with the exciton model predict neutron emission with only a very small part of pre-equilibrium emission, whereas direct contributions to the spectra in (1) are constant (about 200 mb) and independent of incidence energy.
At higher incident energies the exciton model calculations show a remarkable part of pre-equilibrium emission which is separated on the energy scale from the main range of direct (collective) excitation. At 14 MeV the present analysis overestimates the part of emission spectra, where both the direct (collective) contribution and the pre-equilibrium part of the EM calculation are in the same order of magnitude.
This might be caused by a double-counting of emission processes from $n_0 = 3$ states in the EM and the direct (two-step) contribution.
Further investigations for other nuclei are needed for coming to conclusions about the possibilities of the use of the parametrization proposed for nuclear data evaluations.

References

/ 1/ Proceedings of the IAEA AGM on "Nuclear Data for Fusion Reactor Technology" Gaussig, December 1-5, 1986; IAEA-Techdoc - Vienna, 1987

/ 2/ D. Seeliger: Status of experimental and theoretical double-differential neutron emission data in /1/, page

/ 3/ D. Seeliger: Measurements of Cross Sections and Spectra for Neutron Emitting Channels by Fast Neutron Spectroscopy, INDC (NDS) - 173/GI and INT (85)-J; IAEA, Vienna, Sept. 1985, ed. M.K. Metha, p. 26-61

/ 4/ J.J. Griffin: Phys. Lett. 17 (1966) 478; 24 B (1967) 5

/ 5/ M. Blann: Ann. Rev. Nucl. Sci. 25 (1975) 123

/ 6/ K. Seidel, D. Seeliger, R. Reif, V.D. Toneev: Particles and Nuclear 7 (1976) 499

/ 7/ D. Seeliger, K. Seidel, D. Wolfarth: Proc. Neutron Conf., Kiev, 1971, Vol. I, p. 243-252, Naukova Dumka, Kiev 1972

/ 8/ C. Kalbach, F.M. Mann: Phys. Rev. C 23 (1981) 112

/ 9/ H. Kalka: PhD-Thesis, Technical University Dresden, 1986

/10/ P. Oblozinsky, I. Ribansky, E. Betak: Nucl. Phys. A 226 (1974) 347

/11/ C.Y. Fu, Nucl. Sci. and Eng. 86 (1984) 344

/12/ W. Dilg et al.: Nucl. Phys. A 217 (1973) 269

/13/ M. Torjman, H. Kalka, D. Hermsdorf, D. Seeliger: to be published as INDC-report

/14/ N. Austen, Direct Nuclear Reaction Theories, N.Y., Interscience-Wiley, 1969

/15/ H. Feshbach, A.K. Kerman, S. Koonin: Ann. Phys. 125 (1986) 429

/16/ T. Tamura, T. Udagawa, H. Lenske: Phys. Rev. C 26 (1982) 379

/17/ A.I. Blokhin et al.: IZV AN USSR 49 (1985) 962

/18/ M. Torjman, Diploma Work, TU Dresden, 1987

/19/ D. Schmidt et al.: EXFOR 32001, 1983

/20/ S.P. Simakov et al.: Yad.Fiz. 37 (1983) 801

/21/ A. Takahashi et al.: Report OKTAVIAN-A-83-01 (1983)

/22/ D. Hermsdorf et al.: ZfK-277(Ü), 1975

/23/ A. Marcinkovski et al.: Nucl. Sci. and Eng. 83 (1983) 13

/24/ G.N. Lovchikova et al.: FEI-Report 1603 (1984).

Figure captions

Fig. 1 Experimental integrated emission spectra at ε = 5.2, 6.2, 7.2, and 9 MeV /19,20/; dotted line exciton model; broken line - parametrizations (13) of direct contributions, full line - sum of both contributions.

Fig. 2 As fig. 1 for ε = 14 MeV, experiments from /21/

Fig. 3 As fig. 1 for ε = 20 MeV and 25.7 MeV, experiments from /23,24/.

Fig. 4 Legendre coefficients of angular distributions for 5.2, 6.2, 7.2, and 9 MeV /19,20/; broken lines - $a_L(\varepsilon')$, full lines - $f_L(\varepsilon,\varepsilon')$ for L = 1.2

Fig. 5 As fig. 4 for ε = 14 MeV, data from /21/.

Fig. 6 As fig. 4 for ε = 25.7 MeV, data from /23/.

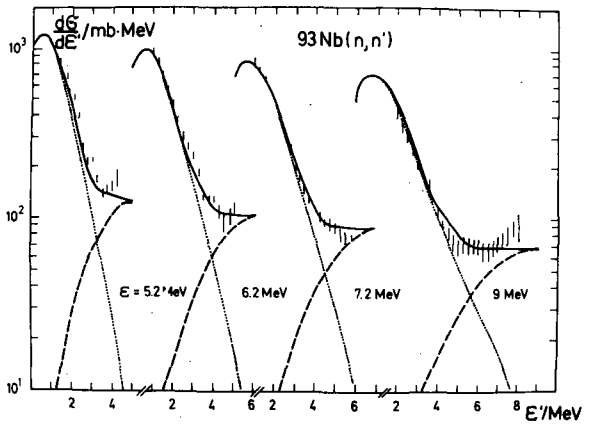

Fig. 1.

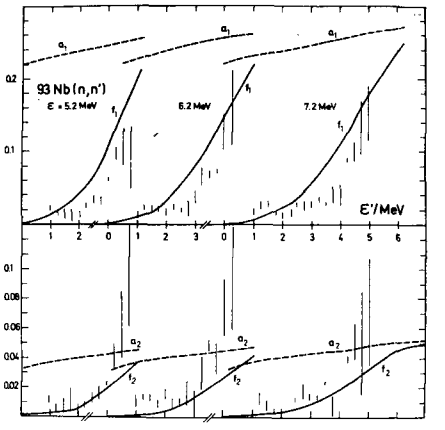

Fig. 4.

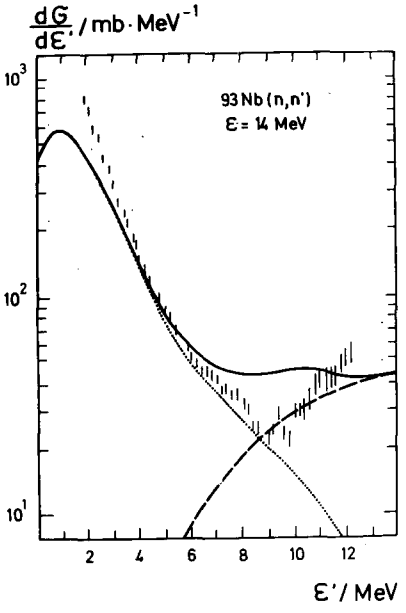

Fig. 2.

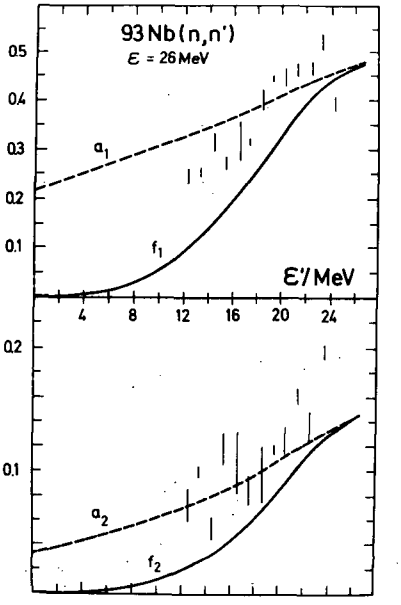

Fig. 5.

Fig. 3.

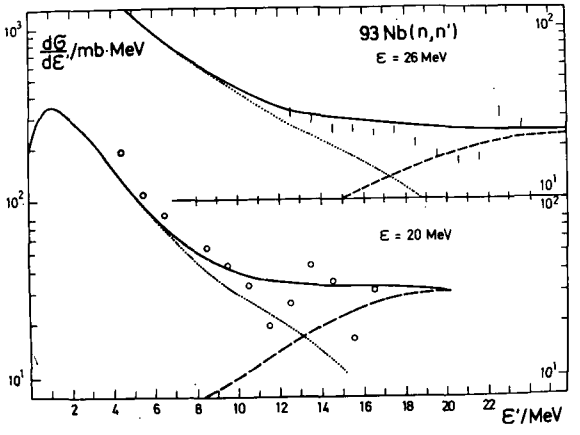

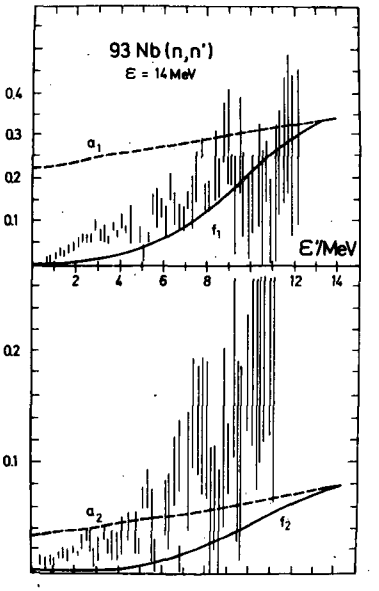

Fig. 6.

NEW SET OF ONE-FERMION LEVEL DENSITY PARAMETERS

Capote R., Herrera E., Kabin E.†, Lopez R., Osorio V.
Institute of nuclear science & technology,
P.O.Box 6122, Havana, Cuba
† Institute for nuclear research, Moscow state university,
117234, Moscow, USSR

ABSTRACT: A new set of level density parameters for unified preequilibrium and equilibrium calculations is obtained. Systematics for this parameters are proposed. The new parameters guarantee the consistency between the sum over all possible particle-hole components and the one-fermion total level density.

The achievement of consistency between the sum over all possible particle-hole components and the one-fermion total level density

$$\sum_{p=h} \omega_1(p,h,U-D) = \frac{\exp\left[2\sqrt{a(U-D)}\right]}{\sqrt{48}\ (U-D)} \qquad (*)$$

is a real need in unified preequilibrium and equilibrium model calculations[1]

However commonly used a and D Dilg's parameters[2] don't satisfy mentioned condition(*see fig.* 1), because they are obtained by fitting experimental data using two-fermion level density formula. In the present contribution a new set of level density parameters a_1 and D_1 for nuclei with mass number $40 \le A \le 250$ were obtained. For this new set of parameters the relation (*) is valid and therefore the consistency is achieved. Calculations using different level density parametrizations were compared with experimental data. A good agreement was achieved by using a_1 and D_1 parameters (*see fig.*2). A sistematics for the parameters in the range $50 \le A < 150$ also is proposed :

$$a_1 = (.184 \pm .007)A - (4.7 \pm .5) \quad \text{for} \quad 50 \le A \le 85$$

$$a_1 = (.113 \pm .003)A \quad \text{for} \quad 86 \le A \le 150$$

$$D_1 = P - (96 \pm 9)A^{-1} \quad \text{for} \quad 50 \le A \le 150$$

where P is calculated with Kummel's parametrization[3]

New parameters a_1 and D_1 allow the practical use of the pairing correction for p-h state densities proposed by Ignatiuk and Sokolov[4] as was suggested by Fu[5]

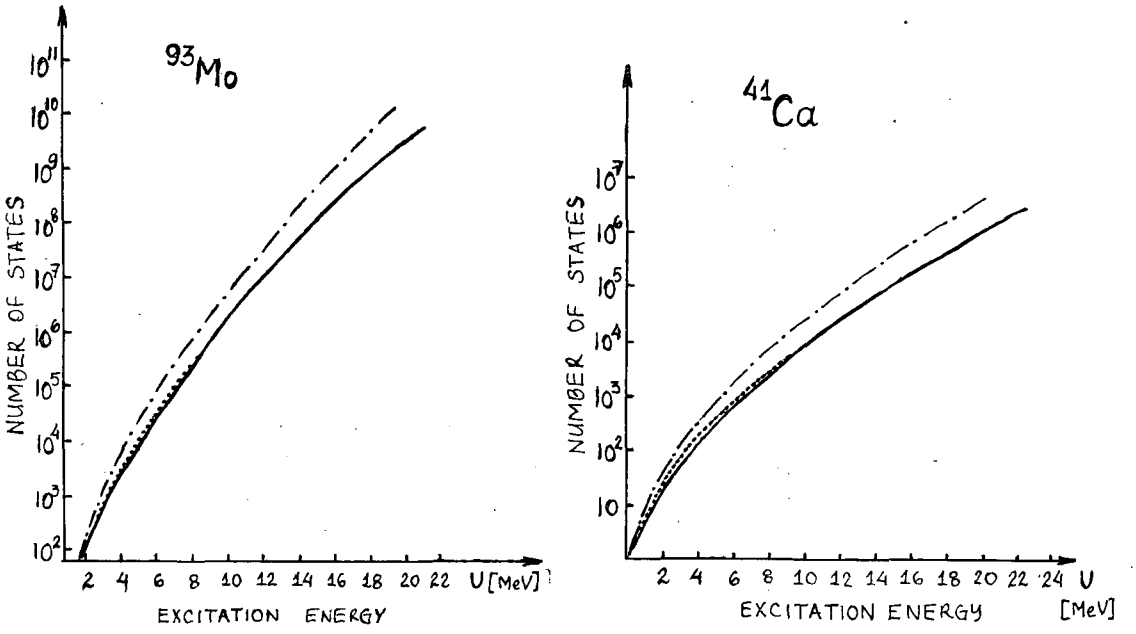

Fig.1 Fits of particle-hole state density sum with Dilg's parameters a and D [—·—] and a_1, D_1 parameters [——] to the one-fermion total level density [·····].

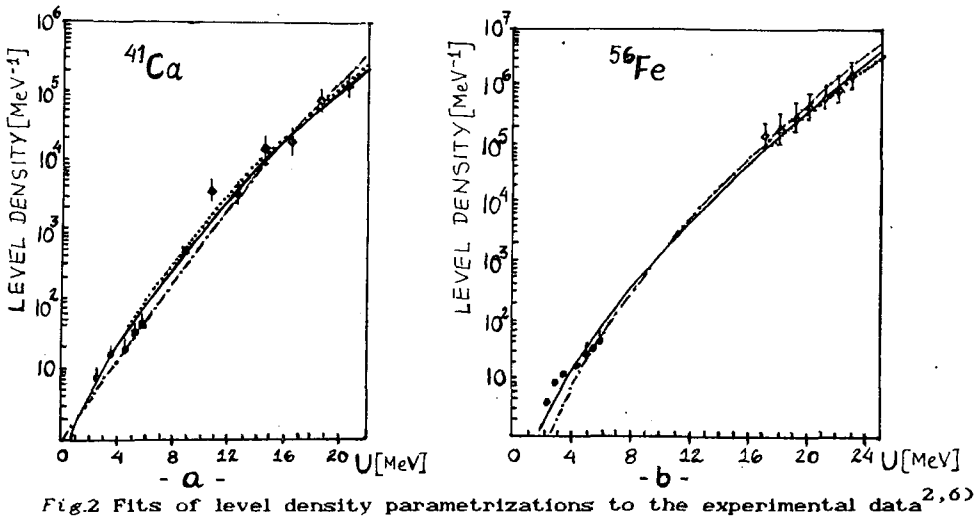

Fig.2 Fits of level density parametrizations to the experimental data[2,6]

—— Dilg's parametrization[2]

-·- Gilbert & Cameron parametrization[7]

····· One-fermion total level densities with a_1, D_1 parameters

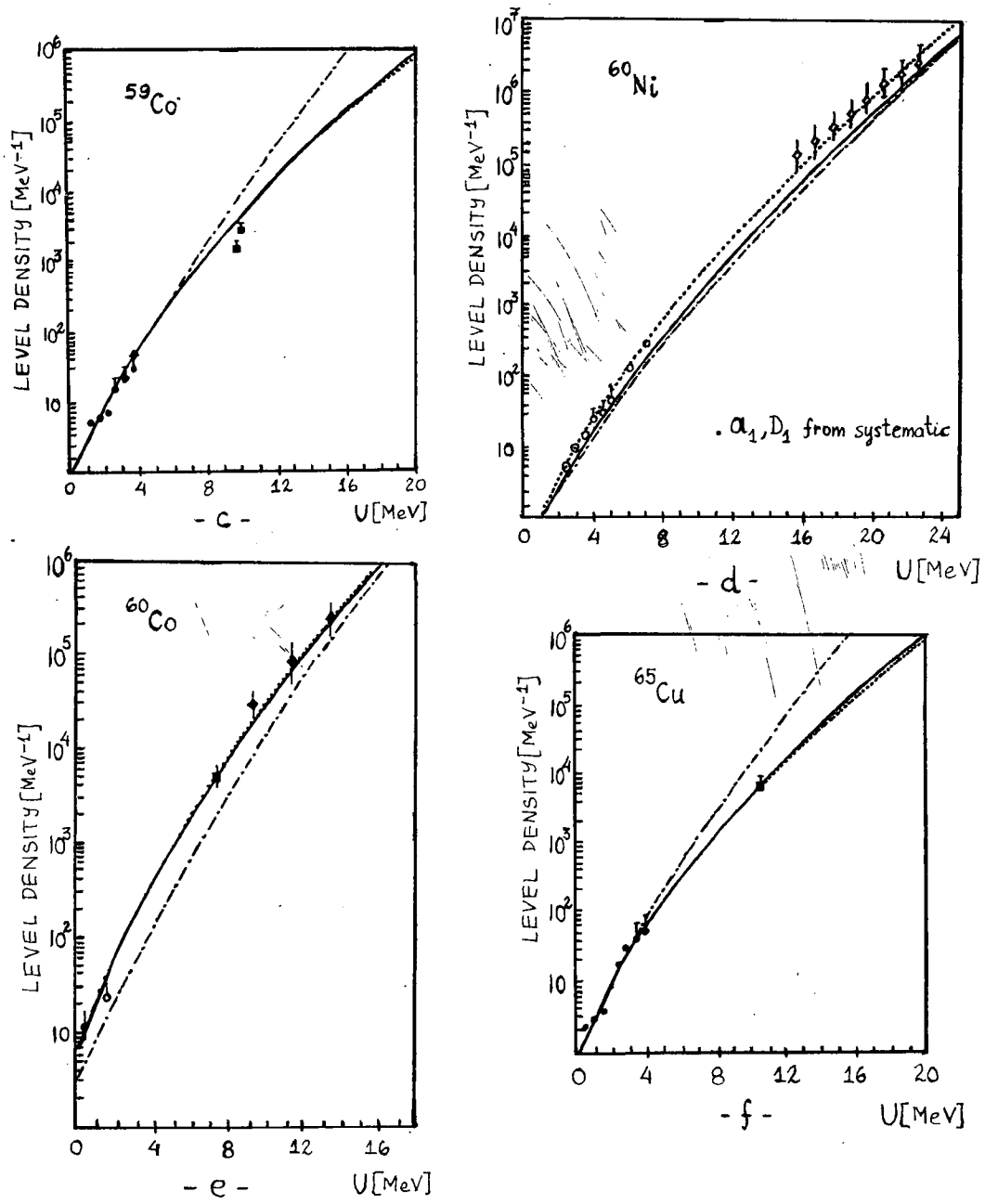

Fig.2 Fits of level density parametrizations to the experimental data[2,6].

—— Dilg's parametrization[2]

—·— Gilbert & Cameron parametrization[7]

····· One-fermion total level densities with a_1, D_1 parameters

Table 1.Level density parameters a_1 (Mev^{-1}) and D_1 (MeV).

	$I = 0.5\ I_{rig}$		$I = I_{rig}$	
Even - even nuclei:				
Ca-20/44	4.78	1.60	4.95	1.35
Ti-22/48	4.79	1.13	5.31	1.23
Ti-22/50	4.80	2.43	5.04	2.18
Cr-24/54	4.71	.87	5.44	1.09
Fe-26/58	5.44	1.22	6.18	1.32
Ni-28/62	5.85	1.40	6.64	1.55
Zn-30/68	6.58	1.14	7.28	1.19
Ge-32/74	9.16	1.44	9.42	1.30
Se-34/78	8.87	1.51	9.81	1.50
Sr-38/88	8.06	2.49	8.52	2.39
Zr-40/92	9.12	1.51	10.01	1.51
Mo-42/96	9.53	1.17	10.44	1.17
Mo-42/98	10.15	1.00	11.10	.99
Ru-44/100	9.97	.87	10.83	.83
Ru-44/102	11.04	.80	11.97	.78
Pd-46/106	12.35	1.50	13.38	1.49
Cd-48/112	12.52	1.59	13.77	1.60
Cd-48/114	13.33	1.73	14.63	1.73
Sn-50/118	12.30	1.72	13.53	1.73
Sn-50/120	12.00	1.66	13.25	1.63
Te-52/124	12.53	1.38	13.77	1.40
Te-52/126	12.77	1.57	14.03	1.56
Xe-54/130	12.45	1.33	13.67	1.31
Xe-54/132	12.59	1.60	13.84	1.61
Ba-56/136	12.55	1.74	13.77	1.73
Ba-56/138	10.87	1.63	12.06	1.64
Nd-60/144	14.22	1.76	15.43	1.74
Nd-60/146	15.34	1.57	16.57	1.55
Sm-62/148	14.47	.93	15.58	.89
Sm-62/150	16.45	.88	17.67	.85
Sm-62/152	15.78	.26	17.00	.25
Gd-64/156	15.52	.42	16.81	.39
Gd-64/158	15.21	.54	16.55	.53
Dy-66/162	15.19	.41	16.43	.39
Dy-66/164	13.98	.11	15.19	.10
Er-68/168	15.32	.42	16.54	.41
Yb-70/172	16.05	.53	17.49	.52
Yb-70/174	15.65	.72	17.10	.70
Hf-72/178	16.77	.55	18.04	.53
Hf-72/180	16.47	.64	17.63	.63
W-74/184	16.77	.66	18.30	.65
Os-76/188	16.77	.97	18.30	.96
Os-76/190	17.07	.83	18.59	.82

Table 1.(continued)

	$I = 0.5\ I_{rig}$		$I = I_{rig}$	
Pt-78/196	16.67	.98	18.25	1.00
Hg-80/200	13.76	.80	15.14	.82
Hg-80/202	13.60	1.10	14.98	1.10
Pb-82/208	7.83	1.95	9.25	2.19
Th-90/230	22.06	.49	23.76	.46
U-92/234	21.42	.33	23.10	.31
U-92/236	22.97	.58	24.66	.56
Pu-94/240	23.15	.78	25.13	.78
Cm-96/246	21.04	.41	22.69	.39
Odd - odd nuclei:				
Sc-21/46	5.17	-1.59	5.40	-1.77
V-23/52	4.72	-1.65	5.05	-1.75
Mn-25/56	5.28	-1.93	5.86	-1.88
Co-27/60	5.81	-1.54	6.23	-1.58
Cu-29/64	6.84	-.66	7.63	-.64
Cu-29/66	7.19	-.32	8.10	-.24
Ga-31/70	7.75	-.57	8.62	-.55
Ga-31/72	7.92	-1.36	8.87	-1.28
As-33/76	8.95	-1.12	9.91	-1.06
Br-35/80	9.09	-.96	10.02	-.94
Br-35/82	9.78	-.32	10.78	-.31
Rb-37/86	7.11	-.69	7.83	-.67
Y-39/90	7.18	.00	8.16	.07
Nb-41/94	10.44	-.35	10.97	-.43
Rh-45/104	12.28	-.73	13.53	-.71
Ag-47/108	12.41	-.61	13.64	-.60
Ag-47/110	13.26	-.65	14.58	-.63
In-49/114	13.26	.05	13.99	.00
In-49/116	13.37	-.44	14.13	-.49
Sb-51/122	12.64	-.90	13.76	-.89
Sb-51/124	11.97	-1.05	12.96	-1.05
I-53/128	12.66	-.90	13.81	-.88
Cs-55/134	11.93	-.98	12.93	-.98
La-57/140	11.66	-.77	12.81	-.75
Pr-59/142	13.02	-.15	14.33	-.14
Eu-63/152	18.26	-.76	19.69	-.76
Eu-63/154	18.11	-.39	19.53	-.41
Tb-65/160	16.17	-.71	17.63	-.71
Ho-67/166	15.49	-.74	16.75	-.74
Tm-69/170	16.36	-.57	17.86	-.57
Lu-71/176	16.91	-.49	18.23	-.50
Ta-73/182	16.68	-.60	18.02	-.61
Re-75/186	17.27	-.56	18.74	-.56

Table 1.(continued)

	$I = 0.5\ I_{rig}$		$I = I_{rig}$	
Re-75/188	17.55	-.64	19.07	-.64
Ir-77/192	18.15	-.56	19.75	-.55
Ir-77/194	16.66	-.63	18.20	-.57
Au-79/198	15.02	-.57	16.44	-.57
Tl-81/204	10.28	-.17	11.61	-.07
Tl-81/206	9.32	-.53	10.54	-.43
Bi-83/210	9.26	-.96	10.48	-.86
Np-93/238	23.03	-.45	24.85	-.46
Odd nuclei:				
Ar-18/41	4.05	-.28	4.91	.07
K-19/41	3.49	-1.51	4.39	.05
Ca-20/41	3.68	-.33	4.39	.05
Ca-20/43	4.15	-.54	4.98	-.01
Ca-20/45	4.41	-.20	5.27	.14
Ti-22/47	4.19	-.57	4.98	-.12
Ti-22/49	4.83	.58	5.74	.84
V-23/49	4.35	-.60	5.08	-.28
V-23/51	6.61	1.45	5.80	.73
Cr-24/51	4.26	-.24	5.03	.13
Cr-24/53	4.58	.30	4.69	.42
Cr-24/55	4.69	-.42	5.66	-.04
Mn-25/51	3.79	-1.13	4.53	-.71
Mn-25/53	4.16	-.53	4.91	-.13
Mn-25/55	4.25	-.85	4.90	-.61
Fe-26/55	4.37	-.18	5.14	.16
Fe-26/57	4.69	-.44	5.60	.03
Co-27/55	4.44	1.26	5.22	1.39
Co-27/57	4.69	.20	5.54	.52
Co-27/59	4.94	-.19	5.68	.04
Ni-28/59	4.40	-.63	5.19	-.21
Ni-28/61	5.12	-.46	6.03	-.07
Ni-28/63	6.04	.52	7.22	.87
Ni-28/65	6.25	.51	7.41	.72
Cu-29/61	4.52	-.91	5.39	-.52
Cu-29/63	5.16	-.40	5.98	-.18
Cu-29/65	4.91	-.42	5.62	-.25
Zn-30/65	6.39	-.53	7.29	-.41
Zn-30/67	7.05	.24	8.09	.32
Zn-30/69	6.62	.01	7.64	.11
Ge-32/71	7.57	-.80	8.56	-.70
Ge-32/73	7.96	-.78	9.00	-.72
Ge-32/75	7.30	-.89	8.33	-.80
Ge-32/77	8.41	.00	9.56	.01

Table 1.(continued)

	$I = 0.5\ I_{rig}$		$I = I_{rig}$	
Se-34/75	8.47	-.71	9.48	-.65
Se-34/77	8.43	-.69	9.46	-.64
Se-34/79	8.90	-.19	9.99	-.17
Se-34/81	9.28	.08	10.45	.10
Se-34/83	8.56	.31	9.79	.35
Sr-38/85	9.12	.29	10.17	.33
Sr-38/87	9.15	1.19	10.32	1.26
Sr-38/89	6.98	1.15	8.20	1.32
Zr-40/91	8.22	.84	9.41	.93
Zr-40/93	10.00	1.08	11.36	1.13
Zr-40/95	10.08	.76	11.39	.79
Mo-42/93	8.41	.93	9.50	1.01
Mo-42/95	9.15	.47	10.32	.54
Mo-42/97	9.81	.11	11.00	.15
Mo-42/99	11.02	-.23	12.31	-.20
Mo-42/101	13.80	.04	13.85	.06
Ru-44/103	10.42	-.78	11.66	-.74
Ru-44/105	12.50	-.17	13.93	-.15
Cd-48/113	12.24	-.13	13.60	-.11
Cd-48/115	13.52	.03	15.00	.04
Sn-50/113	13.48	.97	14.79	.95
Sn-50/115	11.82	.77	13.10	.77
Sn-50/117	12.76	.67	14.14	.66
Sn-50/119	12.86	.93	14.36	.94
Sn-50/121	13.69	1.17	15.24	1.17
Sn-50/123	12.91	1.20	14.57	1.23
Sn-50/125	12.08	.83	13.63	.84
Te-52/123	13.21	.32	14.60	.32
Te-52/125	12.76	-.24	14.11	-.23
Te-52/127	13.40	.14	14.92	.17
Te-52/129	13.08	-.10	14.52	-.09
Te-52/131	13.07	.61	14.66	.63
Ba-56/135	12.92	.04	14.25	.03
Ba-56/137	12.82	1.14	14.28	1.14
Ba-56/139	11.74	.65	13.45	.69
La-57/139	11.33	.42	12.09	.38
Ce-58/137	13.47	.25	14.77	.24
Ce-58/141	14.32	1.49	16.30	1.54
Ce-58/143	15.31	.86	17.27	.90
Nd-60/143	16.48	1.66	18.42	1.69
Nd-60/145	14.31	.55	15.94	.57
Nd-60/147	15.11	-.21	16.73	-.20
Nd-60/151	16.22	-.12	17.92	-.13
Sm-62/151	15.32	-.71	16.90	-.68
Sm-62/153	15.44	-.72	17.01	-.69
Sm-62/155	14.30	-.69	15.80	-.67

Table 1.(end)

	$I = 0.5\ I_{rig}$		$I = I_{rig}$	
Gd-64/153	16.67	-.49	18.22	-.49
Gd-64/155	16.86	-.54	18.43	-.52
Gd-64/157	15.09	-.42	16.58	-.41
Gd-64/159	15.11	-.39	16.67	-.37
Gd-64/161	15.02	-.24	16.61	-.23
Dy-66/157	17.68	-.45	19.20	-.46
Dy-66/159	14.63	-.64	16.05	-.63
Dy-66/161	17.04	-.46	18.61	-.46
Dy-66/163	14.48	-.61	15.93	-.60
Dy-66/165	14.22	-.52	15.75	-.50
Er-68/163	16.86	-.48	18.37	-.48
Er-68/165	15.71	-.48	17.19	-.48
Er-68/167	15.75	-.26	17.30	-.25
Er-68/169	15.42	-.19	17.01	-.18
Er-68/171	15.29	-.23	16.90	-.21
Yb-70/171	15.00	-.59	16.44	-.59
Yb-70/173	15.30	-.27	16.81	-.26
Yb-70/175	15.20	-.13	16.82	-.12
Yb-70/177	15.81	-.04	17.48	-.02
Lu-71/177	16.65	-.12	17.32	-.17
Hf-72/175	16.02	-.48	17.48	-.48
Hf-72/177	16.41	-.23	17.98	-.22
Hf-72/179	16.09	-.17	17.69	-.16
Hf-72/181	16.23	-.04	17.89	-.04
W-74/181	16.95	-.16	18.50	-.16
W-74/183	15.46	-.42	16.98	-.41
W-74/185	15.53	-.61	17.10	-.59
W-74/187	17.12	.05	18.91	.05
Os-76/187	16.39	-.48	17.92	-.47
Hg-80/199	14.68	-.39	16.11	-.40
Hg-80/201	11.92	-.31	13.30	-.27
Pb-82/205	11.07	.19	12.44	.26
Pb-82/207	8.16	.79	9.47	.97
Pb-82/209	7.72	.52	9.28	.75
Th-90/231	22.66	-.40	24.67	-.40
Th-90/233	22.41	-.37	24.50	-.37
U-92/233	22.49	-.20	24.39	-.21
U-92/235	22.01	-.17	24.03	-.16
U-92/237	22.63	-.05	24.71	-.04
U-92/239	23.40	-.37	25.52	-.37
Pu-94/239	20.70	-.31	22.54	-.31
Pu-94/241	21.42	-.45	23.35	-.45
Am-95/243	20.48	-.34	21.86	-.36
Cm-96/245	21.36	-.17	23.28	-.17
Cm-96/247	20.10	-.34	22.04	-.33
Cm-96/249	21.53	-.38	23.58	-.38

References

1) BNL-NCS-51694(1983),"IAEA Advisory group meeting on basic and applied problems of nuclear level densities"
2) Dilg W.,Schantl W. et al. Nucl.Phys.A217(1973) 269
3) Kumel H., Mattauch J.H. et al. Nucl.Phys. 63(1965) 1
4) Ignatiuk A.V.,Sokolov Yu.V. Sov.J.Nucl.Phys 17(1973) 376
5) Fu C.Y. Nucl.Sc.& Eng.86(1984) 344
6) Lu C.C.,Vaz L.C., Huizenga J.R. Nucl.Phys.A190(1972) 229
7) Gilbert A., Cameron A.G.W. Can.J.Phys. 43(1965) 1446

IS THE NEUTRON WIDTH INDEPENDENT OF THE FORMATION MODE OF THE COMPOSITE NUCLEUS ?

L. Łasoń, M. Przytuła
Institute of Physics, Lodz University, Lodz, Poland

Abstract: Neutron decay probabilities calculated according to a semiclassical description are different for neutron and alpha-particle entrance channels. This implies a deviation from the compound-nucleus theoretical predictions. To test this experimentally, some appropriate cases for study are proposed.

1. INTRODUCTION

It is commonly accepted to consider two extreme models for description of the nuclear reaction mechanism, the compound-nucleus model and the direct interaction one. Either of these two models individually provides a satisfactory approximate description of reactions induced respectively by low and high energy particles. In the case of intermediate energy region, when it is impossible to describe reactions by these models used individually, the procedure for separation contributions appropriate to each model is employed. Such procedure is rather a formal classification and can not be treated as a literal picture of the physical reality. In this case it may be not meaningful to conceive of a demarcation line between these models, the problem boils down rather to understand what occurs in the excited nucleus from its formation to its decay.

The discrepancy between measured characteristics of nuclear reactions and expectations based on outlined models can be lie within the measurements accuracy, so they should not give indication of incorretness of the model assumptions. Thus only increasing the measurements accuracy or analysis of effects, sensitive to changes in model assumptions, may reveal defects in our understanding of the reaction mechanism.

It is known that difficulties in description of particle spectra from reactions at medium energies may be obviated by introduction of mechanism of preequilibrium decay and use Griffin's model 1) or its versions. This success inspired to use analogous approach in description of neutron induced reactions, although these reactions are traditionally thought to pass through the compound nucleus stage. As a result of using the new approach (so called semiclassical description) the essence of which is the assumption that the decay process goes together with the process of step by step energy redistribution, was the satisfactory explanation of the average reduced neutron widths and the partial radiative widths dependence on number of neutrons in nucleus 2,3). Moreover the additional assumptions make it possible to obtain reasonable estimations of the average widths of neutron resonances 7). Further considerations and calculations which were carried out on a basis of this approach lead to a suggestion, that in the case of neutron resonances the so called "independence hypothesis" may be not fullfilled. According to this hypothesis intermediate excited nucleus completely "forgets" how it is formed, and this means independence of the decay of the entrance channel.

The purpose of this work is to give the reasons for possibility of deviation from the independence hypothesis in the case of resonance states of intermediate nucleus excited by neutrons and alpha-particles. Earlier indications are 4) that the nucleus "amnesia" is not complete if nucleus is excited by neutron capture. Here we present quantatitative estimations of degree of expectate violation for a num-

ber of selected nuclides and resonances.

2. THE FOUNDATIONS OF SEMICLASSICAL DESCRIPTION

In the semiclassical description presented in ref. 2) and used to analyse resonance states excited by neutron capture, the redistribution of energy is assumed to be a result of two-body collisions of nucleons. As a consequence of these collisions the structure of excited nucleus evolves from the simplest configuration after neutron capture when the whole excitation energy is concentrated on the only one nucleon, to configurations in which the excitation energy is redistributed between many nucleons. In the simplest version of the description, the configurations of excited nucleus are characterised only by the number "i" of excited particles (above Fermi level). The probability of finding the excited nucleus at time "t" in configuration with "i" excited particles depends on the initial configuration, the intranuclear transition rates for transitions to the neighbouring configurations $\lambda_i^{\pm}$, and on probability of the decay from the i-configuration per unit time λ_i. There is a competition between a decay process and an equilibrium one, so the decay is liable to occur at any time during the evolution.
The evolution of nuclear structure is treated statistically and is described by the set of coupled master equations in the form:

$$dP_i(t)/dt = \lambda_{i-1}^{+} \cdot P_{i-1}(t) - (\lambda_i^{+} + \lambda_i^{-} + \lambda_i) \cdot P_i(t) + \lambda_{i+1}^{-} \cdot P_{i+1}(t) \qquad /1/$$

where "i" changes from 1 to the maximal number of nucleons "k" which can be raised above the Fermi level at given excitation energy. The general conservation rules remain valid in this process, of course. The mode of decay of excited nucleus are connected only with particular configurations designed as favourable configurations. For example, at low energy resonances the favourable configuration to neutron decay of resonance states is that with i=1. The whole probability of decay into a selected channel depends on mean time which an excited nucleus spends in configuration favourable to this decay. It is given by

$$\Theta_i = \int_0^{\infty} P_i(t)dt \qquad /2/$$

Quantities Θ_i may be extracted from the system of linear algebraic equations obtained from time-integrated master equations /1/ at boundary conditions appropriate for particular projectile. For instance in the case of neutron induced reactions and those induced by alpha-particles the boundary conditions are written as follows

$$P_i(t=0) = \delta_{1,i} \quad \text{and} \quad P_i(t=\infty) = 0 \quad \text{(for neutrons)}$$
$$P_i(t=0) = \delta_{4,i} \quad \text{and} \quad P_i(t=\infty) = 0 \quad \text{(for alpha-particles)} \qquad /3/$$

These boundary conditions denote that the evolution of nucleus excited after neutron capture starts from configuration with i=1, whereas after alpha-particle capture it starts from configuration with i=4. In both cases, for all configurations we have, because of decay, $P_i(t)=0$ when $t \to \infty$.
In the calculation of decay probability the contributions p_i of particular configurations are needed; they are defined by

$$p_i = \Theta_i / \sum_i \Theta_i \qquad /4/$$

The calculation of p_i requires the values $\lambda_i^{\pm}$, λ_i and k. In ref. 2) $\lambda_i^{\pm}$ were calculated from Fermi golden-rule

$$\lambda_i^{\pm} = 2\pi\hbar^{-1}|\bar{M}|^2 \, \omega^{\pm}(i) \qquad /5/$$

with semiempirical expression for matrix element. The level density $\omega_i^{\pm}$ of accesible final states was taken from ref. 5) with the correction factor given in 6). The details relative to λ_i and k calculations may be found in ref. 2)

3. ESTIMATION OF THE PROBABILITIES OF THE NEUTRON DECAY FOR COMPOSITE NUCLEUS FORMED IN REACTIONS INDUCED BY NEUTRONS AND ALPHA-PARTICLES

As mentioned above, according to the compound nucleus model the decay the particular excited state is independent of the mode of its formation. Thus the probability of this process should not depend upon, among other things, the target nucleus and projectile. On the other hand, according to the semiclassical description this dependence allways exists for the kind of projectile defines unambiguosly *) boundary conditions and thus the solution of master equations /1/. The question now is what value of this dependence is, and what reactions should be chosen to obtain strongest effect. Since the expected effect is, from the formal standpoint, the result of different boundary conditions, its magnitude should be increased together with the mass difference of projectiles. The great effects may be expected also when averaging over many configurations is not possible that is when excited nucleus has a simple structure 4) and the number of favourable configurations for given decay channel is as small as possible.
These conditions are fullfilled in the case of reactions initiated by neutron and alpha-particles bombardment of the light nuclei if the exit channel is a neutron one. The course of both these reactions may be then illustrated with the diagram:

$$\boxed{1p\text{-}0h} \rightleftharpoons 2p\text{-}1h \rightleftharpoons 3p\text{-}2h \rightleftharpoons 4p\text{-}3h \rightleftharpoons 5p\text{-}4h \rightleftharpoons \ldots$$

for (n,n) reaction

$$\boxed{1p\text{-}0h} \rightleftharpoons 2p\text{-}1h \rightleftharpoons 3p\text{-}2h \rightleftharpoons 4p\text{-}3h \rightleftharpoons 5p\text{-}4h \rightleftharpoons \ldots$$

for (α,n) reaction

where the initial configuration is enclosed in a circle and the exit one is enclosed in a rectangle. At excitation energies near neutron binding energy the only favourable configuration for neutron decay is that with i=1 as it is shown on the diagram. The low single particle states density in the case of light nuclei provides the simplicity of structure of the excited state.

---

*) In ref. 2) a distinction is not made between neutrons and protons in potential well, so these same effects are expected for reactions induced by particles with the same mass number.

The choice of light nuclei as target ones is also advisable for experimental reasons. The comparatively low Coulomb barier (greater penetrability) and low density of resonances (requirements on resolution are smaller) alleviates measurements. On the other hand, the necessary data on K ($|\bar{M}|^2=K\,U^{-1}A^{-3}$; U- excitation energy, A- mass number) for light nuclei are rather uncertain and introduce additional error into the results of evaluations.

The results of calculations of $p_1^{(n)}$ and $p_1^{(\alpha)}$ - contributions of the favourable configuration, that is the configuration with i=1 for (n,n) and (α,n) reactions respectively, are listed in Table 1 for the most "promising" cases. Other data connected with these reactions (excitation energy and energies of projectiles) are also tabulated.

Table 1. Calculated contributions of configuration favourable to neutron emission.

Target nucleus in (n,n) reaction	(α,n) reaction	Neutron energy (keV)	Alpha-particle energy (MeV)	Excitation energy (MeV)	$p_1^{(n)}$ $\times 10^3$	$p_1^{(\alpha)}$ $\times 10^3$
$^{14}_{7}N$	$^{11}_{5}B$	2230	2.6238	12.915	3.05	3.00
$^{22}_{11}Na$	$^{19}_{9}F$	0.145	2.361	12.4186	0.443	0.402
$^{25}_{12}Mg$	$^{22}_{10}Ne$	79.6	0.6589	11.1701	0.402	0.367
$^{32}_{16}S$	$^{29}_{14}Si$	102.71	1.8493	8.7431	0.500	0.472
		1358.8	3.2353	9.9622	0.278	0.244
$^{33}_{16}S$	$^{30}_{14}Si$	258	4.2416	11.6653	0.134	0.091

All values p_1 are evaluated for K=250 MeV^3, although there are suggestions that this value is too low 8). If this is the case, it results only in increasing $p_1^{(n)}/p_1^{(\alpha)}$ ratio.
The same effect is expected, in principle, in other exit channels but its estimation on the basis of the semiclassical description is somewhat uncertain as yet.

Because $\Gamma_n=p_1\Gamma_{sp}$ the simplest way to obtain experimental values of $p_1^{(n)}$ and $p_1^{(\alpha)}$ is measurement of neutron widths for both kinds of reactions. But in the case of so simple structure of excited state, the doubts may arise as to how determine neutron width from experimental data and the question may be raised as to whether the conception of resonance width is sensible. For this reason it appears that a more appropriate method, although more difficult, is to measure relative neutron yields in both reactions.

Based on the present results such measurements do not seem to be beyond the scope of experimental possibilities, and might throw some new light on the understanding of the reaction mechanism.

Acknowledgments
The authors would like thank to Dr. U. Garuska for her help in preparing the manuscript.

This work was performed under contract CPBP.01.09

REFERENCES

1) J. J. Griffin, Phys. Rev. Lett. 17(1966)478
2) M. Kaczmarczyk, M. Przytuła, Z. Phys. A323(1986)465
3) H. Stańczyk, J. Phys. G 13(1987)1037
4) G. Rohr, Z. Phys. A318(1984)299
5) F. C. Williams, Jr., Phys. Lett. 31B(1970)184
6) I. Ribanský, P. Obložinský, E. Běták, Nucl. Phys. A205(1973)545; Nucl. Phys. A226(1974)347
7) L. Łasoń, M. Przytuła, Proc. 4th Int. Conf. on Nuclear Reaction Mechanisms, Varenna, June 10-15, 1985, Ed. E. Gadioli, v. 1, p. 517
8) M. Kaczmarczyk, Proc. Symp. Nuclear Excited States, Łódź, June 25-29, 1984, WUŁ, Łódź University, p. 207

DECAY OF THE DOORWAY STATES OF THE GIANT DIPOLE RESONANCE (DGR) BY NEUTRON CHANNEL

I.M.Glatky, A.M.Lapik, B.S.Ratner, S.S.Verbitsky, A.V.Veselovsky

Institute for Nuclear Research Academy of Science USSR Moscow

The method of singling out the processes of doorway state decay to the continuum by means of neutron energy spectrum energetic component registration is proposed. The results for some nuclei in the region of N=28 neutron shell closure are considered.

DGR is a collective coherent excitation of a nucleus consisting of a superposition of particle-hole transitions. Simple 1p-1h configurations created on the first stage are chamging by more complicated and neutron (or proton) emission may occur on all stages of the reaction (Fig.1). The states which are generated on the first stage of the reaction - so called doorway states (DS) - describe the amplitude of the closed channel of the reaction which is excited by the interaction with the open channel. DS concept was introduced by H.Feshbach in 1965 1). DS is connected with the continuum by a one-particle operator. In that case the decay result is an emitted neutron and a residual nucleus is in a hole state. The another channel of doorway state evolution is the complication of configurations due to residual interaction resulting in the formation of the compound nucleus and neutron evaporation (preequilibrium emission is possible also).

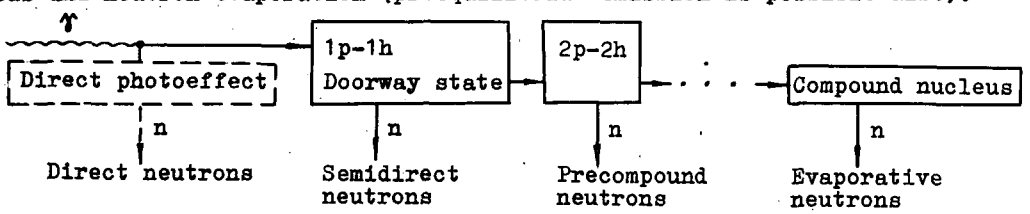

Fig.1. The stages of photoneutron process

DS concept holds true if the probability of transition into more complicated states is not too large. The width of the cross-section structure generated by the DS decay in continuum (intermediate structure-IS) is too small for structure of single-particle type but too large in comparison with compound nucleus resonances. As it is known the DS are most distinct in photonuclear reactions and in reactions of isobar-analog state formation. The study of DS decay features is of great interest and permits to make some advance in a first stage of a nuclear mechanism understanding. In the photonuclear reaction investigation there are the experimental possibilities to select the processes connected with the DS decay to the continuum. One possibility was realised firstly in a classical work 2). In this work it was studied (γ,p) reaction for the nuclei with significant proton-neutron bound energy differeces and therefore with small proton evaporation probability. So called "direct photoeffect" discovered in this work is the manifestation of the DS decay. The alternative possibility to single out the DS decay to the continuum is to discriminate the part of an energetic spectrum of reaction products which is connected mainly with the compound nucleus decay. The analysis of the experimental data for a large amount of a medium-weight and heavy nuclei 3) shows a well defined break in energetic spectra of neutron emitted (Fig.2). This break divides spectrum into two parts: low energetic part which exponentia-

lly falls with the energy and corresponds mainly to neutrons evaporated from compound state and high energy part resulting from nonstatistical processes.It is interesting to note that for nucleon induced reactions this break is much smaller. It seems likely to single out the first stage of the reaction process by the registration of high energy part of emitted photoneutrons spectra only.This method has lower efficiency in the photoproton case due to the absence of such separa - tion of photoproton energetic spectrum into two components which are connected with Coulomb barrier.

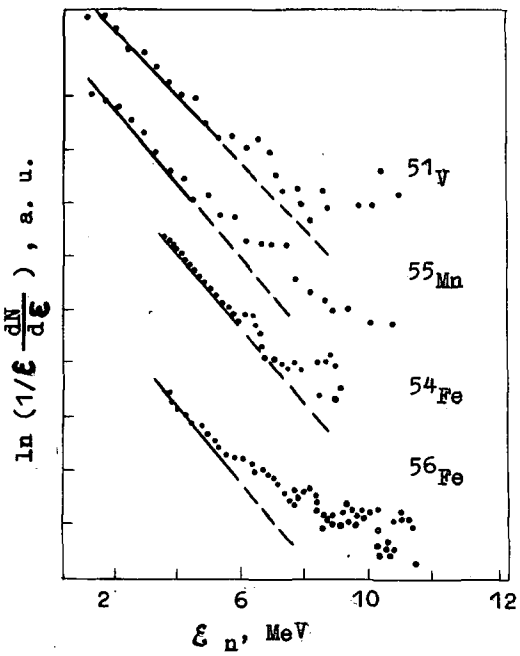

Fig.2.Energy spectra of photoneutrons from some medium-weight nuclei

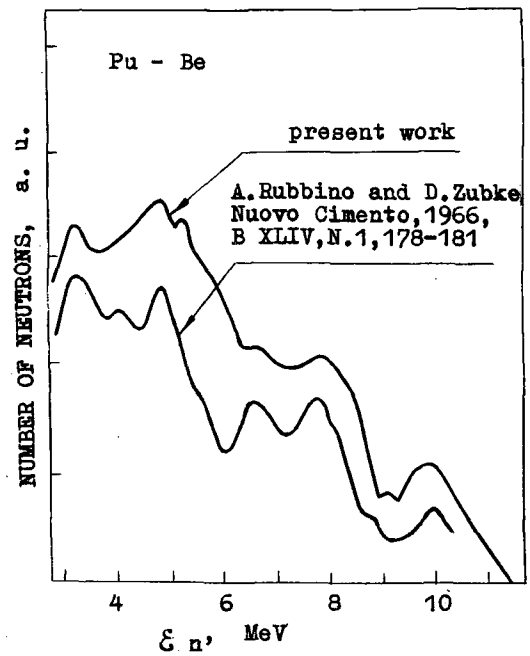

Fig.3.Energy spectra of neutrons from PuBe sourse

In the previous investigations of the (γ,n) reaction on the nuclei ^{58}Ni and ^{60}Ni 4) IS was detected. Authors explained origin of that structure by dipole and quadrupole oscillation interference according to dynamic collective model 5).IS in a cross-section of (γ,n) reaction was observed in a number of other works but the accuracy of results was not good.

The purpose of investigations carried in the photonuclear reactions laboratory of INR since 1975-76 6) was to study mechanism of DGR excited states decay through neutron channel.The experiments were carried out using INR 30 MeV synchrotron.The stability of the bremsstrahlung spectrum tip was maintained with accuracy ± 10 KeV.Neutrons were detected by the scintillation neutron spectrometer with stilbene monocrystal detector 50×50 mm.Energy scale calibration was conducted with PuBe source (Fig.3) and using the photoneutron spectrum from $^{16}O(\gamma,n)^{15}O$ reaction.Registration efficiency of spectrometer geometry was about 2.10^{-3}.A large electron and γ-quanta background was reduced with the help of pulse shape discrimination.The spectrometer electronics in CAMAC standard operated on-line with "Electronika-60"-computer (in the first experiments data were recorded by a multichannel analyser).For the investigations nuclei in the region of a closed N=28 shell were chosen.It was connected with the hope that in the case one or two particles outside the closed shell (or one or two holes)single-particle effects wou-

ld exibit themself more clearly.Energy threshold of photoneutron detection in our experiment was chosen in a region of a break in an energy spectrum i.e. it corresponded $\mathcal{E}_n$=3.5-3.7 MeV.

The results obtained for the iron isotopes ^{54}Fe and ^{56}Fe indicated several peculiar features: 1. Comparison of the total (γ,n) reaction cross-section with the cross-section for energetic neutron emission shows that IS is connected just with the energetic neutron spectrum component (Fig.4).

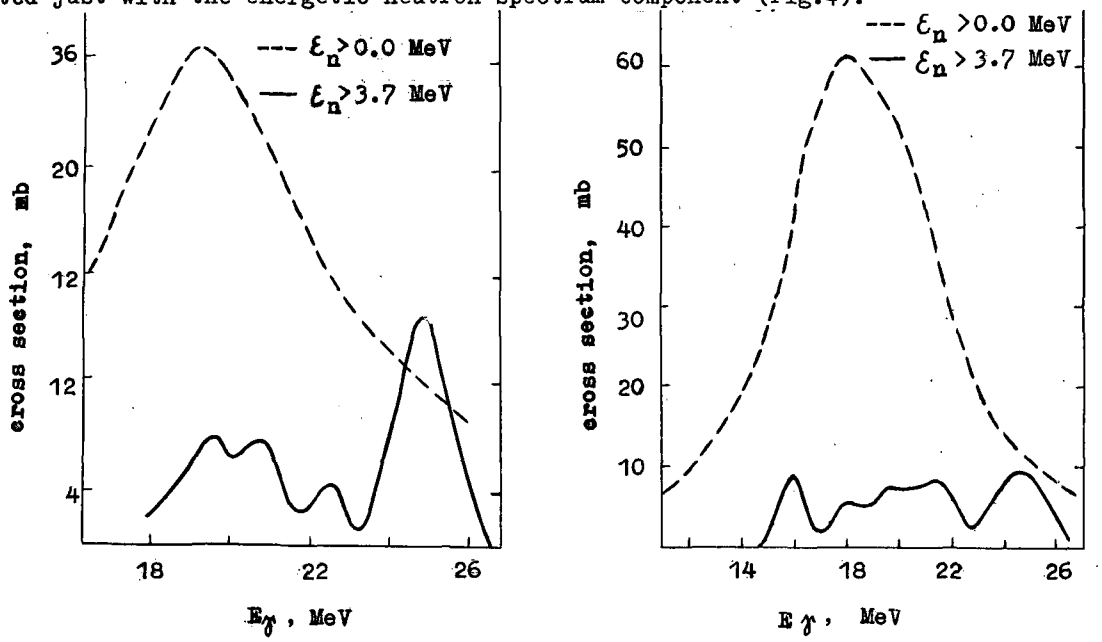

Fig.4. The cross-section of the $^{54}Fe(\gamma,n)^{53}Fe$ and $^{56}Fe(\gamma,n)^{55}Fe$ reactions for all and high energy neutrons

The usefulness of dynamic collective model which claims to explain IS of the (γ,n) cross-section on the spherical nuclei is questionable.2. The location of maxima observed in the photoneutron spectra (Fig.5)measured with different values of $E_{\gamma m}$(maximum energy of γ- quanta in bremsstrahlung) correlates with that of peaks in cross-section for energetic photoneutron emission.Henceforth it was possible to determine positions of the energy levels of the residual nuclei and compare them with the known spectroscopic data.As a rule identification of a decay sceme is unambiguous despite of poor energy resolution of neutron spectrometer. That is due to comparatively large energy distance between lowest levels of final nucleus.3. No decays were observed practicalli in reaction $^{54}Fe(\gamma,n)^{53}Fe$ to the ground state of final nucleus.The resonances at 22.5 and 24.8 MeV both decay to the states with energy E = 0.774 MeV ($3/2^-$) and 1.696 MeV ($7/2^-$) and are superposition at least of two dipole transitions.Absolute values of cross-sections are obtained from the energy neutron spectra by the extrapolation of their low-energetic part with the relation $N(\mathcal{E})= C\cdot\mathcal{E}\cdot EXP(-\mathcal{E}/T)$.In a data given here the mistake of the work 6) which was connected with wrong cross-section calibration is corrected.As is seen from Fig.4 the both curves have very similar shape with notable peak at about 25 MeV.In low energy region the marked difference is pointed out.In the case $^{56}Fe(\gamma,n)^{55}Fe$ reaction peak at E_γ= 16.0 MeV is observed which seems to be connected with dipole transitions of valence 2p3/2 neutrons.

Absence of decays into ground state of the final nucleus,especially notable for resonances at E_γ= 22 and 25 MeV,is interesting feature of the DS created in

(γ,n) reaction on the iron isotops. One of the possible explanations is isospin separation rule which forbids neutron channel decay for the $T_>$ states. Because of that it seems possible proton shells excitation followed by energy transfer to neutron. Partial cross-sections of reactions $^{54}Fe(\gamma,n)^{53}Fe$ and $^{56}Fe(\gamma,n)^{55}Fe$ for $\varepsilon_n > 3.7$ MeV were calculated in 7) on the basis of quasiparticle-optical model. The values of cross-sections calculated appeared rather close to observed (Fig.5).

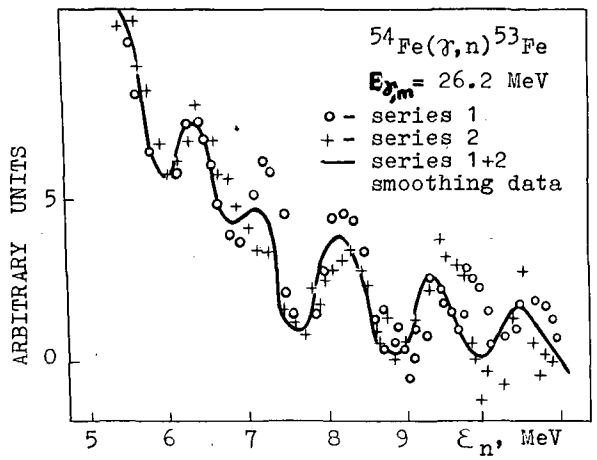

Fig.5. Neutron energy spectrum from $^{54}Fe(\gamma,n)^{53}Fe$ reaction at E_γ = 26.2 MeV

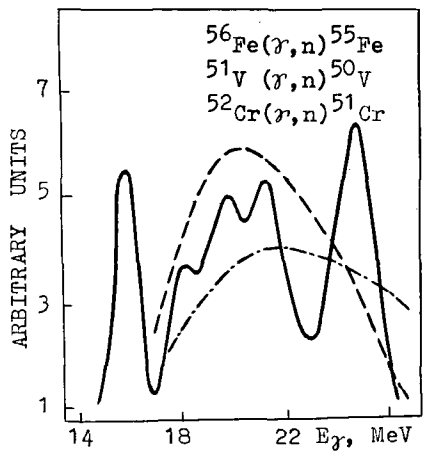

Fig.6. The (γ,n) reaction cross-sections for nuclei with N=28 ($\varepsilon_n > 3.7$MeV)

Indication to the existence of the IS in this calculation was also obtained but contribution of this structure in the cross-section turned out much lower in comparison with the experimental data.

The investigation of the reaction $^{64}Zn(\gamma,n)^{63}Zn$ 8) additionaly supports conclusion of the previous paper about connection of IS in (γ,n) reaction cross-section with energetic photoneutron contribution. In a number of papers the structure in cross-section of reaction $^{64}Zn(\gamma,n)^{63}Zn$ was suggested due to isospin splitting. As it is known two states with difference values of isospin $T = T_0$ and $T = T_0+1$ where T_0 - isospin of initial nucleus are generated in the dipole photoabsorbtion (if $Z \neq N$). In the case of neutron emission lower levels of final nucleus have isospin $T_0-1/2$ and for proton $T_0+1/2$. But the presence of this structure in the cross-section for energetic neutrons emission forces us refuse from isospin splitting hypothesis because of decay of $T_>$ state into the state $T_0-1/2$ by the neutron emission is forbidden due to isospin selection rule.

The curves of cross-sections for energetic neutron emission were also measured for nuclei ^{51}V and ^{52}Cr 9). These nuclei have closed neutron shell 1f7/2 similarly to the nucleus ^{54}Fe but their proton shell 1f7/2 have only 3 and 4 protons, correspondently. As it is seen from Fig.6 the structure in this case is significantly less pronounced. It will be noted that the difference between bound energies of the neutron and proton which defines contribution of the statistical component for ^{51}V and ^{52}Cr nuclei does not differ, essentialy, from that for a ^{56}Fe nucleus. It is the reason why the explanation of the less pronounced structure in cross-section of energetic neutron emission in the case of ^{51}V and ^{52}Cr due to larger contribution of "evaporation" process is not correct. After carrying out automatisation of the experiment 10) the procedure of photoneutron reaction yield measurements was modified: at every $E_{\gamma m}$, neutron energy spectrum was measured. Such pro-

cedure permits to change the value of minimal neutron energy for which cross-section is measured and also to record energy spectra at every $E_{\gamma m}$. In such manner the investigation of reaction $^{58}Ni(\gamma,n)^{57}Ni$ was carried out. Choice of this nucleus caused by the following considerations. 1. Nucleus ^{56}Ni has closed neutron and proton shells (N=Z=28) and two valence neutrons above closed shell. It was possible to expect that interpretation of experimental results in this case would be more unambiguous. 2. Cross-section shape of $^{58}Ni(\gamma,n)^{57}Ni$ reaction for $\mathcal{E}_n>0$ was measured with rather good precision 11). Thanks to that it is especially interest to compare this cross-section with one for $\mathcal{E}_n>3.5$ MeV. Measurements of the yield curve were made from threshold up to $E_{\gamma m}$=20 MeV with the 100 KeV energy steps. Curve of the cross-section calculated by the method of inverse matrix is presented on a Fig.8. Errors indicated are r.m.s. They were obtained by the following pro-

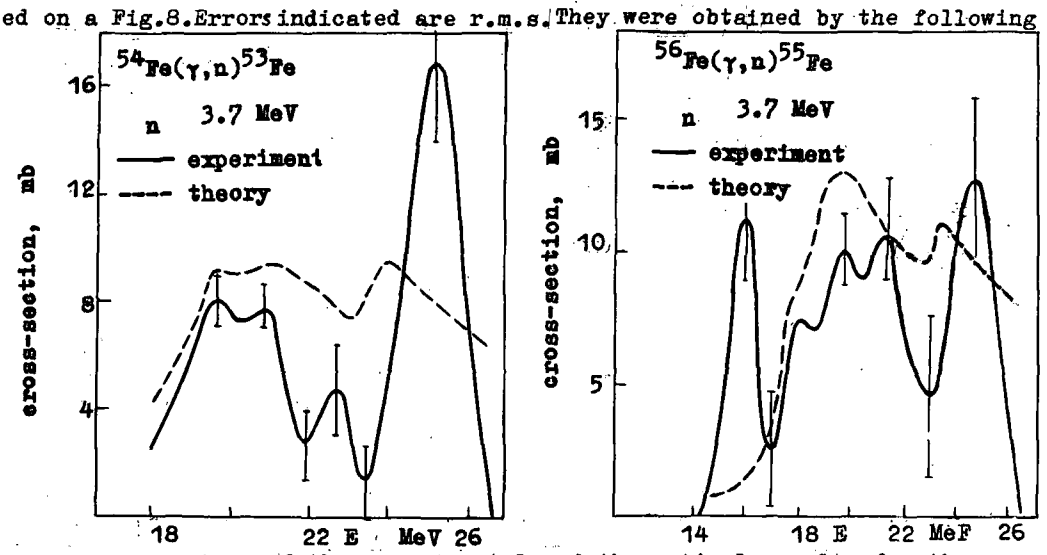

Fig. The comparison of the experimental and theoretical results for the cross-section of the (γ,n) reactions on iron isotopes (for $\mathcal{E}_n>3.7$ MeV)

cedure. Noise with dispersion same as in experiment was added to the smoothed yield curve severel times and in every time cross-section was calculated. Obtained set of cross-sections was used to extract errors in a usual way. These errors give answer to the question whether the existence of the structure in cross-section curve is proved by the yield statistical measurering accuracy.

Widths of resonances are significantly enhanced due to yield curve smoothing procedure. The effect of smoothing can be seen from the part of yield curve near the energy of resonance at E_γ = 18.9 MeV(Fig.9). Appearently, full width of the resonance is less then 100 KeV, so that the life time of DS exceeds 10^{-20}s. Measurements of photoneutron energy spectra at every value of $E_{\gamma m}$ made possible to calculate the cross-section $\sigma(\gamma,n_0)$ for the transition to the ground state of the final nucleus(Fig.10). Since the energy resolution in the energy under discussion is 0.4-0.5 MeV (0.3MeV energy avereging connected with energy step shosen have to be added to energy resolution . It have to be pointed out that positions of all resonances in $\sigma(\gamma,n_{0-3})$ and $\sigma(\gamma,n_0)$ coincide with the exception of the resonance at 18.8 MeV which is absent in $\sigma(\gamma,n_0)$. In the energy region above E_γ=18 MeV the probability of the transition to the ground state decreases appriciable in correspondence with the results obtained for the iron isotopes.

To obtain data on relative widths of resonance state decay to the different states of final nucleus the technique suggested by Gent'group 12) was used: quasi-

monochromatic γ -line is formed by the combination of three bremsstrahlung spectra which have energy shift ΔE from one to another. Neutron spectrum obtained by this method corresponds to 17.9 MeV γ-line with FWHM about 0.5 MeV (Fig.11). Peaks in spectrum correspond to the transitions to ^{57}Ni states with energies E = 2.578 MeV, 1.113 and 0.768 MeV (unresolved) and to the ground state 13).

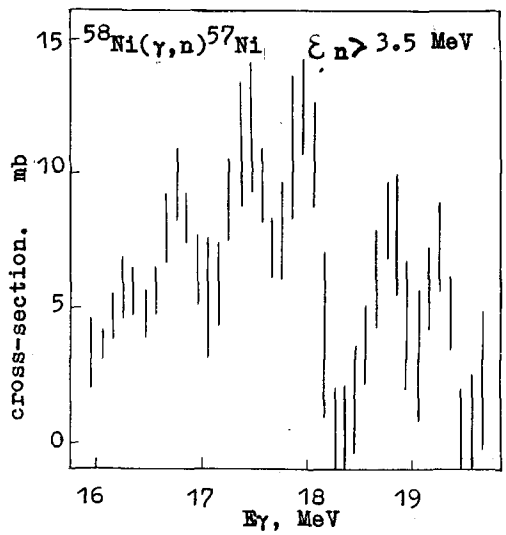

Fig.8. The cross-section of the $^{58}Ni(\gamma,n)^{57}Ni$ reaction for neutron energy $\mathcal{E}_n > 3.5$ MeV

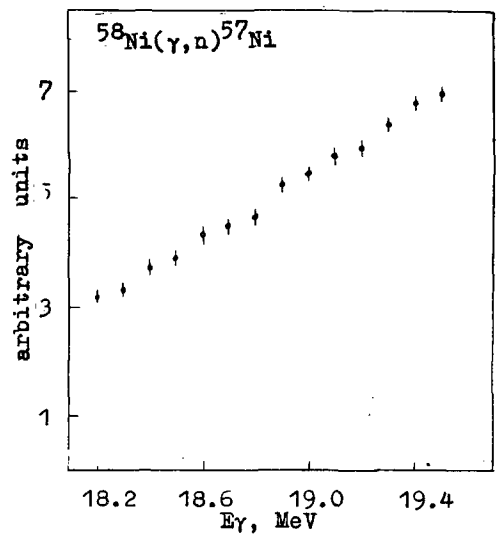

Fig.9. The part yield curve of the reaction near the resonance at E_γ = 18.9 MeV

To compare the cross-section for the energetic neutron emission ($\mathcal{E}_n > 3.5$ MeV) in reaction $^{58}Ni(\gamma,n)^{57}Ni$ with that maasured for all neutrons normalisation was fulfilled using neutron energy spectrum measured at E_γ = 18.8 MeV. The comparison

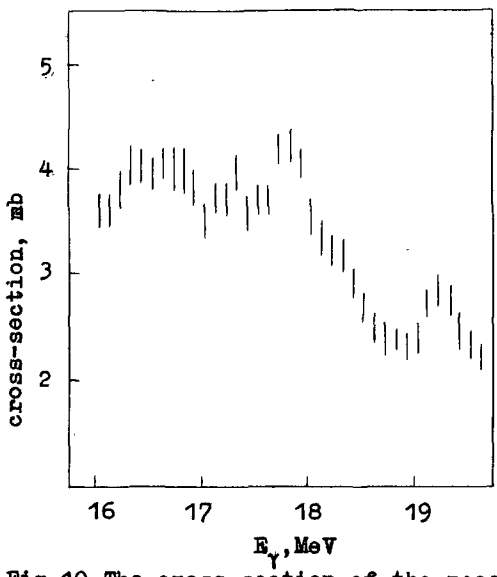

Fig.10. The cross-section of the reaction $^{58}Ni(\gamma,n)^{57}Ni$

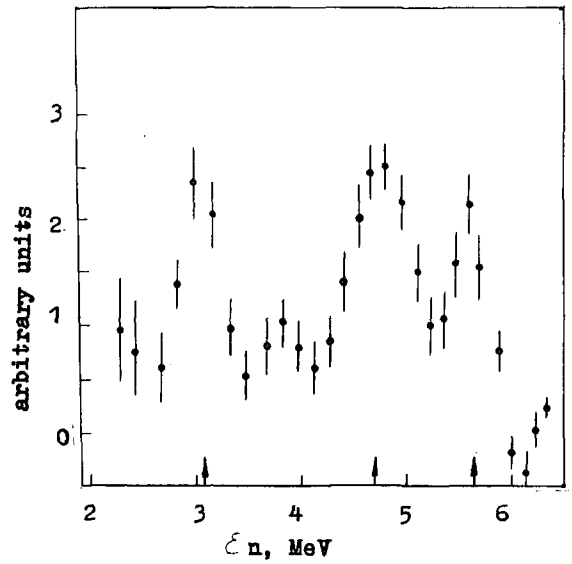

Fig.11. Neutron energy spectrum from quasimonocromatic γ-line with the energy E_γ=17.9±0.3MeV

of both cross-sections is shown on the Fig.12.The discrepancy in the energy of resonances can be explained by the scarsity of experimental points in the peak area of work 11).From Fig.12 we can see that the structure observed in the total cross-section of the reaction is connected with emission of high energy neutrons. Hence the cross-section for emitting low energy neutrons (evaporated from compound state)has very smooth form.It was shown above that contribution of energetic

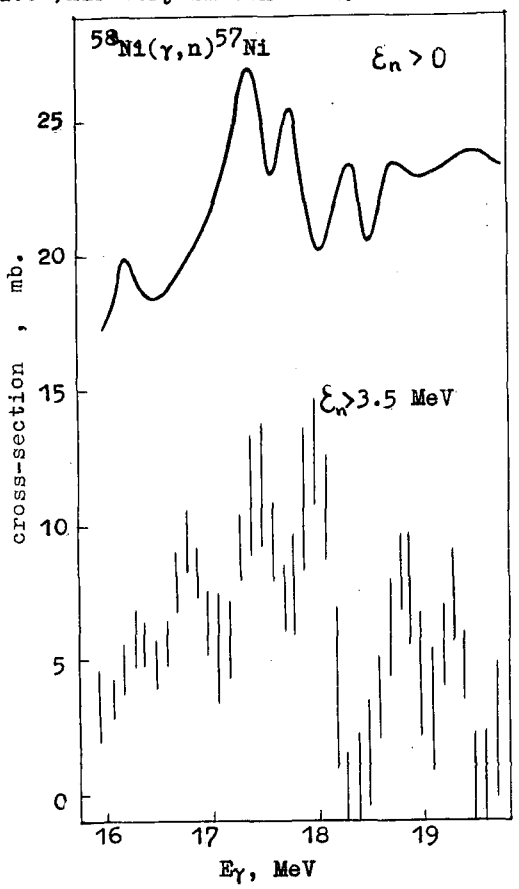

Fig.12. The cross-section of the $^{58}Ni(\gamma,n)^{57}Ni$ for neutron energy $\mathcal{E}_n > 0$ MeV and $\mathcal{E}_n > 3.5$ MeV.

neutrons to the total yield is of less than 0.1.But the cross-section obtained for energetic neutrons corresponds to all neutrons connected with decay to lowest states of final nucleus.Thus the cross-section of the $^{58}Ni(\gamma,n)^{57}Ni$ reaction connected with excitation of lowest states of the final nucleus (having probably hole structure) in the 16 - 20 MeV excitation energy range consists of separeted narrow resonances.For width of this resonances from results of this work it is possible to give the upper estimation only.The additional measurements will be done in narrow energy range using small energy steps.

CONCLUSIONS

1.Present paper describes the method which permits the effective studying of characteristics of the doorway states created in (γ,n) reaction.

2.The doorway states observed in (γ,n) reaction are shown to be connected with the transition to the ground state (at low excitation energy) and to the lowest excited states of the final nucleus which have hole structure in accordance with

nuclear spectroscopy data.

3. FWHM of the resonances related to doorway state decay to the continuum is lower than 50 KeV. This estimation is rather close to results obtained for the reaction Si(p,γ) and for neutron scattering 1). It is necessery to point out that the appropriate value $\Gamma^{\uparrow}$ deduced from (γ,p) reaction is considerably higher (in the case of ^{45}Sc(γ,p) reaction is about 300 KeV 14).

4. In the excitation energy range E_{γ}= 16-19 MeV excited states have isospin $T=T_{<}$. This conclusion is confirmed indirectly by decrease of contribution of transitions to the ground state of final nucleus at E_{γ}>18 MeV.

5. It seems nessesery to give microscopical explanation of doorway state structure observed for the reaction ^{58}Ni(γ,n)^{57}Ni (the number of resonances and their positions).

6. It is of interest that the transitions to the lowest states of final nucleus give considerable contribution to the total cross-section of the ^{58}Ni(γ,n)^{57}Ni reaction. This contribution is abou+ 25 % in the energy range under study.

References

1. H. Feshbach. In: Proc. Intern. Confer. on Study Nucl. Structure with Neutr. N.H. 1966, 257.
2. O. Hirzel, H. Waffler. Helv. Phys; Acta. 20, 373 (1947)
3. B.S. Ratner. Sov. Journ. Particles and Nuclei. 12, 600 (1981)
4. D.G. Owen, E.G. Muirhead, B.M. Spicer. Nucl. Phys. A140, 523 (1970)
5. J.B. Seaborn, D. Drechel, H. Arenhovel, W. Greiner. Phys. Lett. 23, 576 (1966)
6. B.S. Ratner, A.N. Sergiyevsky, S.S. Verbitsky. Nucl. Phys; A285, 71 (1977)
7. V.I. Bondarenko, M.G. Urin. Preprint MIFI, 059-86 (1986)
8. S.S. Verbitsky, A.M. Lapik, B.S. Ratner A.N. Sergiyevsky. JETP Pisma, 27, 315 (1978)
9. A.M. Lapik, B.S, Ratner, S.S. Verbitsky. In: Intern. Confer. on Nucl. Phys. with Electromagn. Interactions. Abstr. of Contrib. Papers
10. S.S. Verbitsky, A.V. Veselovsky, I.N. Efimov, A.M. Lapik, B.S. Ratner. Preprint INR. 0476 (1986)
11. S.C. Fultz, R.A. Alvarez, B.L, Berman, P. Meyer. Phya. Rev. C10, 608 (1974)
12. E. Van Camp, R. Van de Vyver, H. Ferdinande, E. Kerkhove, R. Carchon, J. Devos. Phys; Rev. C22, 2396 (1980)
13. Nucl. Data Sheets. V20, N3, 357
14. D. Ryckbosch, E. Van Camp, R. Van de Vyver, E. Kerkhove, P. Van Otten, P. Berkvens, H. Ferdinande. Phys. Rev. C24, 448 (1982)

ASTROPHYSICAL ASPECTS OF THE PROBLEM OF GIANT RESONANCES IN NUCLEI

V.V. Balashov

Institute of Nuclear Physics, Moscow State University, Moscow 119899, USSR

The advances in astrophysics are closely associated with the development of the physics of atomic nucleus. The urgent astrophysical problems make it necessary at present to treat a very broad class of nuclear problems ranging from the most novel problems bearing on the quark structure of matter to those pertaining to the commonly studied brances of the low-energy nuclear physics.

The aim of the present work is to examine some of the astrophysical aspects of one of the most extensively discussed problems of nuclear physics, namely, the problem of giant resonances. The work has arisen from the rapid evolution of a new trend in the astrophysics and the cosmic ray physics which is called sometimes the high (superhigh) energy gamma-astronomy. We mean the detection of the gamma quanta of energies above 10^{12} - 10^{15} eV in the composition of the galactic (and, maybe, metagalactic) cosmic rays. What is the information about the Universe that they carry back to the Earth? This question has not been answered yet; moreover, we cannot even make sure that the events detected on the Earth, which we attribute to the superhigh-energy gamma-quanta, are actually due to such quanta, rather than to some other (maybe quite new for us) particle species.

The key point of the examined problem is to deal with the origin and the generation mechanisms of such cosmic gamma-quanta. Recently, V.L. Korotkikh, I.V. Moskalenko and the present author proposed a special, so-called photonuclear, mechanism of their generation /1/ which is essentially as follows: A relativistic nucleus of primary cosmic rays (PCR) interacts with the universal microwave radiation or with the soft photons near discrete galactic sources. If the nuclear Lorentz-factor Γ_A is high, the photon energy in the rest-nucleus frame appears to be sufficient for giant resonance or direct photo-disintegration to occur in the nucleus. It is well known in the physics of photonuclear reactions that the product-nuclei generated by the decays of giant resonances remain in their excited states within a high probability. Their de-excitation is accompanied by the gamma-quanta whose energy in the rest-nucleus frame may reach several MeV. In the observer reference frame, an excited relativistic nucleus is a source of narrow-directional gamma-ray emission whose highest energy is of the order of $\Gamma_A \times$ MeV.

The concept of photonuclear mechanism of cosmic gamma-ray generation is a direct extension of the long-known ideas concerning the π^0-meson photoproduction in the interactions of superhigh-energy primary cosmic ray protons with the soft photons of the universal microwave radiation /2/. The two mechanisms are directly relevant to the fundamental problem of the primary cosmic ray energy spectrum cutoff at the high-energy side. It should be borne in mind, however, that our ideas concerning the primary cosmic ray composition are subject to substantial alterations nowadays. For example, whereas all the complex nuclei (heavier than helium) were considered quite recently to constitute a negligible fraction of the PCR composition, the latest data are indicative of quite a different pattern, namely, the data of the Japanese-American Collaboration JACEE /3/ show that at a 10^{15}eV energy the fraction of Fe nuclei in the PCR composition reaches several dozens of percent. In such a situation, the examination of the role of the complex nuclei of PCR belong no longer to the exotic scientific domain, but gets quite practical.

In our first estimates /1/, the nuclear-to-proton PCR component contribution ratio (as calculated for energy per a nucleon) was taken to be 0.1 %. To get a higher definiteness, as regards the nuclear physics, the calculations were carried out for the ^{16}O nucleus whose basic photo-disintegration channels have properly been studied in experiments /4/. In the calculations, use was made of the Planck distribution for the universal microwave radiation with temperature $kT = 2.5 \cdot 10^{-4}$ eV and of the power-law PCR energy spectrum

$i_A(\Gamma_A) = I_A \cdot \Gamma_A^{-s}$, $i_p(\Gamma_p) = I_p \cdot \Gamma_p^{-s}$. The calculations have shown that at the adopted concentration of complex nuclei the photonuclear mechanism contribution to the diffuse gamma-ray emission in the 10^{15} - 10^{17} eV range dominates the contribution of the photomeson mechanism which was considered until now to be of major importance (see Fig. 1). It also dominates the contribution of π°-production in the strong interactions of primary protons with the protons and other components of interstellar gas. The reasons for such dominance are quite obvious; they are (i) a lower nuclear photo-disintegration threshold compared with the pion photoproduction threshold and (ii) a high number density of the photons of the universal microwave radiation.

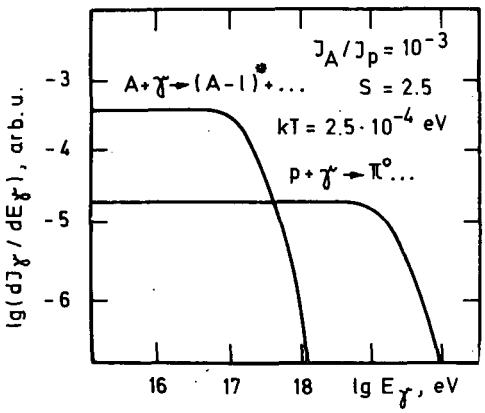

Fig. 1
Energy distribution of gamma-quanta produced by protons and nuclei on the universal microwave radiation photons

The result presented in Fig. 1 is of interest only as regards the methods and should not be related directly to the spectrum of the diffuse gamma-ray emission incoming to the Earth from the Metagalaxy. The fact is that it is just in the range of $E_\gamma = 10^{15}$ - 10^{16} eV where the maximum is known in the gamma-quantum absorption factor due to the interactions of the quanta with the photons of the universal micorwave radiation and, so, the free path of the gamma-quanta of such energies is as small as tens of kpc, i.e. is of the order of the Galactic dimension.

The problem of cosmic gamm-ray generation by the discrete Galactic sources is more interesting. In recent years more and more data were obtained concerning the superhigh-energy gamma-quanta from the well-known Cyg X-3 source /5/. The various models for the source proper have been proposed and are studied theoretically; different versions of the nature of the gamma-ray emission from the source are discussed. Fig. 2 shows the integral spectrum of the gamma-quanta from the discrete Cyg X-3 source together with the results of our calculations /1/ allowing for the photonuclear mechanism (dashed curve 1), the mechanism of π°-meson production on protons (curve 2), and the reaction of π°-meson production in the strong pp-interactions (curve 3). We employed the schematic discrete source model known in astrophysics, namely, the superhigh-energy gamma-rays are generated in the strong and electromagnetic interactions of the source-generated ultrarelativistic protons with the soft photons and baryons near the source. Such a scheme may be used as a first approximation to the physical model of a binary star (a neutron star and companion star) and was actually used earlier when discussing the spectrum of the gamma-ray emission from Cyg X-3 /6/. We have introduced two additional aspects in the model, namely, the nuclear component of the primary corpuscular flux and the photonuclear mechanism of gamma-quantum generation. The PCR is characterized by two parameters, by the relative number density of nuclei and protons I_A/I_p and by the spectral slope S. The gamma-quantum generation medium is also characterized by two parameters, namely, by the photon-to-baryon (nucleon) number ratio $X = N_{ph}/N_B$ and by the mean photon energy $\bar{\varepsilon}$.

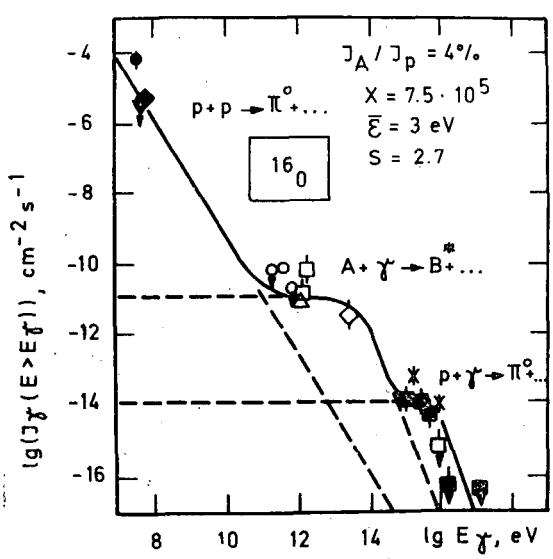

Fig. 2
Integral spectrum of gamma-quanta from the Cyg X-3 discrete source /5/. The solid line summarizes the contribution from the various generation mechanisms (see the text) /1/.

The calculations have shown that in a broad range of the model parameters the resultant gamma-ray spectrum exhibits a characteristic step-like form

with a pronounced contribution from the photonuclear mechanism in the middle of the spectrum. It is just such a step-like form that is exhibited by the integral spectrum of gamma-ray emission from Cyg X-3 constructed using all the data obtained by various groups. Without attributing a significant physical meaning to the particular values of the model parameters displayed in Fig. 2, we shall note that the general form of the gamma-ray-emission from Cyg X-3 in a broad energy range from 10^8 to 10^{17} eV can readily be accounted for in terms of the discussed schematic model. As in Fig. 1, the ^{16}O nucleus is taken as an example of complex nuclei in the PCR composition.

The next step in developing the approach proposed must be to go over to the realistic model parameters. This relates to describing both the primary corpuscular fluxes (their energy spectrum and composition) and the superhigh-energy gamma-quantum generation medium and concerns also the data on the elementary processes of gamma-emiter formation. In our work /7/, to meet the requirements of astrophysics, we substituted Fe nucleus for ^{16}O. Besides, apart from the photonuclear mechanism, we introduced the mechanism of production of excited nuclear fragments in the interactions of the PCR relativistic nuclei with the nucleons of the generation medium. Immediately, this approach gave rise to the problems relevant to nuclear physics. Although the cross section for the gamma-quantum absorption by Fe nuclei has long been known / 8/, we have to know much more, namely, in what manner are the various excited states of product-nuclei excited under the giant-resonance decay? Moreover, the resultant cosmic ray gamma-quantum spectrum depends essentially on the means of the de-excitation of such states, i.e. on the multiplicity and the mean energy of the nuclear gamma-quanta generated by the de-excitation process. The photonuclear reaction physics was not faced earlier with such questions. True, the like questions arose in other problems of nuclear physics (for example, when calculating the relative yield of isomers); however, not a single ready answer can be used.

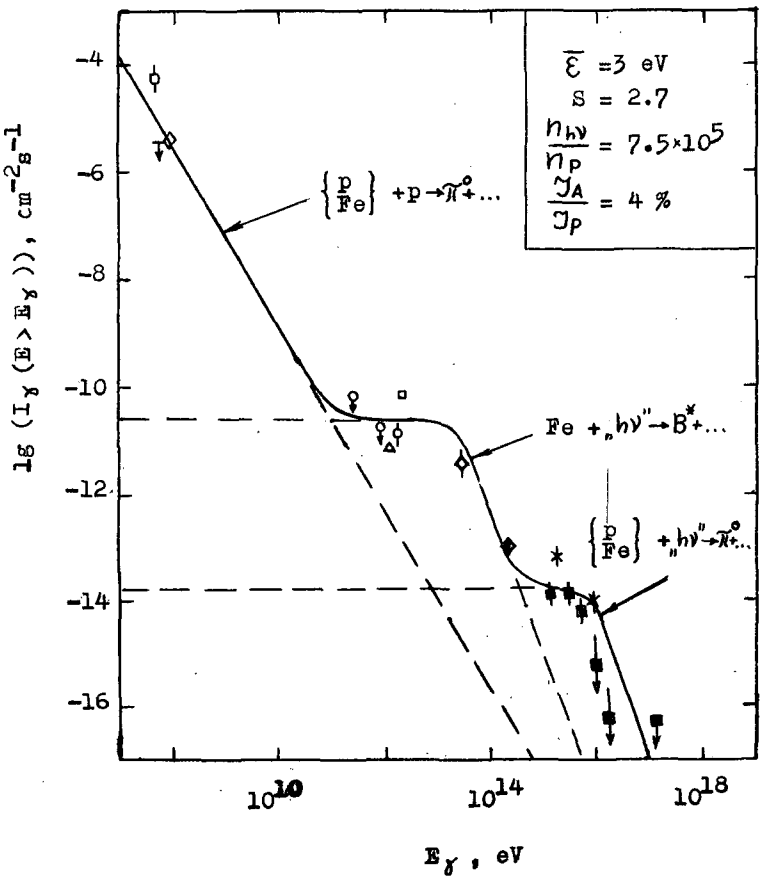

Fig. 3

Integral spectrum of the gamma-quanta of a discrete galactic source. The dashed lines show the calculated contributions from the various generation mechanisms. The solid line is the sum of the contributions. The data are for the Cyg X-3 discrete source /5/.

Fig. 3 shows the result of the calculations where the spectrum of the nuclear gamma-quanta generated as a result of photo-disintegration of Fe nuclei was taken to be uniform in the 0 - 9 MeV range, while the fraction of the transitions directly to the ground states of the daughter nuclei was considered to be negligible. As in our earlier calculations with ^{16}O nuclei, we again obtained the characteristic step-like form of the cosmic ray gamma-ray spectra from the discrete source with a dominating contribution of the photonuclear mechanism in the 10^{11} - 10^{14} eV range (at the effective temperature of the ambient photons of about few eV).

From the study we have concluded that the photonuclear mechanism is absolutely necessary to allow for in any further research bearing on the high- and super-high-energy gamma-ray astronomy. The relevant problems arise also in the nuclear physics. A new and important aspect appears in the problem of the decays of the

highly-excited collective states of nuclei, which has been the most difficult problem in the entire set of the problems relating to giant resonances since the sixties. Namely, we have to know, and be able to predict, the multiplicity and the energy distributions of the secondary gamma-quanta accompanying the giant resonance decays. The problem will prove to be particularly important if the indications are corroborated that the complex nuclei (Fe, etc.) are actually a noticable (and, maybe, dominant) component of the superhigh-energy PCR. In such a case special attention will have to be paid to another mechanism of the cosmic ray gamma-quantum generation in which the gamma-emitters prove to be the excited nuclear fragments produced in the inelastic strong interactions of ultrarelativistic nuclei with protons of medium: $A + p \rightarrow B^* + \ldots$, $B^* \rightarrow B + \gamma$. It has been established reliably nowadays that the production of such excited fragments in the corresponding inverse process $p + A \rightarrow B^* + \ldots$ involves an active role of the multipole giant resonances (very interesting information on how such processes proceed can be derived from the coincidence experiments which get more and more habutual from day to day). As to the existing theory of nuclear disintegration by protons and by other high-energy particles, it has not been applied to the medium and heavy nuclei yet (including the nuclei near Fe which are of particular interest in astrophysics), although it covers the various aspects of the production of excited daughter nuclei and their de-excitation (see, for example, /9/). To extend the theory to the range of medium and heavy nuclei is an urgent task not only in the nuclear physics proper but also in its applications to astrophysics.

References

/1/ Moskalenko I.V. Graduation paper, 1985; Moscow State Un-ty.
Balashov V.V., Korotkikh V.L., Moskalenko I.V. Vestnik Moskovskogo Universiteta, 1987, v. 28, p. 6.

/2/ Zatsepin G.T., Kuz'min V.A. Pis'ma ZETP, 1966, v. 4, p. 144, Greiser K. Phys. Rev. Lett. 1966, v. 16, p. 748.

/3/ Jones W.V. Nucl. Phys. 1984, v. A418, p. 139.

/4/ Coldwell J.T. et al. Phys. Rev. Lett., 1967, v. 19, p. 447.

/5/ Vladimirsky B.M. et al. Uspekhi Phys. Nauk, 1985, v. 145, p. 255.

/6/ Aharonian F.A. et al. Proc. 19th ICRC, 1985, v.I. p. 255.

/7/ Balashov V.V., Korotkikh V.L., Moskalenko I.V. Int. Symp. "Modern Developments in Nuclear Physics", Novosibirsk, 1987.

/8/ Dol'bilkin B.S. et al. Yad. Phys., 1969, v.9.

/9/ Balashov V.V., Dolinov V.K., Korotkikh V.L., Lanskoy D.E. Vestnik Moscowskogo Universiteta, 1986, v. 27, p. 64.

NEGATIVE PARITY STATES IN THE SPECTRUM OF ^{6}Li FROM ELASTIC SCATTERING AND RADIATIVE CAPTURE OF ^{3}He BY ^{3}H.

A. Mondragón and E. Hernández
Instituto de Física UNAM
Apdo. Postal 20-364, 01000 México, D.F. MEXICO

ABSTRACT. The results of a new resonance analysis of the elastic scattering of ^{3}He by ^{3}H in odd parity states and the radiative capture of ^{3}He by ^{3}H in the first excited state of ^{6}Li are presented. We give evidence for a very broad level of ^{6}Li at E_{Li} = 26.5 MeV with $J^\pi = 2^-$ S,T = 1,1 not previously reported. Also, the change in shape in the angular distribution and the broad maximum observed in the cross section for radiative capture of ^{3}He by ^{3}H in the first excited state of ^{6}Li at high energies are explained in terms of the interference of three very wide $^{33}F_j$ overlapping resonances. Numerical values for the resonance energies, the total, elastic and radiative widths are given.

1. INTRODUCTION

The isobaric diagram of nuclei with A = 6 shows that all excited states of ^{6}He and ^{6}Li, and all states of ^{6}Be are unbound with respect to nucleon and to cluster decay(1). In ^{6}Li, the study of the ^{4}He + d system has led to good information about the T = 0 states. The relatively small widths of the 0^+ and 2^+, T = 1, states below 6 MeV have made it possible to study them in several reactions and in inelastic scattering. However, the other states of ^{6}Li are very poorly known, except that it is clear that there are no other sharp or fairly sharp T = 1 states of ^{6}Li below ~ 17 MeV(2). In this work we are particularly interested in the T = 1, negative parity, unbound states of ^{6}Li that are strongly coupled to the ^{3}He + ^{3}H channel. Evidence for these odd parity states comes from the elastic scattering and radiative capture of ^{3}He by ^{3}H in odd orbital angular momentum states.

A phase shift analysis of the elastic scattering of ^{3}He by ^{3}H due to Vlastou et al(3) shows resonances JT = 21,01 at E_{Li} = 21.0 MeV and 21.5 MeV respectively in the $^{33}P_j$ waves (L = 1), and resonances JT = 41,31 at E_{Li} = 25.7 MeV and 26.7 MeV respectively in the $^{33}F_j$ waves (L = 3), but no resonance is reported with JT = 21 for L = 3. The negative parity states of ^{6}Li seen as resonances in the $^{33}P_2$ and $^{33}F_j$ waves in the elastic collision will show up in the radiative capture of ^{3}He by ^{3}H in the first excited state of ^{6}Li, which is a $^{13}D_3$ state(4) at E_{Li} = 2.18 MeV with $J^\pi = 3^+$ and T = 0, but not in the capture in the ground state $J^\pi = 1^+$, T = 0 since the selection rules forbid these transitions. Recently, D. Schenzle and P. Kramer(7) computed the energy spectrum of ^{6}Li taking into account the non-central terms in the nucleon-nucleon interaction. They found the three $^{33}F_j$ states of negative parity split in one $^{33}F_4$ states at E_{Li}= 24.9 MeV, and the $^{33}F_2$ and $^{33}F_3$ state degenerate at E_{Li} = 27.8 MeV. It was also found that these states are almost pure {3,3} partitions. These results strongly suggest that the broad maximum in the excitation function, dots in Fig(2), are due to the presence of three very wide $^{33}F_j$ overlapping resonances, two of which, $^{33}F_2$ and $^{33}F_4$, produce coherent contributions to the photon field that interfere.

2. RESONANCES IN THE ELASTIC SCATTERING OF ^{3}He BY ^{3}H.

The elastic scattering of polarized ^{3}He by ^{3}H was measured by Vlastou et al(3) over the energy range from 20 to 33 MeV. These authors represented the cross section and polarization of the scattered and recoil particles in terms of 18 real phase shifts, which they called solution I, and then they made a parametrization of the resonant phase shifts in terms of the single level R – matrix formalism and found the resonances mentioned above. They also made a second, more realistic analysis

of the same elastic data, called solution II, in terms of 18 complex phase shifts, to account for the possible influence of the open channels. A resonance analysis of the complex phase shifts of the more realistic solution II was not attempted.

In this work we made a χ^2 fit of the single level $S_{\ell j}$ matrix formula

$$S_{\ell j} = e^{i2\phi_{HS}(a)} \left[e^{i2\beta_{\ell j}} |B_{\ell j}| - ie^{2\phi_{\ell j}} \frac{\Gamma_{el,\ell j} \; F_\ell(k)}{E - E_{\ell j} + i\frac{1}{2}\Gamma_{\ell j}} \right] \qquad (1)$$

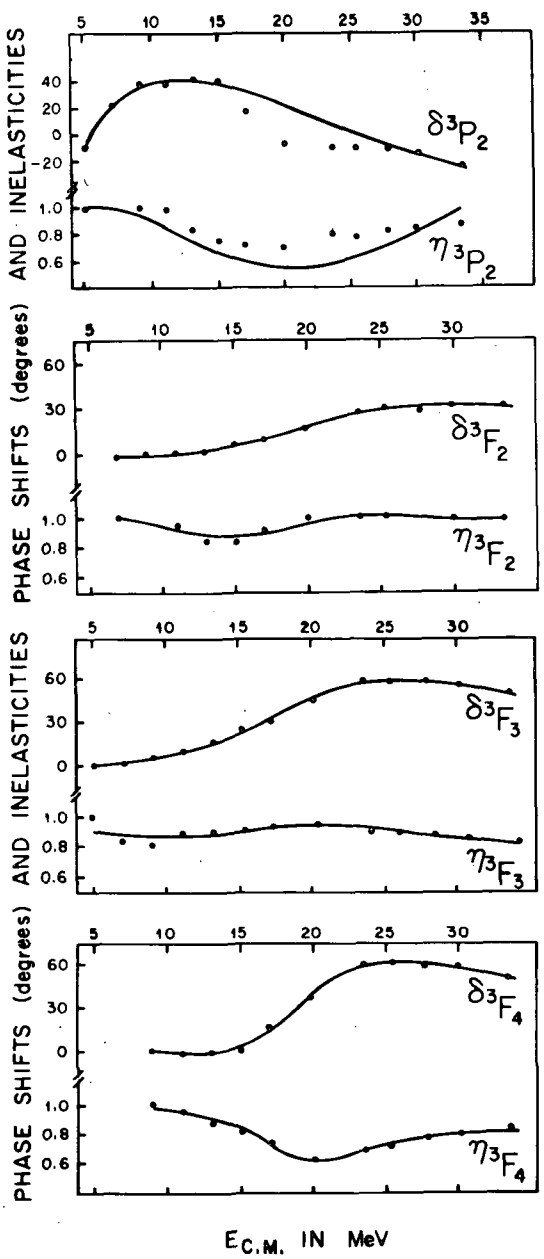

Fig 1. The phase shifts $\delta_{^3L_j}$ and inelasticities $\eta_{^3L_j}$ of the L_j partial waves as function of the ^{3}He Lab energy. The dots show the experimental data of Vlastou et al[6]. The full line —— is the best fit of the single resonance plus background, eq(1), to the data.

to the complex phase shifts of the $^{33}P_2$, $^{33}F_2$, $^{33}F_3$ and $^{33}F_4$ partial waves of solution II of Vlastou et al[3] over the energy range from 5 to 33 MeV. In the notation of Vlastou $S_{\ell j} = \eta_{\ell j}\exp\{2iRe\delta_{\ell j}\}$ and $\eta_{\ell j} = \exp\{-2Im\delta_{\ell j}\}$. In expression (1), $F_\ell(k)$ is the Coulomb penetration factor which is a known function of the masses, charges and relative energy of the two colliding nuclei[9] with no free parameters. $\phi_{HS}(a)$ is the phase shift due to a charged hard sphere of radius a and charge $Z_{He}Z_H$. The magnitude $|B_{\ell j}|$ of the background term, $\beta_{\ell j}$, and the phase of the elastic width $\phi_{\ell j}$ are linear functions of the energy with the same value of the slope. The resonance energy $E_{\ell j}$, the elastic width $\Gamma_{el,\ell j}$ and the total width $\Gamma_{\ell j}$ are constants independent of the energy. Therefore, in (1) there are ten parameters that may be varied.

The fit, was performed using the computer programme FASFIT with an automatic search routine, all the ten parameters were varied in each search cycle until the best set of parameter was found. The quality of the fit to all $^{33}F_2$, $^{33}F_3$ and $^{33}F_4$ complex phase shift data is very good. We found a very broad $^{33}F_2$ level in ^{6}Li at E_{Li} = 10.76 MeV with $J^\pi = 3^-$, S = 1, T = 1, not yet reported. The result of this fit is shown in Fig(1) and the numerical values of the resonance parameters of the elastic channel are shown in Table 1.

3. RESONANCES IN THE DIRECT RADIATIVE CAPTURE OF ^{3}He BY ^{3}H.

The differential cross section for direct capture from the continuum to a bound state of the ^{3}He-^{3}H system with emission of electric dipole radiation, computed in perturbation theory to first order in the electromagnetic field, may be written as

$$\frac{d\sigma}{d\Omega} = \frac{1}{4\pi}\sigma_T + a_2(E)\,P_2(\cos\theta) \qquad (2)$$

where σ_T is the total yield of the reaction

Table 1. Resonance parameters

State	$E_{\ell j}$ (MeV)	$\Gamma_{\ell j}$ (MeV)	$\Gamma_{el,\ell j}$ (MeV)	$\Gamma_{\gamma,\ell j}$ (eV)
$^{33}P_2$	2.49	3.03	3.01	33.58
$^{33}F_2$	10.76	8.74	8.28	77.69
$^{33}F_3$	8.98	6.73	6.11	00.087
$^{33}F_4$	9.18	5.37	4.23	713.58
$\Delta\chi_{12-32} = -48°$	$\Delta\chi_{12-34} = 110°$	$\Delta\chi_{32-34} = -158°$		

$$\sigma_T = \frac{\pi\lambda^2}{(2s+1)} \sum_{\ell j} |Q_{\ell j}|^2 \qquad (3)$$

and

$$a_2 = \frac{3\lambda^2}{8(2s+1)} \sum_{\ell j} \sum_{\ell' j'} \left\{ \left[\frac{1}{3}\delta_{\ell\ell'}\delta_{jj'} - \sqrt{(2\ell+1)(2\ell'+1)}\, Z(\ell\ell';jj') \right] Q^*_{\ell j} Q_{\ell' j'} \right\} \qquad (4)$$

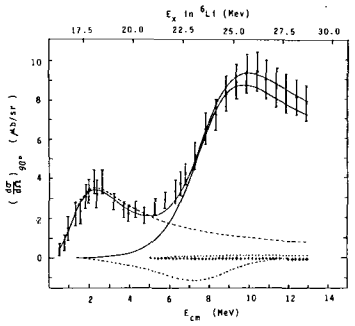

Fig 2. differential cross section for the $^3H(^3He,\gamma_1)^6Li$ reaction at 90° Lab.— Best fit of interference resonances formula to the data.

in these expressions, $Q_{\ell j}$ is proportional to the radial integral of the electric dipole operator between the initial scattering state of $^3He - ^3H$ and the final bound state of ^6Li, s is the channel spin, ℓ is the orbital angular momentum of the relative motion of ^3He and ^3H and j is the total angular momentum of the system, and

$$Z(\ell\ell';jj') = \sum_{M_i} (\ell 0 1 M_i | \ell 1 j)(\ell' 0 1 | \ell' 1 j') \begin{pmatrix} j_f & 1 & j \\ -M_i & 0 & M_i \end{pmatrix} \begin{pmatrix} j_f & 1 & j' \\ -M_i & 0 & M_i \end{pmatrix}$$

In LS coupling, the first excited state of ^6Li is described as a $^{13}D_3$ state[4], hence considering waves up to $\ell = 3$, there are only four partial waves, i.e, $^{33}P_2$, $^{33}F_2$, $^{33}F_3$ and $^{33}F_4$ which can contribute to the electric dipole transition to this state. In order to make apparent the resonant structure in the cross section due to the nucleus-nucleus interaction in the entrance channel we expand the wave function of the relative motion of ^3He and ^3H in terms of Gamow states[8], keeping only one resonant term in each partial wave and dropping the background term, we obtain

$$Q_{\ell j} = \sqrt{(2j+1)}\, i^{\ell+1} e^{i(\sigma_\ell - \sigma_0 + \phi_{\ell j} + \chi_{\ell j})} \frac{\Gamma_{el,\ell j}^{1/2}\, \Gamma_{\gamma,\ell j}^{1/2}\, F_\ell(k)}{(E - E_{\ell j}) + i\frac{1}{2}\Gamma_{\ell j}} \qquad (5)$$

where σ_ℓ is the Coulomb phase , $e^{i\phi_\ell} \Gamma_{el,\ell j}^{1/2}$ is the transition amplitude from the scattering state to the resonant state of energy $E_{\ell j} - i\frac{1}{2}\Gamma_{\ell j}$, $e^{i\chi_{\ell j}} \Gamma_{\gamma,\ell j}^{1/2}$ is the transition amplitude from the resonant state to the first excited state of ^6Li, and $F_\ell(k)$ is the Coulomb penetration factor[9].

The cross section for the reaction $^3H(^3He,\gamma_1)^6Li^*$ was measured by Blatt et al[5] from E_{He}= 1 MeV up to 5 MeV and by Ventura et al[6] from E_{He} = 6 MeV up to 26 MeV. In order to make a fit of expressions (2) - (5) to the experimental data of Ventura et al[6],we proceeded as follows:

i) The numerical values of the total yield, dots in Fig(4), and the coefficient $a_2(E)$ were obtained from a least squares fit of expression (2) to the angular distribution of γ_1 photons Fig(3)

ii) Once we knew the numerical values of σ_T , dots in Fig(4), we inserted the numerical values of the elastic channel parameters in (5) and made a fit of the sum of resonant terms (3) to the numerical values of σ_T and obtained numerical values of the radiative widths $\Gamma_{\gamma_i,\ell j}$. A fit of the resonant expressions (4) and (5) to the numerical values of $a_2(E)$ gave us values of the relative radiative phases $\chi_{\ell j} - \chi_{\ell' j'}$. With this first set

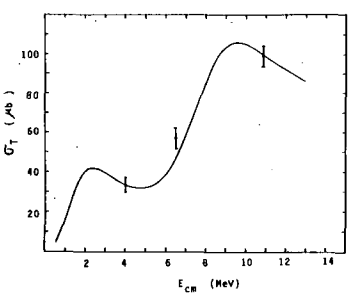

Fig 4. Total yield of the reaction $^3H(^3He,\gamma_1)^6Li$ —— Best fit of interfering resonances formulae to the data.

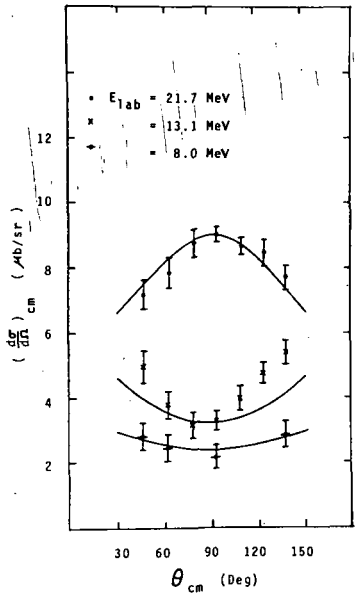

Fig 3. ✝, ✱ and ✝ photon angular distribution of $^3H(^3He,\gamma)^6Li$ reaction. —— Best fit of interfering resonances formulae to the data.

of resonant parameters we made a χ^2 fit to the excitation function taken at 90° Lab. dots in Fig(2), and refined the fits to σ_T and $a_2(E)$ until we obtained the best set of parameters. Some of these results are shown in Table 1. The solid lines in Fig(2),(3) and Fig(4), show the best fit of our formulae to the experimental data.

4. CONCLUSIONS.

From a careful numerical analysis of the elastic scattering of ^3He by ^3H in odd orbital angular momentum, L = 3, in which the unitarity of the resonant S matrix and the threshold behaviour were exactly taken into account, we have found a very broad F - wave level in the spectrum of ^6Li, at E_{Li} = 26.52 MeV with $J^\pi = 2^-$, S = 1 and T = 1 which had not been reported in previous studies. The negative parity level with S = 1, T = 1 and J = 3 was found at E_{Li} = 24.64 MeV that is, shifted by almost 2 MeV to lower energy with respect to the value quoted by Ajzenberg-Selove(1). The negative parity level with S = 1,T = 1 and J = 4 was found at the same energy as in Ajzenberg-Selove. From the numerical analysis of the elastic scattering of ^3He by ^3H in the L = 1 state ($^{33}P_2$ wave) we found a negative parity, S = 1, T = 1,J = 2^- at 18.28 MeV. Most probably this is the 2^- p-level reported by Vlastou et al at ~ 21 MeV.

The identification of the $J^\pi = 2^-$, S = 1,T = 1 state in the spectrum of ^6Li as a very wide resonance in the $^{33}F_2$ elastic wave in the $^3He + ^3H$ channel allowed us to solve a long standing puzzle in the radiative capture of ^3He by ^3H in the first excited state of ^6Li. The change in shape of the angular distribution of the cross section for this reaction observed at E_{He} = 21.7 MeV is produced by the interference of the coherent contribution of the $^{33}F_2$ and the $^{33}F_4$ resonances to the photon field. The broad maximum in the excitation function observed at E_{He} = 21.8 MeV is due to the presence of three very wide overlapping resonances. We also give numerical values of the resonance energies, the total, elastic and radiative widths.

REFERENCES

1) Ajzenberg-Selove F. Nuclear Phys A449, (1984)1

2) Ajzenberg-Selove F. "The Structure of the light nuclei" in Proc. of the International School-Seminar on Heavy Ion Physics. Joint Institute for Nuclear Research, Dubna, USSR, 1986.

3) Vlastou, R., J.B.A. England, O. Karban and S. Baird, Nuclear Phys. A292,(1977)22

4) Inglis, D.F., Rev. Mod. Phys 25, (1953) 390

5) Blatt, S.L.,A.M. Young, S.C. Ling, K.F. Moon and C.D. Porterfield Phys. Rev 176, (1969) 1147.

6) Ventura, E., C.C. Chang and W.E. Meyerkopf Nuclear Phys A173, (1971) 1. Ventura, E., J.R. Calarco and W.E. Meyerkopf Phys Lett. B46, (1973) 364.

7) Kramer, P., G. John and D. Schenzle. "Group Theory and the Interaction of Composite Nucleon Systems".Braunschweig, Friedr. Vieweg und Sohn (1981) pp. 193

8) Hernández E.and A. Mondragón, Phys. Rev. C29, (1984) 722; Mondragón A. and J. M. Velázquez "Lectures Notes in Physics" 263, (1986) Heidelberg Springer Verlag pp 353.

9) Humblet, J., Nuclear Phys. 50, (1964) 1.

POLARIZATION EFFECTS IN THE $^6Li(^3He,\alpha)\,^5Li - \alpha + p$ REACTION AT LOW ENERGIES

S.Burzyński, J.Turkiewicz, K.Rusek, I.M.Turkiewicz and P.Żuprański
Institute for Nuclear Studies, Hoża 69, 00-681 Warsaw, Poland

Abstract: The sequential reaction $^6Li(^3He,\alpha)^5Li - \alpha + p$ has been studied at energies of 1.5, 1.73, 3.0 and 3.5 MeV. From the kinematically complete p-alpha coincidence experiment the angular distributions of protons from the decay of the ^5Li g.s. nucleus have been derived. Their asymmetry relative to the ^5Li momentum has been explained in terms of a polarization of the intermediate ^5Li system.

The energy spectrum of particles emitted in ^3He induced reactions on the ^6Li target contains mainly a continuum coming from the processes with three particles in the final state 1-4): $^6Li+^3He \rightarrow \alpha + \alpha + p$. At low energies the direct break-up in which the three particles in the exit channel are produced simultaneously has a very small cross section 2). The basic mechanism for this reaction is then the sequential break-up characterized by the formation of the intermediate systems from pairs of particles (alpha-alpha) and (alpha-p) which subsequently decay by a particle emission. The reaction proceeding by the intermediate (alpha-p) system which is considered to be ^5Li nucleus is the subject of the present report.

The measurements of the $^6Li(^3He,\alpha)\,^5Li$ reaction were carried out using the ^3He beam from the Van de Graaff accelerators in Warsaw (1.5 and 1.73 MeV) and at the Joint Institute for Nuclear Research in Dubna (3.0 and 3.5 MeV). The target was 100 ug/cm2 thick LiF (enriched up to 95% of ^6Li) layer evaporated onto a 10 um/cm2 carbon foil. The energy loss of the incident ^3He beam in the target ranged from 75 keV to 125 keV depending upon the ^3He energy. The Rutherford cross section for the elastic scattering of the $^3He+^{19}F$ measured simultaneously with the reaction on ^6Li, w as used to obtain the absolute normalisation of the cross section.

The geometrical scheme of the experiment is shown in Fig. 1. The particles emerging from the target were detected by two detectors working in coincidence. Because of favorable kinematical conditions (Q-value for the reaction under study is 16.87 MeV) no identification of particles was necessary. One detector, kept in a fixed position at 90° to the beam had the thickness of the depletion layer adjusted to be a full energy detector for alpha particles from the studied energy range, but a transmission detector for protons. The second detector of a depth of 2.5 mm, was covered by aluminum foil thick enough to stop all particles but protons with energies above 2.5 MeV. Proton detector was set in the reaction plane defined by the incident ^3He and the registered alpha particle. Its position was changed from 30° to 130° of the lab angle in 10° step, on opposite side of the ^3He beam, that means on the side of ^5Li recoil. The coincidences were stored on a magnetic tape as 3-fold events: the energies of an alpha-particle (E_1) and a proton (E_2) and the time difference between them. Time resolution of the prompt peak in the TAC spectrum was typically 50 ns. Random coincidences, monitored by recording events over a vider time range, were negligible. Signals were processed by a Nuclear Data 4420 computer, which controlled the write up of the data on tape and provided for several on-line control displays.

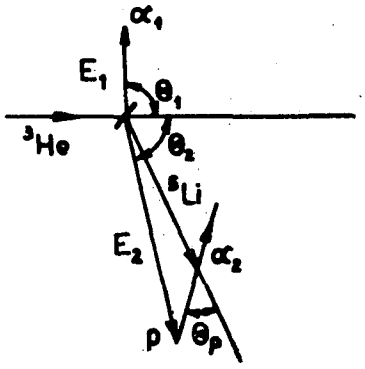

Fig. 1

During the off-line analysis event by event recorded data were sorted to produce bidimentional spectra in the (E_1-E_2) plane, gated by TAC window.
For two detectors used in coincidence at a particular pair of angles, the particles energies E_1 and E_2 are lying in the (E_1-E_2) plane on the well determined contour, resulting from the energy relation for a kinematically complete three--body reaction experiment 5).
Each contour corresponds to the total energy E_T equal to the sum of the reaction Q-value and the kinetic energy brought in by the incident particle.

In our experimental setting only one contour was observed for Q value equal to 16.87 MeV with a width defined by the total energy resolution. Along the locus clusterings of experimental points were observed corresponding to the sequential processes proceeding by the intermediate unbound states (Fig. 2):

^{5}Li, g.s., 3/2-, Γ = 1.5 MeV 6), from the reaction ^{6}Li(^{3}He,α)^{5}Li

^{8}Be, 11.4 MeV, 4+, Γ = 3.5 MeV 6), from the reaction ^{6}Li(^{3}He,p)^{8}Be.

Projection of the kinematical contours onto the E_1 axis yielded the one-dimentional alpha particle spectra. Some of them are shown in Fig. 3. They mainly contain two broad peaks, the higher energy one being a contribution from ^{5}Li g.s. and the lower energy one from the ^{8}Be 11.4 MeV state. The procedure of decomposition of these two contributions was applied by fitting the energy distributions of alpha particles in the frame of final state interaction theories 7).

Alpha particle spectra in the range corresponding to ^{6}Li(^{3}He,α)^{5}Li$_{gs}$ transition were integrated to obtain the (α-p) angular correlations corresponding to the ^{5}Li g.s. decay. They were transformed into the angular distributions of protons in the rest frame of the ^{5}Li using the three body kinematics formula of Ohlsen 5). These angular distributions are shown in Fig. 4. The positive angles correspond to the emission of protons in the direction nearer to the direction of the incident ^{3}He beam. Error bars contain both the statistical errors and the uncertainties resulting from ambiguities in energy spectra separation.

All the presented angular distributions are evidently asymmetric in respect to the direction of the emission of the ^{5}Li, denoted by 0° on the angle axis. The asymmetry observed at 1.5 MeV and 1.73 MeV is of the same type as that observed by Livesey and Piluso 3) at 1.25 MeV, shown also in Fig. 3 for comparison. One must comment on aa close similarity of the angular correlations measured at 1.25, 2.5 and 1.73 MeV, because the energy 1.5 MeV (corrected for energy loss in the target) corresponds to the 17.64 MeV level of the ^{9}B compound nucleus while other two energies fall beyond any know level. It would mean, that the process does not seem to be affected by an excited single level of the compound nucleus, contrary to the interpretation suggested in ref. 2). The smooth change of the measured angular distributions with the ^{3}He beam energy rather points to the direct process governing the reaction mechanism. The angular distribution measured at 3.0 MeV is rather flat. However at 3.5 MeV the asymmetry is again quite pronounced, but in this case more protons are observed at negative proton emission angles then at positives - just opposite to that at lower energies.

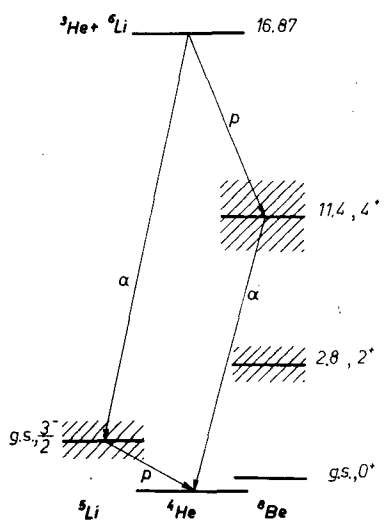

Fig. 2

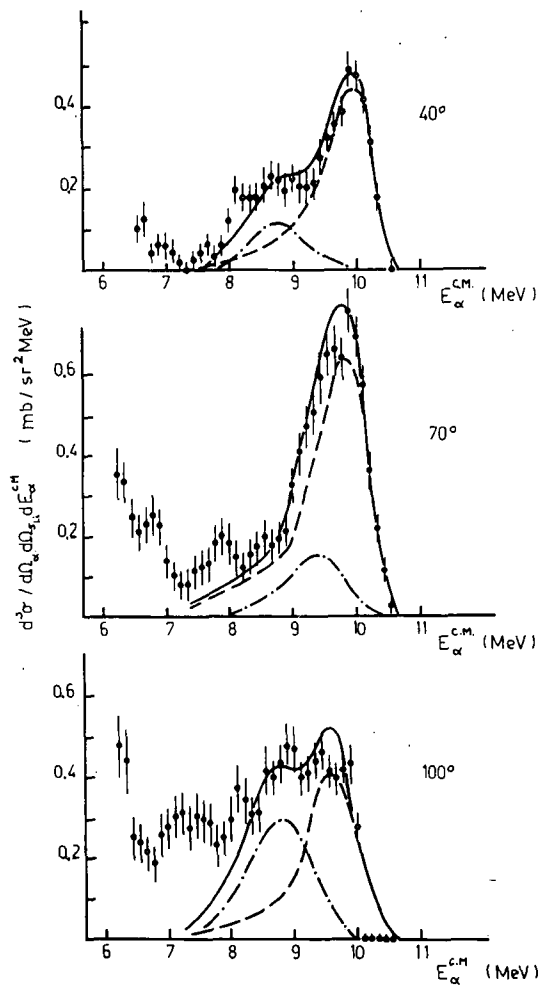

Fig. 3

The asymmetry of the ^{5}Li decay can be understood if one assumes, that this nucleus is formed during the first stage of the reaction in a polarized state. The angular distribution for the particle with spin s to decay into two particles with spins s_1 and s_2 is described in the rest frame of the decaying particle by the general expression given e.g. by Simonius 8):

$$W(\theta,\phi) = \sum_{kq} \frac{4\pi}{2k+1} A_k t_{kq} Y^*_{kq}(\theta,\phi)$$

t_{kq} are the spherical polarization tensors of rank k, which describe the polarization of the decaying particle,
$k=0,1,\ldots 2s$, $-k \leq q \leq +k$;
(θ,φ) are the angles defining the direction of the emission of one of the decay products;
A_k, the decay amplitudes are real and q-independent. Parity conservation in the decay implies $A_k=0$ for odd k. Thus the decay of ^{5}Li ground state of spin 3/2 into an alpha particle and a proton is completely determined by the polarization tensors t_{00}, t_{20}, t_{21} and t_{22}. Assuming A_0 equal to 1 according to the usual conventions 13) one can calculate $A_2=-1$. Using the coordinates in which the experimental angular distributions are presented, the angular distributions for the particular case of the ^{5}Li proton decay proceeding in the reaction plane can be written in a form:

$$W(\theta) = t_{00} - \frac{1}{2} t_{20} (3\cos^2\theta - 1) + \sqrt{6}\, t_{21} \sin\theta\cos\theta - \frac{3}{2} t_{22} \sin^2\theta$$

From this expression one can see immediately that the asymmetric angular distribution results from the term containing t_{21} component of the ^{5}Li tensor polarization. To describe the measured proton angular distributions this formula was transformed into

$$W(\theta) = A - B\cos^2(\theta - \theta_0)$$

where A, B and θ_0 are the following functions of the tensor components:

$$A = t_{00} - \frac{1}{4} t_{20} - \frac{1}{2}\sqrt{\frac{3}{2}}\, t_{22} + \frac{1}{2}\sqrt{\left(\frac{3}{2} t_{20} - \frac{3}{2} t_{22}\right)^2 + 6t_{21}^2}$$

$$B = \sqrt{\left(\frac{3}{2} t_{20} - \frac{3}{2} t_{22}\right)^2 + 6t_{21}^2}$$

$$\theta_0 = -\frac{1}{2}\, tg^{-1}\left(\frac{\sqrt{6}\, t_{21}}{\frac{3}{2} t_{20} - \sqrt{\frac{3}{2}}\, t_{22}}\right)$$

They were free parameters in the fit to the experimental angular distributions. The solid curves presented in Fig. 4 are the results of these fits. The best fit parameters are smoothly dependent on the incident energy, what indicates that the correct description of the experimental data is not fortuitous.

Parameters A and B determine the overall normalization and anisotropy of the distribution. The asymmetry is related to θ_0, where θ_0, the arctg function of all three tensor polarization components depends very strongly on their relative signs and magnitudes. Thus the observed experimentally change of the possition of the minimum in the proton angular distributions should reflect the energy dependence of the tensor polarization of ^{5}Li. In fact it contains also a hidden angular dependence on the energy-dependent ^{5}Li emission angle kinematically coupled to a fixed (90°) alpha-registration angle.

The source of this strong polarization can be found in the dynamic conditions of the reaction. It is well known that a strong angular momentum mismatch forces the transfer to occur in the reaction plane (see e.g. von Oertzen 10). Thus the transferred angular momentum l is perpendicular to the reaction plane (having a z-component $m_z=0$). The polarization of the transferred orbital angular momentum is transmitted to the total angular momentum transfer and hence to the polarization of outgoing particles through the coupling between l transfer and spins of the participating nuclei given by an appropriate Clebsch-Gordon coefficient 9). The ^{5}Li nucleus being the product of the very mismached reaction should then have very large vector and tensor polarization. Our measurements of the angular correlations are sensitive only to the second rank polarization 8) as explained above.

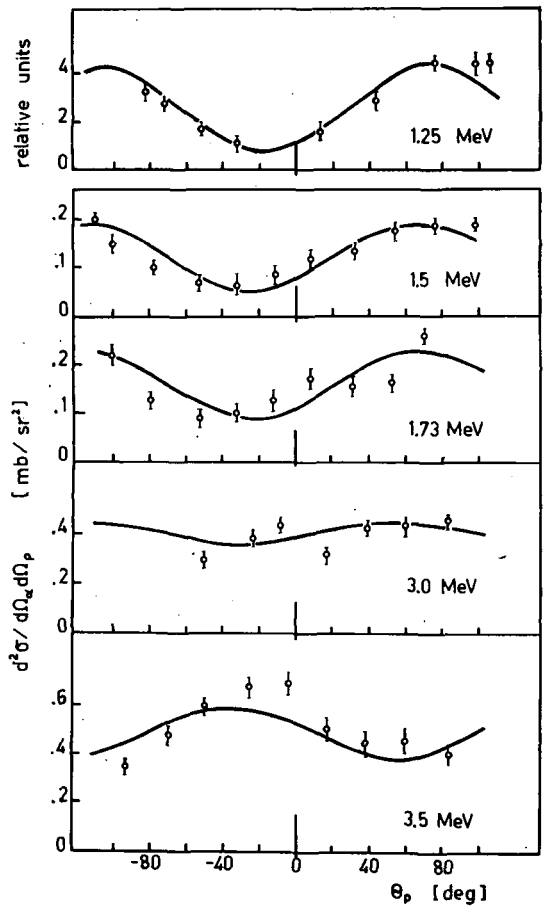

Fig. 4

REFERENCES

1. M.A.Reimann, P.W.Martin and E.W.Vogt, Can.J.Phys. 46(1968)2241.
2. D.T.Thompson and G.E.Tripard, Phys.Rev. C6(1972)452.
3. D.L.Livesey and C.J.Piluso, Can.J.Phys. 52(1974)1167.
4. J.C.Heggie and P.W.Martin, Phys.Lett. B43(1973)289.
5. G.G.Ohlsen, Nucl.Instr.Meth. 37(1965)240.
6. F.Ajzenberg-Selove and T.Lauritsen, Nucl.Phys. A413(1984)1.
7. S.Burzyński, J.Turkiewicz, K.Rusek, I.M.Turkiewicz and P.Żuprański, to be published in Nucl.Phys.
8. M.Simonius, Lecture Notes in Physics, 30(1973)38, Polarization Nuclear Physics.
9. G.R.Satchler, Direct Nuclear Reactions, Clarendon Press, 1983.
10. W.von Oertzen, Invited talk at XII Summer School on Nuclear Physics, 2-14 September 1979, Mikołajki, Nukleonika 25(1980)939.

$^7Li(^7Li, ^6He)^8Be$ SINGLE-PROTON STRIPPING REACTION ABOVE COULOMB BARRIER

O.V. Bochkarev, L.V. Chulkov, A.A. Korsheninnikov, E.A. Kuz'min, I.G. Mukha, G.B. Yankov

Abstract: The $^7Li(^7Li, ^6He)^8Be$ (Q = 7.28 MeV) reaction has been measured at $E_{lab}(^7Li)$ = = 22 MeV. Exact finite-range DWBA calculations reproduce the shape of angular distributions of the $^8Be(0^+)$ and $^8Be^+(2^+)$ states. The contribution of the compound reaction mechanism is less than 10 %.

1. Introduction

Transfer reactions are being studied for a long time. As far back as in 1959 $^9Be(^7Li, ^8Li)^8Be$ reaction was investigated /1/ as involving a transfer of a neutron from one of the initial nuclei to the other. At that time it was also expected that the $^7Li(^7Li, ^6He)^8Be$ reaction proceeded by a direct transfer of one proton between the colliding ^7Li nuclei /2/. But the measured angular distributions of ^6He at incident energies below the Coulomb barrier (2.5 MeV) have exhibited /3,4/ the absence of a strong structure, an almost total isotropy and small cross sections. Since there are no other publications about this reaction in the literature, it would be interesting to have new data at incident energies far above the Coulomb barrier.

In the present work the results of the $^7Li(^7Li, ^6He)^8Be$ measurements at the lithium energy of 22 MeV are given. Deduced angular distributions for the ground (0^+) and first excited (2^+) states of ^8Be are compared with the theoretical models of direct interaction and compound nucleus.

2. Experimental Procedures and Results

The $^7Li(^7Li, ^6He)^8Be$ reaction was induced by accelerating double-ionized ^7Li particles to 22 MeV using the I.V. Kurchatov IAE isochronous cyclotron. Beam currents were up to 400 nA. The target was made by evaporating 1.23 mg/cm^2 of ^7Li(99.7 %) metal onto a thin carbon backing. The target thickness was about 1 MeV to the 22 MeV lithium beam. ^6He spectra were measured by steps of 1.0 - 1.5^o in the angle range of 6 - 30° lab and by 2.5^o in the 30 - 60° lab one. With the account of the particle identity in the entrance channel, the angle range of 6 - 60° lab corresponds to the 10 - 170° cm one. Particle identification was effected by means of the E(1.2 mm) and E(32 μm) silicon detectors with the 2 x 10^{-4} sr solid angle. Typical ^6He spectra are shown in fig. 1. These spectra exhibit well-pronounced and resolved peaks for the first two states of ^8Be (0 and 3.04 MeV), as well as a smooth background. No special investigation of the background sources was performed. But it was supposed that the continuum could be due to the two-step reaction $^7Li(^7Li, \alpha)^{10}Be^* \rightarrow {}^6He + \alpha$. Experimental spectra were approximated by the curves consisting of three components: two Breit-Wigner distributions from the peaks and the Gauss distribution from the background near the peaks (fig. 1)

Fig. 2 gives the results of the experimental angular distributions of the ^6He particles corresponding to ^8Be (g. s.; 0^+) and $^8Be^*$ (3.04 MeV; 2^+). The systematic error in the absolute cross section is taken to be ± 10 and ± 15 % for the first excited and ground states, respectively. Both the angular distributions are anisotropic and have a strong structure unlike that of the data at incident energies near the Coulomb barrier /3,4/.

3. Analysis

The angular distributions are compared with the exact finite-range DWBA calculations using the LOLA code /5/. The radius parameter of 2.00 fm and diffusenes of 0.65 fm were used in the calculation of the bound state wave functions. The bound state potentials

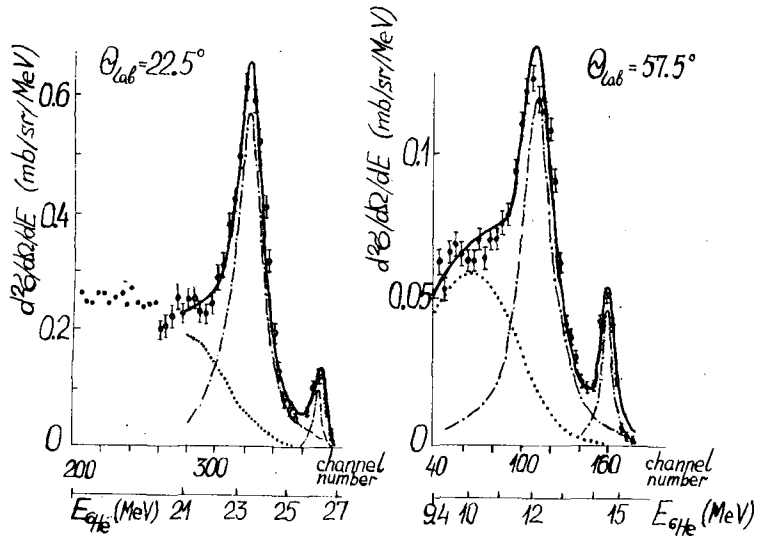

Fig. 1 ^{6}He spectra from the ^{7}Li(^{7}Li, ^{6}He)^{8}Be reaction at the lithium lab energy of 22 MeV and lab angles of 22.5 and 57.5°. The solid lines are the results of the approximation, while the broken lines are the components of the approximation.

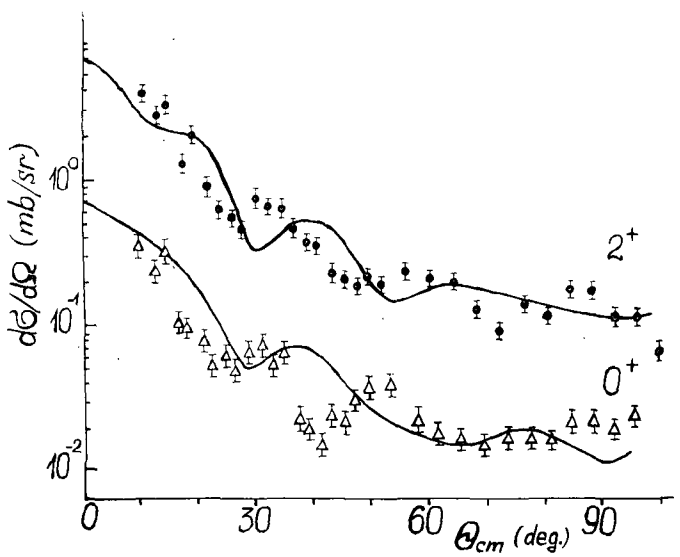

Fig. 2 ^{6}He experimental and DWBA angular distributions for the ^{7}Li(^{7}Li, ^{6}He)^{8}Be (0^+ and 2^+) reaction at E_{lab}(^{7}Li) = 22 MeV

were determined by allowing the depth to vary until the experimental binding energies were achieved. On the basis of the shell model, one expects a stripped proton to be captured into the 1p-state. For the transition leaving ^{8}Be in its 0^+ ground state, only the $1p_{3/2}$ capture is allowed. For the 2^+ first excited state both the $1p_{3/2}$ and $1p_{1/2}$ captures are allowed. According to the selection rules, the l-transfer values are equal to 0, 1 and 2 for the $p_{3/2}$ final state, while for $p_{1/2}$ only 1 and 2 are realized. Since the difference between the cross sections for the $p_{3/2}$ and $p_{1/2}$ states is essential only at forward angles (0_{cm} 10°), one expects that only the $1p_{3/2}$ capture is allowed for both the final ^{8}Be states (0^+ and 2^+).

The optical-model parameters used for the entrance and exit channels were taken from

the analysis of the ^{7}Li(24 MeV) + ^{9}Be reaction by Cook /6/. The DWBA calculations are shown in fig. 2 together with the experimental angular distributions. The single-proton stripping calculations reproduce, in general, the shape of angular distributions, as well as the rate of fall-off with increasing angle but not the details of these distributions, in particular, the positions of maxima and minima. The attempts at varying the optical--model parameters failed to improve the calculations.

The single-proton spectroscopic factors were deduced by comparing the experimental and DWBA cross sections at the forward angles. They are 1.1 and 1.3 for the ground and first excited states of ^{8}Be, respectively. The theoretical data are 2.898 and 1.119 /7/. The discrepancy is not too larga to speak about some dominat mechanism other than the one-step direct proton transfer. But this discrepancy and phse problem can be an argument for the existence of two-step contributions or the need for other types of the optical-model potential.

To estimate the contribution of the compound process in the $^{7}Li(^{7}Li, {}^{6}He)^{8}Be$ reaction at 22 MeV, calculations have been made using the Hauser-Feshbach model. The deduced cross sections are less than 12 and 7 % of the experimental cross sections for the ground and first excited states of ^{8}Be, respectively.

4. Conclusion

The angular distributions of ^{6}He have been measured for the ground and first excited states of ^{8}Be from the $^{7}Li(^{7}Li, {}^{6}He)^{8}Be$ reaction at the lithium energy of 22 MeV far above the Coulomb barrier. Clear indications have been obtained that the direct mechanism is the dominant one. The comparison of the experimental and theoretical DWBA data shows that the angular distributions are, on the whole, satisfactorily described by the single-proton stripping mechanism. The phase problem in the DWBA calculations remains open. The contribution of the compound-nucleus mechanism is negligible.

References

/1/ E. Norbeck, J.M. Blair, L. Pinsonneault and R.J. Gerbracht, Phys., 1959, v. 116, p. 1560

/2/ E. Norbeck, Jr. und C.S. Littlejohn, Phys. Rev., 1957, v. 108, p. 754

/3/ R.R. Carlson, R.L. McGrath, E. Norbeck, Phys. Rev., 1964, v. 136, p. B1687

/4/ R.A. Stryk and J.M. Blair, Phys. Rev., 1968, v. 169, p. 767

/5/ R.V. DeVries, Phys. Rev., 1973, v. C8, p. 951

/6/ J. Cook, Atomic Data and Nucl. Data Tables, 1981, v. 26, p. 19

/7/ C. Cohen and D. Kurath, Nucl. Phys., 1967, v. A101, p. 1.

A MEASUREMENT OF THE FORWARD DIFFERENTIAL CROSS SECTION OF THE REACTION $^1H(n,d)_\gamma$ AT E_n=25 MeV

P. Michel, K. Möller, J. Mösner, G. Schmidt
Central Institute for Nuclear Research, Rossendorf, G.D.R.

In recent years it has become obvious that the forward differential cross section of the reaction $^1H(n,d)_\gamma$ and its inverse, the photodisintegration, is a sensitive probe for studying the nucleon-nucleon interaction and the electromagnetic transition operator. To test different theoretical approaches to this reaction requires accurate experimental data.
The present experimental and theoretical situation is shown in Fig. 1. Most theoretical approaches predict a minimum in the differential cross section at about E_γ=10 MeV. But up to now no clear decision can be made by the experimental data whether the minimum exists. The experimental data are mainly by the Mainz/1,7/, Louvin/4,6/, Frascati/2,5/, IUCF/3/ and RUG-Gent/8/ groups.
Theoretical calculations have been performed by Partovi/9/, Laget/10/, Friar/11/, Jaus/12/, Cambi/13/, Hwang/14/, Pandey/15/ and others.
Fig. 1 exhibits two main features:

i) Most theoretical approaches give a poor description of the experimental data.
ii) Due to the very small cross section of the reaction the experimental errors are large.

In the present paper an experiment has been performed to add a new data point to Fig. 1 for E_n=25.6 MeV (corresponding to E_γ=15 MeV). The experimental set-up is shown in Fig. 2. The neutrons are produced by bombarding a Ti-^3H target (manufactured by Kolomiez et al., Institute of Nuclear Research of the Ukrainian Academy of Science, Kiev/ USSR) with 9.5 MeV deuterons from the Rossendorf Tandem accelerator. The capture deuterons are produced in a gaseous ^1H target and then detected in a spectrometer consisting of a telescope and two position sensitive multistep avalanche chambers /MSC/.
The target gas cell contains two MWPCs which ensure that the detected particles are originated within the gas cell.
The two scintillation counters (SC1, SC2) serve for measuring the time of flight and the response of the charged particles and the MSCs are used for the determination of the track coordinates in order to reconstruct the neutron-deuteron angle. Detectors are coupled via CAMAC electronics to a small computer KRS 4201(Robotron). Details of the experimental arrangement are given in refs. /16-18/.
Using Monte Carlo simulation we deduce the zero-degree cross section from the measured angular distribution. The result is

$$\left(\frac{d\sigma}{d\Omega}\right)^{cm.}_{\theta=0°} = (5.8 \pm 2.3)\ \mu b/sr$$

The main error is due to the statistics of the measurement. A comparison of the capture reaction measurement with corresponding photodisintegration experiments /1,7,8/ shows that in the latter cases about 100 times larger reaction rates are possible and therefore essentially smaller statistical errors can be achieved.
The result is in good agreement with a lot of theoretical predictions but because of the relativly large error more detailed conclusions cannot be drawn.

REFERENCES

/1/ Huges, R.J. et al., Nucl. Phys. A 267 (1976) 329
/2/ De Pascale, M.P. et al., Phys. Lett. 114 B (1982) 11
/3/ Meyer, H.O. et al., Phys. Rev. Lett. 52 (1984) 1759
/4/ Ninane, A. et al., Phys. Rev. C 35 (1987) 402
/5/ De Pascale, M.P. et al., Phys. Rev. C 32 (1985) 1830
/6/ Dupont, C. et al., Nucl. Phys. A 445 (1985) 13
/7/ Zieger, A. et al., Few-Body Syst. 1 (1986) 135
/8/ De Graeve, A. et al., Spring Meeting Groningen (1987) March
/9/ Partovi, F., Ann. Phys. 27 (1964) 79
/10/ Laget, J.M., Can. J. Phys. 62 (1984) 1046
/11/ Friar, J.L. et al., Phys. Rev. C 30 (1984) 441
/12/ Jaus, W. et al., Nucl. Phys. A 431 (1984) 669
/13/ Cambi, A. et al., J. Phys. G: Nucl. Phys. 10 (1984) L11
/14/ Hwang, W.T.P. et al., Ann. Phys. 149 (1983) 335
/15/ Pandey, L.N. et al., Phys. Rev. C 32 (1985) 1842
/16/ Stiehler, T. et al., Nucl. Instr. Meth. A 236 (1985) 343
/17/ Stiehler, T. et al., Annalen der Physik 43 (1986) 602
/18/ Michel, P. et al., ZfK-621, Annual report (1986) 126 and 127

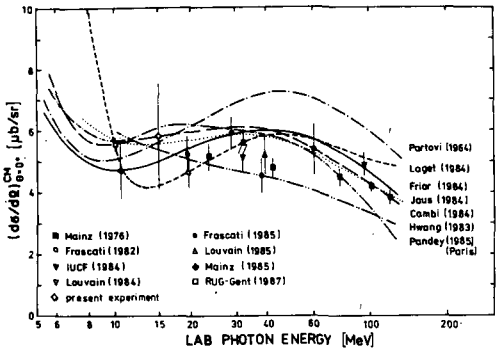

Fig.1: Forward differential cross section of the photodisintegration (Mainz(1976)/1/, Frascati (1982) /2/, IUCF (1984) /3/, Louvain (1984) /4/, Frascati (1985) /5/, Louvain (1985) /7/, RUG-Gent (1987) /8/, Partovi (1964) /9/, Laget (1984) /10/, Friar (1984) /11/, Jaus (1984) /12/, Cambi (1984) /13/, Hwang (1983) /14/, Pandey (1985) /15/)

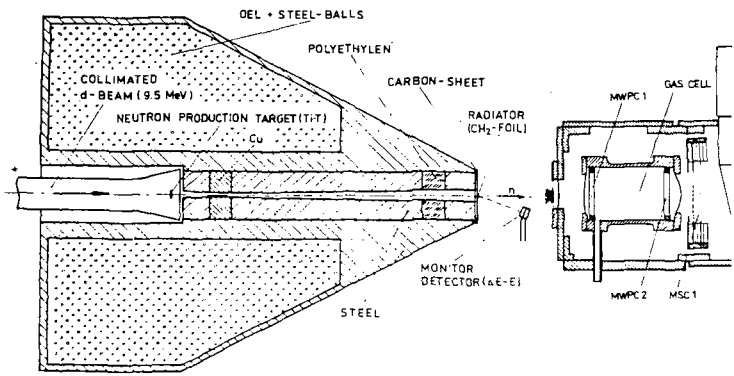

Fig. 2: Experimental set up

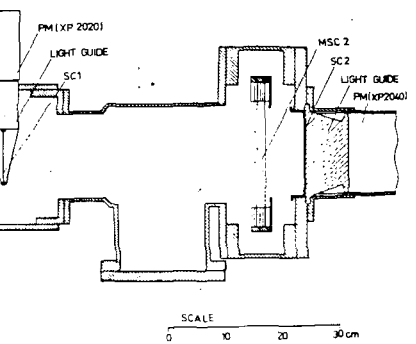
PM (XP 2020)
LIGHT GUIDE
SC1
MSC 2
SC2
LIGHT GUIDE
PM(XP2040)
SCALE
0
10
20
30 cm

FOLDING-POTENTIAL ANALYSIS OF ELASTIC AND INELASTIC ALPHA'SCATTERING PROCESSES AND OF (p,α) AND (α,p) REACTIONS ON LIGHT NUCLEI

G. Staudt, H. Abele, R. Neu, Ch. Striebel, M. Walz, S. Welte
Physikalisches Institut der Universität Tübingen, D-7400 Tübingen
H. Oberhummer, H. Cech, Institut für Kernphysik, Technische Universität Wien, A-1020 Wien
P.D. Eversheim, F. Hinterberger, Institut für Strahlen- und Kernphysik, Universität Bonn, D-5300 Bonn

Abstract

Differential cross sections of elastic and inelastic α-scattering have been measured on some light nuclei at E = 48.7 and 54.1 MeV. The experimental results were analysed in terms of the optical model and the coupled-channels method using a double-filded α-potential. Previous investigations of some (p,α) and (α,p) reactions have been reanalysed employing these α-potentials. The angular distributions as well as the correct absolute magnitude of the (p,α) and (α,p) cross sections are well reproduced.

Introduction

Elastic alpha-nucleus scattering processes are generally described by optical potentials whose parameters are adjusted to reproduce the scattering data. Furthermore optical potentials are needed in the analysis of inelastic α-scattering data using a coupled-channels procedure. Finally, the knowledge of α optical potentials is necessary in the calculation of (p,α) and (α,p) reactions in the framework of the DWBA.

In order to analyse elastic alpha-nucleus scattering processes the simple Saxon-Woods shape is generalized by introducing terms of higher order of the well-known Saxon-Woods function. Further "model-independent" parametrizations of the optical potential are commonly used employing either a sum of Gaussians or a sum of Fourier-Bessel functions added to a Saxon-Woods form factor /1/.

A systematic optical model analysis of $^{16}O(\alpha,\alpha)$ elastic scattering has been presented by Michel et al. /2/. For the real part of the optical potential they found a new parametrization. The extracted potential, which has only two smoothly - varying - energy - dpendent parameters, gives a precise description of the α-^{16}O elastic scattering data in the energy range between 30 and 150 MeV. The analysed data were shown to allow the elimination of the well.known so-called discrete ambiguity. The real volume integral per nucleon pair of this potential which is about 400 MeV fm^3 at low energies, descreases with energy with a slope comparable to that found for higher mass targets.

A further approach to the determination of optical model potential constitutes the double-folding procedure. Recently the α-particle scattering was analysed by Kobos et al. within the framework of this concept /3/. The resulting volume integrals $J_R/4A$ vary between 300 and 400 MeV fm^3. The model yields a good account for α-scattering in an energy regime of 25 to 100 MeV for nuclei in the mass region between ^{40}Ca and ^{208}Pb.

We have measured the elastic and inelastic α-scattering on some light nuclei in the mass region A = 11 - 24 at incident energies E_α = 48.7 and 54.1 MeV. In order to analyse the data optical model and coupled-channels calculations have been carried out using a potentials based on the folding concept. Furthermore we reanalysed previous investigations of some (p,α) and)α,p) reactions employing double-folded α potentials in the DWBA calculations.

Experimental Procedure

The measurements were performed by using α particle beams from the Bonn isochronous cyclotron. Typically, intensities between 20 and 400 nA were utilized with a beam resolution of $5 \cdot 10^{-4}$. Target foils of about 50 μg/cm^2 thickness (^{11}B, ^{24}Mg) and gas targets with a pressure of about 500 mbar ($^{12,13}C$, $^{14,15}N$, $^{16,17,18}O$, $^{20,22}Ne$) have been used.

The detector system consisted of four E-E-telescopes fixed on two turntables. The detectors were of the surface barrier type with a thickness of about 200 µm (E) and 2000 µm(E). The detector signals were amplified and registered by means of standard particle identification techniques. Great care was taken to fix the zero-degree direction which could be determined with an accuracy of about 0.1 degree.

The inelastic α-scattering on ^{24}Mg has been measured at the Heidelberg post accelerator utilizing the multistep spectrometer. With an energy resolution of better than 100 keV in the particle spectrum all members of the ground state and the γ-band up to E_x = 8 MeV could be well separated.

The α-Nucleus Double-Folding Potential

The real part of the folding potential is described by

$$U_F(r) = \lambda \int d\mathbf{r}_1 \int d\mathbf{r}_2 \rho_T(\mathbf{r}_1)\rho_\alpha(\mathbf{r}_2) \cdot t(E,\rho_T,\rho_\alpha,\mathbf{s}=\mathbf{r}+\mathbf{r}_2-\mathbf{r}_1)$$

where r is the separation of the centers of mass of the colliding target nucleus and the α-particle, $\rho_T(\mathbf{r}_1)$ and $\rho_\alpha(\mathbf{r}_2)$ are the respective nucleon densities, and λ is an overall normalization factor. The quantity t is the energy and density dependent effective nucleon-nucleon interaction

$$t(E,\rho,s) = g(E,s)f(E,\rho)$$

with the M3Y interaction

$$g(E,s) = 7999\frac{\exp(-4s)}{4s} - 2134\frac{\exp(-2.5s)}{2.5s} - 276(1-0.005E)\delta(s)$$

and

$$E = E_\alpha^{c.m.}/4$$

where $E_\alpha^{c.m.}$ is the c.m. kinetic energy of the α-target-system. The density dependence is given by

$$f(E,\rho) = C(E)[1+\alpha(E)e^{-\beta(E)\rho}]$$

with $\rho = \rho_T(\mathbf{r}_1)+\rho_\alpha(\mathbf{r}_2)$. The parameters C(E), α(E) and β(E) were determined by fitting the volume integral of t(E,ρ,s) to a parametrized form of the real part of a G-matrix interaction obtained from Brueckner-Hartree-Fock calculations for nuclear matter for various densities ρ and at various nucleon energies E. /4/

By the use of the computer code FOLD the real part of the optical potential $U_F(r)$ was calculated /5/. For the density distributions of the target nuclei ρ_T and of the α-particle ρ_α the charge densities measured in electron scattering were used.

In order to gain a sufficient flexibility in the shape of the absorptive part of the optical model potential a "model independent" form was chosen expressing the imaginary part of the potential as a sum of Fourier-Bessel functions of six terms

$$W(R) = \sum_{v=1}^{6} a_v j_0\left(v\frac{\pi}{R_c}r\right).$$

A cut-off radius R_c = 10 fm was used. All fits were performed using the computer code GOMFIL /6/, where the only adjustable parameters are the six Fourier-Bessel coefficients a_v of the imaginary part and the normalization constant λ of the real part of the potential.

Optical Model Analysis of Elastic α-Scattering

The double-folding potential was first applied to an analysis of the elastic α-scattering on ^{16}O. For this nucleus elastic scattering data are known covering a broad energy range. The experimental data together with the results of the calculation are shown in fig. 1. The quality of the fits compares well with the best available phenomenological optical description /2/ provided the double-folding potential is renormalized by a factor

$\lambda \sim 1.35$ in agreement with the findings of Kobos et al. /3/.

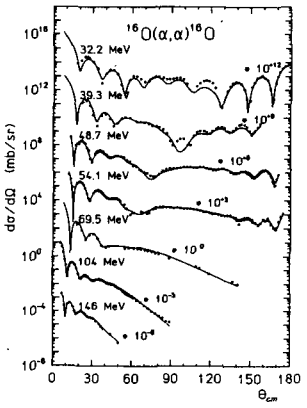

Fig. 1. Elastic α-scattering on ^{16}O: Experimental data and optical model fits, calculated by using the double-folding potential.

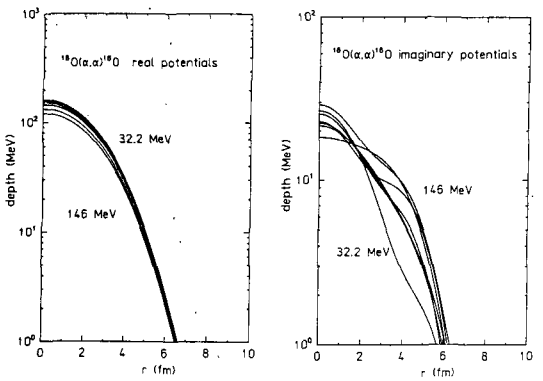

Fig. 2. Real and imaginary part of the optical potential as used in the calculations of fig. 1

The real parts of the renormalized folding potential and the imaginary parts obtained by the fitting procedure are shown in fig. 2. The renormalization factors λ, the volume integrals and the rms radii are listed in table 1. The real potentials are in excellent agreement with those obtained by Michel et al. for both their depth and shape /2/. Recently, Wada and Horiuchi have shown /7/, that $\alpha + {}^{16}O$ RGM calculations which reproduce the spectroscopic data of the ^{20}Ne levels also fit well the elastic scattering cross sections up to high energies. The equivalent local potential derived from the resonating-group method is found to be very similar to the optical potential calculated by the double-folding procedure. Thus it is concluded that a significant part of the energy dependence of the real part of the $\alpha + {}^{16}O$ potential is due to the internucleus antisymmetrization.

The imaginary potentials derived by the procedure described above are shallower than the potentials of Saxon-Woods type. On the other hand they resemble in shape to the real potentials as obtained by the folding procedure. As for the real part, the depth of the imaginary part decreases slightly for increasing incident energy. However, the radial range and the volume integrals $J_I/4A$ slopes up with energy. This means, that for increasing energy the absorption is pushed more to the surface. The rms radii for the imaginary potential are for all energies larger than those for the real part.

Table 1. Renormalization factor λ, volume integrals and rms radii from an optical model analysis with a double-folding potential for elastic α-scattering on ^{16}O

E_α (MeV)	λ	$J_R/4A$ (MeV fm^3)	$\langle r_R^2\rangle^{1/2}$ (fm)	$J_I/4A$ (MeV fm^3)	$\langle r_I^2\rangle^{1/2}$ (fm)
32.2	1.395	407	3.61	51.1	4.33
39.3	1.389	400	3.61	56.9	4.20
48.7	1.390	397	3.61	74.8	4.40
54.1	1.354	383	3.61	76.6	4.28
69.5	1.332	369	3.61	93.8	4.23
104[a]	1.288	339	3.62	101	4.12
146	1.275	313	3.63	108	3.97

[a] exp. data renormalized by the factor 0.73 /ref. 2/

Now we analyse all our data measured at an incident energy of 54.1 MeV in terms of double-folding model. The results are shown in fig. 3 and in table 2. Not unexpectedly, the comparison of the fit to the experimental data of elastic scattering is the less favourable, the more the nucleus is deformed. Inspecting sections for the ^{11}B, ^{12}C, ^{20}Ne, and ^{24}Mg it becomes evident, that it is beyond the scope of an optical model analysis to interpret the angular distributions of elastic scattering for strongly deformed nuclei. This statement, though less stringent, is also valid for nuclei like ^{13}C and ^{18}O.

Table 2. Renormalization factor λ, volume integrals and rms radii from a optical model analysis with a double-folding potential for elastic α-scattering on light nuclei at incident energy E = 54.1 MeV

Target nucleus	λ	$J_R/4A$ (MeV fm^3)	$\langle r_R^2\rangle^{1/2}$ (fm)	$J_I/4A$ (MeV fm^3)	$\langle r_I^2\rangle^{1/2}$ (fm)
^{11}B	1.32	393	3.46	122	4.35
^{12}C	1.32	367	3.37	115	3.12
^{13}C	1.32	375	3.46	97.2	4.12
^{14}N	1.31	368	3.47	80.8	4.11
^{15}N	1.35	381	3.57	89.1	4.52
^{16}O	1.35	383	3.61	76.6	4.28
^{17}O	1.32	375	3.66	93.8	4.60
^{18}O	1.30	364	3.66	112	4.68
^{20}Ne	1.21	352	3.86	127	4.50
^{22}Ne	1.11	307	3.81	114	4.42
^{24}Mg	1.15	323	3.86	116	4.26

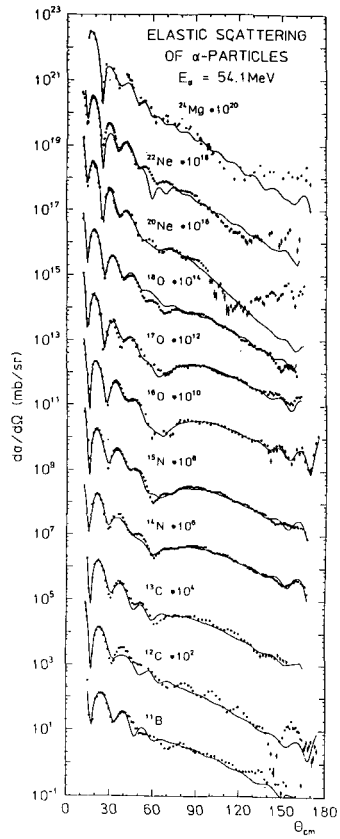

Fig. 3. Elastic α-scattering on some light nuclei at E_α = 54.1 MeV: Experimental data and optical model fits, calculated by using the double-folding potential.

Coupled-Channels Analysis of Inelastic α-Scattering

For the elastic and inelastic scattering on deformed nuclei coupled-channels calculations are adequate to analyse the experimental data. It is well known that at low-medium energies α-scattering is very sensitive to multistep processes in the excitation of the target nucleus. Therefore we analysed the elastic and inelastic α-scattering cross sections for the excitation of collective states in ^{13}C, ^{18}O, ^{20}Ne, ^{22}Ne and ^{24}Mg in terms of the coupled-channels method utilizing the program ECIS /8/. An investigation of the α-scattering on ^{12}C is in progress.

For the nuclei ^{13}C, ^{18}O, ^{20}Ne and ^{22}Ne the concept of the symmetric rotor model is employed. The calculations give a reasonable description of the data, s. figs. 4 and 5. The inelastic α-scattering on the strongly collective nucleus ^{24}Mg has been analysed within the framework of triaxial rotor model /9/ extended to hexadecapole degrees of freedom. The results are given in fig. 6.

In all the coupled-channels calculations again a folding potential was used for the

optical potential. Measuring the strength of the imaginary potential by the volume integral, this integral is much smaller in the case of a coupled-channels analysis as compared to an optical model analysis (s. fig. 7). This trend is expected since the strength of the absorptive part of an optical potential has to take into account all the couplings into inelastic channels. As can be seen in fig. 7, the correlation between the volume integrals $J_I/4A$ obtained in optical model analyses and the deformation parameters β_2 is striking. On the other hand, the values of the volume integrals $J_I/4A$ obtained in coupled channels calculations are actually similar to those extracted from the optical model analysis of the elastic α-scattering on the spherical nucleus ^{16}O.

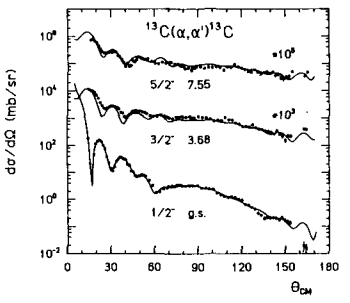

Fig. 4. Elastic and inelastic α-scattering on ^{13}C at E_α = 54.1 MeV: Experimental data and coupled-channels fits, calculated by using the double-folding potential. β_2 = -0.24, β_4 = -0.04.

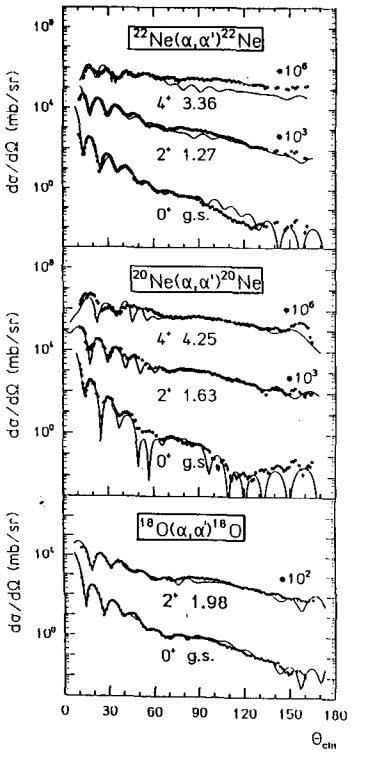

Fig. 5. Same as fig. 4, but for the nuclei ^{18}O: β_2 = 0.18; ^{20}Ne: β_2 = 0.27; β_4 = 0.04; ^{22}Ne: β_2 = 0.28, β_4 = 0.02.

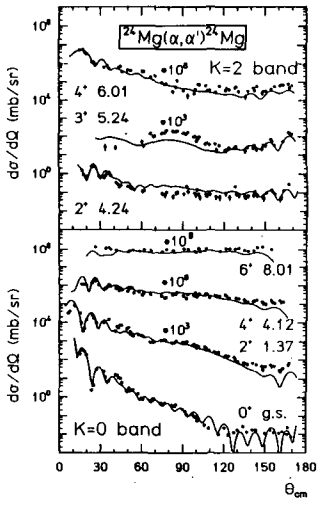

Fig. 6. Same as fig. 4, but for the nucleus ^{24}Mg: β_2 = 0.27, β_4 = -0.10.

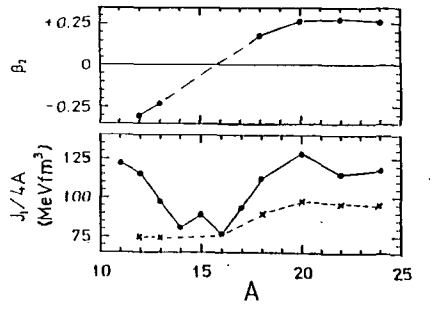

Fig. 7. Mass dependence of the deformation parameter β_2 and of the volume integral per nucleon of the optical potential deduced from optical model calculations (points) and from coupled-channels fits (crosses).

DWBA Analysis of (p,α) and (α,p) Reactions

During the last few years much attention has been paid to the absolute normalization of the cross section of (p,α) or (α,p) reactions. Recent microscopic analyses reveal striking discrepancies between the measured absolute values σ_{exp} and the theoretical predictions σ_{th} /10-12/. The enhancement factor

$$\varepsilon = \frac{\sigma_{exp}}{\sigma_{th}}$$

required to obtain agreement between both values varied up to three orders of magnitude. This discrepancy may be due to unrealistic NN potentials, the omission of multi-step processes and the use of insufficient single-particle wave functions in the calculation of the form factor. The influence of the optical α-potential in the exit (or entrance) channel of the DWBA transition amplitude has been investigated by Brunner et al. /10/ for the transfer $^{27}Al(p,\alpha)^{24}Mg$ and by Hamill and Kunz /11/ for the $^{40}Ca(\alpha,p)^{43}Sc$ reaction. Both analyses conclude that the employance of deep optical α-potentials of Saxon-Woods form results in an acceptable description of the differential cross sections whereas this type of potentials require large enhancement factors ε to renormalize the theoretical predictions. On the other hand, when using shallow Saxon-Woods potentials small enhancement factors are needed but the resulting angular distributions of cross section and analyzing power are unacceptable.

The situation is drastically altered if an optical α-potential based on the double-folding concept instead of a Saxon-Woods potentials is adopted. Stimulated by the recent success of the folding model in the description of the elastic and inelastic α-scattering we reanalysed previous investigations of some (p,α) and (α,p) reactions using double-folded α-potentials in the DWBA calculations. The computer code TROMF was developed which allows a least-square fit to the experimental elastic scattering data in the entrance and exit channels as well as to the experimental differential cross sections of the transfer reaction, simultaneously /13/. The code optimises the free parameters of the optical potentials in the entrance and exit channels as well as the microscopic form factor. For the proton channel Saxon-Woods potentials are aused, whereas for the α channel a "model independent" form was chosen expressing the imaginary part as a sum of Fourier-Bessel functions of six terms and the real part as a sum of Fourier-Bessel functions of six terms added to the α-folding potential. The elastic scattering cross sections were calculated using the optical model code included in the code DWUCK V /14/. The three-nucleon transfer (p,α) or (α,p) was determined using a microscopic finite range DWBA model /12/. Thereby we used the finite range DWBA code DWUCK V and the microscopic form factor code TRANSØ4 /15/.

As an example I will discuss the reaction $^{27}Al(p,\alpha)^{24}Mg$ (g.s.). The experimental data have been taken from ref. 12. As a first result of the least-square fit procedure the best-fit parameters of the single-particle bound-state potentials give reasonable values, approximately the same as for instance the parameters given by Malaguti and Hodgson /16/. The resulting microscopic form factors deduced from both parameter sets are shown in fig. 8. Secondly, the best-fit α-optical potential is quite similar to the folding potential for the elastic α-scattering on ^{24}Mg at E_α = 42 MeV /17/ as shown in fig. 8. Both potentials give an excellent fit to the experimental $^{24}Mg(\alpha,\alpha)^{24}Mg$ data at 42 MeV.

Finally, the $^{27}Al(p,\alpha)^{24}Mg$ differential cross section and analyzing power values are well fitted (solid lines of fig. 9). The angular distribution of the cross section and the analyzing power as well as the absolute magnitude of the cross section are reproduced using an enhancement factor of ε = 1.20.

In order to estimate the sensitivity of the computed cross section and analyzing power we performed calculations using both the form factors and both the α-optical potentials shown in fig. 8. The results of this variation are given as dashed and dashed-dotted lines in fig. 9. As can be seen, the variation of the reaction cross section and analyzing power

is more marked than that of the microscopic form factors and α-optical potentials. This shows the sensitivity of the reaction data to slow variations in the shape of the form factor and the α-optical potential.

The most interesting result of our best-fit search is the following: even we only fitted to the experimental elastic differential cross sections of the entrance and exit channel as well as to the angular distribution of the (p,α) cross section, we obtained also the correct absolute magnitude of this cross section. In all the work up till now it was impossible to get the absolute magnitude and the angular distribution of the (p,α) - or (α,p) cross section simultaneously. The progress in fitting the (p,α) and (α,p) experimental data is due to the use of optical α-potential which is of the folding model instead of the Saxon-Woods type.

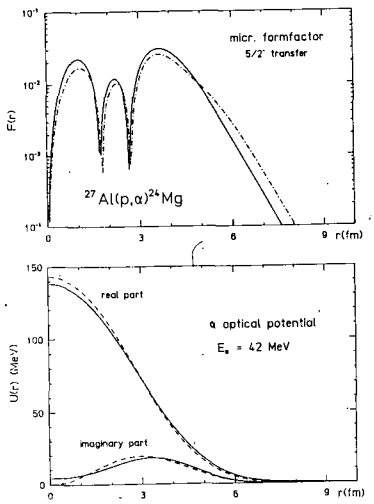

Fig. 8. Best-fit form factor and best-fit α optical potential (solid lines), form factor calculated with the parameters of ref.16 (dashed-dotted line), folding potential for the elastic scattering on ^{24}Mg at E_α = 42 MeV (ref.17)(dashed line).

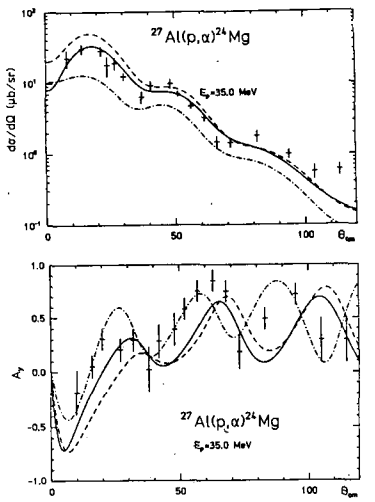

Fig. 9. Differential cross section and analysing power for ^{27}Al(p,α)^{24}Mg at E_p = 35 MeV: Experimental data and DWBA results calculated with the form factors and α optical potentials given in fig. 8.

We also investigated the energy dependence of this reaction. Again the experimental data have been taken from ref. 12. In the calculations with E_p = 24 and 45 MeV the same form factor was used as it results from the search procedure with E_p = 35 MeV as given above. Again the elastic scattering and reaction data are fitted but only with free optical model parameters and with free values. As one can see from fig. 10 the experimental elastic p- and α-cross sections as well as the (p,α) reaction cross sections are reproduced excellently by the microscopic finite range DWBA calculations.

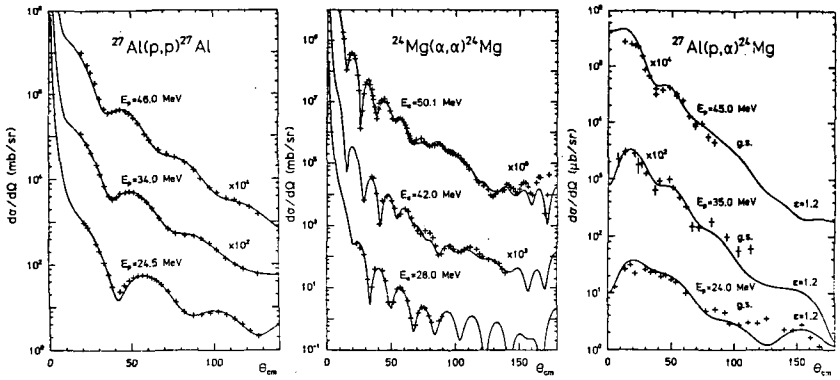

Fig. 10. Energy dependence of $^{27}Al(p,p)^{27}Al$, $^{24}Mg(\alpha,\alpha)^{24}Mg$ and $^{27}Al(p,\alpha)^{24}Mg$: Experimental values together with the results of optical model and finite range DWBA calculations using a microscopic form factor. In all cases the absolute reaction cross section is well reproduced if a normalization factor of only $\varepsilon = 1.2$ is used.

Conclusions

A study of elastic and inelastic α-scattering processes on several light nuclei at an incident energy near 50 MeV has been performed. The experimental results were analysed in terms of the optical model and the coupled-channels procedure. It could be shown that the double-folding potential calculated by means of the DDM3Y nucleon-nucleon interaction describes rather well the experimental differential cross sections for a broad energy range from 30 up to 150 MeV.

Furthermore these potentials have been used in the analysis of (p,α) and (α,p) reactions in the framework of microscopic finite-range DWBA calculations. It was possible to obtain almost the correct magnitude of the cross section, while in previous work the absolute value was generally underestimated by about two orders of magnitude. Simultaneously the angular distribution of both the experimental cross sections and the analyzing powers could be reproduced.

Acklowledgements

This work has been supported by the BMFT under contract no. 06 TÜ 460.

References

1. W.L. Put, A.M.J. Paans, Nucl. Phys. A291 (1977) 93
   F. Michel, R. Vanderporten, Phys. Rev. C16 (1977) 142
   E. Friedman, C.J. Batty, Phys. Rev. C17 (1978) 34
   H.J. Gils, E. Friedman, H. Rebel, J. Buschmann, S. Zagrowski, H. Klewe-Nibenius, B. Neumann, R. Pesl, G. Bechtold, Phys. Rev. C21 (1980) 1239
   H.P. Gubler, K. Kiebele, H.O. Meyer, G.R. Plattner, I. Sick, Nucl. Phys. A351 (1981)29
2. F. Michel, J. Albinski, P. Belery, Th. Delbar, Gh, Grégoire, B. Tasiaux, G. Reidemeister, Phys. Rev. C28 (1983) 1904
3. A.M. Kobos, B.A. Brown, R. Lindsay, G.R. Satchler, Nucl.Phys. A 425 (1984) 205
4. J.P. Yeukenne, C. Mahaux, Z. Phys. A302 (1981) 233
5. H. Clement, University of Tübingen, computer code FOLD (unpublished)
6. H. Leeb, Technical University of Vienna, computer code GOMFIL (unpublished)
7. T. Wada, H. Horiuchi, Phys. Rev. Lett. 58 (1987) 2190
8. J. Raynal, University of Paris, computer code ECIS (unpublished)
9. A.S. Davydov, G.F. Filippov, Nucl. Phys. 8 (1958) 237
10. F. Brunner, H.H. Müller, C. Dorninger, H. Oberhummer, Nucl. Phys. A398 (1983) 84
11. J.J. Hamill, P.D. Kunz, Phys. Lett. 129 (1983) 5
12. F. Hoyler, H. Oberhummer, T. Rohwer, G. Staudt, H.V. Klapdor, Phys.Rev. C31 (1985) 17

13. M. Walz, University of Tübingen, computer code TROMF (unpublished)

14. P.D. Kunz, University of Colorado, computer code DWUCK V (unpublished)

15. K. Preisinger, Technical University of Vienna, computer code TRANØ4 (unpublished)

16. F. Malaguti, P.E. Hodgson, Nucl. Phys. A215 (1973) 243

17. R. Neu, H. Abele, G. Staudt, P.D. Eversheim, F. Hinterberger (to be published)

LOW ENERGY BEHAVIOUR OF THE OPTICAL POTENTIAL IN ALPHA PARTICLE SCATTERING

M. Brenner, K.-M. Källman, P. Manngård, Å. Sjöberg

Department of Physics, Åbo Academi, Turku, Finland

Z. Máté, S. Szilágyi, L. Zolnai

Institute of Nuclear Research, Debrecen, Hungary

ABSTRACT:

Elastic and inelastic alpha-particle differential cross sections have been measured at 12.80, 14.56, 16.34 and 18.13 MeV on ^{62}Ni. The results were analysed with the optical model and coupled channel calculations were done. The energy dependence of the volume integrals was compared with the theoretical prediction. A similar study is in progress for ^{50}Cr and ^{34}S.

Recent papers [1), 2), 3), 4)] report on rapid variations and anomalous behaviour of the nucleus-nucleus potential for energies E in the vicinity of the top of the Coulomb barrier. It was shown that there are general theoretical arguments[5)] for expecting such an energy dependence of the potential parameters at low energies, based on the dispersion relation which connects the real and imaginary parts of the complex optical potential. This relation which is based on the causality principle has the following form:

$$V(r,E) = V_o(r,E) + \frac{P}{\pi} \int_0^\infty \frac{W(r,E')}{(E'-E)} dE'$$

Here P is the "principal value", V_o is a slowly and smoothly E depending term. It is expected that W(r,E') decreases rapidly for energies below the Coulomb barrier. Because of the above mentioned formula the real part is expected to be bell shaped near the top of the Coulomb barrier. In order to confirm this principle the $\alpha+^{62}$Ni elastic and inelastic scattering was studied in this work.

The experiment was performed using the sector focusing cyclotron of the Åbo Academy. The collimated α-particle beam was momentum analyzed in a 110° magnet. Using four surface-barrier Si detectors angular distributions were measured for the elastic and inelastic (2_1^+) scattering of α-particles by ^{62}Ni in steps of 2 and 4° at laboratory energies 12.80, 14.56, 16.34 and 18.13 MeV. The target was a 150-200 μg/cm^2 thick foil enriched in ^{62}Ni (97.94 %). The overall energy resolution was about 100 keV in the experiment while the energy loss in the target was 35 keV for 16 MeV bombarding alpha energy. The measured cross-sections are shown in figures 1 and 2.

First we analysed the data in the frame of the optical model. As it can be expected the volume integrals J_V and J_W cannot be determined unambiguously from the low energy scattering by ^{62}Ni. We obtained good agreement with several very different optical parameter sets and very strongly varying volume integrals. These parameter sets and the corresponding volume integrals with the χ^2-s are given in table 1. Later we made coupled channel calculations using the program ECIS [6)]. The coupling constant was set to 0.16 in accordance with the value obtained in [7)]. The parameters for this case are given in table 2. The experimental data and the results of calculations are compared in figures 1 and 2.

The volume integrals are compared with prediction of [5)] in figures 3 and 4. The

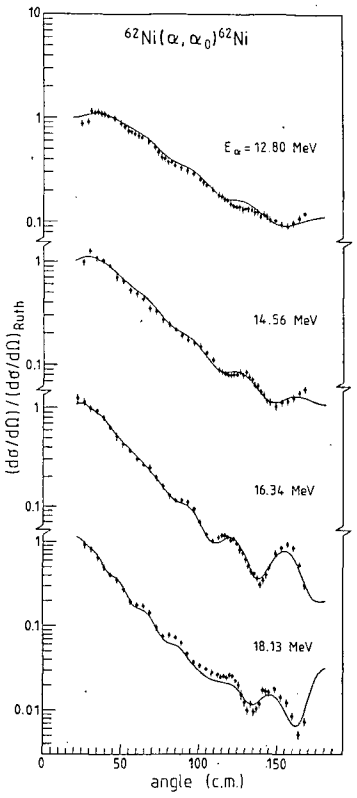

Fig.1. The experimental angular distributions for elastic scattering of α-particles by ^{62}Ni compared with results from coupled channel calculations using the optical potential parameter set from table 2 giving the best χ^2 (the solid lines).

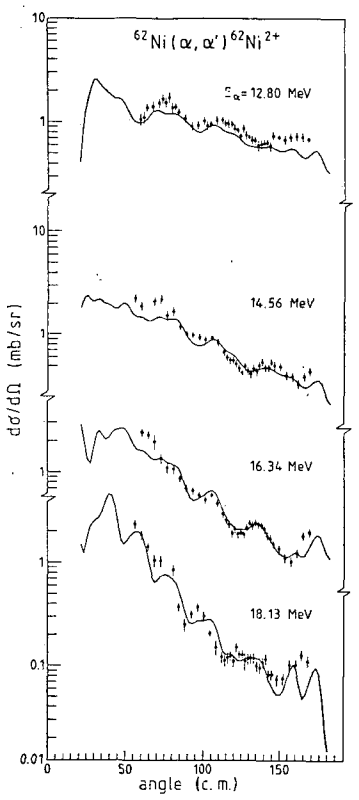

Fig.2. The experimental angular distributions for inelastic (2_1^+) scattering of α-particles by ^{62}Ni compared with results from coupled channel calculations using the same parameter set as in fig. 1 (the solid lines).

Table 1. The parameters obtained from the optical model calculations

E_α [MeV]	V [MeV]	r_V [fm]	a_V [fm]	W [MeV]	r_W [fm]	a_W [fm]	J_V [MeV fm^3]	J_W [MeV fm^3]	$\chi^2_{el.}$
12.80	210.8	1.40	0.56	12.4	1.80	0.14	667	76	0.5
14.56	207.0		0.51	32.7	1.00	0.62	646	42	0.4
16.34	211.2		0.52	14.1	1.70	0.20	659	73	1.0
18.13	198.1		0.58	16.1	1.69	0.39	631	84	1.6
12.80	137.2	1.45	0.58	11.9	1.79	0.21	481	72	0.6
14.56	133.6		0.54	12.5	1.63	0.38	463	59	0.5
16.34	133.0		0.54	16.55	1.48	0.14	462	57	1.9
18.13	126.3		0.59	13.1	1.71	0.41	445	71	1.8
12.80	104.6	1.50	0.56	10.5	1.81	0.52	402	65	0.5
14.56	101.8		0.52	10.84	1.66	0.34	387	53	0.5
16.34	105.0		0.50	10.3	1.72	0.15	397	55	1.2
18.13	94.6		0.58	11.7	1.72	0.39	366	64	2.0
12.80	60.5	1.55	0.54	9.86	1.58	0.50	254	43	0.8
14.56	57.0		0.53	7.67	1.67	0.36	239	39	0.6
16.34	58.0		0.52	14.4	1.67	0.24	242	80	6.1
18.13	31.5		0.72	5.61	1.86	0.47	139	39	2.6

Table 2. The parameters obtained when the inelastic (2_1^+) channel was coupled to the elastic one

E_α [MeV]	V [MeV]	r_V [fm]	a_V [fm]	W [MeV]	r_W [fm]	a_W [fm]	J_V [MeV fm^3]	J_W [MeV fm^3]	$\chi^2_{el.}$	$\chi^2_{inel.}$
12.80	196.7	1.40	0.59	14.4	1.78	0.32	629	87	1.2	3.1
14.56	191.2		0.55	14.2	1.69	0.37	604	73	1.0	3.3
16.34	192.2		0.55	14.6	1.69	0.36	607	75	2.4	6.8
18.13	200.4		0.40	20.0	1.09	1.45	605	58	1.8	4.7
12.80	129.2	1.45	0.55	12.9	1.47	0.10	450	43	1.4	4.5
14.56	126.3		0.54	14.0	1.46	0.09	439	45	0.9	2.5
16.34	124.2		0.55	13.9	1.46	0.10	433	46	0.8	2.6
18.13	117.3		0.60	15.7	1.49	0.18	414	50	2.4	4.8
12.80	99.1	1.50	0.54	10.5	1.47	0.66	379	39	1.3	2.2
14.56	96.2		0.52	13.4	1.30	0.81	366	39	1.44	2.5
16.34	95.6		0.55	8.49	1:75	0.23	366	48	2.5	3.5
18.13	86.3		0.65	12.9	1.72	0.48	340	73	23	5.5
12.80	56.6	1.55	0.54	8.24	1.40	0.20	238	24	1.8	1.6
14.56	54.9		0.507	5.72	1.78	0.26	232	34	1.0	1.6
16.34	52.6		0.58	6.00	1.76	0.27	234	35	4.1	2.5
18.13	65.2		0.62	9.6	1.77	0.33	280	57	12.1	6.8

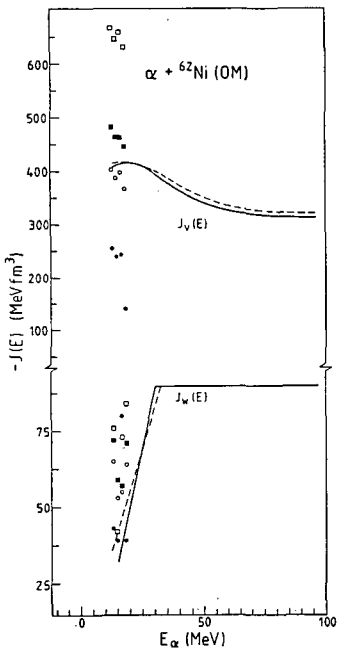

Fig.3. Comparison of the volume integrals obtained from the optical model calculation with the prediction of 5).

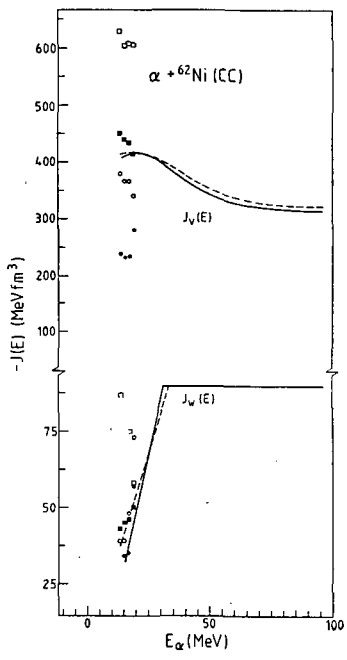

Fig.4. Comparison of the volume integrals obtained from the coupled channel calculation with the pediction of 5).

different symbols correspond to different parameter sets given in tables 1 and 2. It can be seen that the best fit values in the coupled channel case are close to the predicted ones.

Similar experiments have been performed for target nuclei ^{50}Cr and ^{34}S. The analysis of the data is in progress. Preliminary results for an angular distribution of elastic α-scattering on ^{34}S measured at the cyclotron of INR (Debrecen) are shown in figure 5.

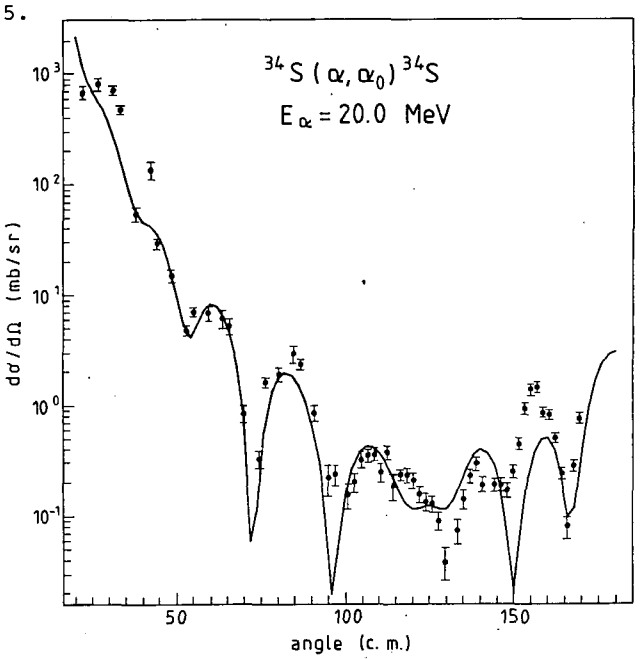

Fig.5. Preliminary results for the experimental angular distribution of elastic scattering of α-particles on ^{34}S compared with the results of optical model calculations.

REFERENCES

1) Lilley J S, Fulton B R, Nagarajan M A, Thompson I S, and Banes D W, 1985 Phys. Lett. 151B 181
2) Fulton B R, Banes D W, Lilley J S, Nagarajan M A, Thompson I J, 1985 Phys. Lett. 162B 55
3) Baeza A, Bilwes R, Diaz J and Ferrero J L, 1984 Nucl. Phys. A419 412
4) Michel F, Albinski J, Belery P, Delbar Th, Grégoire Gh, Tasiaux B, and Reidemeister G, 1983 Phys. Rev. C28 1904
5) Mahaux C, Ngô H and Satchler G R, 1986 Nucl. Phys. A449 354
6) Raynal J, Notes on ECIS (Service de Physique Theorique, CERN-Sacley 91101 GIF-sur-Yvette CEDEX)
7) Rebel H, Löhken, R, Schweiner G W, Shatz G and Hauser G, 1972 Z. Phys. 256 258

РЕАКЦИИ (n,α) ПРИ ЭНЕРГИИ НЕЙТРОНОВ 3 Мэв

Я. Оравец, И. Сарка, М. Флорек, К. Голы
Comenius University, Department of Nuclear Physics; CSSR 842 15 Bratislava

Г. Гельфер, У. Ян
Technische Universität Dresden, Sektion Physik; DDR 8027 Dresden

Анотация

Измерялись эффективные сечения редких (n,α) реакций на ядрах среднего веса 51-V, 55-Mn, 69-Ga, 95-Mo, 143-Nd при энергии нейтронов 3 Мэв, обсуждение экспериментальных результатов было сделано на основе статистического моделя Хаузера-Фешбаха и сравнены с вычисленными данными по [3]. Все эксперименты были сделаны на нейтронном генераторе ТУ Дрезден.

1. Введение

Реакции (n,α) при энергии нейтронов 3 Мэв на ядрах среднего веса и средне тяжелых ядрах протекают глубоко под куломбовским барьером с очень низкой правдеподобностью ($\sigma_\alpha \div 10^{-33}$ м^2). В основном они проходят через стадию составного ядра и их можно считать очень редкими реакциями [1].

Исследование этих редчайших реакций (n,α) является новой областью нейтронной спектрометрии, которая начала свое развитие в 60-тых годах. Эти исследования дают в первую очередь новую информацию о физическом поведении и структуре высоко возбужденных состояний атомных ядер. Дают сведения о самом процессе альфа-распаде и лучше обясняют представления о механизме этих реакций.

Экспериментальное исследование этих реакций затрудняется тем, что получение нейтронов с энергией 3 Мэв в нейтронных генераторах на основе реакции $D(d,n)^3He$ плотность потока нейтронов ниже плотности потока нейтронов из реакции $T(d,n)^4He$ премерно на два порядка ниже 14-Мэв нейтронов. Сечения реакций (n,α) в области энергии нейтронов 3 Мэв на ядрах среднего веса и средне тяжелых ядер, измерены для таких нуклидов, где величина σ_α относительно высокая, $\sim 10^{-31}$м^2, например реакции на ядрах ^{58}Ni, ^{54}Fe [2]. Коэффициенты трансмиссии для частиц альфа, для нами используемых нуклидов следующие например $^{55}Mn \div 10^{-7}$, $^{95}Mo \div 10^{-5}$, $^{143}Nd \div 10^{-6}$, по сравнению с $^{58}Ni \div 10^{-2}$. Для атомных ядер, сечения реакций $(n,\alpha) \div 10^{-33}$м^2 существуют только теоретические данные [3].

2. Эксперимент

Для измерения сечений редких реакций (n,α) на ядрах среднего веса и средне тяжелых ядрах при энергии нейтронов 3 Мэв, мы использовали метод нейтронно-активационного анализа в сочитании с бета-гамма спектрометра, метод прямых измерений с использованием ионизационной камеры и газово-полупроводникового телескопа.

Метод активационного анализа был использован для тех ядер, у которых после реакции (n,α) остаются дочерные бета-гамма радиоактивные ядра с полупериодом распада несколько минут или часов. Этим методом были измерены сечения реакций (n,α) на ядрах ^{55}Mn и ^{69}Ga [4].

Ценную информацию о характере реакций получаем когда измеряем прямо энергетический спектр альфа данной реакции. Из этих данных можно прямо определить переходы альфа для отдельных возбужденных уровней дочерных ядер и тем самым высчитать парциальные эффективные сечения реакций (n,α). Для этого был использован газово-полупроводниковый телескоп для ядер: σ_{α_c} - ^{55}Mo, σ_{α_c} и σ_{α_1} для ^{143}Nd [5,6].

Измерения с ионизационной камерой с сеткой ядра ^{67}Zn, не привели к успеху, хотя теоретические предсказания эффективного сечения для (n,α) реакции для этого ядра были довольно высаки - σ_α - 878 микробарн. Таблица №1 показывает наши расчотные и измеренные эффективные сечения (n,α).

Таблица №1

Ядро мишени	^{51}V	^{55}Mn	^{67}Zn	^{69}Ga	^{95}Mo	^{143}Nd	
Теория (μb)	17	12	878	28	α_0 110	α_0 α_1	51 12
Экспер. (μb)	<100	(7±3)	<700	(70±50)	(90±40)		(130±60) (30±20)

Теоретические величины в таблице №1 были вычислены на основе статистической модели Хаусера-Фешбаха модификацией программы STAPRE, где были приняты во внимание каналы n, p, α. Плотность возбужденных состояний, программа определяет расчотом по [7] из дискового набора (в области дискретных состояний). Величины параметров плотности возбужденных состояний "a" и энергетических щелей "Δ" были взяты из [8]. Для расчота трансмиссионных коэффициентов на основе оптической модели были использованы процедуры из программы SCAT [9]. Также использовался глобальный потенциал Мек Фадена и Сачлера [10]. Протонный канал был описан потенциалом Бечети и Гринлес [11]. Трансмиссионные функции для нейтронов были расчитаны нелокальным глобальным потенциалом Пери и Бук [12].

3. Обсуждение результатов

В области ядер среднего веса были измерены эффективные сечения (n,α) реакций для ядер ^{55}Mn, ^{69}Ga, ошибка в результатацх была выше у ядра ^{69}Ga. Причиной этого был изотопически состав естественного галия, где E_γ из изотопа ^{70}Ga в реакции $^{69}Ga\ (n,\gamma)^{70}Ga$ близка по энергии возбуждения дочерного ядра ^{66}Cu. Нам удалось определить реакцию $^{69}Ga\ (n,\alpha)^{66}Cu$ на основе разницы полупериодов дочерных ядер ^{66}Cu и ^{70}Ga. Данные ядра имеют малую плотность возбужденных состояний. Все энергетически разрешены переходы составного ядра реализуются на дискретных уровнях. В случае глубоко подбариерных реакций расхождение между теорией и экспериментом можно считать минимальным.

В случае ^{95}Mo и ^{143}Nd распад альфа осуществляется глубоко под кулоновским барьером (для ^{95}Mo; E_{α_0} = 9,2 Мэв, высота борьера дла частицы альфа 18 Мэв и для ^{143}Nd, E_{α_0} = 12,4 Мэв а высота барьера 25 Мэв). Эти ядра имеют высокую степень плотности возбужденных состояний. Из измереных величин σ_{α_0} и σ_{α_1} у ^{143}Nd получается, что большинство эмитированых частиц идет на основное состояние и только 23% идет на первый возбужденный уровень (по теоретическим расчетам 21%). У ядра ^{143}Nd расчет дает заниженные значения. Из исследованных изотопов эфективные сечения реакций (n,α), в энергетическом ин-

тервале 1 Мэв были расчитаны начиная с энергий 2 Мэв в каталогу JAERI-M 84-103 [3] для изотопов ^{51}V, ^{55}Mn, ^{95}Mo. Рисунок №1 показывает зависимость расчетных эффективных сечений σ_α от энергии E_n на этих ядрах из [3] и также наше экспериментальные результаты для энергии 3 Мэв. Из сравнения этих величин хорошее согласие дает ^{95}Mo. В области ядер среднего веса (^{51}V, ^{55}Mn) экспериментальные данные занижены по сравнению с расчетными.

Для дальнейшего развития проблематики нужно в дальнейшем уточнить до сих пор существующие экспериментальные результаты и расширить энергетический интервал и количество изотопов.

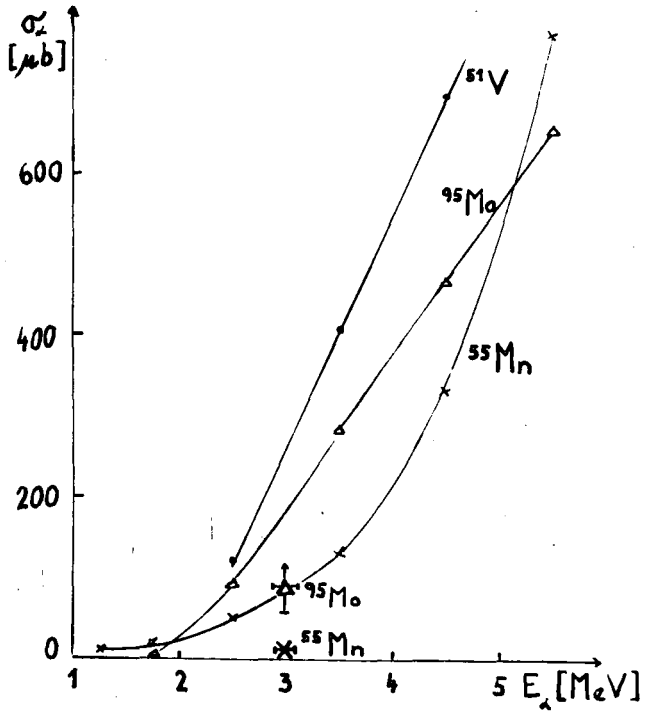

Рис.№1; Функции возбуждения, расчитаны по [3] для ядер ^{51}V, ^{55}Mn, ^{95}Mo и наши экспериментальные величины.

Литература

1. Florek M., Oravec J., Szarka I., Usačev S., Antalík R., Helfer H., Sassonov S., Proseedings of the 2-th Int. Symp., June 1979, Smolenice, Veda Bratislava /1980/103.
2. Salisbury S.R., Chalmers R.A., Phys. Rev. 140 /1965/B 305.
3. Nakagawa T., JAERI-M 84-103 /1984/.
4. Florek M., Oravec J., Szarka I., Holý K., Jahn U., Helfer H., Czech. J. of Phys. B34 /1984/.
5. Szarka I., Florek M., Oravec J., Holý K., Helfer H., Jahn U., Nucl.Inst. and Meth. B17 /1986/472-474.
6. Florek M., Szarka I., Oravec J., Holý K., Mišianiková E., Helfer H., Jahn U., Popov Ju.P., Proc. of the 4-th Int.Symp., Smolenice, June 1985, Veda Bratislava /1986/74.
7. Lang D.W., Nucl. Phys. 77/1966/545.
8. Dilg W. et al., Nucl. Phys. A217/1963/269.
9. Smith W.R., Comp. Phys. Comm. 1/1969/106.
10. McFadden L., Satchler G.R., Nucl. Phys. 84/1966/177.
11. Becchetti F.D., Greenleess G.W., Phys. Rev. 182/1969/1190.
12. Perey F., Buck B., Nucl. Phys. 32/1962/353.

FROM TOTAL NEUTRON CROSS SECTIONS TO THE SYSTEMATICS OF NUCLEAR CHARGE RADII*

I.Angeli, J.Csikai, and A.Algora Pineda
Institute of Experimental Physics, Kossuth University,
H-4001 Debrecen, Pf. 105. Hungary

Experimental investigations and model calculations on fast neutron cross sections lead to a comprehensive study of rms charge radii. The deviation from the rough A dependence follows simple trends with discontinuities at magic neutron numbers as well as at the inset of strong deformations. A correlation between variations of radii and binding energy has been established. The rms radii measured by electron scattering are - on the average - less than those measured by muonic atom X-rays.

1. Fast neutron cross sections and the mass number dependence of the radius parameter $r_o(A)$

The roots of the investigations to be presented here go back to about twenty years. The equipments available to us at that time (neutron generator, scintillation detectors, etc.) set a limit to the fields to be studied. Having this in mind total cross sections of 30 elements were measured at 14 MeV. The aim of these measurements was to search for eventual fine structure in the mass number dependence of total cross sections. Although significant deviations from the smooth mass number dependence was found, these deviations could not be attributed to any simple effect (e.g. odd-even, or N-Z symmetry) 1). The smooth mass number dependence of the total cross sections was described by a simple semi-classical optical model 2, 3, 4). During this work, the role of nuclear radius, the fine structure in its mass number dependence, and its connection to the binding energy per nucleon 5), arose over and over again.

An analysis of nonelastic neutron cross section data at 14 MeV resulted in the mass number dependence of the radius parameter

$$r_o(A) = 1.21 + \frac{4.0}{A^{2/3}} - \frac{15}{A^{4/3}} \text{ (fm)} \qquad (1)$$

if the expression

$$\sigma_{NE} = \pi(r_o(A)A^{1/3} + \lambda\!\!\!^{-})^2 \qquad (2)$$

is used, and

$$r_o(A) = 1.27 + \frac{5.6}{A^{2/3}} - \frac{17}{A^{4/3}} \text{ (fm)} \qquad (1')$$

if $\lambda\!\!\!^{-}/2$ is used instead of $\lambda\!\!\!^{-}$ in (2).

*This work was supported by the Hungarian Research Foundation (Contract No. 259.)

However, small systematic deviations from this smooth mass number dependence can not be unambiguously established because the accuracy of nonelastic cross section data is limited and no data on series of separated isotopes are available. Therefore, our attention turned to the fine structure in nuclear charge radii.

2. Fine structure in the mass number dependence of nuclear charge radii

The present-day sources of nuclear charge radii yield the quantity $r=\langle r^2\rangle^{1/2}$, or differences thereof for neighbouring nuclei; both r and Δr are more or less model independent. Fast electron scattering, characteristic X-rays from muonic atoms may yield both r and Δr values, while optical isotope shifts (including modern versions using laser techniques) and K_α isotope shifts yield only Δr differences between isotopes of elements. Composing literature data measured with these methods, long series of $r_Z(N)$ values can be constructed. It is worth to normalize these experimental data by the well-known formula

$$r_C = \sqrt{\tfrac{3}{5}}\, r_o(A)\, A^{1/3}, \tag{3}$$

where

$$r_o = 1.15 + \frac{1.8}{A^{2/3}} - \frac{1.2}{A^{4/3}} \quad (\mathrm{fm}). \tag{4}$$

For the isotopes of a given element, the increase of radii with neutron number N is systematically less than expected from the above simple formula. This can be illustrated 6) by plotting the ratio

$$\varrho_Z(N) = \frac{r_Z(N)}{r_C(A)} \tag{5}$$

as a function of N. These points lie very close to a straight line, the coefficient of correlation being generally higher than 0.95. Therefore, we may write

$$\varrho_Z(N) = a_Z N + b_Z = \left(\frac{\partial \varrho}{\partial N}\right) N + b_Z \tag{6}$$

The good linearity means that the derivative $\left(\frac{\partial \varrho}{\partial N}\right)$ is constant in a wide range of neutron numbers. It would be interesting to find a connection between this derivative and some - approximately constant - property of the nucleus: average density, compressibility? .

It should be noted, however, that there is a sudden increase in the slopes a_Z at magic neutron numbers, showing the effect of neutron shells on the charge distribution. The slopes a_Z depend on the mass number and neutron number in two distinct ways: firstly, the absolute value of a_Z decreases roughly as 1/A, and secondly, there are sudden changes at magic neutron numbers. The 1/A dependence can be explained simply by the liquid drop model. Allowing for this dependence by multiplying a_Z by the average mass number $\bar{A}_Z$ of the element in question, a plot of $a_Z\bar{A}_Z$ products shows up a characteristic saw-tooth structure with drastic changes at magic neutron numbers and at the inset of large deformations 6).

An attempt to the interpretation of the systematic behaviour described above could reproduce the average trend, but not the pronounced shell effects 7). So, a theoretical interpretation of this systematics is still lacking.

3. Correlation in the fine structure of nuclear charge radii and binding energies

An interesting relation between radii and binding energies is worth mentioning. Plotting the quantity

$$\beta_N = \Delta_{2N} \left[\left(\frac{B_{exp}}{B_S} \right) 8A \right] \qquad (7)$$

where B_{exp} is the experimental binding energy,

B_S is calculated by Seeger's semiempirical formula, we have the "reverse" of the $a_Z \bar{A}_Z$ plot 8). It should be noted that β_N values derived from different isotopic sequences, follow approximately the same dependence on N. This is the reason why Nir calls it a "universal" function 9). This universality results in a broad predictive power 8).

4. Differences between radii determined by electron scattering and muonic atom X-rays

In principle, the root-mean-square (rms) radius for a given nuclide should be the same value, irrespective of the method of measurement. However, this does not seem to be true for rms radii determined by electron scattering r_{el} and muonic atom X-rays r_{mu}. Ruckstuhl 10) has measured r_{mu} for the nucleus ^{12}C, and concluded that there is a 2.4 x (standard deviation) difference between the two radii:

$$r_{el} - r_{mu} = -2.4 \text{ st. dev.}$$

This difference is tentatively attributed to a short-range additional weak interaction between muon and nucleons. Dispersive effects at electron scattering may also cause appreciable $r_{el} - r_{mu}$ differences 11). An analysis of up-to-date r_{el} and r_{mu} data has shown 12) that the average difference is

$$\overline{r_{el} - r_{mu}} = -0.006 (\pm 0.002) \qquad \text{(fm)}.$$

Its absolute value is higher for light nuclei, and decreases with increasing mass number. The mass number dependence of the difference may perhaps help in deciding the right interpretation: cross section normalization, dispersive effects in electron scattering, nuclear polarization, or additional weak interaction in muonic atoms? If neither of these can be held responsible for the difference, this would render the issue even more challenging.

References

1) I.Angeli, J.Csikai, J.Nagy, T.Scharbert, T.Sztaricskai and D.Novák: Acta Physica Hungarica, 30 (1971) 115
2) I.Angeli and J.Csikai: Nuclear Physics, A148 (1970) 389
3) I.Angeli and J.Csikai: Nuclear Physics, A170 (1971) 577
4) I.Angeli, P.Nagy and J.Csikai: Nuclear Science and Eng. 55 (1974) 418
5) I.Angeli, J.Csikai and I.Hunyadi: Physics Letters, 29B (1969) 36; Acta Physica Hungarica, 28 (1970) 87
6) I.Angeli and M.Csatlós, Nuclear Physics, A288 (1977) 480
7) I.Angeli, M.Beiner, R.J.Lombard and D.Mas: Journal of Physics G: Nuclear Physics, 6 (1980) 303
8) I.Angeli: Physics Letters, 82B (1979) 313; I.Angeli and R.J.Lombard: Zeitschrift für Physik, A324 (1986) 299
9) D.Nir: Physical Review, C18 (1978) 1022
10) W.Ruckstuhl, B.Aas, W.Beer, I.Beltrami, K.Bos, P.F.A.Goudsmit, H.J.Leisi, G.Strassner, A.Vacchi, F.W.N.De Boer, U.Kiebele and R.Weber: Nuclear Physics, A430 (1984) 685
11) E.A.J.M.Offermann, L.S.Cardman, H.J.Emrich, G.Fricke, C.W.De Jager, H.Miska, D.Rychel and H.de Vries: Phys. Rev. Letters, 57 (1986) 1546
12) I.Angeli and R.J.Lombard: (to be published)

ON THE USE OF NUCLEAR REACTION THEORY METHODS IN APPLIED CALCULATIONS OF NEUTRON FLUX FUNCTIONALS

Ippolitov, V.T., Korolyov E.V., Pozdnyakov A.V.

V.G. Khlopin Radium Institute, Leningrad,USSR

The expression for the real part of an optical potential is obtained on the basis of real nucleon-nucleon forces. The results of cross section calculations are performed. This method is recommended for neutron cross sections calculations for nuclei range where experimental data do not exist.

Neutron flux functionals are the objects of practical interest in the calculations of neutron fields in different assemblies:

$$Y = \iiint F(\vec{r}, E, \vec{\Omega})\, P(\vec{r}, E, \vec{\Omega})\, d\vec{r}\, dE\, d\vec{\Omega}, \qquad (1)$$

where F is a neutron flux density, P is a given function.

The Monte Carlo method is most often used in calculations of assemblies, that have the complicated geometries and compositions. Using the Monte Carlo method it is possible to calculate the functional (1) by averaging of some random quantity on neutron trajectories, not determining the neutron flux density in the all phase space.

The determination of the neutron path length in complicated geometries is one of the principal difficulties of the neutron trajectories simulation. The modern Monte Carlo codes allow to solve this problem and to reduce to minimum the calculational error connected with a simplification of the real geometry.

A representation of energy dependent neutron cross sections is an another problem of neutronics calculations. The multigroup approximation with use of group constants libraries is widely practised for solution of this problem. Increasing the number of groups up to several thousand in the energy range up to 15 - 20 MeV it is possible to decrease the methodical error of group constants and to make it comparable with initial data uncertainties.

The group constant libraries are generated from evaluated data files based on experimental data. The results of differential experiments are far from being complete and they have many discrepancies. In the process of data evaluation the calculations based on the nuclear reaction theory are often used. The reliability of the results depends on an adequate choice of a nuclear model.

The Fig. 1 presents the total cross sections for ^{238}U calculated with use of the coupled channel model /1/ and the data from multigroup neutron cross section library RIYaD /2/ (the number of group is 2293 in energy interval from 10^{-5} eV to 20 MeV). The RIYaD constants for uranium isotopes were generated from ENDF/B-IV files.

With use of both data the Monte Carlo calculations of K for infinite natural uranium medium were carried out. The results of calculations performed a good agreement with each other and with experimental data /3/ (the discrepancies are 0,5 %).

The calculation of the nuclides accumulation and transmutation is the object of the great practical interest. The receipt of reliable results is prevented by an absence of cross section experimental data for the majority of fission products. In this case the problem of nuclear data prediction based on nuclear reaction theory arise.

The nuclear data prediction in a region which is difficult for experimental investigations for example in the region of fission products, is hampered since the information about nuclear level schemes, deformation parameters and optical potential parameters do not exist. In contrast to stable nuclei region where the optical potential parameters for concrete nucleus may be determined by fitting of calculated cross sections to experimental data, the optical potential for fission products has to have the greater predictional potency and, therefore, has to be constructed within limits of microscopic approach.

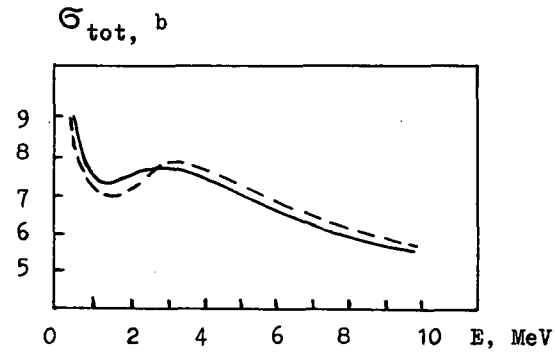

Fig. 1 The total cross sections for ^{238}U: full line - the results of coupled channel calculations; dashed line - the multigroup library RYDaD data

Let consider in detail a possibility of an optical potential real part construction based on the real nucleon-nucleon forces.

As NN-interaction we use nucleon-nucleon potentials of one-boson-exchange model (OBEP). Expanding them in series on zero-range velocity dependent potentials and limiting by square terms of relative transfer momentum it is possible to obtain an expression for an effective nucleon-nucleon interaction making a contribution to the central nuclear field /4/:

$$V_{12} = t_0\{1+x_0\hat{P}_\sigma\}\delta(\vec{r}_1-\vec{r}_2)-\frac{1}{8}\{t_1+x_1\hat{P}_\sigma\}\left[(\vec{\nabla}_1'-\vec{\nabla}_2')^2\delta(\vec{r}_1-\vec{r}_2) + \delta(\vec{r}_1-\vec{r}_2)(\vec{\nabla}_1-\vec{\nabla}_2)^2\right]+\frac{1}{4}\{t_2+x_2\hat{P}_\sigma\}(\vec{\nabla}_1'-\vec{\nabla}_2')\delta(\vec{r}_1-\vec{r}_2)(\vec{\nabla}_1-\vec{\nabla}_2), \quad (2)$$

where P is the spin-exchange operator, is the gradient operator acting only on the left, -acts only on the right, the coefficients t_k and x_k are defined via masses and coupling constants of exchange mesons.

The effective interaction (2) allows to receive, in the Hartree-Fock approximation, the analytical expression for an equivalent energy dependent potential V(r, E), which may be considered as the real part of a nucleon-nucleus optical potential (see /4/). In particular, for a neutron-nucleus potential we have:

$$\begin{aligned} V(r, E) &= V^o_{av}(r)+V^E_{av}(r)E+V^o_\tau(r)+V^E_\tau(r)E, \\ V^o_{av}(r) &= \rho(r)g(r)\left[c_o+c_1\rho^{2/3}(r)+c_2\frac{\nabla^2\rho(r)}{\rho(r)}\right], \\ V^E_{av}(r) &= \frac{2\gamma_1+\gamma_2}{2}\rho(r)g(r), \\ V^o_\tau(r) &= \Delta\rho(r)g^2(r)\left[b_o+b_1\rho(r)+b_2\rho^{2/3}(r)+b_3^{5/3}\rho(r)+b_4\nabla^2\rho(r)\right], \\ V^E_\tau(r) &= \frac{\gamma_2}{2}\Delta\rho(r)g^2(r) \end{aligned} \quad (3)$$

Here V_{av} and V are the isoscalar and the isovector components of the real part of the optical potential, (r) is the nuclear density distribution,

$$\Delta\rho = \rho_n(r)-\rho_p(r),$$

$$g(r)=((1+\frac{2\gamma_1+\gamma_2}{2})\rho(r))^{-1},$$

E is the incident energy. The coefficients c_i, b_i, γ_i depend only on the coupling constants and masses of the exchange mesons.

In other words, now we have the relation between OBEP parameters and parameters of Re Vopt.

In the considered approach all the components of V(r, E) have different formfactors whose shapes are basically determined by the tensor forces connected with the one-pion exchange. The calculations have shown /5/, that all versions of OBE-potentials taking into account the one-pion exchange (the PVS-models) lead to an appearance of discontinuities in the formfactors for all the components of V(r, E). It is probably associated with features of NN-potential expansion. Limiting this expansion by square terms of relative transfer momentum we inexactly take into account the contribution of long-range tensor forces connected with one-pion exchange. Decreasing the pion-nucleon coupling constant, i.e. decreasing the tensor forces contribution it is possible to eliminate the formfactor discontinuities in all PVS-models. Decreasing the one-pion exchange contribution into NN-interaction we pass on to a some effective nucleon-nucleon interaction, which differs from the vacuum one. The presence of surrounding nucleons must influence in the first place on the processes connected with the pion exchange, since such processes are characterized by transfer momentum less than K_F and their contribution, according to Pauli principle,must be suppressed. In the case of heavy mesons exchange (scalar and vector mesons) a typical transfer momentum is greater than K_F and Pauli principle has no importance.

The direct comparison of the real part of the optical potential calculated on the basis of meson theory of NN-potentials, Re V^M_{opt}, with phenomenological optical model potentials is hampered since Re V^M_{opt} has the formfactor that differs from the Saxon-Wood's one. Therefore the value of g^2 was chosen by comparison of the neutron cross sections, calculated with Re V^M_{opt} , with experimental data and the cross sections calculated with help of phenomenological potentials for ^{208}Pb. The calculations were carried out with the OBE--potential /6/ taking into account the exchange of real mesons and resonances only. A Saxon-Wood's distribution with r_o = 1.2 fm, a = 0.5 fm and (0) = 0.17 fm^{-3} was taken as (r). Since in the offered approach only the real part of a central potential is calculated it is necessary to choose Im Vopt and a spin-orbital potential V_{SO} for the neutron cross sections calculations. In principle, in our approach there is a possibility to construct V_{SO} , but for the simplification of calculation we use the phenomenological spin--orbital potential. In the concrete calculations Im Vopt and V_{SO} of the potential /7/, whose parameters were determined on the basis of totality of experimental data for nuclei with A 40 and incident energy E_n 50 MeV were used.

The performed calculations show that using Re V^M_{opt} calculated from NN-potential /6/ with g^2 = 2.0 and phenomenological Im V_{opt} /7/ it is possible to describe (with discrepancies 10 %) the neutron cross sections for spherical nuclei with A 80 in the energy interval from 1 to 16 MeV.

Fig. 2 presents the neutron total and elastic cross sections calculated for ^{107}Ag using both Re V^M_{opt} and phenomenological potential /7/. In the same picture the data from ENDL files are shown. It is necessary to emphasize that used optical potential real part has the only free parameter g^2 which have been determined by fitting of calculated cross sections to ENDL data for ^{208}Pb and have not been changed in subsequente calculations.

When g^2 = 2.0 the isoscalar component of Re V^M_{opt} practically coincide with phenomenological $V^o_{av}(r)$ 3 /7/, but isovector component has the shape which differs from Saxon--Wood's one and essentially differs from phenomenological ones. Therefore the suggested potential will have the greatest difference from phenomenological potentials for nuclei with A Z (A Z), in particular, for fission products. Since V(r, E) have been constructed proceeding from sufficiently common physical conceptions the use of it in neutron cross sections calculation for fission products is more reasonably than extrapolation into this region of phenomenological optical potentials which were obtained from analysis of experimental data for stable nuclei.

We believe that the afore-cited examples of concrete calculations illustrate the feature of our approach consisting in a development of nuclear reaction theory and nuclear models on the more fundamental basis that is necessary for providing of growing nuclear data requirements for applied neutronics calculations.

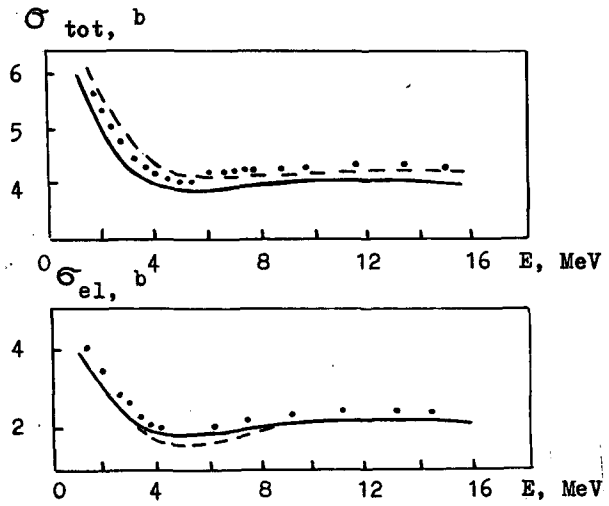

Fig. 2 The cross sections tot and el for ^{107}Ag, calculated with V(r, E) when g^2 = 2.0 (full line), dashed line - the cross sections calulated with phenomenological potential /7/, points - ENDL data

References

/1/ Lagrange Ch., Report NEANDC (E) 228 "L", CEA, 1982

/2/ Dushin V.N., Korolyov E.V., Matveev G.V., Atomnaya Energiya, 1987, v. 63, N 6, p. 452

/3/ Nikolaev M.H. et al., JETF, 1958, v. 34, p. 752

/4/ Pozdnyakov A.V. et al., Bull. Acad. Sci. USSR, Phys., 1980, v. 44, p. 2316

/5/ Pozdnyakov A.V. et al., Bull. Acad. Sci. USSR, Phys., 1982, v. 46, p. 874

/6/ Gerstew A. et al., Phys. Rev., 1971, v. D3, p. 2076

/7/ Becchetti F.D. et al., Phys. Rev., 1969, v. 182, p. 1190

СПЕКТРЫ НЕЙТРОНОВ УТЕЧКИ ИЗ УРАНОВОЙ И ТОРИЕВОЙ СФЕР С КАЛИФОРНИЕВЫМ ИСТОЧНИКОМ НЕЙТРОНОВ

С.П. Симаков, А.А. Андросенко, П.А. Андросенко, Б.В. Девкин, Б.В. Журавлев, М.Г. Кобозев, В.А. Талалаев

Физико-энергетический институт, Обнинск, СССР

В.А. Загрядский, Д.Ю. Чувилин

Институт атомной энергии им. И.В. Курчатова, Москва, СССР

I. Введение

Целью интегральных экспериментов и сравнения их данных с результатами расчетов является проверка файлов оцененных ядерных данных, а также тестировка программ и методов, используемых в расчетах переноса излучений в веществе /I/ . Среди различных типов интегральных экспериментов эксперименты со сферическими сборками и нейтронным источником в центре характиризуются наиболее простой (сферически симметричной) геометрией, что позволяет прежде всего эффективно решать задачу тестировки нейтронных данных. К этому типу относится эксперимент, описанию которого посвящена настоящая работа.

Наш интерес к этой работе вызван также еще двумя обстоятельствами. Во-первых, насколько известно из литературы, данных по спектрам нейтронов утечки из U и Th сфер с калифорниевым источником нет. Во-вторых, в описываемом эксперименте спектр нейтронов утечки измерялся методом времени пролета, в то время как ранее в подобных экспериментах с калифорниевым источником всегда применялся амплитудный метод. Поэтому представляет интерес исследование возможности приложения метода времени пролета к интегральным экспериментам со спонтанно распадающимся нейтронным источником.

2. Эксперимент

Измерения спектров нейтронов утечки из U и Th сфер проводились методом времени пролета на установке, схематически изображенной на рис. I. Источником нейтронов являлась быстрая ионизационная камера со слоем ^{252}Cf, нанесенным на один из двух плоских электродов /2/ . Электрический сигнал с камеры использовался для получения стоп-сигнала для временного анализатора нейтронов утечки и для счета числа актов деления за время эксперимента. Уровень дискриминации в усилителе-формирователе устанавливался таким, чтобы отсечь сигналы соответствующие α-частицам. Интенсивность калифорниевого источника нейтронов на момент проведения эксперимента составила $5 \cdot 10^5$ нс.

Исследуемые сборки, выточенные из металлического урана и тория, представляли собой полые сферы с размерами, приведенными в таблице I. Камера с ^{252}Cf вводилась внутрь сферы через цилиндрический канал диаметром 5 см. Ториевая сфера очехлована сверху алюминиевой фольгой толщиной I,5 мм.

Нейтроны, вылетающие из сборки, регистрировались сцинтилляционным детектором, расположенным детектором, расположенном в защите. Детектор состоял из кристалла стильбена Ø 6,3 см и высотой 4 см и ФЭУ I43-I /3/ . Порог регистрации нейтронов равнялся 0,I МэВ, суммарное временное разрешение детектора и камеры с ^{252}Cf - 3 нс, пролетное расстояние источник-детектор - 385 см. Для определения вклада фоновых нейтронов, рассеянных помещением, между

сферой и детектором устанавливался металлический конус длиной 100 см. Благодаря массивной защите вокруг детектора временное распределение фоновых нейтронов было равномерным, а отношение эффект/фон ≃ 15.

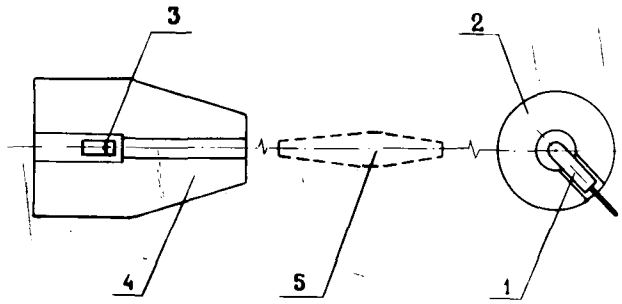

Рис. I Схема эксперимента: I. Камера с ^{252}Cf, 2. Сборка, 3. Детектор, 4. Защита, 5. "Теневой" конус,

Таблица I. Параметры исследованных сфер

Элемент	радиус, см		Вес, кг
	внешний	внутренний	
^{238}U (0,4 % ^{235}U)	I2	4	I30
^{232}Th	I3	3	I05

После вычитания фона временной спектр нейтронов утечки преобразовался в энергетический. Так как стоп-сигналы от камеры деления распределены во времени статистически, то в спектр вводилась поправка на их случайные наложения /4/ . При средней частоте поступления стоп-сигналов $1{,}3 \cdot 10^5$ сек $^{-1}$, поправка имела величину 3 - 10 %. Эффективность регистрации нейтронов детектором измерялась в такой же последовательности и такой же геометрии эксперимента, когда источник нейтронов устанавливался один без сфер.

Искомый спектр нейтронов, вылетевших с поверхности сфер в телесный угол на один нейтрон источник и на единицу энергии, находился согласно следующему выражению:

$$L(E) = \frac{N_{сф}(E)}{N_{ист}(E)} \cdot \frac{M_{ист}}{M_{сф}} \cdot S(E) \qquad (1)$$

Где $N_{сф}(E)$ и $M_{сф}$ зарегистрированный детектором спектр нейтронов и соответствующее ему число актов деления в случае измерения со сферой,
$N_{ист}(E)$ и $M_{ист}$ - то же самое, для случая измерения с голым источником.

Спектр мгновенных нейтронов спонтанного деления ^{252}Cf и $S(E)$ задавался в виде распределения Максвелла с параметром $T = 1{,}42$ МэВ и корректирующей функцией $\mu(E)$, как это рекомендавано в работе /5/ :

$$S(E) = 2\sqrt{E/\pi \cdot T^3}\ \exp(-E/T)\ \mu(E) \qquad (2)$$

Из выражения (I) видно, что спектр нейтронов утечки $S(E)$ получается из отношения экспериментальных величин, измеряемых в близких экспериментальных условиях: камера с ^{252}Cf, окруженная исследуемой сборкой, и без нее. Отсюда следует, что измерения являются относительными и $L(E)$ не содержит таких систематических погрешностей как, например, погрешность определения эффективности детектора или числа нейтронов, вылетевших из источника. Погрешность спектра нейтронов утечки, измеренная таким способом будет определяться в основном статистической точностью (в нашем случае она равна 0,5 - I0 % для интервала энергий I МэВ в диапазоне I - 9 МэВ), стабильностью работы аппаратуры ($\simeq$3 %) и точностью, с которой известен спектр нейтронов деления ^{252}Cf ($\simeq$2 % /5/). Таким образом полная погрешность экспериментальных данных составляет 4 - II %.

3. Результаты измерений и расчетов

Экспериментальные данные и результаты расчетов по спектрам нейтронов утечки из U и Th сфер показаны на рис. 2 и 3, а также приведены в таблице 2, проинтегрированные по энергии в указанных интервалах. Все расчеты в настоящей работе выполнены по программе BRAND /6/, моделирующей процесс переноса излучений в веществе методом Монте-Карло. В программе в качестве константного модуля используется NEDAM /7/ , основанная на библиотеке оцененных нейтронных данных ENDL- 75. В расчетах спектр нейтронов источника задавался согласно выражению /2/ .

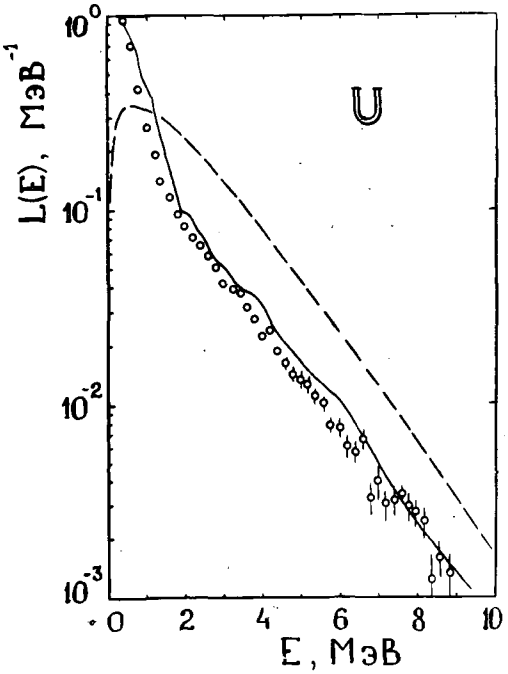

Рис. 2 Спектры нейтронов утечки из урановой сферы: - эксперимент, - расчет, Спектр нейтронов калифорниевого источника (2):

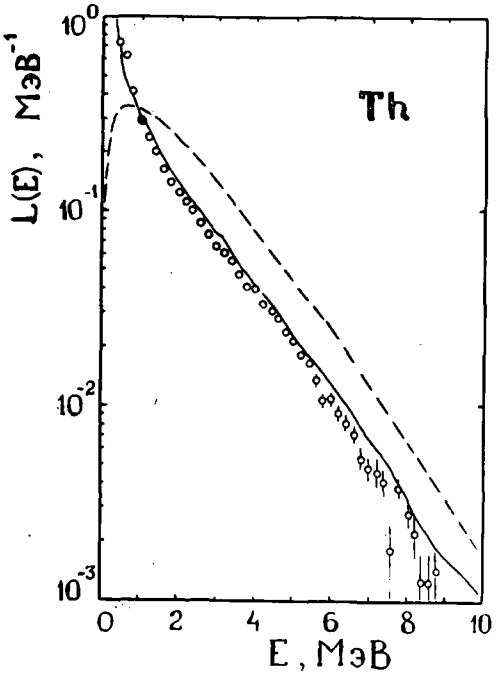

Рис. 3 Тоже, что на рис. 2, для ториевой сферы.

При сравнении экспериментальных и нейтронных данных прежде всего возникает вопрос о влиянии на экспериментальные результаты таких факторов, как рассеяние нейтронов источника на конструкционных элементах камеры, точность метода измерения по времени пролета, наличие канала в сборках. Оценка влияния перечисленных факторов проводилась расчетным путем.

Таблица 2 Результаты измерений и расчетов

Ядро	E, МэВ	Ф1	Ф2	Ф3	$\int L(E)dE$, н/1н источника		Расчет
					эксперимент	расчет	эксперимент
U	0,4-1	1,01	1,03	1,00	0,3470 ± 0,0130	0,3968 ± 0,0018	1,14 ± 0,04
	1-2	1,00	1,02	1,04	0,1491 ± 0,0054	0,2120 ± 0,0016	1,42 ± 0,05
	2-3	1,00	1,01	1,03	0,0636 ± 0,0025	0,0710 ± 0,0011	1,12 ± 0,04
	3-4	0,99	1,01	1,01	0,0346 ± 0,0014	0,0408 ± 0,0008	1,18 ± 0,05
	4-5	0,99	1,00	1,00	0,0189 ± 0,0010	0,0221 ± 0,0005	1,17 ± 0,06
	5-6	0,98	1,00	1,00	0,0109 ± 0,0006	0,0136 ± 0,0004	1,25 ± 0,08
	6-7	0,98			0,0057 ± 0,0004	0,0073 ± 0,0003	1,28 ± 0,11
	7-8	0,98			0,0032 ± 0,003	0,0033 ± 0,0002	1,03 ± 0,12
	8-9	0,97			0,0018 ± 0,0002	0,0020 ± 0,0002	1,11 ± 0,17
	0,4-9				0,634 ± 0,023	0,7689 ± 0,0029	1,21 ± 0,04
Th	0,4-1	1,01	1,02	1,01	0,3150 ± 0,0110	0,2583 ± 0,0011	0,82 ± 0,03
	1-2	1,00	1,01	1,02	0,1957 ± 0,0071	0,2040 ± 0,0010	1,04 ± 0,04
	2-3	1,00	1,00	1,02	0,0958 ± 0,0035	0,1010 ± 0,0007	1,05 ± 0,04
	3-4	0,99	0,99	1,02	0,0523 ± 0,0019	0,0585 ± 0,0006	1,12 ± 0,04
	4-5	0,99	0,99	1,01	0,0295 ± 0,0011	0,0315 ± 0,0004	1,07 ± 0,04
	5-6	0,98	0,99	1,01	0,0148 ± 0,0008	0,0163 ± 0,0003	1,10 ± 0,05
	6-7	0,98			0,0075 ± 0,0004	0,0091 ± 0,0002	1,21 ± 0,07
	7-8	0,98			0,0036 ± 0,0003	0,0049 ± 0,0002	1,36 ± 0,13
	8-9	0,97			0,0016 ± 0,0001	0,0020 ± 0,0001	1,25 ± 0,11
	0,4-9				0,716 ± 0,026	0,6856 ± 0,0018	0,96 ± 0,03

Искажение спектра нейтронов источника происходит главным образом за счет рассеяния на электродах (диски ø 20 мм, толщиной δ = 0,18 мм) и стенках камеры (δ = 0,35 мм). Как видно (см. поправку Ф1 (E) в таблице 2) происходит незначительное "смягчение" спектра нейтронов источника.

Отличие геометрии исследуемой сборки от сферически симметричной обусловлено наличием отверстия, через которое источник вводится внутрь сферы. Расчеты показали, что отношение Ф2 (E) спектров утечки из целой сферы и из сборки с каналом имеет величину не превышающую величину соответствующего отношения масс 1,03.

При измерении спектров нейтронов утечки методом времени пролета из массивных образцов, строго говоря, нарушается связь между временем пролета и энергий нейтроноа. Это происходит из-за задержки нейтрона, испытывающего многократные рассеяния в таком образце. Для оценки величины соответствующей поправки в расчетах по BRAND моделировался эксперимент по времени пролета и процедура обработки данных. Вначале рассчитывался временной спектр нейтронов утечки с учетом реального времени пролета на пути источник-сфера-детектор и эффективность детектора. Далее временной спектр преобразовывался в энергетический L_t (E) и сравнивался с прямым расчетом энергетического спектра нейтронов утечки L_E(E). Как видно из таблицы 2, соответствующая поправка Ф3(E) = L_E(E)/L_t(E) также сравнительно невелика.

Приведенные на рис. 2 и 3 и в табл. 2 экспериментальные данные уже поправлены на перечисленные выше факторы (т.е. на функцию $\Phi(E) = \Phi 1^{-1} \Phi 2 \Phi 3$) и соответствуют таким образом спектру нейтронов утечки из сферически симметричной сборки с источником нейтронов в центре с распределением по энергии (2).

Там же приведены расчетные данные по спектрам нейтронов утечки, выполненные по программе BRAND с оцененными нейтронными данными из библиотеки NEDAM. Как видно, расхождения между рассчетными и экспериментальными данными во многих энергетических интервалах превышает их суммарную погрешность, что свидетельствует о неточности использованных в расчетах файлов оцененных нейтронных данных. Интересно отметить, что для урановой сферы согласие заметно более худшее. Аналогичный результат был получен нами для спектров нейтронов утечки из этой урановой сборки с I4 МэВ - источником нейтронов в центре /8/ : в интервале энергий вторичных нейтронов 0,4 - I0 МэВ отношение расчет/эксперимент равнялось I,27 ± 0,08. Использование в расчетах данных из библиотеки ENDF/BIV дало отношение I,05 ± 0,06. Таким образом в обеих случаях (с I4 МэВ и Cf -источниками нейтронов) обнаруживается плохое качество библиотеки оцененных данных

4. Заключение

В настоящей работе спектр нейтронов утечки из сферических сборок со спонтанно делящимся источником нейтронов ^{252}Cf в центре измерен методом времени пролета. По сравнению с амплитудным методом, применявшимся в других работах для подобных измерений /I/ , следует отметить ряд преимуществ.

Во-первых, измерения спектров нейтронов утечки и определение эффективности детектора происходит по существу в одном эксперименте и в одной геометрии. Таким образом нет необходимости, как в случае амплитудного метода, калибровать детектор относительно других источников излучений, что в конечном счете повышает надежность измеряемой информации. Кроме того, спектрометр по времени пролета обладает функцией отлика, которую в случае измерения сплошных энергитических распредений можно, как правило, считать δ -функцией, поскольку ее относительная ширина сравнительно мала (в нашем случае $\Delta E/E \simeq 8$ %). В амплитудном методе функция отклика детектора на основе органического сцинтиллятора представляет собой более или менее равномерное распределение амплитуд импульсов от нейтронов с определенной энергией. Поэтому здесь возникает задача тщательного определения функции отклика спектрометра и восстановления энергетического распределения из аппаратурного, что вносит дополнительные погрешности.

С другой стороны, приложение метода времени пролета к измерениям спектров нейтронов утечки из интегральных сборок со спонтанно делящимся источником нейтронов вносит свои характерные особенности. Речь идет о случайном наложении стоп-сигналов, нарушении связи между энергией нейтрона и временем пролета, влиянии ионизационной камеры на спектр нейтронов источника. Как было показано выше, влиянием перечисленных факторов можно либо пренебречь, либо сравнительно легко учесть. Но в других случаях, например, измерениях спектров утечки из сборок больших размеров оно может заметно возрастать.

Полученные в работе экспериментальные данные по спектрам нейтронов утечки из U и Th сфер с Cf -источником нейтронов в центре сравнивались с расчетами, в которых в качестве константного модуля использовалась библиотека оцененных нейтронных данных NEDAM. Обнаруженные заметные расхождения, особенно в случае урановой сферы, свидетельствуют о неточности данных в этой библиотеке.

Литература

/I/ И.Г. Горячев, Ю.И. Колеватов и др. "Интегральные эксперименты в проблеме переноса ионизирующих излучений", М., Энергоиздат, I985

/2/ В.Я. Барыба, Н.В. Корнилов и др. Вопросы атомной науки и техники, Сер. Реакторостроение, I977, вып. 5 (I9), с. 45

/3/ В.А. Талалаев, С.П. Симаков и др., Доклад на международной конференции по нейтронной физике, (22 - 25 сентября I987 г., г. Киев)

/4/ Н.В. Корнилов, Препринт ФЭИ - 467, Обнинск, I974 г.

/5/ J. Grundl, C. Eisenhauer, Report IAEA-208, Vienna, 1978, v. 1, p. 53

/6/ Андросенко А.А., Андросенко П.А., Вопросы атомной науки и техники. Сер. Физика и методы расчета ядерных реакторов. М., ЦНИИАИ, I985, с. 33.

/7/ Андросенко П.А. Там же, с. 45.

/8/ Андросенко А.А., Андросенко П.А. и др. Доклад на международную конференцию по нейтронной физике (22 - 25 сентября I987 г., г. Киев).

COINCIDENCE EXPERIMENTS ON LIGHT NUCLEI WITH INTERNAL TARGET IN ELECTRON STORAGE RING

S.G. Popov
Institute of Nuclear Physics, 630090 Novosibirsk, USSR.

The properties of an electron as a perfect probe of nuclear matter are well-known: point-like character, good knowledge of electromagnetic interaction which is weak in comparison with nuclear forces. However, corresponding cross sections are small and the presence of the radiation tail impose strict demands on the experimental statistics. High beam intensity and large target thickness are standard conditions for high luminosity. Experiments are carried out usually with linear electron accelerators.

Coincidence experiments being necessary for modern nuclear physics can be performed with the high duty factor only which is not the case for conventional linear accelerators. Recently a few facilities of new generation became available and several projects have been suggested. The Table 1 gives a list of machines in operation and in construction for energies in a broad range 100 MeV - 4 GeV.

The alternative method using a superthin internal target in an electron storage ring has been developed in Novosibirsk. The main advantages of this methodics are

i) high efficiency of utilizing the accelerated electron beam
ii) high duty factor
iii) high energy and kinematical precision at high luminosity
iv) excellent possibilities of detecting secondary particles
v) possibilities to use exotic targets as well as beams.

By means of this methodics electroexcitation coincidence experiments on light nuclei (12-C, 14-N, 16-O) were carried out at excitation energies up to 70 MeV. Various reaction mechanism (direct, resonant, preequilibrium and statistical) are separated and analysed.

As an illustrative example, Fig. 1 shows the dependence of the proton temperature (for "equilibrium" proton component with isotropic angular distribution and quasi-Maxwellian spectrum) on excitation energy for 16-O and 14-N. Increase of accuracy and detailed analysis are necessary to understand roughly the constant behaviour of temperature.

The next important step in the progress of electron-nuclear physics will be connected with using longitudinally polarized particles.

Most of results of Novosibirsk group were overviewed in the talk presented at the International Symposium on Modern Developments in Nuclear Physics (Novosibirsk, 1987).

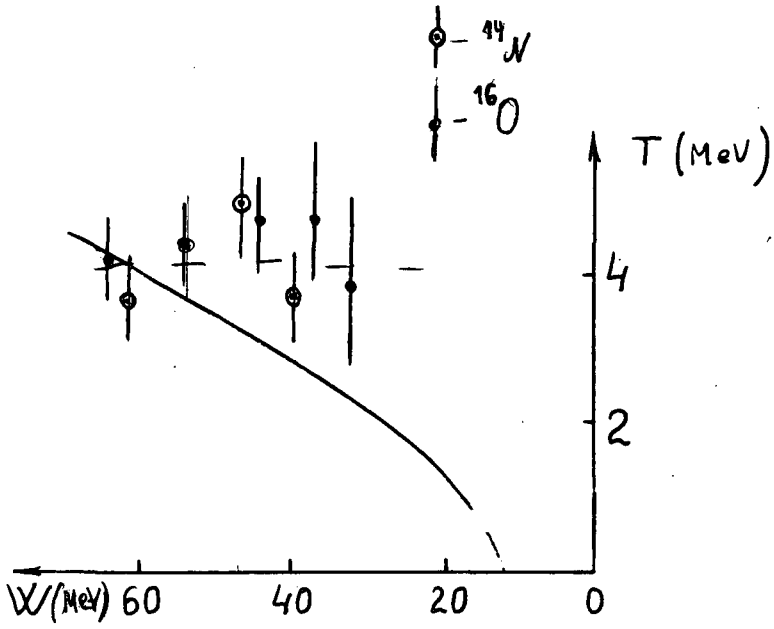
^{14}N
^{16}O
T (MeV)
4
2
W(MeV) 60
40
20
0

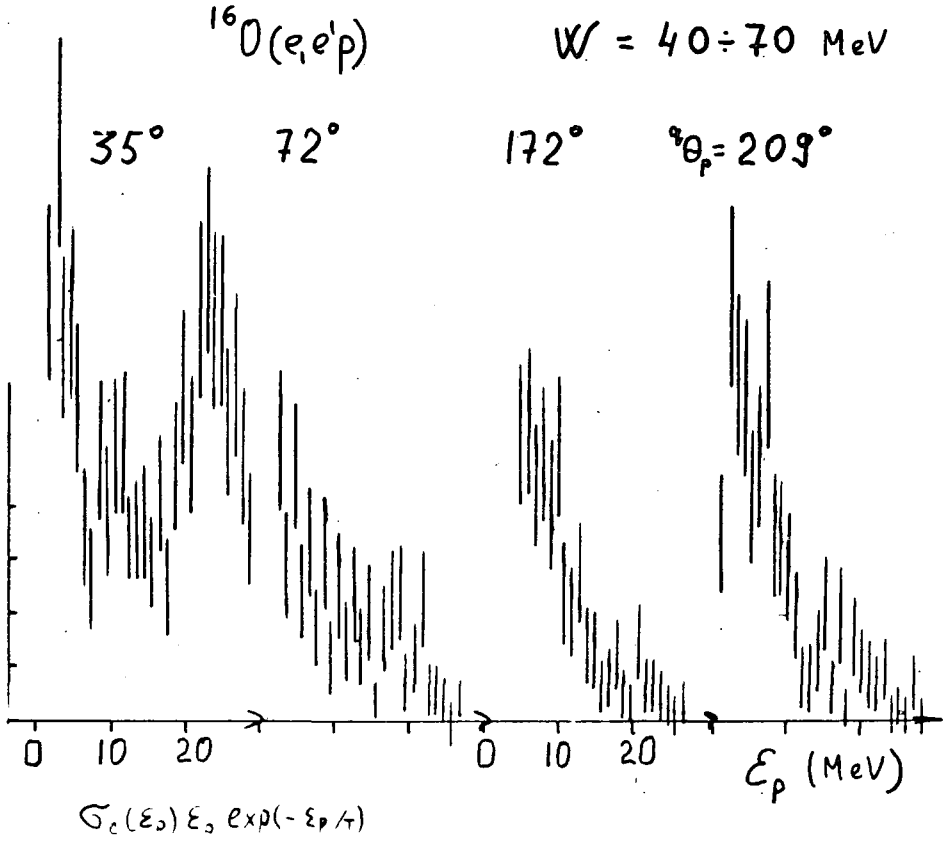
$^{16}O(e,e'p)$
W = 40÷70 MeV
35°
72°
172°
θ_p = 209°
0
10
20
0
10
20
ε_p (MeV)
$\sigma_c(\varepsilon_p)\,\varepsilon_p\,\exp(-\varepsilon_p/T)$

TABLE 1 THE CONTINUOUS ELECTRON BEAM FACILITIES

LABORATORY	TYPE OF ACCEL.	ENERGY, MEV	D.F. %	AVERAGE CURR., MKA
NOVOSIBIRSK, USSR				
1. VEPP-2	SIT	100 -500	90	0.5 A
2. VEPP-3	SIT	400 -2100	100	0.1 A
STANFORD, USA				
3. LINAC	LA	70 -120	75	20
4. PEP	SIT	2-15 GeV	100	50 mA
5. ILLINOIS, USA	RM	67	100	2
6. AMSTERDAM, NETH.	LA	500	2.5	20
7. SACLAY, FRANCE	LA	600	1.0	1.0
8. MAINZ, FRG	RM	180	100	10
9. MIT, USA	LA	700	1.0	0.5
10. TOCHOKU, JAP.	ST	150	80	0.5
PROJECTS				
11. DARMSTADT, FRG	LA	130	100	20
NBS, USA				
12. RTM-1	RM	185	100	550
13. RTM-2	RM	1000	100	300
14. LUND, SVEDEN	ST	100 -550	100	10
15. SASCATOON, CAN	LA	300	80	
16. SAO PAULO, BRAS.	LA+ST	17	100	100
17. SACLAY, FRANCE	LA+ST	500 -2000	100	100
18. MAINZ, FRG	RM	840	100	100
19. CEBAF, USA	RM	500 -4000	80	240
20. ILLINOIS, USA	RM	450	100	20
21. MIT, USA	SIT	250 -1000	100	80 mA
22. ARGONNE, USA	RM	4000	100	300
23. BONN, FRG	ST	3500	60	
24. MSU, USSR	RM	110	100	100
25. KHARKHOV, USSR	ST	2000	100	
26. NOVOSIBIRSK, USSR	SIT	100 -220	90	1.0 A
27. FRASCATI, ITAL.	ST	500	100	100
28. MONTREAL, CAN.	RM	200	100	300
29. TSUKUBA, JAP.	LA	500	2.0	100

LA - Linear accelerator; RM - Racetrac microtron; ST - Stretcher;

SIT - Superthin internal target.

NEW EXPERIMENTAL INSIGHTS INTO THE NUCLEAR FISSION REACTION

J.P. Theobald, Institut für Kernphysik der Technischen Hochschule Darmstadt, D-6100 Darmstadt

Abstract
Experimental results on cold-deformed fragmentation, spontaneous nuclear tripartition, alpha particle associated nuclear fission and on fission fragment kinetic energy fluctuations in resolved neutron resonances are presented and discussed.

Preface

This is a report on experimental work, which has been done with my friends and colleagues: M. Mutterer, C. Budtz-Jørgensen, H.H. Knitter, B. Leroux, M.S. Moore and my students: F.J. Hambsch, P. Heeg, P. Koczon, F. Kraske, J. Pannicke, Patricia Schall, and K. Weingärtner.

1.) Introduction

Recent experiments which we have performed with the fission product spectrometer "COSI FAN TUTTE" at the high flux reactor of the Institute v. Laue-Langevin (ILL) in Grenoble (France), with the "GELINA" supported neutron time-of-flight spectrometer at the Central Bureau for Nuclear Measurements at Geel (Belgium) and with the kinematic spectrometer "DIOGENES" at ILL and in our Institut für Kernphysik der Technischen Hochschule Darmstadt (IKDA), have given us new messages from the nuclear fission process. These news we have partly already transmitted to the scientific community by publications)[1, 2, 3] or by contributions to conferences)[4, 5, 6, 7, 8].

These information refer to (in brakets the names of the instruments with which the corresponding experiments have been performed are quoted):

- cold-deformed or so called "hot" fragmentations)[1, 12], (COSI FAN TUTTE),
- spontaneous nuclear tripartition)[2], (DIOGENES),
- alpha particle associated fission)[4, 5, 6], (DIOGENES), and
- kinetic energy fluctuations of fission fragments in resolved neutron resonances)[3, 7, 8], (GELINA).

As the first two items have been presented and discussed in ref.)[1, 2], I shall only summarize the main observations in chapters 2 and 3. In continuation of my last contribution at Gaussig in 1985),[5] I shall inform you more thoroughly about our latest results on alpha accompanied fission in chapter 4 and discuss the fragment energy fluctuation more detailed for those of you, which have not been at the Kiev Conference on Neutron Physics in September this year)[8] in chapter 5.

2.) "Hot" fragmentation

The scission point configuration of the fissioning nucleus can be characterized by the free energy in this system:

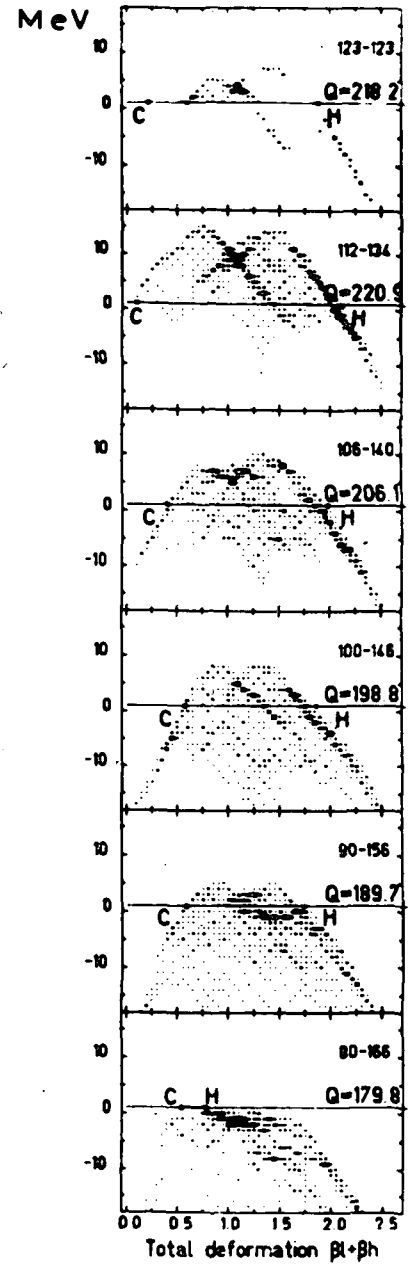

Fig.1. Free energy at the scission for mass splits 123-123, 112-134, 106-140, 100-146, 90-156 and 80-166 amu as function of the total deformation. The thin line is the reaction Q value. Each symbol represents the sum of Coulomb interaction and deformation energies corrected for shell and pairing effects as a function of total deformation. The size of the symbol is a measure of realisation frequency of the corresponding deformation. Cold fragmentation is marked with C and "hot" one with H. In both cases the free energy is equal to zero.

$E_{free} = Q - (V_{int} + V_{LD}$ + shell and pairing corrections) V_{int} is the nascent fragment Coulomb and nuclear interaction energy and V_{LD} the liquid drop energy of the individual fragments. E_{free} is a function of the total deformation energy at scission which is approximatively the sum of the light and heavy fragment deformations

$\beta_L + \beta_H$. For some fragment mass ratios of the $^{245}Cm(n_{th},f)$ reaction the function E_{free} (ε) is displayed in figure 1. This function has two zero points: one for the lowest possible deformation, when the reaction Q-value is tied up essentially in Coulomb potential energy and another one for the highest possible deformation when minimum energy is left for Coulomb repulsion. These two situations characterize cold (C) and "hot" (H) fragmentation. Instead of "hot" the more correct but less stylish notation "cold-deformed" has been suggested.)[13]

Cold fragmentation has been subject of several experiments)[9, 10] and there exist excellent reviews of the experimental and theoretical results)[11]. "Hot" fragmentation has been investigated only recently)[1, 12]. As the results have already been published)[1] and discussed)[13], I shall restrict my report to a summary of the main features of this rare process:

i) "Hot" fragment mass spectra show, like cold mass spectra, fine structures caused by (shell) stabilized fragment masses, and, what has certainly to be confirmed,

ii) "Hot" fragments do not necessarily deexcite by neutron emission, if they do not stay on a 10 ns time scale in a shape isomeric state, which could cause retarded neutron emission, which is not detectable in this experiment.

The latter observation is supported by an experiment of V.P. Zakharova and D.K. Ryazanov)[14], which find zero neutron emission for certain "hot" mass splits.

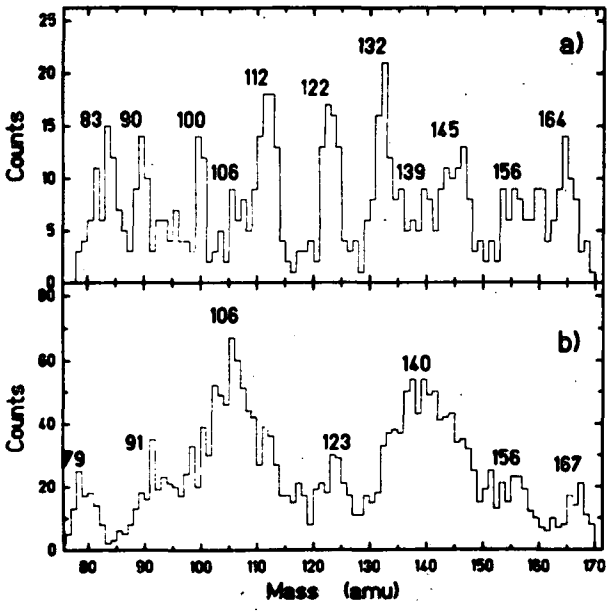

Fig.2. Cold (a) and "hot" (b) fragmentation mass yields of the highest (a) and the lowest (b) kinetic energy observed. Fine structure is marked with mass numbers.

Figure 2 shows for the $^{245}Cm(n_{th},f)$-reaction cold and "hot" fragment mass spectra on a 10^{-5}/MeV yield level. "Hot" fragmentation is an interesting process for the investigation of shell effects on the stability of very deformed nuclei)[13]

3.) Spontaneous tripartition of ^{252}Cf

With the inner part of our toroidal angular position sensitive ionization chamber "DIOGENES")[5], constructed and successfully applied for the investigation of alpha particle associated fission, we have measured energy- and relative angular distributions of the three reaction products from spontaneous ternary fission of ^{252}Cf. Experimental details, in particular techniques to discriminate random triple coincidences of binary fragments are described in ref)[2]. Energy and mass spectra obtained are displayed in figure 3.

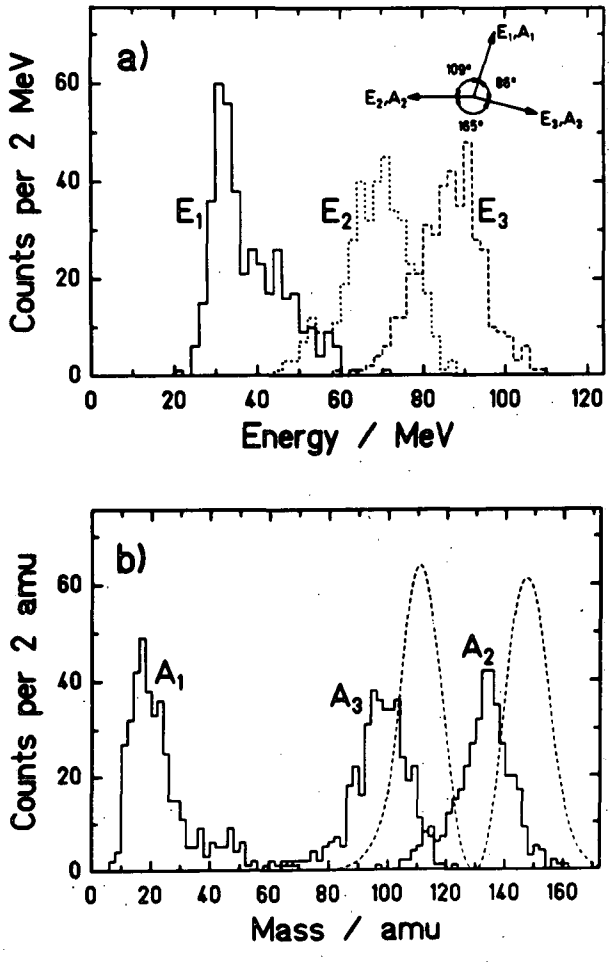

Fig.3a) Energy spectrum of ^{252}Cf ternary fission events, measured with a low-energy threshold of 25 MeV. The inset indicates the corresponding mean angles.
b) Mass distribution calculated from the measured energies and angles using momentum conservation. The binary fission mass spectrum of ^{252}Cf is represented by dashed lines.

While the energy spectra agree quite well with results published by M.L. Muga and collaborators)[15] the mass spectra show significant differences. These discrepancies in the mass assignments are due to the fact that M.L. Muga did not measure the relative angular distribution of the three reaction products but assumed instead a nearly 120° / 120° / 120° / angular correlation. Consequently we do not confirm on the 10^{-6} yield level near symmetric tripartition but the well known charged particle associated fission. For near symmetric tripartition we can give upper limits as listed in table I.

Table I

Mass of the Lightest Particle		$\sigma_{ternary}/\sigma_{binary}$
$12 < A < 30$	"Light-Particle Accompanied Fission"	$\approx 10^{-6}$
$30 \leq A < 70$	"Asymmetric Tripartition"	$< 8 \cdot 10^{-8}$
$70 \leq A \leq 95$	"Symmetric Tripartition"	$< 2 \cdot 10^{-9}$

With the results ends hopefully a 20 years old discussion about the existence of low energy near symmetric tripartition, which could never be identified by radiochemical analyses.

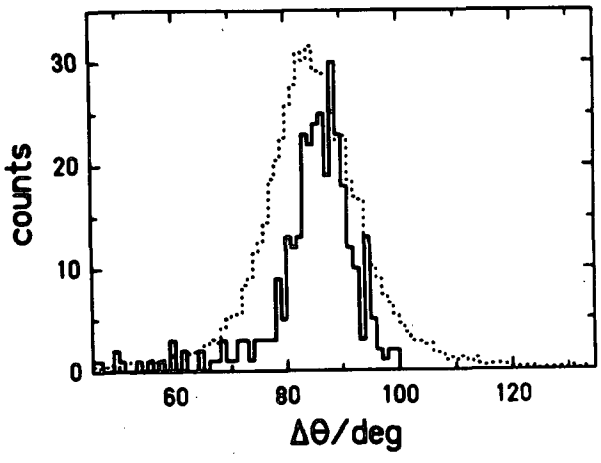

Fig.4. Distribution of the angles between light particles with $Z \geq 6$ and light fragments, peaked at 87° with a FWHM of 12°. The dashed line shows for comparison the corresponding distribution of longrange alpha particles, peaked at 84,9° with a width of 18,3° FWHM.

From the evaluation of our spectra together with the measured angular distribution of the light charged particles relative to the lighter main fragment as shown in figure 4 we can draw the following conclusions:

i) Light particles with nuclear charge numbers $Z \geq 6$ are emitted from all types of main fragment mass splits.

ii) These particles are emitted close to the scission point, where already two Coulomb fields of the nascent fragments have a focussing effect on the particles angular distributions.

This means that these ternary fission events have the most characteristic features in common with alpha particle associated fission, the subject of the next chapter, however, with minor differences:

iii) Compared to alpha particles the heavier light nuclei have a smaller width of the angular distribution and a mean emission angle closer to 90°
These observations are probably a consequence of a more restricted spatial origine of these particles.

4.) Alpha particle associated fission

With the angular position sensitive double torus ionization chamber "DIOGENES" we have measured kinematic observables of alpha particle accompanied fission. A quarter section of the detector system is presented in figure 5, more details have been given in ref.)[5].

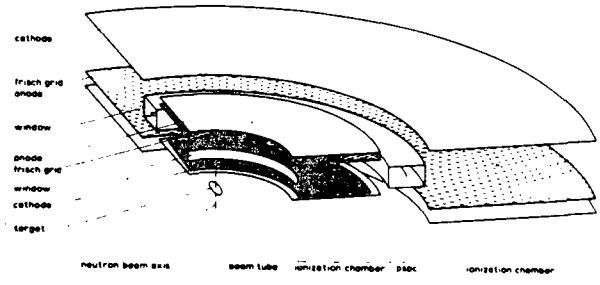

Fig.5. Detectorsystem "DIOGENES"

From the measured quantities, particle - particle, particle - fragment and fragment - fragment parameter correlations can be deduced. Some examples are displayed in figure 6 for the case of the ^{235}U (n,αf)-reaction. Similar data are available for ^{239}Pu (n,αf) and ^{252}Cf(s.f.). Of course, there exist all cuts through these two dimensional distributions, all mean values and all projections on the coordinate axes. In figure 7 distributions of the alpha particle emission angles are displayed for the above mentioned reactions. For theoretical investigations all data are available on magnetic tapes. I shall now discuss some aspects of these data and put the emphasis on the following two questions,

i) the classical one about the information provided by ternary alpha particles on the scission point configuration of the essentially binary fission process.

ii) and a more provocative one about essential differences between binary and alpha particle associated fission.

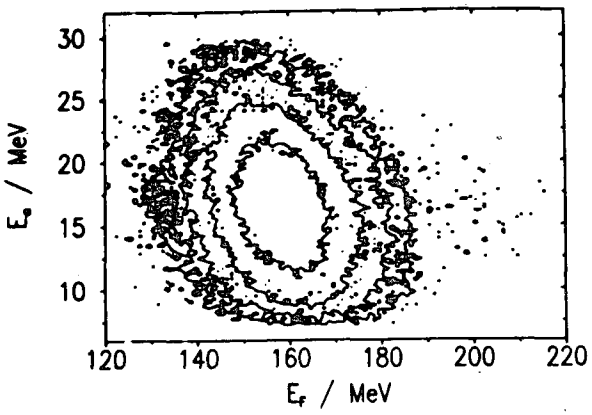

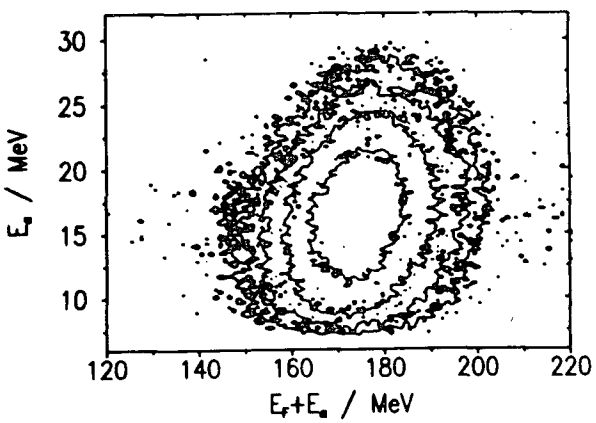

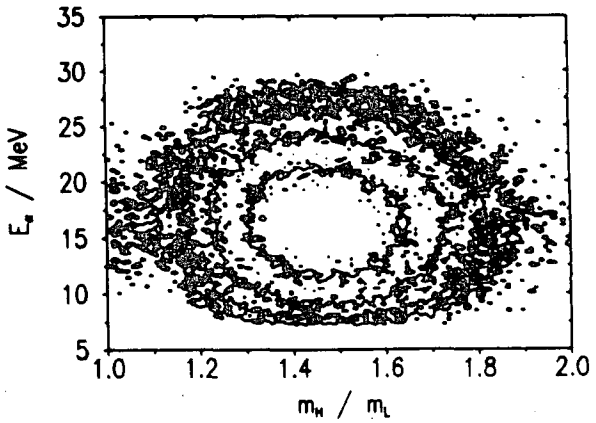

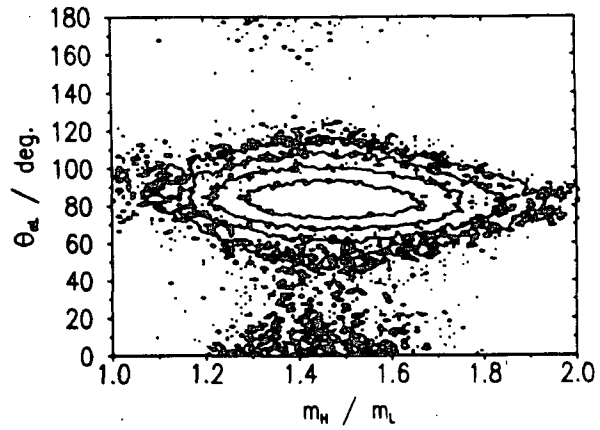

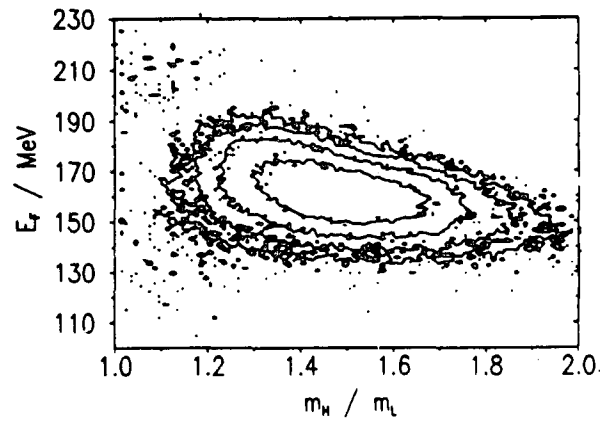

Fig.6. Correlations between ternary fission parameters,
m_H/m_L : heavy-to-light fragment mass ratio
E_F : total fragment kinetic energy
E_α : α-particle energy
$\Theta_{\alpha L}$: α-particle emission angle rel. to light main fragment for the reaction $^{235}U(n,\alpha f)$

Concerning

i) In the past trajectory calculations have been used to transform measured kinematic observables like alpha particle energies E_α, emission angles $\Theta_{\alpha l}$ and fragment kinetic energies E_{ff} into the corresponding microscopic scission point parameters $E_\alpha^{(o)}$, $\Theta_{\alpha L}^{(o)}$ and $E_{ff}^{(o)}$ The particle and fragment motion is calculated in the Coulomb plus nuclear potential of nascent fragments. Their finite sizes are taken into account by shape parametrization of the scission point configuration known from binary fission theory.
We performed also such trajectory calculations: for each of the fragment mass ratios 1.2, 1.4, 1.6, and 1.8 more than 10^6 trajectories with the initial parameters randomly distributed inside the following windows

$$0 \text{ MeV} \le E_\alpha^{(o)} \le 10 \text{ MeV}$$

$$0 \text{ MeV} \le E_{ff}^{(o)} \le 70 \text{ MeV}$$

$$0^o \le \Theta_{\alpha l}^{(o)} \le 180^o$$

The scission point shape of the fragments was assumed to be ellipsoidal.
By a selection procedure, described in ref.)[6], we separated subgroups of trajectories which reproduce more than 99 % of our data. This was the situation, when I gave my talk here in November 1985. In the meanwhile we know that subgroups of trajectories with these properties can be generated for quite different scission point configurations and microscopic parameters)[16].
The transformation of measured "macroscopic" kinematic observables into "microscopic" scission point parameters by trajectory calculations is far from being unequivocal.

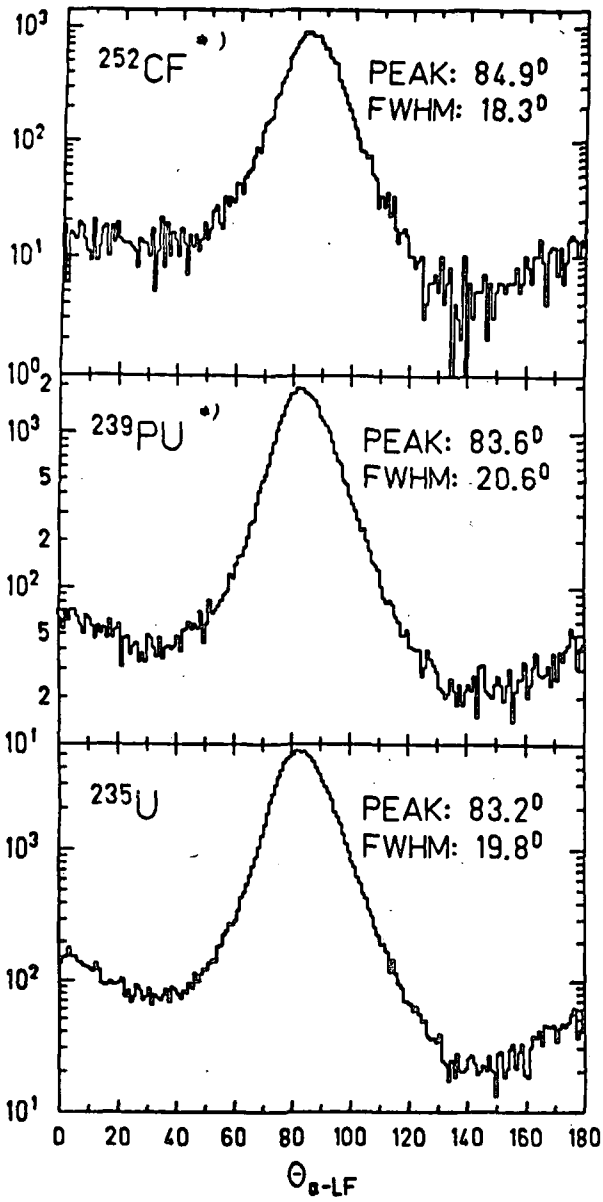

Fig.7. Angular distributions of α particles for the reactions $^{235}U(n,\alpha f)$, $^{239}Pu(n,\alpha f)$ and $^{252}Cf(sf)$
*preliminary data

Now the question raises, if the experimental data carry scission point configuration effects at all. In order to elicit this point we have separated the measured most probable emission angles $\Theta_{\alpha l}$ and the widths of the angular distributions $\Delta\Theta_{\alpha l}$ for more compact ($E^* < \bar{E}^*$) and more stretched ($E^* > \bar{E}^*$) scission point configurations, for which the kinetic energies of the main fragments are higher or lower than the average values. Figures 8 and 9 are plots of $\Theta_{\alpha l}$ and $\Delta\Theta_{\alpha l}$ as functions of the main fragments mass ratios for cold and hot fission events[23], also the integral functions are displayed. There is a small but clear indication for nuclear configuration effects on both observables $\Theta_{\alpha l}$ and $\Delta\Theta_{\alpha l}$ at the instant of particle emission. However, it is debatable whether these effects are also relevant for the investigation of the usual binary fission.

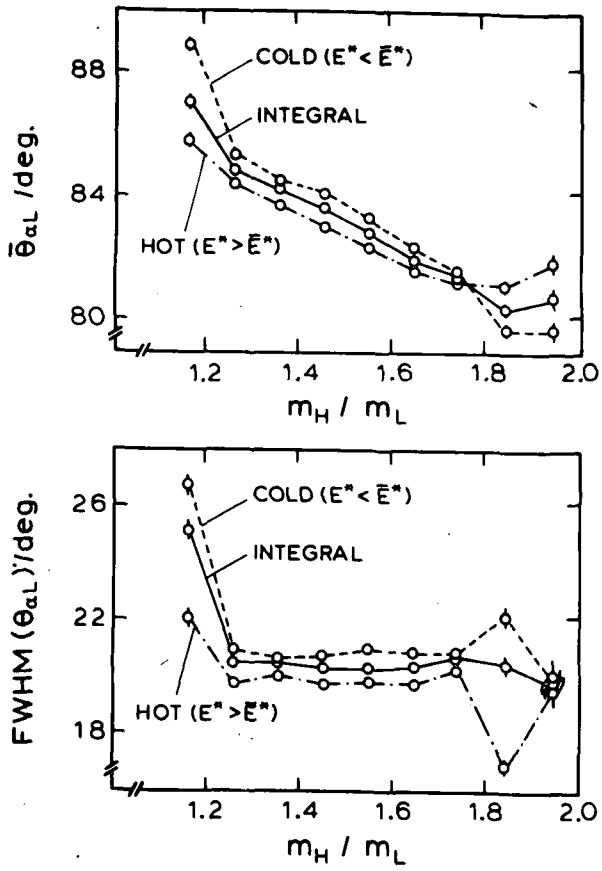

Figs.8 and 9. Most probable emission angles and widths of the angular distributions for cold, integral and hot fragment mass ratios.)[23]

In figure 9 another configuration effect is obvious: the strong increase of the width of the angular particle distribution close to main fragments mass symmetry. We know from the saw tooth shape of the $\bar{\nu}$ function, the average number of emitted neutrons for a given fragment mass, that mass symmetric fission at the scission point is deformation asymmetric. Most probably this fact can explain the increase of the angular width mentioned above.

Although there are nuclear configuration effects, they are obviously not accessible by trajectory calculations. Therefore O. Tanimura and T. Fließbach have started to develop a quantum mechanical theory of ternary fission)[17] They calculated energy and angular distributions of alpha particles from the fissioning nuclear system $^{235}U+n$ by solving the Schrödinger equation with a time dependent potential. Figure 10 shows their results for the alpha particle intensity as function of emission angle and kinetic energy for more or less elongated fission shape configurations compared to our experimental results displayed on the top of this figure.

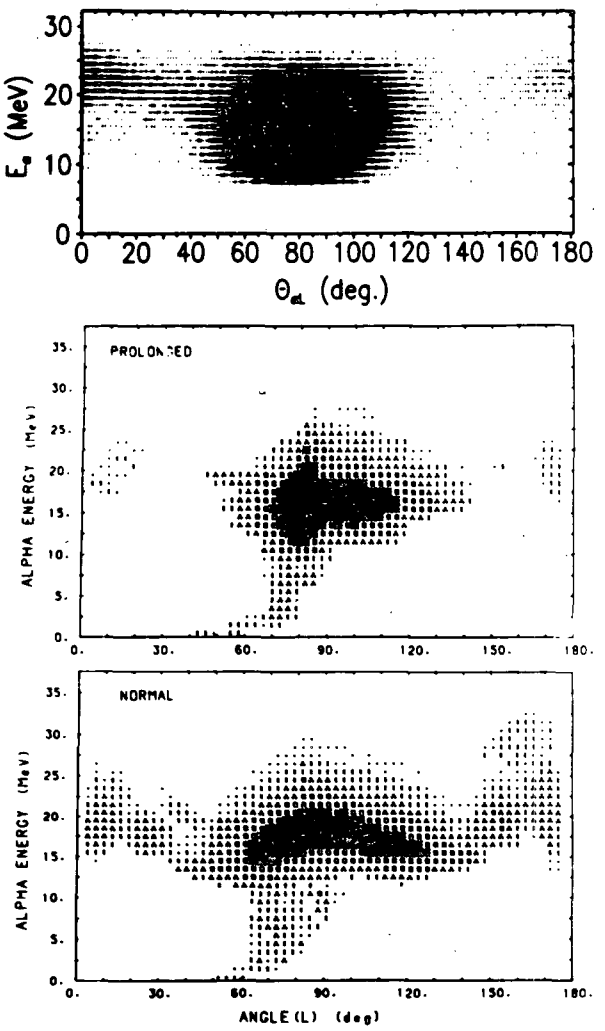

Fig. 10 Alpha particle yield as function of emission angle and kinetic energy a) experimental data for the $^{235}U(n,\alpha f)$ reaction b1, b2) theoretical results for more or less elongated nuclear deformation)[17].

Table II

"Normal" means typical for binary fission "stretched" means that the elongation parameter is 30 % above "normal" Δ: FWHM.

Table II

	$\Theta_{\alpha\ell}$	$\Delta\Theta_{\alpha\ell}$	E_α	ΔE_α
Experiment (^{236}U)	83.2° ± 0.3°	$19.8^{+0.5}_{-1.0}$°	16.4 ± 0.6 MeV	10.0 ± 0.6 MeV
Theory				
"normal" configuration	84°	30°	18.0 MeV	5 MeV
"stetched" configuration	83°	13°	16.2 MeV	5 MeV

Table II presents the most probable emission angles and kinetic energies of the alpha particles for more or less stretched nuclear shapes as well as the widths of angular and kinetic energy distributions compared to experimental results. In contrast to classical trajectory calculations this theory can reproduce the increased focussing effect of more elongated fission configurations as shown in figure 9.

Another result is worthwhile to mention: equatorial alpha particle emission occurs before polar one.

There is a good qualitative agreement between theory and experiment, but by far not the complete congruence of experimental and theoretical data we know from our trajectory calculations, (which are most probably misleading). However, the theory of O. Tanimura and T. Fließbach is based on more fundamental physical arguments and the results on nothing more than the time dependency of the deformation parameters of the nuclear potential during fission as compared to ordinary radioactive alpha decay. As in their calculations this time dependency has been assumed to be essentially linear, the results are surprisingly good.

ii) We are now left with the question on differences between binary and ternary fission. Is the old assumption correct, that the alpha particles, emitted in a few permillages of essentially binary fission do not disturb significantly the general fission process and carry only information about the (binary) scission configuration?

A more detailed examination has shown that this assumption is not valid. The alpha particle is not only a spectator but a participant in the fission process. This becomes evident from the comparison of the total kinetic energies released in ternary and binary fission by the three and two reaction products respectively. For the cases $^{235}U(n,\alpha f)$ and $^{235}U(n,f)$ as examples, these quantities together with their average values and the corresponding maximum Q-values are plotted as functions of the heavy main fragment masses in figure 11. The deformation energy of the main fragments is in ternary fission substantially lower than in binary fission. This is valid for all nuclear systems we have investigated: $^{235}U(n,\alpha f)$, $^{239}Pu(n,\alpha f)$, $^{252}Cf(s.f.)$, and also $^{245}Cm(n,\alpha f)$ we have studied with the time-of-flight spectrometer COSI FAN TUTTE extended by a series of semiconductor detectors around the fissile target. The differences between Q-values and mean total kinetic energies for binary and ternary fission are shown in figure 12 for the above nuclei.

The consequence is, that the main fragments in ternary fission are less deformed than in binary fragmentation. The alpha particles modify the nuclear

fission configuration.

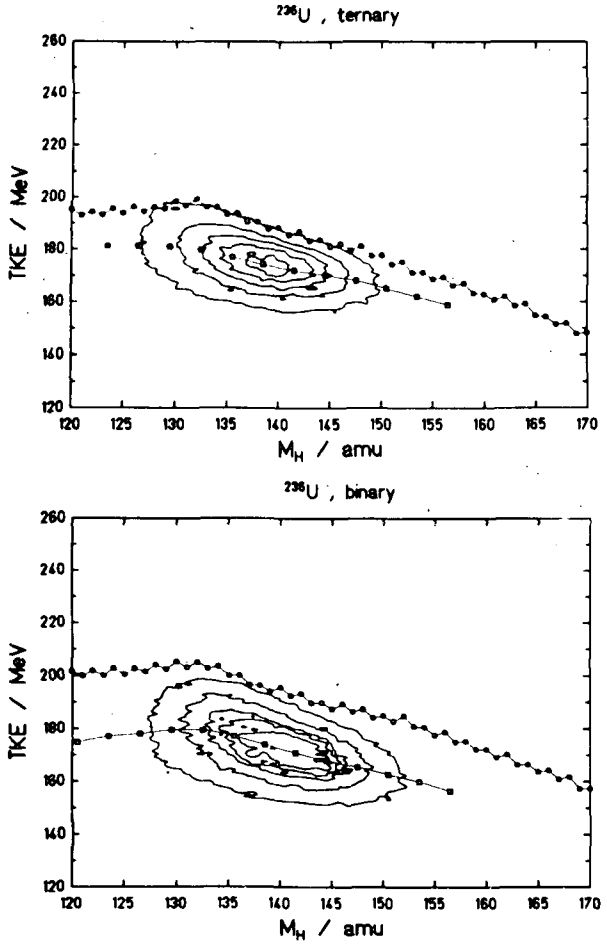

Fig.11. Distributions of the total kinetic energy for ternary (top) and binary (bottom) fission as function of heavy fragment masses together with corresponding averages and Q-values.

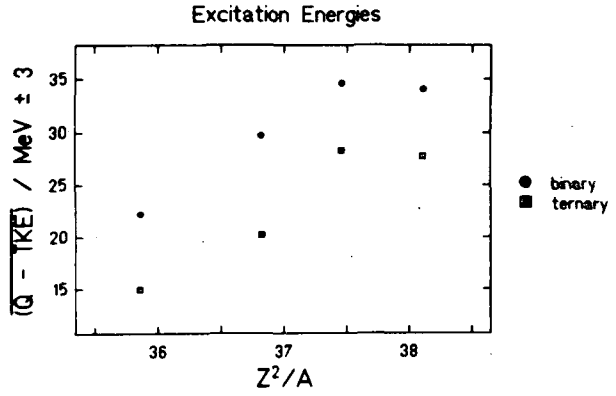

Fig.12. Average excitation (deformation) energies of binary and ternary fission fragments as function of Z^2/A of the compound nucleus: ^{236}U, ^{240}Pu, ^{246}Cm and ^{252}Cf.

5.) Fission fragment kinetic energy and mass fluctuations in resolved neutron resonances

With the neutron time-of-flight spectrometer of the BCMN at Geel in Belgium we have measured fragment kinetic energy- and derived fragment mass-distributions in resolved resonances (or groups of resonances) of the $^{235}U(n,f)$ reaction in the neutron energy range from thermal up to about 125 eV)[18,7,8] and we found strong total kinetic energy fluctuations. These fluctuations are anticorrelated with variations of $\bar{\nu}$, the average number of neutrons per fission event)[19] as displayed in figure 13.

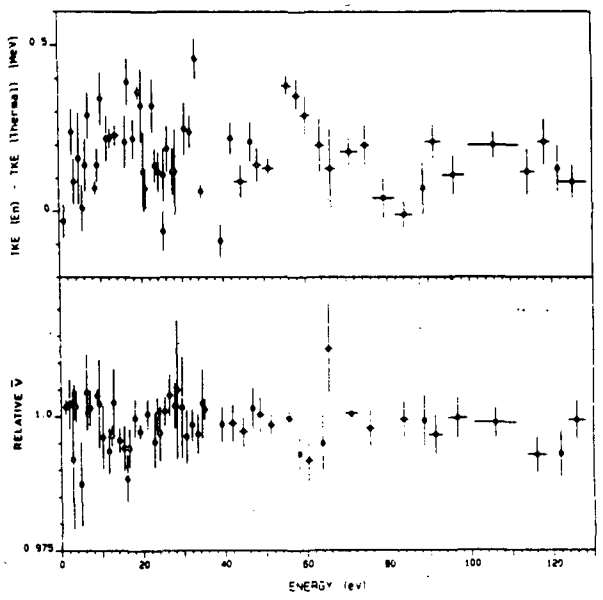

Fig.13. Fluctuations of the fragment total kinetic energy as function of the incoming neutron energy together with fluctuations of $\bar{\nu}$)[19]

In resolved resonances, fragment mass distributions of high statistical accuracy have been determined. In figure 14 two examples are shown for the resonances at 12.40 and 19.30 eV incoming neutron energy. I cannot discuss here correlations between the measured energy fluctuations and fluctuations of other fission parameters from resonance to resonance, which have been used in the past for mostly spurious resonance channel spin assignments)[20]. This discussion is the main subject of ref.)[18] and would not fit into the frame of this report.

Instead I shall try to interpret these fluctuations in the framework of the recent exit-channel model of fission developed by U. Brosa, S. Grossmann, and A. Müller)[21].

In our context, the essential aspect of this model is that it introduces new decision elements for fragment mass and energy distributions into the development of the fission process. This process is in general described by the motion of a "configuration point" in the potential landscape of the fissioning nucleus, i.e. a mapping of the shell and pairing corrected liquid drop nuclear po-

tential as function of deformation coordinates.

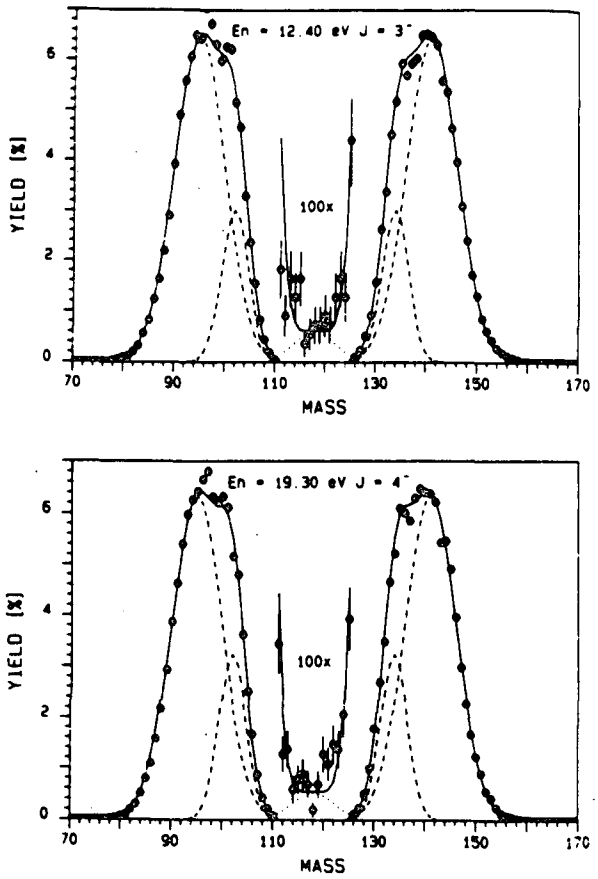

Fig.14. Mass distributions of fission fragments in the resolved resonances at 12.40 eV and 19.30 eV of the $^{235}U(n,f)$ reaction. The dotted lines are five Gauss-distributions which fit the experimental data.

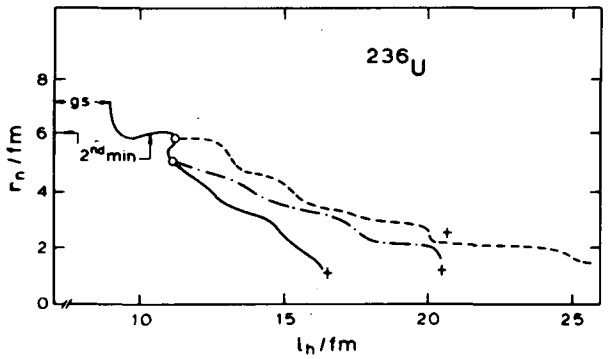

Fig.15. Fission paths in the deformation space of ^{236}U. r_n is the neck radius and l_h the half elongation of the fissioning nucleus. (Courtesy of U. Brosa).

The new decision elements are "bifurcation points", where the path of the configuration point in the potential landscape splits into two (or more) directions. Figure 15 illustrates the situation for ^{236}U, where three fission paths or exit channels are distinguishable. A consequence of these three paths is the break-up of the fragment mass and energy distributions into three components)[3]. This theoretical prediction is supported by our data in figure 16, the mass distribution of thermal neutron induced fission of ^{235}U, which could be decomposed into three partial distributions W_1, W_2 and W_3. In ref.)[3,8] we have demonstrated that the partial distribution parameters are in fair agreement with the model calculations)[21].

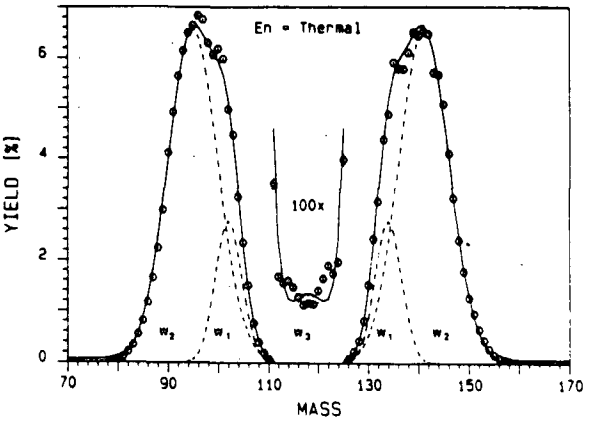

Fig.16. The same as in figure 14 for thermal neutrons.

On the basis of these considerations we compare now the fragment kinetic energy fluctuations plotted in figure 13 with fluctuations of the branching ratio W_1/W_2 in figure 17.

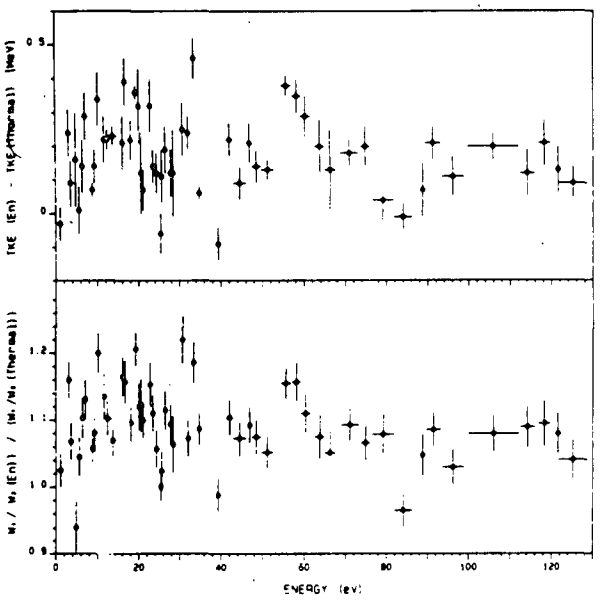

Fig.17. Comparison of the measured energy fluctuations of figure 13 and the fluctuations of the ratio W_1/W_2, the two Gaussians fitting the asymmetric fragment mass distributions.

We recognize a strong correlation, which is confirmed by a correlation coefficient of $r = 0.81 \pm 0.05$.

6.) Summary and Conclusions

In chapters 2 - 5 we have shown some points of growth of the physics of nuclear fission.

- Cold - deformed or "hot" fragments are candidates for very deformed shell stabilized nuclei.
  There is some evidence that they do not deexcite by neutron emission or stay on a 10-100 ns time scale in shape isomeric states
- Down to a yield level of 10^{-9} per binary fission no spontaneous symmetric tripartition is observed for ^{252}Cf(s.f.).
- Alpha particle associated nuclear fission is a self-ruled process, which cannot be used to study binary fission configurations)[22].
  There is for the first time an "ansatz" for a quantum mechanical theory of alpha particle accompanied nuclear fission.
- Fluctuations of fragment kinetic energies in resolved neutron resonances are not correlated with the channel spin. Most probably they are due to fluctuating branching ratios at the bifurcation points in the Brosa-Grossmann-Müller model of nuclear fission.

Finally it has to be pointed out, that all the above results are standing in juxtaposition. There is no dynamical theory of nuclear fission as a unification of the different experimental observations.

Acknowledgement

I have to thank T. Fließbach, O. Tanimura, U. Brosa, and R. Hasse for stimulating discussions.

References

1). P. Koczon, M. Mutterer, J.P. Theobald, P. Geltenbort, F. Gönnenwein, A. Oed, and M.S. Moore
Phys. Lett. B 191 (1987) 249

2). Patricia Schall, P. Heeg, M. Mutterer, and J.P. Theobald
Phys. Lett. B 191 (1987) 339

3). H.-H. Knitter, H.-J. Hambsch, C. Budtz-Jørgensen, and J.P. Theobald
Z. Naturforsch. 42a (1987) 786

4). P. Koczon, M. Mutterer, J.P. Theobald, M.S. Moore, F. Gönnenwein, P. Geltenbort, A. Oed, and J. Pannicke
Radiation Effects 92-96 (1986) 385
and
Proceedings of the International Conference "Nuclear Data for Basic and Applied Science", Santa Fe, USA, May 13-17, 1985, p. 385

5). J.P. Theobald
Proceedings of the "XV-th International Symposium on Nuclear Physics" Dresden-Gaussig, 1985 report ZfK-592, p. 43

6). J.P. Theobald
Proceedings of the "Seminar on Fission" Castle of Pont d'Oye, Habay-la-Neuve, May 1986, C. Wagemans, Ed.
report BLG 586, Brussels, p. 63

7). F.-J. Hambsch, H.-H. Knitter, C. Budtz-Jørgensen, M. Mutterer, and J.P. Theobald
Proceedings of the "International Symposium on Collective Phenomena in Nuclear and Subnuclear Long Range Interactions in Nuclei",
Bad Honnef, May 1987, P. David Ed. in press.

8). H.-H. Knitter, C. Budtz-Jørgensen, F.-J. Hambsch, Ch. Straede, and J.P. Theobald
Proceedings of the International Conference on "Neutron Physics"
Kiev, Sept. 1987, in press

9). C. Signarbieux, M. Montoya, M. Ribrag, C. Mazur, C. Guet, P. Perrin, and M.J. Maurel
J. de Phys. 42 (1981) L 437

10). H.-G. Clerc, W. Lang, M. Mutterer, C. Schmitt, J.P. Theobald, U. Quade, K. Rudolph, F. Gönnenwein, H. Schrader, and D. Engelhardt
Nucl. Phys. A452 (1986) 277

11). F. Gönnenwein
Proceedings of the "Seminar on Fission" Castle of Pont d'Oye, Habay-la-Neuve, May 1986, C. Wagemans, Ed.
report BLG, Brussels, p. 106

12). P. Koczon, PhD. Thesis, T.H. Darmstadt, 1987

13). R.W. Hasse
Proceedings of the "All-Union Symposium on Physics and Chemistry of Fission", Obninsk, USSR, June 1987, in press.

14). V.P. Zakharova and D.K. Ryzanov
Sov. J. Nucl. Phys. 30 (1979) 19

15). M.L. Muga
Proceedings of the International Conference on "Physics and Chemistry of Fission", Vol. 2, Salzburg 1965, (IAEA Wien, 1965), p.409
Phys. Rev. 142 (1966) 716 , see references in)[2]

16). F. Kraske, Diploma Thesis,
TH Darmstadt, 1987

17). O. Tanimura and T. Fließbach, University Siegen 1987
Z. f. Physik, in press

18). F.-J. Hambsch, PhD Thesis,
T.H. Darmstadt, 1987

19). R.E. Howe, T.W. Phillips, and C.D. Bowman,
Phys. Rev. C13 (1976) 195

20). R. Vandenbosch and J.R. Huizenga
Nuclear Fission, Academic Press, New York (1973)p94

21). U. Brosa, S. Grossmann, and A. Müller,
Proceedings of the "XVI-th Symposium on Nuclear Physics", Dresden-Gaussig, (1986)

22). G.A. Pik-Pichak
Sov. J. Nucl. Phys. 40 (1984) 215

23). In this chapter the notations cold and hot are not used in the strict sense of chapter 2

ENERGY DISSIPATION IN FISSION CLOSE TO THE BARRIER

F. Gönnenwein[+], J.P. Bocquet[++] and R. Brissot[++]

[+]Physikalisches Institut, University of Tübingen, Morgenstelle 14, D-7400 Tübingen, FRG
[++]Institut Laue-Langevin, BP 156x, F-38042 Grenoble-Cedex- France

Abstract

Measurements of the nuclear charge distributions of fission fragments for fission processes close to the barrier are reviewed. The emphasis is put on thermal neutron induced fission. The nuclei studied range from Th up to Cf. It is shown that the observed odd--even effect of the fragment charge yield and the odd-even staggering of the total kinetic energy may be evaluated to yield the energy dissipated in the course of fission between the saddle and the scission point. The dissipated energies found are rather small. They vary smoothly with Z^2/A of the compound nucleus and increase from about 3 MeV for ^{230}Th up to 11 MeV for ^{250}Cf.

1. Introduction

The total energy Q released in nuclear fission is shared between the total kinetic energy TKE and the total excitation energy TXE of the fragments. The energy distributions for both, TKE and TXE, have been extensively studied experimentally for many fission reactions. However, for a deeper insight into the fission mechanism these global energy distributions are probably not too helpful. This is due to the fact that again both, TKE and TXE, receive contributions from at least two different terms. The kinetic energy TKE is the sum of the Coulomb repulsion energy E_{Coul} of the nascent fragments at scission and any prescission kinetic energy ε the fragments may already have acquired at the time of neck rupture. Similarly, the final excitation TXE of the fission fragments at infinity is made up from the fragment deformation energy E_{Def} at scission and the energy E_{int} already transformed into internal excitation energy at this stage of the fission process. For a fission reaction where the available energy is just sufficient to overcome the fission barrier, this internal excitation energy E_{int} has to be identified with the energy E_{Dis} dissipated through viscous forces between saddle and scission. This situation is nearly met for thermal neutron fission. At the scission point, then, part of the available energy, viz. the sum of E_{Coul} and E_{Def}, is still tied up as potential energy E^{sci}_{pot}. On the other hand, the prescission kinetic energy and the dissipation energy are both fed by the energy gained in going from the fission prone parent nucleus to the scission configuration. In the case of induced fission close to the fission barrier, this energy gain may be visualized as the potential energy drop ΔE_{pot} between the saddle and the scission point. The energetics for this special case is sketched schematically in Fig. 1. Put into formulas,

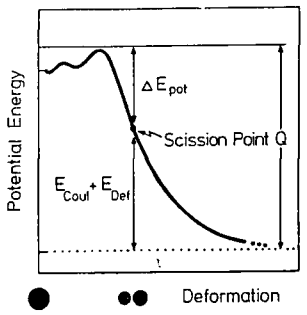

Figure 1: Schematic presentation of the energetics for near-barrier fission.

the above statements for near barrier fission read

$$Q = TKE + TXE = (E_{Coul} + \varepsilon) + (E_{Def} + E_{Dis})$$
$$= (E_{Coul} + E_{Def}) + (\varepsilon + E_{Dis}) = E^{Sci}_{pot} + \Delta E_{pot}. \quad (1)$$

Any detailed theory of nuclear fission will have to calculate the energy terms of eq. (1) individually. For a close comparison with theory also experiments should aim at determining these quantities.

The static potential energy surface PES of a fissioning nucleus has been and still is extensively studied. The degree of sophistication in the calculations has moved from macroscopic (liquid drop) to either macroscopic - microscopic (inclusion of shell and pairing effects via the Strutinski recipe) or purely microscopic approaches. The correlation between the fine structure of the PES in the vicinity of the fission barrier and the observation of spontaneously fissioning isomers is well known. More recently a rich structure of the PES beyond the saddle point has come back into focus /1,2/. While all models agree that the energy gain ΔE_{pot} between saddle and scission increases with the fissility $x \sim Z^2/A$ of the fissioning nucleus, the exact figures for ΔE_{pot} are strongly model dependent. A subtle point in this context is the proper definition of the scission configuration, i.e. the determination of the neck radius at which a sudden necking-in occurs /3/. In dynamical calculations of the fission path also inertial and viscous forces will play a role.

Calculations of the dynamical type give information on the prescission kinetic energies ε /4,5/. Experimentally ε becomes accessible by studying ternary fission. In the evaluation of the experimental data the measured angular and energy distributionsof the ternary particles are compared to trajectory calculations. An input parameter to these calculations is the prescission energy ε of the fragments. Unfortunately, the results are extremely sensitive to other model parameters like the emission mechanism of ternary particles, the size of fragments and nuclear forces. The spread in what may be tentatively called "experimental" values for ε is accordingly large and ranges between 10 and 50 MeV /6-9/. Thus, the situation is not very satisfactory.

The energy E_{Dis} dissipated in moving from the saddle to the scission point is directly linked to the viscosity of nuclear matter. Numerous theoretical studies have been devoted to this subject. Concepts which have been discussed in recent years for tackling nuclear friction are one-body and two-body dissipation mechanism (see ref./10/ for a review of the literature) and microscopic descriptions of the intrinsic excitation of fissioning nuclei. The latter are reviewed in /11/.

The present paper surveys the available experimental information on the energy E_{Dis} dissipated between saddle and scission in low excitation nuclear fission. Two types of experiments have so far been proposed with that purpose in mind: the dependence of the symmetric to asymmetric fission yields on the excitation energy of the compound nucleus /12/ and the odd-even effects in the nuclear charge yields of fission fragments. In both cases the measured observables have to be correlated to the physical quantity of interest, E_{Dis}, by a model.

The basic idea, why E_{Dis} may be deduced from the proton odd-even effect is the following: starting from an (even,even) fissioning nucleus, any odd charge number Z of the fragments indicates that at least one proton must have been broken in the course of fission; on the other hand, pairs are broken by the internal excitation energy the fissioning nucleus already has at the saddle point and/or accumulates during the descent from saddle to scission. Hence, from a comparison of the even and odd charge yields of the fragments it should be possible to infer the excitation energy of the fragments at scission.

It should be stressed that, stated in terms of radiochemistry, only the independent fragment yields carry the relevant information, since for these yields the primary charge distribution has not been blurred by β-decay. These charge distributions are directly accessible to physical measurement techniques. In contrast with the proton number Z, the primary odd-even effect of the neutron number N (and hence the mass number A) is difficult - if not impossible - to observe, since neutron evaporation is much faster than any fragment identification method. An exception to this rule is, however, given in the cold

fragmentation regime of fission. In cold fragmentation one studies the limiting case of fission where no neutrons are emitted. Therefore, here the odd-even effect in the neutron numbers carries a similar information to the one in the proton numbers of the fragments.

In the following we will mainly dwell on recent and partly unpublished results on the proton odd-even effect in a variety of actinides, studied by thermal neutron fission at the High Flux Reactor of the Institut Laue-Langevin in Grenoble, France.

2. Experimental Techniques

Radiochemical methods were the first to determine nuclear charge distributions of fission fragments. A huge amount of data covering many different types of fission reactions has been collected. The data are complete in the sense that they range from the lightest up to heaviest nuclear charges occurring in fission /13/. Mass spectrometry, counting of β-decay length and X-ray spectroscopy has also, but more occasionally, been used for the problem at hand.

A systematic series of measurements of fragment nuclear charge distributions has been started a few years ago on the mass separator Lohengrin installed at the High Flux Reactor of the Institut Laue-Langevin in Grenoble. The fission target is placed close to the reactor core and the recoiling fragments are analysed as to mass number A and kinetic energy E by the separator /14/. To take nuclear charge data a special detector is installed in the focal plane of the separator. In the first version of this detector the energy loss ΔE of fragments in a carbon foil was determined by a time-of-flight technique /15/. In a later version of the detector, the ΔE carbon absorber was replaced by parylene and the residual energy behind the absorber was measured by a high resolution ionization chamber /16,17/. More recently a ΔE-E_{rest} ionization chamber has been put into operation on Lohengrin /18/, where both, ΔE and E_{rest}, are measured. This method yields very clean and reliable results.

Some of the charge data to be reviewed were taken just by placing a ΔE-E_{rest} ionization chamber in front of a fissile target being irradiated by thermal neutrons /19/. For fission reactions like ^{229}Th(n,f), showing a well pronounced odd-even effect on the charges, this relatively simple method has proven to give useful information.

Also the fission fragment spectrometer Cosi fan tutte of the Institut Laue-Langevin /20/, which is complementary to Lohengrin, has been pushed to measure nuclear charges. On this instrument the charges are inferred from the ranges of fragments with known mass and energy in an axial ionization chamber /21/. First results are available for the reaction ^{241}Pu(n,f) /22/.

The charge resolving power $Z/\Delta Z$ of the above physical methods is limited to roughly $Z/\Delta Z = 50$. This means that, in contrast ro radiochemistry, only the nuclear charges of the light fragment group can be studied. However, since the charge identification by physical techniques only takes a few micro-seconds, the interference through β-decay is virtually outruled. The measured charge numbers are those of the primary fragments and the sum of the charges for the two complementary fragments of binary fission has to be strictly equal to the charge of the fissioning nucleus. It is, therefore, sufficient to know the charge distribution of one fragment group only. A further asset of the physical methods is that nuclear charge distributions may be scanned for a given kinetic or excitation energy of the fragments.

3. Experimental Results

A sample of experimental charge distributions obtained at the Institut Laue-Langevin for thermal neutron fission of actinides ranging from ^{229}Th(n,f) through ^{249}Cf(n,f) is shown in the Figs. 2a through 2d, respectively. The original data may be found for ^{229}Th in ref. /19/, for ^{235}U in ref. /16/, for ^{239}Pu in ref. /17/ and for ^{249}Cf in ref. /23/. The measured primary charge distributions of fission fragments are presented as the charge yields

of the heavy fragment group, normalized to 100 % within the group. Evidently for the light actinide ^{229}Th one observes a striking odd-even effect, with even Z charge numbers being much more favoured than odd ones. As one moves to the heavier actinides this effect becomes less pronounced. For the heaviest nuclide studied, ^{249}Cf, the effect has almost disappeared. It should be noted that all charge distributions in Figs. 2a to 2d have been averaged over the fragments' kinetic energies.

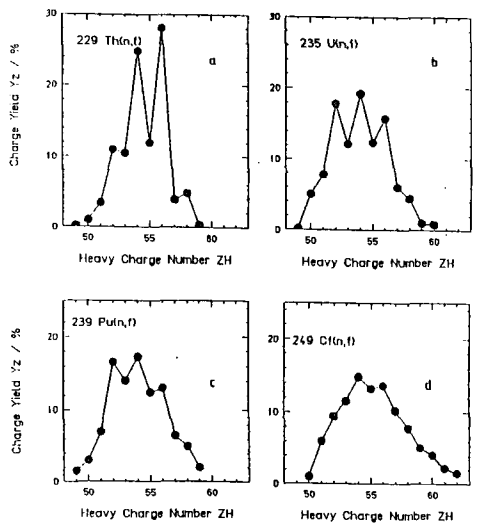

Figure 2: Charge distribution of heavy fragment for thermal neutron fission of the actinides ^{229}Th, ^{235}U, ^{239}Pu and ^{249}Cf.

It is a longstanding practice to quantify the odd-even effect δ of the charge yields by

$$\delta = (Y_e - Y_o) / (Y_e + Y_o), \qquad (2)$$

with Y_e and Y_o the sum of yields for even and odd charge fragmentations, respectively. With this definition a preponderance of even over odd Z-yields is equivalent to a positive $\delta > 0$.

The proton odd-even effect δ is plotted in Fig. 3 as a function of Z^2/A of the fissioning nucleus. This latter parameter is proportional to the fissility, a notion first introduced in liquid drop model calculations. The figure summarizes all data obtained so far for thermal neutron fission of (even,even) compound nuclei /16,17,19,22,23/.

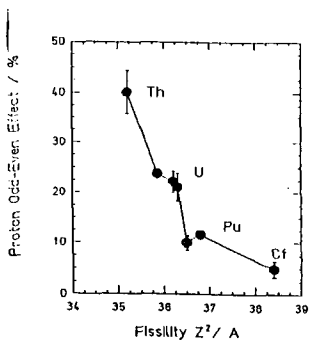

Figure 3: Proton odd-even effect of fragments vs. fissility Z^2/A of the compound nucleus for thermal neutron fission.

Obviously, there is a close correlation between the odd-even effect and the fissility. On the other hand, no such correlation is observed between the odd-even effect and either the fission barrier height B_f, or the neutron binding energy B_n, or the difference (B_n-B_f) between these two energies. The latter energy, (B_n-B_f), is available at the saddle point as internal excitation energy, E_{Sad}, for thermal neutron fission. From this experimental fact it is concluded that the main contribution to pairbreaking in thermal neutron fission is not due to the excitation energy at the saddle. Instead, one has to look for a pairbreaking mechanism beyond the saddle point. Once having passed the saddle point, a fission prone nucleus will slope down the potential energy surface, until it reaches the scission point, where a rapid necking-in of the neck connecting the nascent fragments

occurs. All theoretical calculations - from macroscopic to microscopic models - of the potential energy surface agree that the potential energy gain ΔE_{pot} (s. Fig. 1) between saddle and scission increases smoothly with the fissility Z^2/A of the compound nucleus. As an example, in Fig. 4 the figures for ΔE_{pot}, as reported by M. Asghar and R.W. Hasse for a liquid drop model calculation /24/, are plotted as a function of Z^2/A.

This behaviour of ΔE_{pot} is intriguing for the following reason. If nuclear matter shows any viscosity, the dissipated energy E_{Dis} has to be supplied by the energy gain ΔE_{pot} and one would hence expect E_{Dis} to follow a trend similar to ΔE_{pot} as a function of Z^2/A. But if the dissipated energy E_{Dis} gets larger with increasing Z^2/A, this should favour pairbreaking the higher the Z^2/A values are. Therefore, the odd-even effect should slope downwards when plotted versus Z^2/A. This is exactly what is observed experimentally. In the following we will take the conjecture for granted that in thermal neutron fission of the actinides the majority of proton (and neutron) pairs are broken in the descent from the saddle to the scission point.

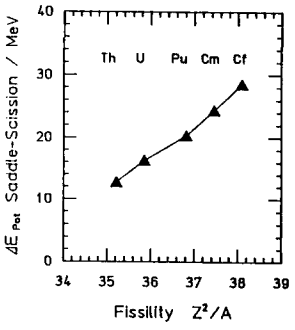

Figure 4: Gain in potential energy between saddle and scission vs. fissility Z^2/A of the compound nucleus.

So far we have considered the odd-even effect averaged over the fragment energies. But the physical charge measurements to be presented here contain more detailed information. In Fig. 5 we show the dependence of the odd-even effect δ on the kinetic energy E_L of the light fragment. Evidently, the odd-even effect gets more pronounced with the kinetic energy increasing. From energy conservation, an increase of the kinetic energy has to be compensated by a decrease of the excitation energy of the fragments. It is to be expected that for a small measured excitation energy, both terms contributing (s. eq. (1)), viz. the potential energy of deformation and the internal excitation at the scission point, will be small. Therefore, the observed dependence of the odd-even effect on the kinetic energy corroborates the idea that the probability for pairbreaking is directly linked to the internal excitation energy and that a large odd-even effect points to a small internal excitation energy and vice versa.

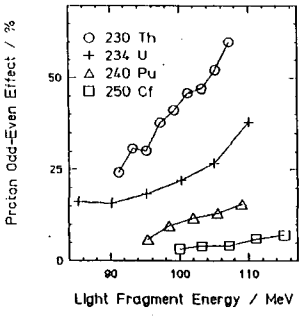

Figure 5: Proton odd-even effect vs. light fragment kinetic energy for thermal neutron fission of ^{229}Th, ^{233}U, ^{239}Pu and ^{249}Cf.

The odd-even effect sloping upwards with kinetic energy in Fig. 5 means that the higher the kinetic energies the more even charge yields of fragments are enhanced as compared to odd ones. Stated otherwise, the kinetic energy distributions of even charge fragments are shifted to higher energies relative to the distributions for odd-charge neighbors. The mean light fragment kinetic energy E_L for a given light fragment charge Z_L is shown in Fig. 6 for some of the compound nuclei studied by thermal neutron induced fission. A well

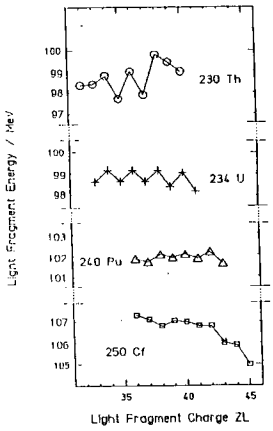

Figure 6: Light fragment kinetic energy vs. light fragment charge for thermal neutron fission of ^{229}Th, ^{233}U, ^{239}Pu and ^{249}Cf.

detectable pronounced odd-even staggering of the mean light fragment kinetic energy is manifest. Similarly to the odd-even effect in the yields, the size of the odd-even staggering of the kinetic energies gets smaller the higher the fissility Z^2/A of the compound nucleus is. For the heaviest nucleus studied, $^{249}Cf(n,f)$, the staggering is barely visible. This dependence of the odd-even staggering on fissility is not readily obvious and will have to be interpreted in terms of a model in the next section.

4. Evaluation of Data

The qualitative arguments having been put forward so far, suggesting a correlation between the proton odd-even effect δ and the internal excitation energy E_{int} at scission, and hence also the energy E_{Dis} being dissipated in fission, have now to be supported by a more quantitative analysis. As already pointed out, starting from a (even,even) compound nucleus any observed odd-Z fragments indicate that proton pairs have been broken. In fact, in principle it is sufficient to break one proton pair only and to distribute the two protons with equal probability onto the two fragments in order to completely wash out any odd-even effect δ. It is thus seen that δ is very sensitive to pairbreaking.

Several models have been proposed linking the odd-even effect to pairbreaking and internal excitation energy or intrinsic temperature at scission. Within the framework of the very successful version of the scission point model by B.D.Wilkins et al. /25/ the odd--even effect δ is related to the pairing gap parameter /12,26/. The parameter Δ depends on the intrinsic temperature or excitation energy. For high temperatures the gap parameter Δ decreases. This facilitates pairbreaking and for high internal excitation energies the odd-even effect δ is predicted to converge to zero.

A different approach being based on the statistics of quasiparticle excitations has been suggested by G. Mantzouranis and J.R. Nix /27/. The final reasoning is very similar to the one just described. Let us stress that in both these models the increase of the potential energy gain ΔE_{pot} with fissility Z^2/A will entail a raise in the intrinsic temperature through viscosity effects and hence will lead to a drop of the odd-even effect δ, in fair agreement with experiment.

For the quantitative evaluation of the present data we have chosen to rely on yet another description of the odd-even effect δ, since this description appears to depend less on the details of the underlying nuclear fission model. From a purely combinatorial analysis of pairbreaking H. Nifenecker et al. /28/ have derived the following formula for the proton odd-even effect δ:

$$\delta = (1 - 2p\varepsilon q)^{N_{max}}. \qquad (3)$$

In eq. (3) N_{max} is the maximum number of proton and neutron pairs which may be broken, q is the probability to break a pair, ε is the probability for this pair to be a proton pair, while p is the probability for the individual nucleons of a pair to go into comple-

mentary fragments. The maximum possible number of broken pairs N_{max} will depend on the excitation energy made available in the course of fission. With the probability q from eq. (3) the average number of broken pairs $\langle N \rangle$ is simply

$$\langle N \rangle = q\, N_{max}. \tag{4}$$

The two probabilities ε and p from eq. (3) may be fixed by simple arguments. The probability ε for the broken pair to be a proton pair is set to be proportional to the proton number Z out the A nucleons:

$$\varepsilon = Z/A \sim 0.39. \tag{5}$$

For the probability p it is assumed that the two protons from a broken pair have an equal chance to end up either in one single fragment, or in the two fragments of binary fission. This assumption is in line with the view that nucleon pairs are broken in the long descent between saddle and scission. Accordingly we put

$$p = 1/2. \tag{6}$$

Even with the simplifications brought about by eqs. (5) and (6), one is not in a position to calculate from the measured odd-even effect δ the number of broken pairs, unless the basic probability q to break a pair is known. However, fortunately enough the probability q does not enter in a crucial way into the calculation of the internal excitation at scission, the quantity we are finally interested in. In fact, this energy may be calculated from

$$E_{int} = 2\Delta \langle N \rangle = 2\Delta q N_{max} \tag{7}$$

if it is assumed that it always takes the energy 2Δ = const to create a two quasiparticle excitation from pairbreaking. This approximation tends to overestimate the calculated energy E_{int}. For 2Δ we adopt the figure re-commended by H.C. Britt and J.R. Huizenga /29/ for the gap parameter at the saddle point, namely

$$2\Delta = 1.7 \text{ MeV}. \tag{8}$$

From eqs. (3) and (7) the excitation energy may now be deduced from the measured odd-even effect by treating q as a free parameter. Letting vary q between its limiting values q = 0 and q = 1 one finds $E_{int} = -4.36 \ln\delta$ and $E_{int} = -3.44 \ln\delta$, respectively. Evidently, the calculated energy E_{int} is not sensitive to the exact figure of q. We therefore propose as the final formula we are looking for

$$E_{int} = -4 \ln\delta \quad \text{MeV}. \tag{9}$$

This corresponds roughly to the choice q = 0.5.

Eq. (9) tells that for no pairbreaking at all (δ = 1) there cannot be any excitation either (E_{int} = 0), while the more pairs are broken (δ 0), the higher is the internal excitation energy. The formula thus reproduces in a strikingly simple way the physical input.

Turning now to the evaluation of the thermal neutron data, we make use of the observation discussed in section 3 that here the main pairbreaking mechanism is viscous heating between saddle and scission. To first approximation we therefore identify the internal excitation energies E_{int}, calculated from the charge measurements with the help of eq. (9), with the energies E_{Dis} dissipated in the course of fission. Some of these energies E_{Dis} for the actinides under study are displayed in Fig. 7. For comparison with the gain in potential energy ΔE_{pot} values between saddle and scission, the ΔE_{pot} values from Fig. 4 have again been plotted in Fig. 7. As anticipated intuitively, the dissipated energy E_{Dis} closely follows the trend of ΔE_{pot} with fissility. Moreover, the ratio $E_{Dis}/\Delta E_{pot}$ is fairly constant and it is concluded that 30 - 40 % of the available energy is converted into excitation. It should be stressed that the quoted figure for the percentage of dissipation, which in a way is a measure for the viscosity of nuclear matter, is liable to large errors. This is due, first, to the simplifications which were necessary to derive

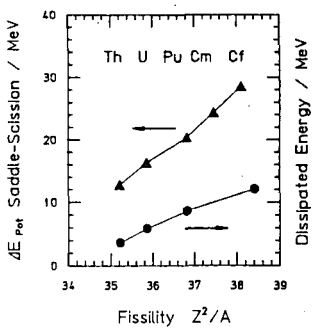

Figure 7: Dissipated energy vs. fissility Z^2/A for thermal fission of ^{229}Th, ^{235}U, ^{239}Pu and ^{249}Cf. The potential energy gain between saddle and scission from Fig. 4 is given for comparison.

eq. (9) and, second, to the uncertainties in the calculation of the potential energy drop ΔE_{pot}, which depends strongly on the fission model.

There is, however, a slight inconsistency in the treatment of data presented in Fig. 7 which has to be remedied. We recall that the energy gain ΔE_{pot} calculated from fission models is the potential energy drop between the saddle and the scission point. For a fair comparison with theory one should, therefore, get hold of precisely the energy dissipated through viscosity in the descent from saddle to scission. The energy E_{int} having been discussed in connection with the breaking of proton pairs in eq. (9) is in general made up from the truly dissipated energy E_{Dis} and the excitation energy E_{Sad} the nucleons already has at the saddle point, i.e.

$$E_{int} = E_{Dis} + E_{Sad} \quad . \tag{10}$$

This equation states that internal excitation energies at the saddle and those accumulated through viscous forces between saddle and scission are treated on an equal footing as far as pairbreaking is concerned. For thermal neutron fission E_{Sad} is much smaller than E_{Dis} and this means that the interpretation of thermal neutron fission data we have given above is to first approximation justified. This is no longer true for fast neutron fission.

For neutron induced fission reactions where the incoming neutron energies do not exceed the range of first chance fission, the excitation energy of the compound nucleus from which fission proceeds is well defined. Assuming that any energy which is not needed to overcome the fission barrier stays with the fissioning nucleus as excitation energy E_{Sad} at the saddle, one has

$$E_{Sad} = B_n + E_n - B_f \tag{11}$$

with B_n and E_n the neutron binding and kinetic energy, respectively, and B_f the fission barrier height.

With the help of eqs. (10) and (11) it now becomes feasible to have an independent test or even calibration for the δ-thermometre of internal excitation put forward in eq. (9). In fact, any change dE_n in incoming neutron energy is equivalent to a change dE_{Sad} of the saddle point energy and hence a change dE_{int} of the total excitation energy. Upon varying E_n (and hence E_{int}) by known amounts and measuring the corresponding shift in the odd-even effect δ the basic equation (9) may be checked. In view of the many assumptions which had to be made when deriving this equation, an experimental test of eq. (9) is highly desirable.

Unfortunately, there is only one fission reaction, viz. $^{235}U(n,f)$, where nuclear charge measurements have been performed for at least two different neutron energies E_n. Besides thermal neutron measurements, radiochemical data are available for E_n = 1.9 MeV /30/ and E_n = 3.0 MeV /26/. The proton odd-even effect deduced from these data is given in Fig. 8. As expected from the general discussion given above, δ decreases rapidly with increasing neutron or internal excitation energy. This is a gratifying result since it confirms by experiment the ideas put forward for the interpretation of δ. Yet, the error bars in the data are large and prevent detailed conclusions to be drawn. But taking the data points seriously one readily realizes that they are in conflict with the predictions from eq.(9).

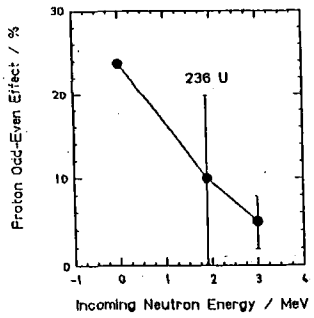

Figure 8: Proton odd-even effect vs. incoming neutron energy for $^{235}U(n,f)$.

Instead, the experimental data from Fig. 8 are well reproduced by the equation

$$E_{int} = -2\ln\delta \quad \text{MeV} . \tag{12}$$

This could indicate that the excitation energies calculated from eq. (9) are overestimated by a factor of two. Since it has already been pointed out in the derivation of eq. (9) that this formula should yield upper limits to E_{int}, the above result is not at all surprising. Still, for a reliable calibration of the δ-thermometre more accurate experimental data are needed. Charge measurements from (d,pf) reactions are under way which - at least preliminarly - seem to favour more eq. (9) than eq. (12). We will, therefore, continue to use eq. (9) in the following.

In the next step we put together all available data on the proton odd-even effect, both for thermal and fast neutron fission. From the measured odd-even effect δ, the total internal excitation energy E_{int} is calculated using eq. (9) and from eqs. (10) and (11) the energy E_{Dis} dissipated between saddle and scission is deduced. Figure 9 summarizes all E_{Dis} data having been collected up to date /15,16,17,19,22,23,26,30/ and displays their

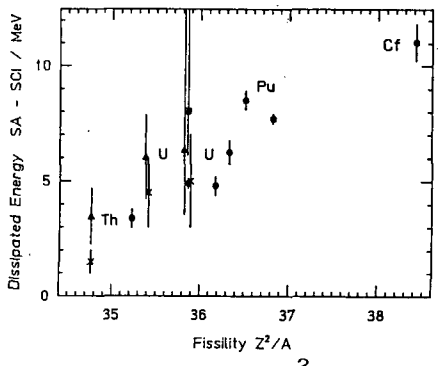

Figure 9: Energy dissipated between saddle and scission for the actinides Th,U,Pu and Cf. Full circles: thermal neutron fission, physical method. Triangles: fast neutron fission, radiochemistry [30]. Squares: fast neutron fission, radiochemistry [26]. Crosses: fast neutron fission, radiochemistry [12].

dependence on the fissility Z^2/A. Similarly to Fig. 7 the smooth variation of the energy E_{Dis} with the fissility is fairly well established. The thermal and fast neutron data fit together quite satisfactorily. Also included in Fig. 9 are values for E_{Dis} which have been obtained from radiochemistry by J.E. Gindler et al. /12/ for fast neutron fission of ^{232}Th, ^{235}U and ^{238}U. Since in this case the approach used to deduce E_{Dis} is completely different from the present one, it is reassuring to find a close agreement between the two methods.

Upon comparing the energy E_{Dis} dissipated (Fig. 9) with the energy ΔE_{pot} available between the saddle and the scission point (Fig. 4) one notices that the ratio $E_{Dis}/\Delta E_{pot}$ stays fairly constant for all Z^2/A in the range studied. A similar conclusion had already been reached from the first approximate evaluation of thermal neutron fission data (s. Fig. 7). The figure which is obtained for this ratio with E_{Dis} from eqs.(9) to (11) and ΔE_{pot} from ref. /24/ is $E_{Dis}/\Delta E_{pot} \sim 0.3$. Again it is difficult to give error bars for this latter quantity. Despite these uncertainties as to the absolute value of $E_{Dis}/\Delta E_{pot}$, the constancy of $E_{Dis}/\Delta E_{pot}$ for the nuclei studied appears to be well established. This allows for a simple parametrization of nuclear viscosity in fission processes.

So far we have only considered the odd-even effect δ averaged over the kinetic energy distributions of the fragments. We finally have to discuss the variation of δ with the

kinetic or total excitation energy of the fragments (Fig. 5) and the odd-even staggering of the kinetic energy with the fragment charge (Fig. 6) for thermal neutron fission.

Neglecting neutron evaporation, the relation between the light fragment kinetic energy E_L and the total kinetic energy TKE reads TKE = $E_L A_F/A_H$, with A_F and A_H the masses of the fissioning nucleus and the heavy fragment, respectively. With the help of this equation the measured odd-even staggering δE_L of the light fragment energy is converted into the odd-even staggering δ TKE of the total kinetic energy. For thermal neutron fission of the nuclei studied, the correlation between the odd-even effect in the charge yields δ and the staggering of the total kinetic energies δTKE is given in Fig. 10. There is evidently one Uranium data point to the right of the figure spoiling on otherwise clear correlation between δ and δTKE. This point stays for the $^{232}U(n,f)$ reaction which has been studied by the ΔE-E ionization chamber method (s. section 2). Later tests have shown that this method may be subject to considerable errors as to the energy dependence of charge yield measurement. It is therefore justified to discard this data point from the discussion.

The correlation between δ and δTKE has led to the conjecture that the energy necessary to break a pair is taken from the prescission kinetic energy. With the premise that at most one proton pair is broken H.-G. Clerc et al. /31/ have derived the formula

$$\delta TKE = 2\Delta \frac{2\delta}{1+\delta}. \tag{13}$$

Adopting for the pairing gap parameter the value 2Δ = 2.3 MeV a rather good fit to the data in Fig. 10 is achieved. However, the assumption that only one proton pair has been split is not consistent with the analysis having been outlined for δ as a function of fissility.

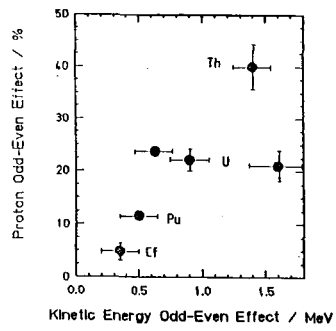

Figure 10: Correlation between proton odd-even effect and odd-even staggering of total kinetic energy of fragments for thermal neutron fission.

A more general combinatorial treatment, but again assuming that pair breaking drains prescission kinetic energy, leads to a slightly more involved relation between δ and δTKE /28/:

$$\delta TKE = 2\Delta\, \delta \ln\delta/(\delta^2-1) \tag{14}$$

Again choosing 2Δ = 2.3 MeV, the fit for the Cf, Pu and U data points is satisfactory but one fails to reproduce the Th data. It is questionable whether a proper choice for 2Δ can be found at all, since the data seem to imply a linear relationship between δ and δTKE which is not foreseen from eq. (14). In fact, the basic ad hoc assumption to correlate δ and δTKE, invoking the prescission kinetic energy, may be put into question. After all, first there is an odd-even effect δ Q already present in the available energy Q and second for even and odd charge fragments the deformabilities may be different leading to different scission configurations and hence Coulomb energies.

Another approach to the correlation between δ and δTKE goes back to Fig. 5 showing the dependence of the odd-even effect δ in the charge yields on the kinetic energy E_L of the light fragment. As already argued qualitatively in the preceding section, the slope $d\delta/dE_L$ is intimately connected to the odd-even staggering δE_L (s. Fig. 6). Switching from E_L to the total kinetic energy TKE one can indeed deduce the following relation /32/:

$$\delta TKE = 2\sigma^2_{TKE}(d\delta/dTKE) \tag{15}$$

with σ^2_{TKE} the variance of the TKE distribution. For the ^{230}Th nucleus with the steepest slope $d\delta/dE_L$ in Fig. 5 one calculates a slope $d\delta/dTKE \sim 1$ % MeV. The dependence of δ from TKE is thus seen to be rather weak as compared to the dependence of δ from the internal excitation energy E_{int} at scission. In fact, from eq. (9) one finds for the slope $d\delta/dE_{int}$ for the same ^{230}Th nucleus on the average $d\delta/dE_{int} = -10$ % MeV. This factor of ten for the ratio between the two slopes is also observed for the other actinides. The reason for the proportionality between the two slopes may be understood from

$$d\delta/dTKE = (d\delta/dE_{int})(dE_{int}/dTKE). \tag{16}$$

Since we are concerned here with thermal neutron fission one may substitute E_{int} by the energy E_{Dis} dissipated between saddle and scission and find

$$d\delta/dTKE = (d\delta/dE_{int})(dE_{Dis}/dTKE). \tag{17}$$

From eq. (9) one has for the first factor

$$d\delta/dE_{int} = -\delta/4 \qquad MeV^{-1}. \tag{18}$$

The second factor is expected to be rather universal and at least in principle is available from theory. The calculation should take into consideration that both the prescission kinetic energy and the Coulomb energy at scission contribute to TKE. The width of the TKE distribution then comes about by letting move the location of the scission point on the potential energy curve vs. deformation of Fig. 1. A similar argument has been used to explain the variation of the average odd-even effect δ with fissility Z^2/A in the above discussion. Of course, if the factor $dE_{Dis}/dTKE$ in eq. (17) were to be constant, then the two slopes $d\delta/dTKE$ and $d\delta/dE_{int}$ would be strictly proportional to each other. Since E_{Dis} and TKE show a smooth trend, though opposite in sign, with the deformation of the scission configuration, at least a near constancy of $dE_{Dis}/dTKE$ is anticipated.

Putting together the eqs. (15, (17) and (18) one finally obtains

$$\delta TKE = -\frac{\delta}{2}\,\sigma^2_{TKE}\,(dE_{Dis}/dTKE) \qquad MeV. \tag{19}$$

Though for a quantitative comparison with experiment the last term on the right hand side of eq. (19) has not yet been calculated, the formula shows that δTKE and δ are proportional to each other. This feature is in good agreement with experiment (s. Fig. 10). Last not least is should be pointed out that, due to the linear correlation between δ and δTKE, the dependence on fissility Z^2/A of the average odd-even effect δ entails a similar dependence of the odd-even staggering δTKE of the kinetic energy. The experimental observation from Fig. 6 with δTKE tapering off for increasing fissilities thus finds a simple explanation.

5. Conclusions

It has been shown that measurements of the nuclear charge distributions and, more specifically, the proton odd-even effects of fission fragments from (even,even) compound nuclei may be evaluated to yield the energy E_{Dis} dissipated between the saddle and the scission point. The idea behind is that - in the dynamical evolution of a fissioning nucleus - dissipative forces will lead to internal excitation energies, which in turn induce nucleon pairs to be broken; the number of broken pairs serves as a measure of the dissipated energy on one hand, while on the other hand it governs the magnitude of the observable odd--even effects.

It is found that the dissipated energy E_{Dis} increases smoothly with the fissility Z^2/A of the fissioning nucleus for all actinides studied, from Th up to Cf. This behaviour is similar to the one calculated from various fission models for the potential energy gain ΔE_{pot} between saddle and scission. The close correlation between E_{Dis} and ΔE_{pot} is

considered to be a proof for the conjecture that, in the descent from the saddle to the scission point of fission, nuclear viscosity is responsible for the breaking of nucleon pairs.

Especially for fast neutron fission any pair breaking which may already occur at the saddle point has to be taken into account. In the present approach this has been done by simply treating excitation energies at the saddle and those generated by the fission process itself on equal grounds. It could be shown that with this procedure the values obtained for the dissipated energy E_{Dis} from thermal and fast neutron fission agree reasonably well with each other, if due allowance is made for the simplifying assumptions in the evaluation. It should be stressed that the quoted figures for E_{Dis} (s. Fig. 7) are upper limits and that the actual values may be down by a factor of two.

From the present analysis a typical value for the dissipated energy in the standard $^{235}U(n,f)$ reaction is $E_{Dis} \sim 5$ MeV. From theoretical calculations /5,11/, the figure $E_{Dis} \sim 14$ MeV is reported. Evidently, the discrepancy is rather large (and gets even larger considering that our value is thought to be an upper limit). It should be pointed out, however, that in the theoretically calculated energy of dissipation, besides a proper choice of the viscosity forces, the definition of the scission or exit point enters as a crucial parameter.The above discrepancy could be largely removed if in the calculations the exit point of fission were to be placed at smaller deformations of the scission configuration. This would entail both, smaller potential energy drops ΔE_{pot} and dissipation energies /5,11/. By the way, the ratio $E_{Dis}/\Delta E_{pot}$ calculated in /5,11/ is pretty close to the figure deduced in the present work. In fact, the energies ΔE_{pot} given in /24/ for ^{236}U and used here are by a factor 2 or even more smaller than in /5/ and /11/. Since also the dissipated energies E_{Dis} deduced from our charge measurements are smaller by about this factor than in /5,11/, the agreement for the ratio $E_{Dis}/\Delta E_{pot}$ may be rather fortuitous. It nevertheless appears that the theoretical models could be made to come into agreement with the E_{Dis} values found in the present study. In this context it is interesting to note that the figure $E_{Dis} = 8.2$ MeV has been claimed in /33/ for $^{235}U(n,f)$ from a semi-empirical analysis of experimental data combined with potential energy calculations for the scission configuration.

Finally, it should be stressed that though in fission pairing or superfluidity is not fully preserved the damping forces nevertheless are rather small, with the dissipated energies ranging between 3 and 11 MeV in going from $^{229}Th(n,f)$ to $^{249}Cf(n,f)$.

In thermal neutron fission, experimental data for both, the dependence of the odd-even effect δ on the fragment kinetic energy and the odd-even staggering of the total kinetic energy δTKE, have been presented. The analysis shows that not only the slope $d\delta/TKE$, but also the average odd-even effect δ in the charge yields is proportional to δTKE. Different models have been discussed trying to understand the correlation between δ and δTKE. A new model has been proposed which is based on a similar reasoning as already employed for the interpretation of the average δ data and their dependence on fissility. This latter approach seems to offer a simple explanation for the linear correlation between δ and δTKE. However, for a quantitative test of this model the calculation of the variation of the dissipated energy E_{Dis} with the total kinetic energy TKE is still missing.

References

1. P. Möller, J.R. Nix and W.J. Swiatecki, Int. School-Seminar on Heavy Ion Physics, Dubna, USSR, 1986, p. 167
2. U. Brosa, S. Grossmann and A. Müller, Z. Naturforsch. 41a (1986) 1341
3. K.T.R. Davies et al., Phys. Rev. C 16 (1977) 1890
4. A.J. Sierk and J.R. Nix, Phys. Rev. C 21 (1980) 982
5. J. Moreau et al., Journées d'Etudes sur la Fission, Arcachon, France 1986
6. C. Guet et al., Nucl. Phys. A 314 (1979) 1

7. H.M.A. Radi et al., Phys. Rev. C 26 (1982) 2049
8. G.A. Pik-Pichak, Sov. J. Nucl. Phys. 40 (1984) 215
9. J.P. Theobald, Report IKDA 85/22, T.H. Darmstadt, 1985, FRG
10. J.R. Nix and A.J. Sierk, Int. School-Seminar on Heavy Ion Physics, Dubna, USSR, 1986, p. 453
11. G. Schütte, Phys. Rep. 80 (1981) 113
12. J.E. Gindler, L.E. Glendenin and B.D. Wilkins, Proc. 4th IAEA Symp., Jülich 1979, Vienna 2 (1980) 111 and Lecture Notes Vol. 158 (1982) 145, Springer Verlag
13. A.C. Wahl, Phys. Rev. C 32 (1985) 184
14. E. Moll et al., Kerntechnik 19 (1977) 374
15. W. Lang et al., Nucl. Phys. A 345 (1980) 34
16. C. Schmitt et al., Nucl. Phys. A 430 (1984) 21
17. H.G. Clerc et al., Nucl. Phys. A 452 (1986) 277
18. J.P. Bocquet, R. Brissot and H.R. Faust, to be published
19. M. Djebara et al., Nucl. Phys. A 425 (1984) 120
20. A. Oed et al., Nucl. Instr. and Meth. 219 (1984) 569
21. A. Oed, P. Geltenborg and F. Gönnenwein, Nucl. Instr. and Meth. 205 (1983) 451
22. P. Schillebeeck , private communication
23. J.P. Bocquet et al., Verhandl. DPG (VI), Vol. 22 (1987) IV, C-1.2 and Journées d'Etudes sur la Fission, Arcachon, France 1986, to be published
24. M. Asghar and R.W. Hasse, J. de Physique C 6 (1984) 455
25. B.D. Wilkins, E.P. Steinberg and R.P. Chasman, Phys. Rev. C 14 (1976) 1832
26. G. Mariolopoulos et al., Nucl. Phys. A 361 (1981) 213
27. G. Mantzouranis and J.R. Nix, Phys. Rev. C 25 (1982) 918
28. H. Nifenecker et al., Z. Phys. A 308 (1982) 39
29. H.C. Britt and J.R. Huizenga, Phys. Rev. C 9 (1974) 435
30. S. Amiel, H. Feldstein and T. Izak-Biran, Phys. Rev. C 15 (1977) 2119
31. H.-G. Clerc et al., Proc. 4th IAEA Symp. Jülich, 1979, Vienna 2 (1980) 65
32. A. Guessous, thesis, Univ. of Grenoble, 1983, unpublished
33. H. Schultheis and R. Schultheis, Phys. Rev. C 20 (1979) 403

FLUCTUATIONS OF FISSION CHARACTERISTICS AND THE STRUCTURE OF FISSION CHANNELS.

V.I.Furman and J.Kliman*.

Joint Institute for Nuclear Research, Dubna, P.O.Box 79, Moscow, USSR.
*Institute of Physics EPRC,Dubravska cesta 9, Bratislava, Czechoslovakia.

Abstract: The fluctuations of the total kinetic energy, the independent yields and the anisotropy of an angular distribution of fission fragments in the individual resonances with J =4 are analysed. The possible way to unify the standard channel picture of a fission with recent ideas about fission paths are investigated.

1. Introduction

Impressive advances recently obtained at the study of detailed fission fragments characteristics 1),2),3) and also the successes 4) in theoretical treatment of their mass and kinetic energy distributions somewhat overshadowed quantum mechanical aspects of fission physics. The cause, may be, is in that this aspects clearly appear only in the rare cases when the fission results from individual states of nuclei. The quantum - mechanical effects can appear in the first place in the form of interference between fission channel amplitudes, observed in the (n,f) cross sections 5)as well as in the P-even 6) and P-odd 7),8) angular correlation of fission fragments. Secondly, the sharp changes in the differential and integral characteristics of fission for different initial states of a fissile nucleus with given spin and parity that appear, for example, in strong fluctuations of fission widths of neutron resonances 5), in relative yield fluctuations9) of given fission fragments, and also in an anisotropy variation of fission fragments angular distribution 10), are related to the fact that the number of fission channels is limited to a few units and each of them has its wave function 11). If we suppose that the nucleus conserves the axial symmetry during the process of fission the wave function of a channel on the way to scission point is characterised by the values of spin J and its projection K to the deformation axis. Thus, the angular characteristics in a fixed channel are described 11) by the wave function of symmetric top $\mathcal{D}^{J}_{MK}(\theta)$, and the internal properties of channels are determined by the detailed features of movement in the nuclear space of large deformations. The basic properties of the fission fragments, the coupling of amplitude of forming separate fragments have to be programmed into the channel wave function $\psi_f^{J\pi K}$, since without this it is impossible to understand the existence the above-mentioned interference effects. Let us remark that the theoretical description of P-even and P-odd angular correlations, observed in the study of (n,f) reactions with slow polarized neutrons 12),13) was constructed on basis of direct generalisation of Bohr's idea.

The aim of our paper is the modification of the fission picture proposed in 11) to insert into (this approach) the quasiclassic characteristics of different fission paths which may define 4) the main features of mass and kinetic energy distributions of fission fragments. The generalization is based on analysis of the experimental data sets for a compound nucleus ^{236}U, unique in its completness. The knowledge of spin separated cross - sections of (n,f) reaction 14) permits to analyse in detail the fluctuation (from one resonance to other) of mean kinetic energies 1), of the fission fragment yields 9),15),16) and also of the fragments angular anisotropy coefficients 10). The important part of our analysis consists

in the use of the results 17), where authors obtain the weights of separate fission channels in neutron resonances extracted from the detailed investigation of the interferences revealed in the fission cross-sections 14) of $^{235}U(n,f)$ reaction.

2. The basic formulas.

The wave function of compound state with the characteristics J,π,M is described in the form

$$\psi_\lambda^{J\pi M} = \sum_K a_{K\lambda}^J \psi_f^{J\pi MK} + \psi_{\lambda\, n.f.}^{J\pi M} \tag{1}$$

where $\psi_{\lambda\, n.f.}^{J\pi M}$ denotes the part of function $\psi_\lambda^{J\pi M}$ not connected to fission, and quantum fission channel is described by a standard function of the deformed nucleus (see e.g. 18) formulas 4.19 or 4.39). Further the projection of J to the z-axis in a laboratory system of coordinates denoted by M is omitted. The coefficients $a_{K\lambda}^J$ defining the value of admixture of a given fission channel (here for simplicity we take into account only one channel with fixed J,π,K) to the state λ randomly fluctuate for different λ-s. Due to strong mixing in K 19) caused by Coriolis interaction we have $\langle a_{K\lambda}^{J2}\rangle_\lambda \simeq$ const/(2J+1).
In the frame of statistical approach to the structure of neutron resonances $\langle a_{K\lambda}^{J2}\rangle \sim 1/N_\lambda$, where $N_\lambda \gg 1$ is the total number of components in the wave function (1). Moreover we suppose that

$$\psi_f^{J\pi K} = \sum_d \sqrt{\alpha_d^K}\, \psi_d^{J\pi K} \tag{2}$$

where the function $\psi_d^{J\pi K}$ describes the properties of the bulk of fission fragments connected to path of fission 4) (walley) ''d''. The coefficients α_d^K of dynamical mixing of contributions of walleys to a given channel J,π,K are normalised by

$$\sum_d \alpha_d^K = 1 \tag{3}$$

taking into account the orthogonality of functions $\psi_d^{J\pi K}$ for different d. Then the total fission width, of the state , has the form

$$\Gamma_{f\lambda}^{J\pi} = \sum_K (a_{K\lambda}^J)^2 \Gamma_f^{J\pi K} \equiv \sum_K \Gamma_{f\lambda}^{J\pi K} \tag{4}$$

where

$$\Gamma_f^{J\pi K} = \sum_d \alpha_d^K \Gamma_d^{J\pi K} \tag{5}$$

The nontrivial meaning of the dependence of "partial" width $\Gamma_d^{J\pi K}$, related to the sum of contributions of all fragments from a given walley d to the total probability of fission, on the value of K lies in the fact that the height of the fission barrier is naturally connected with the saddle configuration of nucleus on the fission path d in a full analogy with ref.4). Transmission of the fission barrier in channel J,π,K is formed by dynamical weighting (via the coefficients α_d^K) of transmissions in separate walleys.
We introduce the relative contribution of the channel J,π,K in the total fission widths

$$P_{K\lambda}^{J\pi} \equiv \Gamma_{f\lambda}^{J\pi K} / \Gamma_{f\lambda}^{J\pi} \quad \text{with} \quad \sum_K P_{K\lambda}^{J\pi} = 1 \tag{6}$$

So in a given resonance λ the relative yields of fission fragments (i,j) (M_i,Z_i, M_j,Z_j,E_k^{ij}) with kinetic energy of relative movement E_k^{ij} we describe in the form

$$Y_{f\lambda}^{J\pi}(i,j)/Y_{f\lambda}^{J\pi} = \sum_K P_{K\lambda}^{J\pi} \Gamma_f^{J\pi K}(i,j)/\Gamma_f^{J\pi K} \simeq \sum_d \mathcal{F}_d(i,j)\, W_{d\lambda}^{J\pi} \tag{7}$$

In analogy with the paper 1) we assume that the mass and energy distribution belonging to a given walley d may be described through the universal (normalised) function $\mathcal{F}_d(i,j)$ while the weights of walley $W_{d\lambda}$ may fluctuate for different λ. We omit below the indices J,π, if it does not lead to misunderstanding. The weights $W_{d\lambda}$ are expressed by the relation

$$W_{d\lambda} = \sum_K P_{K\lambda} \alpha_d^K \Gamma_d^K / \Gamma_f^K \tag{8}$$

with

$$\sum_K W_{d\lambda} = 1 \tag{9}$$

Finally as is follows from (7) the mean total kinetic energy (over all fission fragments) for the fission through a state λ may be written as

$$\bar{E}_\lambda = \sum_d \bar{E}_d W_{d\lambda} \tag{10}$$

where

$$\bar{E}_d = \int dM_i\, dZ_i\, E_k^{ij} \mathcal{F}_d(i,j) \tag{11}$$

3. The analysis of experimental data and discussion of results.

If we consider a compound - nucleus ^{236}U formed by s-neutron capture there exist only states with $J = 4^-$ and 3^-. As it has been shown in ref 14) for the resonances with $J = 4^-$ essential contribution give only two fission channels having K=1 and 2. This is connected to the forbideness of the channel having $J,\pi,K = 4^-0$ under the condition of the axial symmetry of a fission and to the strong hindrance of the channels having K=3 and 4 caused by a low transmission of the fission barrier. For the states with $J^\pi = 3^-$ the situation is more complex because an essential contribution give at least three values of K=0,1 and 2, so below we restrict ourselves only to an investigation of fission characteristics of the compound - states with $J^\pi = 4^-$.

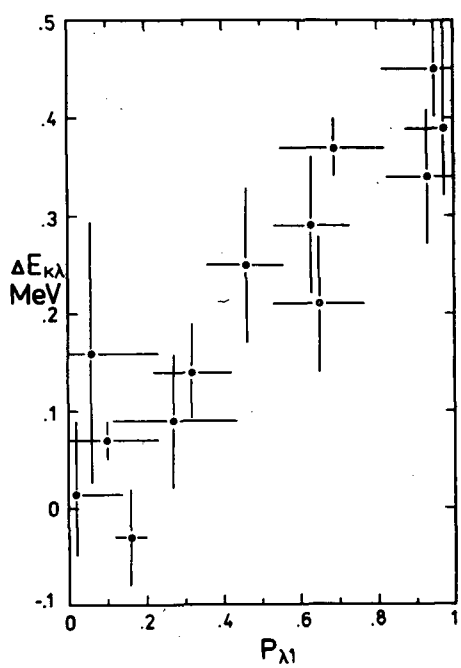

Fig. 1. Correlation of the weights of the fission channel with $J^\pi K = 4^-1$ with respect to the total kinetic energy fluctuations.

Let us consider firstly the fluctuation for different states λ of the mean total kinetic energy $\bar{E}_\lambda$, measured in the paper1) as a difference $\bar{E}_\lambda - \bar{E}_{th}$, where $\bar{E}_{th}$ is the value of total kinetic energy for thermal neutrons. Taking into accounts only two channels K=1 and 2 and using formulas (8),(6) and (10) one has

$$\Delta \bar{E}_\lambda = \bar{E}_\lambda - \bar{E}_{th} = \sum_d \bar{E}_d \Delta W_{d\lambda} + \langle \bar{E}_\lambda \rangle_\lambda - \bar{E}_{th} \tag{12}$$

where

$$\Delta W_{d\lambda} = W_{d\lambda} - \langle W_{d\lambda} \rangle_\lambda = (P_{1\lambda} - \bar{P}_{1\lambda}) \left(\frac{\alpha_d^1 \Gamma_d^1}{\Gamma_f^1} - \frac{\alpha_d^2 \Gamma_d^2}{\Gamma_f^2} \right) \tag{13}$$

It is clear that $\Delta \bar{E}_\lambda$ has to depend linearly on $P_{1\lambda}$, as it is confirmed by fig.1, where the relation between values $\Delta \bar{E}_\lambda$ and $P_{1\lambda}$ from ref. 17) for resonances λ with $J^\pi = 4^-$ lying in the interval neutron energy 1 eV $\leq E_n \leq$ 35 eV is shown. (We use in our analysis only rather definite resonances, with very small $J^\pi = 3^-$ admixture.)

Hence we may conclude that the fluctuations of the total kinetic energy are satisfactorily described taking into account only random contributions of two fission channels with K=1 and K=2.

Note, that from (12) easily follows the correlation between $\Delta \overline{E}_\lambda$ and $\omega_\lambda = (W_{I\lambda}/W_{II\lambda})/(W_I^{th}/W_{II}^{th})$ established in the paper 15). Indeed as implied by 1) the superlong walley can be neglected, if we consider the values directly determined by the symmetric fission yield. So from (9) it follows that $\Delta W_{I\lambda} \simeq -\Delta W_{II\lambda}$ Then

$$\omega_\lambda = \left(\frac{\langle W_{I\lambda}\rangle}{W_I^{th}} \Big/ \frac{\langle W_{II\lambda}\rangle}{W_{II}^{th}}\right)\left(1 + 2\,\frac{\Delta W_{I\lambda}}{\langle W_{II\lambda}\rangle}\right) \tag{14}$$

and

$$\Delta \overline{E}_\lambda \simeq \Delta W_{I\lambda}\,(\overline{E}_I - \overline{E}_{II}) + Const. \tag{15}$$

Using the formula (13) we are able to explain simultaneously the small magnitudes of the fluctuations $\Delta W_{d\lambda} \lesssim 0{,}03$ and the large ones of $P_{1\lambda}$ ($P_{1\lambda} \lesssim 0.5$), if the difference $(\alpha_d^1 \Gamma_d^1/\Gamma_f^1 - \alpha_d^2 \Gamma_d^2/\Gamma_f^2) \leq 0{,}1$.
Such a situation is fully attainable.

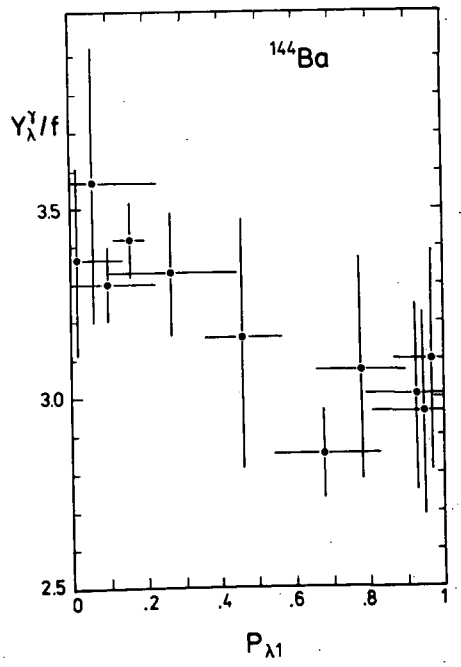

Fig. 2. Correlation of the independent yields of ^{144}Ba with respect to the weights of the fission channel $J^\pi K=4^-1$.

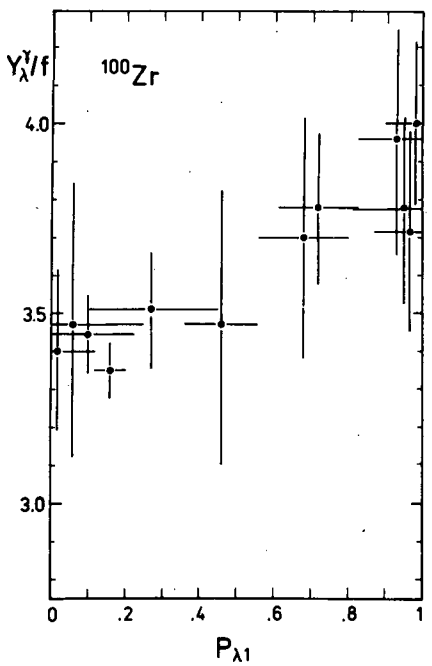

Fig. 3. The same as a Fig.2 for the yields of ^{100}Zr.

In Fig. 2 and 3 the fluctuations of the independent yields of nuclei ^{144}Ba and ^{100}Zr are shown in a correlation with $P_{1\lambda}$. As it follows from (7)

$$\Delta\,(Y_{f\lambda}(Ba)/Y_{f\lambda}) \simeq -\,\mathcal{F}_{II}(Ba)\,\Delta W_{I\lambda} \tag{16}$$

$$\Delta\,(Y_{f\lambda}(Zr)/Y_{f\lambda}) \simeq [\mathcal{F}_I(Zr) - \mathcal{F}_{II}(Zr)]\,\Delta W_{I\lambda} \tag{17}$$

In last formula $[\mathcal{F}_I(Zr) - \mathcal{F}_{II}(Zr)] > 0$ so using (13) we can qualitatively describe by the relations (16) and (17) the experimental situation. However it is necessary to note that the magnitudes of the yield fluctuations are larger than expected

in comparison with the energy fluctuations $\Delta\overline{E}_\lambda$.

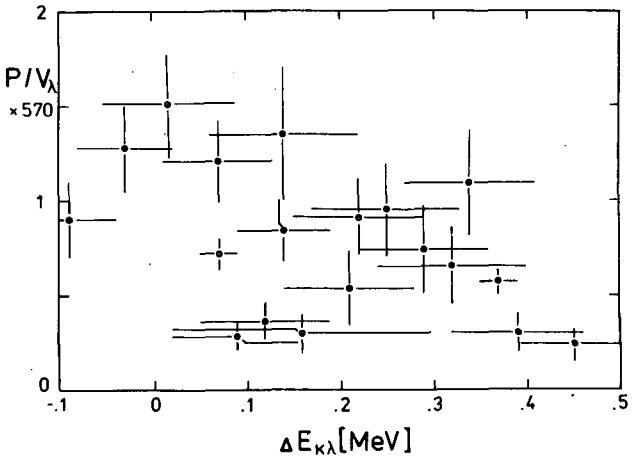

In Fig.4 we compare the ratios $\delta_\lambda = Y_{f_\lambda}(Peak)/Y_{f_\lambda}(Walley)$ from ref.15) with the values $\Delta\overline{E}_\lambda$. It is important to note that the large fluctuations (100%) of δ_λ cannot be explained if we take into account only two fission channels with K=1;2. If one include the channels having K=3 and 4 with small weights it permits in principle to explain the absence of the correlation between δ_λ and $\Delta\overline{E}_\lambda$ and a large dispersion of δ_λ, too.

Fig. 4. Comparison between the fluctuations of the total kinetic energy and of the peak-to-walley yields ratio for the compound states ^{236}U with $J^\pi = 4^-$.

In ref.10) the authors have measured the anisotropy of an angular distribution of fission fragments and extracted the values of so called A_2^{obs}, expressed for by the formula

$$A_2^{obs}(E_n) = \frac{A_2^{3^-}\sigma_{nf}^{3^-}(E_n) + A_2^{4^-}\sigma_{nf}^{4^-}(E_n)}{\sigma_{nf}^{3^-}(E_n) + \sigma_{nf}^{4^-}(E_n)} \tag{18}$$

The coefficients $A_{2\lambda}^{J\pi}$ for the fixed neutron resonance λ may be written as

$$A_{2\lambda}^{J\pi} = \sum_K A^{J\pi K} P_{K\lambda}^{J\pi} \tag{19}$$

where $A_2^{J\pi K}$ depends only on the angular variables. As a measure of a spin purity of $A_2^{obs}(E_n)$ we use the value of an effective spin

$$J_{eff} = 3 + \frac{\sigma_{nf}^{4^-}(E_n)}{\sigma_{nf}^{3^-}(E_n) + \sigma_{nf}^{4^-}(E_n)} \tag{20}$$

In the Fig. 5 together with the respective values of $P_{1\lambda}$ the coefficients $A_2^{obs}(E_n)$ for neutron energies E_n where $J_{eff} \geqslant 3.5$ (and hence $A_2^{obs} \approx A_{2\lambda}^{4^-}$) are shown. For the case under study $A_{2\lambda}^{4^-} = -1.31\ P_{1\lambda}^{4^-} - 1.17$ and the large fluctuations of $A_{2\lambda}^{4^-}$ have to exist. As it is seen from Fig.5 this relation qualitatively describes the experimental situation.

However it is necessary to keep in mind that the values $A_2^{obs}(E_n)$ are rather sensitive to the small contributions of fission channels with K = 3 and K = 4.

It has been stressed that in our approach there is a natural explanation for the small fluctuations of the total kinetic energy of the fission fragments and the large fluctuations of the coefficients $A_{2\lambda}$.

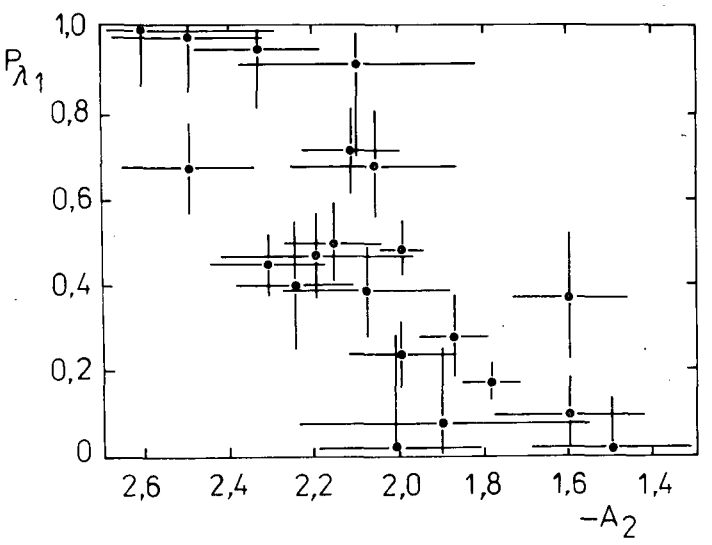

Fig. 5. Correlation of the weights of the fission channel $J^{\pi}K = 4^{-}1$ with respect to the anisotropy coefficients $A_{2\lambda}$.

In conclusion it may be noted that our analysis gives the direction of a possible way to unify the standard channel picture of a fission 11) with the recent ideas 4) about fission paths.

The authors are indebted to Drs. A.B.Popov and S.G.Kadmensky for the valuable discussions.

References.

1) H.-H.Knitter,F.-J.Hambsch,C.Budtz-Jørgensen and J.P.Theobald,Z.Naturforsch. 42a(1987)786.
2) E.K.Hulet,J.F.Wild,R.J.Dougan et.al.,Phys.Rev.Lett.56(1986)313.
3) P.Koczon,M.Mutterer,J.P.Theobald, et.al., Phys.Lett., B191(1987)249.
4) U.Brosa and S.Grossmann,Z.Phys. A310(1983)177.
5) J.E.Lynn, The theory of neutron resonance reactions,Claredon Press,Oxford, 1968, p.351.
6) N.V.Borovikova,V.A.Vesna,A.I.Egorov, et.al., Pisma JETP 30(1979)527.
7) G.V.Danilyan,B.D.Vodennikov,V.P.Dronyaev,et.al.,Pisma JETP 26(1977)197.
8) A.K.Petukhov,G.A.Petrov,S.I.Stepanov,et.al.,Pisma JETP 32(1980)324.
9) G.A.Cowan, B.P.Bayhurst,R.J.Prestwood,et.al.,Phys.Rev.C2(1970)615.
10) N.J.Pattenden and H.Postma,Nucl.Phys.,A167(1971)225.
11) A.Bohr, Proc.First Int.Conf. on the Peaceful Uses of Atomic Energy, P/911, Vol.2, p.151 and 220,(1956), United Nations, N.Y.
12) O.P.Suskov and V.V.Flambaum, Usp.Phys.Nauk,136(1982)4.
13) V.E.Bunakov,V.P.Gudkov,Nucl.Phys.,A401(1983)93.
14) M.S. Moore, J.D. Moses, G.A. Keyworth et al. Phys. Rev. C 18 (1978) 1328
15) F.-J. Hambsch, Ph.D. Thesis, Internal Report, VG./1796/87, TH Darmstadt, FRG, and C.B.N.M. Geel, Belgium, 1987
16) N.A. Gundorin, A. Duka-Zolyomi, J. Kliman and V.I. Furman, Preprint JINR, P3-87-718, Dubna, 1987
17) M.S. Moore, G. de Saussure and J.R. Smith, Proc. of the IAEA Consultants Meeting on Uranium and Plutonium Isotope Resonance Parameters, INDC(NDS 129 GJ), Vienna, 1981, ed. D.E. Cullen, IAEA, Vienna
18) A. Bohr and B.R. Mottelson, Nuclear Structure, Vol. 2, W.A. Bendjamin, M.C. Reading, Massechusetts, USA, 1975
19) S.G. Kadmensky, V.P. Markushev, Yu.P. Popov, I. Furman, Sov. Nucl. Phys., 39 (1984) 7.

CONSISTENT THEORETICAL DESCRIPTION OF ENERGY AND ANGULAR DISTRIBUTIONS OF PROMPT FISSION NEUTRONS

H. Märten, A. Ruben, and D. Seeliger
Technische Universität Dresden, GDR

Basic requirements to be met for the physically consistent calculation of energy and angular distributions of prompt fission neutrons are summarized. Main emphasis is pointed to an adequate statistical-model approach (SMA) to cascade neutron evaporation from a fragment diversity specified by the occurrence probability $P(\{p_f\})$ as function of a fragment parameter set $\{p_f\}$ ("internal" consistency) as well as to the SMA application to any fission reaction depending on the $P(\{p_f\})$-description as function of the fissioning-nucleus parameters $\{p_{FN}\}$ ("external" consistency).

1. Introduction

A large number of microscopic measurements has shown that the energy spectrum of prompt fission neutrons (PFN) is an evaporation-like distribution phenomenologically described by either a Maxwellian or a Watt spectrum. Most of the observations are consistent with the theoretical concept of neutron emission from highly excited and rapidly moving fragments. However, PFN emission has to be understood as a superposition of different components corresponding to specific mechanisms.[1] In addition to the main one, the so-called "scission neutron" emission due to rapid nuclear-potential changes close to scission, the neutron emission during fragment acceleration (probably including non-equilibrium effects), and neutron emission from n-unstable light charged particles (^5He, $^6He^+$, etc.) after ternary fission can be assumed. The possible role of these secondary mechanisms has been discussed in Refs. 1,2.
Several characteristics of secondary neutrons (mostly considered as a central component in the lab. frame of fissioning nucleus) have been derived from experimental PFN data (in particular, the dependence of the probability distribution on emission angle) in comparison with statistical-model approaches to the predominant evaporation component. It has been emphasized in Ref. 1 that most of the contradictions of informations deduced are due to rough ansatzes for the description of PFN spectra in the centre-of-mass system of fragments (CMS) and the neglection of the intricate fragment occurrence probability $P(\{p_f\})$, i.e. average fragment parameters are used. Furthermore, the CMS spectra have been often adjusted on the basis of the experimental distributions themselves.
Several questions appear:

(i) What are the requirements to be met in adequate calculations of PFN characteristics?
(ii) What role do secondary mechanisms play?
(iii) Is their consideration necessary for practical SMA applications to PFN emission at all?
(iv) How can the distribution $P(\{p_f\})$ be predicted, in particular in the case of induced fission reactions as function of incidence energy?

The questions stated above concern basic problems of PFN theory and their practical application.

2. "Internal" consistency of PFN theory

Several attempts have been made to describe PFN energy and angular distributions assuming that all prompt neutrons are evaporated from fully accelerated fragments (SMA).[3-7] These approaches can be classified according to

(i) the ansatz of an evaporation spectrum as function of $\{p_f\}$ (either Hauser-

Feshbach or Weisskopf-Ewing or approximative),

(ii) the complexity of $P(\{p_f\})$ considered.

The physical constraints of a pure SMA have been emphasized in a recent review.[8] The importance of the consideration of a complex $P(\{p_f\})$ distribution for the precise description of PFN emission distributions has been studied in the framework of the cascade evaporation model (CEM)[7,9] indicating certain deviations if neglecting special features of PFN emission. However, the applicability of a SMA is restricted in most cases due to the lack of knowledge of the $P(\{p_f\})$ distribution. Provided that $P(\{p_f\})$ is known accurately, the agreement of SMA calculations with experimental data (energy and angular distributions, in particular as function of certain $\{p_f\}$ variables) is a measure of the "internal" physical consistency of the SMA. It should be assumed that any deviations are due to

- the influence of secondary-neutron emission as discussed above,
- the non-adequate SMA ansatz (e.g. neglection of PFN characteristics).

In the case of ^{252}Cf spontaneous fission, $P(\{p_f\})$ can be deduced from experimental data on neutron and γ-ray emission as function of fragment variables (mass number A, charge number Z, total kinetic energy TKE, excitation energy E^*, angular momentum I) with reliable precision.[7]

The CEM considering the whole dependence of PFN emission on A, TKE, and E^*, e.g. $\{p_f\} = \{A, TKE, E^*\}$, as well as on averages $\bar{Z}(A)$ and $\bar{I}(A)$, has recently been used to describe new experimental data[10] on energy and angular distributions $N(E,\Theta)$ of ^{252}Cf(sf) PFN. In particular, the center-of-mass system anisotropy of neutron emission (due to fragment angular momentum) and neutron/γ-competition of de-excitation, have been considered.[11] As shown in Appendix A, the parameter-free CEM reproduces the measured data within the experimental as well as theoretical uncertainties.

No significant indications of secondary neutrons have been found. The upper limit of their relative yield was estimated to be $\lesssim 5$ %.

At present, the CEM can obviously be assumed as a "internally" consistent SMA to describe the whole distribution $N(E,\Theta)$. In particular, the crucial polar regions at E close to the average fragment kinetic energy per nucleon E_f, i.e. at low centre-of-mass frame energy, have satisfactorily been reproduced due to the consideration of neutron/γ-ray competition and reliable choices of the global optical potential.[8,11]

Concerning the analysis of $N(E,\Theta:\{p_f\})$ data, a more detailed investigation should provide further informations on PFN emission. The new experimental data obtained by Knitter and Butz-Jørgensen,[12] i.e. $N(E,\Theta:A,TKE)$, are a comprehensive base for further studies.

The Madland-Nix model (MNM) has widely been used for the description of PFN spectra N(E). It incorporates an approximative spectrum ansatz. Furthermore, the calculations are performed for average fragment parameters $\bar{p}_f$ of both groups in binary fission reactions. The consideration of the spectrum dependence on A has been introduced in the generalized MNM (GMNM)[13], i.e. $\{p_f\} = \{E^*, A\}$, $\overline{TKE}(A_1/A_2)$, $\bar{E}^*(A)$, $\bar{Z}(A)$, $\bar{I}_{total}$. However, some refinements had to be taken into account to obtain a consistent description of $N(E,\Theta)$ for any fission reaction, namely the consideration of n/γ-competition (simulated by a low limit T_0 of rest-nucleus temperature) as well as semi-empirical level density parameter a(A) instead of the Fermi-gas model approach $a \sim A$.[8,11] Including these modifications, the GMNM provides the basis for a reliable prediction of PFN <u>energy and angular</u> distributions. The a(A) scaling factor considered as well as the limit T_0 are handled as model parameters defining the spectrum hardness and the shape of angular distribution at E close to E_f, respectively. Both have been adjusted on the basis of ^{252}Cf(sf) data. They are not changed in case of GMNM applications to any fission reaction. Both the CEM and the GMNM are suitable to describe <u>$N(E,\Theta)$</u> for ^{252}Cf(sf) with adequate accuracy, i.e. within experimental <u>as well as theoretical</u> uncertainties (internal consistency). However, their application to any fission reaction requires the knowledge of the relevant $P(\{p_f\})$ distribution.

A reliable prediction of $P(\{p_f\})$, i.e. the precondition of the "external" consistency of PFN theory, is only possible in the framework of the more simple GMNM.
In the case of CEM, it can be derived neither from fission theory nor from experimental data with sufficient accuracy and/or completeness. Hence, we'll focus on GMNM discussing possibilities of $P(\{p_f\})$-prediction for any fission reaction.

3. Prediction of fragment distribution for complex SMA applications

As outlined above, the application of complex SMA requires the knowledge of $P(\{p_f\} : \{p_{FN}\})$, where $\{p_{FN}\}$ denotes a parameter set of the fissioning nucleus as mass and charge number, excitation energy, angular momentum, etc. Since basic fission theories fail to reproduce this occurence probability with adequate accuracy, the GMNM has been combined with semi-empirical fission theories providing $P(A;\overline{E}^*(A),\overline{TKE}(A_1/A_2) : A_{FN},Z_{FN},E^+_{FN})$ for actinide fission (Th-Cf) at E^*_{FN} below about 25 MeV:

(i) two-spheroid model (TSM)[14], i.e. a scission point model including semi-empirical, temperature-dependent shell correction energies, for the prediction of $\overline{E}^*(A)$ and $\overline{TKE}(A_1/A_2)$ (energy partition as function of mass asymmetry);

(ii) 5-Gaussian approach[15] (justified theoretically[16] as well as experimentally[17]) for the prediction of $P(A:A_{FN},Z_{FN},E^*_{FN})$ (mass yield curve);

In addition, the angular distribution of fragments with reference to incident-beam direction, $W(\beta)$, which causes a PFN anisotropy with reference to incident-beam direction, is approximated by a

(iii) statistical-model description[18] of $W(\beta:A_{ZN},Z_{FN},E^*_{FN})$ based on the distribution in angular-momentum projection (K) depending on fissioning-nucleus temperature (calculations based on an adjustment to experimental data).

In the case of multiple-chance fission reactions, e.g. (n,xnf)-reactions, the fragment occurence probability is predicted for each chance separately. Consequently, the GMNM can be applied to each chance. In our first applications, this has been done for average $\overline{E}^*_{FN}$ for $x \geq 1$. The weight of each chance, i.e. the partial fission cross section $\sigma_{f,x}$, as well as the spectra of pre-fission neutrons are calculated within the Hauser-Feshbach model including fission channel (code STAPRE).[19] In summary, the following scheme should be realized:

<u>Input</u>: $\underbrace{\overline{E}^*_x(A),\overline{TKE}_x(A_1/A_2),P_x(A)}$

$\Downarrow$

GMNM

$\Downarrow$

$\overline{\nu}_x(A),N_x(E,\theta),N_x(E)$, etc.

$\Downarrow \longleftarrow W_x(\beta)$

$G_x(E,\Psi)$ (emission probability with reference to incident-particle direction)

<u>Results</u>: $$\overline{\nu}_{tot} = \sum_x \frac{\sigma_{f,x}}{\sigma_{f,tot}} \cdot (\overline{\nu}_x + x)$$

(multiplicity including pre-fission and post-fission neutrons)

$$\sigma(E,\Psi) = \sum_x \sigma_{f,x} \cdot \overline{\nu}_x \cdot G_x(E,\Psi)$$

(cross-section of post-fission neutron emission)

etc.

(For some applications, see Appendix B as well as Refs. 20,21).
The semi-empirical fission theories mentioned above reproduce the following remarkable trends in the dependence of fragment variables on E^*_{FN}:

(i) Due to the diminution of shell effects with increasing scission point temperature (which increases as E^*_{FN} increases), $\bar{E}^*(A)$ and consequently, $\bar{\nu}(A)$ changes in a definite manner: The strong saw-tooth like behaviour becomes less pronounced with increasing E^*_{FN}. $\bar{E}^*(A)$ shows the strongest rise at A around 132 (double-magic fragment) as a consequence of the diminuished stiffness. The TSM reproduces the energy partition results as measured (cf. Refs. 22,23).[24]

(ii) Position, width, and weight of the 5 Gaussians describing the mass yield curves (two asymmetric "standard" fission paths, one symmetric fission path[16]) have been adjusted on the basis of experimental data as in Ref. 19.
The higher E^*_{FN},
- the higher the weight of the symmetric mode,
- the higher the widths.

The relative weights of both asymmetric modes depend on E^*_{FN}. Whereas $\bar{A}_H$ (mass number of the heavy-fragment group) is almost independent on A_{FN} at very low E^*_{FN}, it is remarkably dependent on E^*_{FN} itself.

(iii) The fragment anisotropy decreases with increasing E^*_{FN}(except threshold region where special fission channels are important).

It should be emphasized that experimental fragment occurence probabilities are commonly used for the calculations if they are known with sufficient accuracy. This is necessary in the case of threshold fission specifically. Here, channel effects are considerable. So far, they are not included in the semi-empirical fission theories.
The reliable description of $P(\{p_f\}: \{p_{FN}\})$ is of high importance to predict PFN data for any induced fission reaction ("external" consistency of PFN theory). Some results are shown in Appendix B. So, it becomes possible to study $\bar{\nu}(E^*_{FN})$, $\bar{E}(E^*_{FN})$, and, in particular, the correlation function $E(\bar{\nu})$ (cf. Ref. 25).
As shown in Appendixes A and B, the shape of PFN spectra is neither Maxwellian nor Watt type. Whereas E increases as E^*_{FN} increases, the shape of the PFN spectrum with reference to Maxwellians corresponding to given E is little changed. However, this result is a pure theoretical one. So far, the accuracy of measured PFN spectra is not sufficient to confirm this behaviour found for pure (n,f)-reactions. In the case of multiple-chance fission, remarkable deviations from the approximatively linear increase of $\bar{E}$ and $\bar{\nu}$ with increasing incidence energy appear at higher-order thresholds ($x \geq 1$).[20,25] This is due to the diminished E^*_{FN} for $x \geq 1$ as a consequence of pre-fission neutron emission.

4. Conclusions

(i) PFN energy and angular distributions $N(E,\theta)$ can be well described by a complex SMA based on the assumption that all neutrons are evaporated from fully accelerated fragments characterized by an intricate occurence probability $P(\{p_f\})$ (CEM without free parameter, GMNM based on parameters adjusted for $^{252}Cf(sf)$).

(ii) However, such a SMA should probably simulate emission probability distributions of secondary neutrons (scission neutrons, neutrons emitted during fragment acceleration) to a certain extent. In contrast to previous assymptions (central component[26]), recent theoretical works[27,28] indicate that scission neutrons are preferentially emitted in polar direction. Further, the neutron component during fragment acceleration is strongly influenced by dissipation mechanism (relaxation)[2].

(iii) The TUD concept for calculations of PFN spectra, angular distributions, and multiplicities in any fission reactions relies on a combination of GMNM with semi-empirical fission theories, since basic fission theories fail to reproduce the fragment occurence probability in a complete and sufficiently accurate manner. In

spite of this alternative compromise, PFN data are well described/predicted. Especially, multiple-chance fission reactions are considered separately in connection with Hauser-Feshbach theory including fission channel for the calculation of scattered-neutron cross sections, fission cross-sections, and γ-production cross sections.

Appendix A

Selected results of CEM and GMNM calculations for ^{252}Cf(sf) (check of internal consistency)

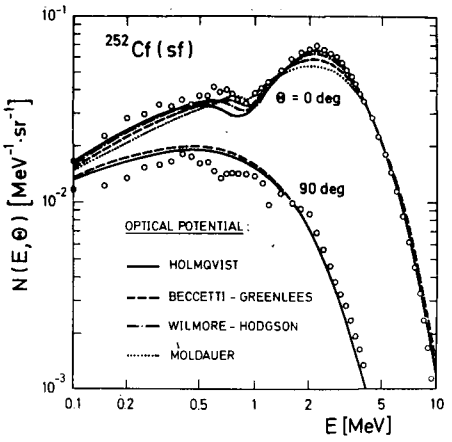

Fig. A 1
Differential ^{252}Cf(sf) neutron spectra for polar ($\theta=0^o$) and equatorial direction ($\theta=90^o$). Experimental data [10] are compared with CEM calculations based on several optical potentials as indicated

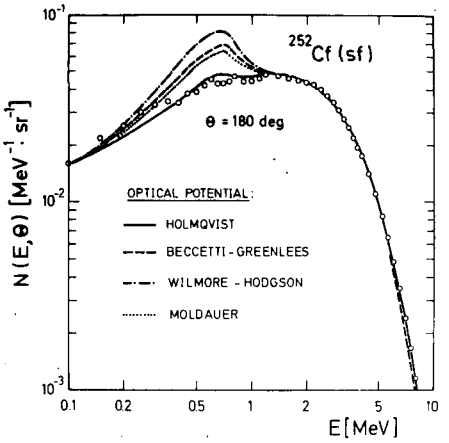

Fig. A 2
As for Fig. A 1, but for $\theta=180^o$

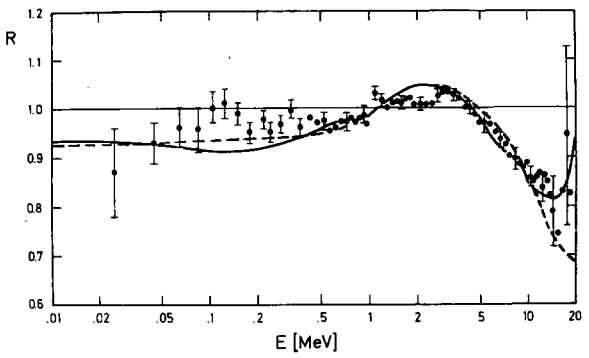

Fig. A 3
Ratio R of the Cf neutron spectrum to a Maxwellian with 1.42 MeV temperature parameter (dots - evaluated data[29], continuous line - CEM, dashed line - GMNM)

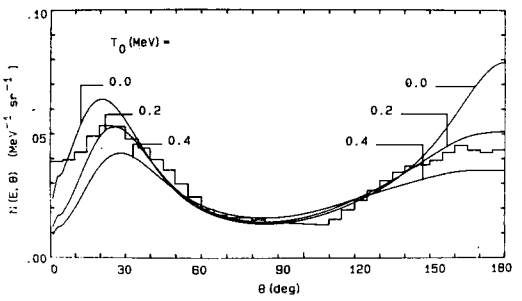

Fig. A 4
Cf neutron angular distribution at E = 1.0 MeV (histogram - experimental data[10], curves - GMNM based on different parameters T_0, i.e. low limit of rest-nucleus temperature simulating n/γ-competition)

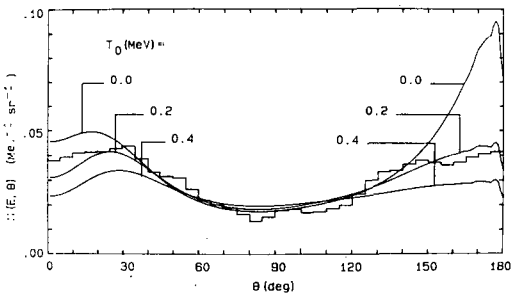

Fig. A 5
As for Fig. A 4, but for E = 0.55 MeV

Appendix B

GMNM applications to induced fission reactions

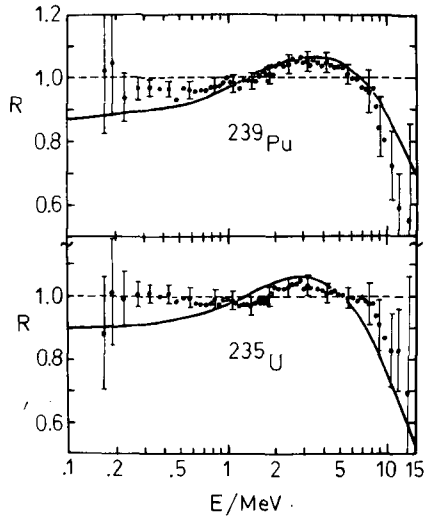

Fig. B 1
Ratio of PFN spectra calculated in the framework of GMNM (curves) to reference Maxwellians with T = 1.383 MeV and T = 1.318 MeV for n-induced fission of ^{239}Pu and ^{235}U, respectively (dots - experimental data[30])

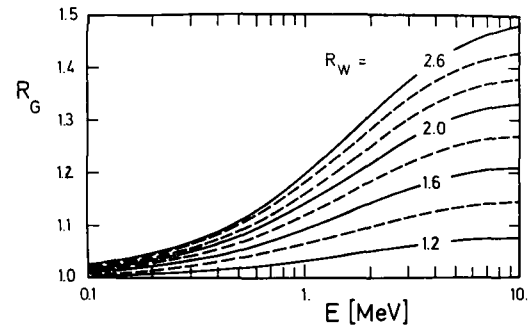

Fig. B 2
Anisotropy ratio R_G ($0^o/90^o$) of PFN emission with reference to fragment anisotropy ratio R_W (parameter) for actinide fission (average behaviour) (cf. Ref. 30 for experimental data)

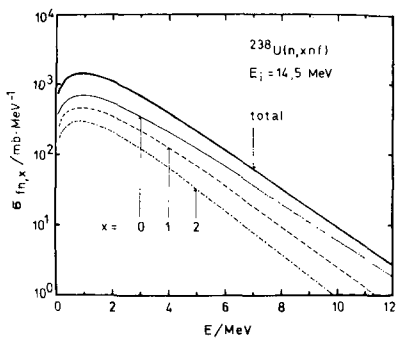

Fig. B 3
Partial PFN cross sections for ^{238}U fission induced by 14.5 MeV neutrons (cf. Ref. 21)

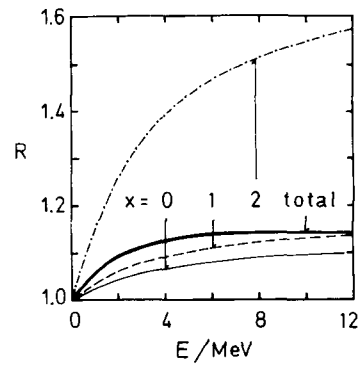

Fig. B 4
Partial PFN anisotropies R of PFN emission with reference of incidence beam direction for ^{238}U induced by 14.5 MeV neutrons

References

1 H. Märten et al., Proc. Int. Symp. Nucl. Phys. - Nuclear Fission - Gaussig, 1985, ZfK-592 (1986) 1

2 H. Märten, D. Seeliger, J. Phys. G (1988)

3 E. Nardi et al., Phys. Lett. 43B (1973) 259

4 J.C. Browne, F.S.Dietrich, Phys. Rev. C10 (1974) 2545

5 D.G. Madland, J.R. Nix, Nucl. Sci. Eng. 81 (1982) 213

6 B.F. Gerassimenko, V.A. Rubchenya, IAEA-TECDOC-335 (1985) 280

7 H. Märten, D. Seeliger, J.Phys. G 10 (1984) 349

8 H. Märten, Proc. IAEA Advisory Group Meeting on Nuclear Theory for Fast Neutron Nuclear Data Evaluation, Beijing, Oct. 1987, in print

9 H. Märten et al., Proc. IAEA Consultants' Meeting, Smolenice, 1983, INDC(NDS)-146/L (1983) 199

10 H. Märten et al., Nucl. Instr. Meth. A 264 (1988) 375

11 H. Märten et al., Proc. Int. Conf. Neutron Physics, Kiev, 1987, in press

12 C. Budtz-Jørgensen, H.H. Knitter, Rad. Eff. 93 (1986) 5

13 H. Märten, D. Seeliger, Nucl. Sci. Eng. 93 (1986) 370

14 H. Märten et al., Proc. Int. Symp. Nucl. Phys., Gaussig, 1986, ZfK-610 (1986) 169

15 D. Lucas, H. Märten, to be published

16 U. Brosa et al., loc. cit. (14), 162

17 C.A. Straede, Thesis, CBNM, Geel (1985)

18 J.R. Huizenga, R. Vandenbosch, Nuclear Fission (1973)

19 M. Uhl, Proc. Int. Symp. Nucl. Phys., Gaussig, 1982, ZfK-491 (1982) 155 and A.V. Ignatyuk et al., Yad. Fiz. 47 (1988) 355

20 H. Märten et al., these proceedings, p. 39

21 H. Märten et al., ibid, p. 160

22 J. Drochon et al., Nucl. Phys. A 318 (1979) 63

23 H. Yamamoto et al., J. Nucl. Sci. Techn. 16 (1979) 779

24 H. Märten et al., these proceedings, p. 156

25 H. Märten et al., Proc. Int. Conf. on Nuclear Data for Science and Technology, Mito, 1988

26 H.R. Bowman et al., Phys. Rev. 126 (1963) 2120

27 P. Mädler, Z. Phys. A 321 (1985) 343

28 B. Milek et al., KFKI-1987-19/A (1987)

29 W. Mannhart, IAEA-TECDOC-410 (1987) 194

30 P.I. Johansson et al., NBS SP 425 (1975) 572

FISSION ENERGETICS AND PROMPT FISSION NEUTRON EMISSION

H. Märten, A. Ruben, D. Seeliger
Technische Universität Dresden, Dresden, GDR

Abstract

Fission energetics are studied in the framework of a simple two-spheroid model including semi-empirical shell correction energy. For the neutron induced and the multiple chance fission the calculated energy partitions are discussed in comparison with experimental results. A further application of this model shown in this paper is the evaluation of neutron multiplicities.

1. Introduction to the Two-Spheroid-Model

For several applied purposes, for instance the calculation of fission neutron spectra, the exact knowledge of the total kinetic energy (TKE) and the average excitation energy (E^*) of the fragments is required. The Two-Spheroid-Model (TSM) /1/ allows the calculation of those energy partitions on the basis of a general treatment of energy.
The foundation of the TSM is according to Terrell /2/ the assumption of spheroidically shaped fragments, whose major semi-axes nearly meet at the scission point. The deviation from the spherical shape effects the deformation energy (E-def) of the fragments, which is assumed to be quadratic in radius change and linear in the deformability parameter o. The total kinetic energy (TKE) is equal to the coulomb energy of the two charges, effectively located at the centres of the two fragments.
Setting up a general energy balance we introduce a nuclear potential F, which is equal to the sum of kinetic and deformation energies of the complementary fragments. By using the classical method of minimizing this potential at the scission point we get a set of equations, which allows to deduce TKE and E-def of the fragments, if knowing the deformability parameter α.
According to Kildir and Arras /3/ α is determined by the fragment shell correction energies δw with reference to the α-value deduced in the framework of the liquid drop model. In the energy balance the dissipative energy according to the results of Gönnenwein /4/ and a simple approximation of pairing effects are included.
On the basis of the well-known fragment data for 252-Cf(sf) and 235-U(n,f) we deduce the deformability parameter α and the shell correction energies δw of the fragments for both fission reactions. Using the formalism of Bohr and Mottelson /5/ to fixe these shell energies for the nucleare temperature $\tau=0$ we get a set of shell correction energies as the foundation for several applications. The results of further researches have pointed out, that the δw-values of other fission reactions are nearly linear in the mass of the fissioning nucleus.
Interpolating the parameter-sets deduced and taking into account the diminuation of the shell effects due to the intrinsic temperature τ at scission it is possible to calculate by the TSM the fragment deformability parameters α for a fission reaction of any actinide nucleus. These parameters allow then the calculation of the TKE and E^* as a function of mass split within the minimizing equations described above. With a further energy balance, it is possible to calculate the average fragment neutron multiplicities.

2. Application to neutron induced fission

In the following part of this paper the calculated energy partitions and neutron multiplicities are discussed in comparison with experimentally received values. A systematic study of the dependence of the total kinetic energy on the incidence energy and the fragment mass showed in the case of the neutron induced fission of 235-U a behaviour similar

to Straedes experimental results /6/ (Fig. 1-3).
The maximum of TKE is stipulated by the extrem negative shell correction energies of the heavy fragments around the mass number 130, which lead to a strong stiffness. An increasing incidence energy causes the diminution of shell effects. The stiffness decreases and the TKE-maximum has a smaller value. In the region of the positive shell correction energies, for instance in the symmetrical region, the washing-out of shell effects leads to an increasing fragment stiffness, which is connected with higher TKE-values.

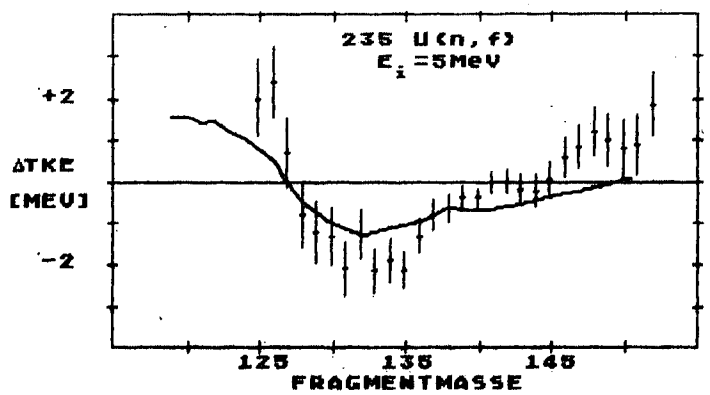

Fig. 1
TKE-differences between 5 MeV and thermal neutron induced fission of 235-U as a function of mass split
line - TSM, points - Straede et al. /6/

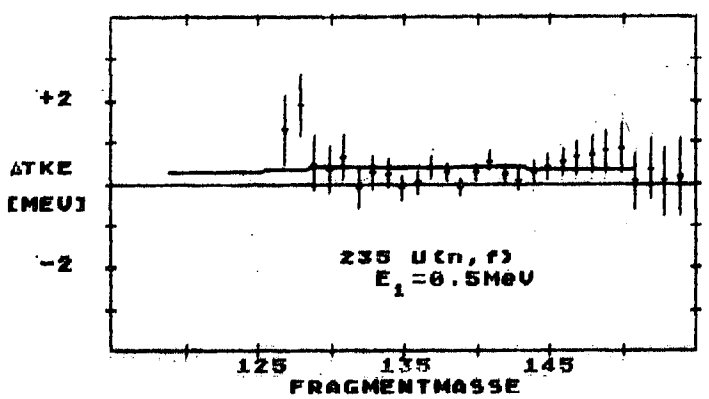

Fig. 2
The same as for figure 1, but for 0.5 MeV incidence energy

In the first two figures, the calculated differences between the TKE of thermal and higher-energetic induced fission of 235-U as a function of fragment mass are shown in comparison with the results of Straede et al. /6/. The small differences between the calculated and experimental values point to a stronger washing out of the shell effects than assumed up to now. Figure 2 shows the increasing TKE in the whole mass region in the range of small incidence energies caused by pairing effects, considered in the calculation of the level density parameter according to Ignatjuk /7/.

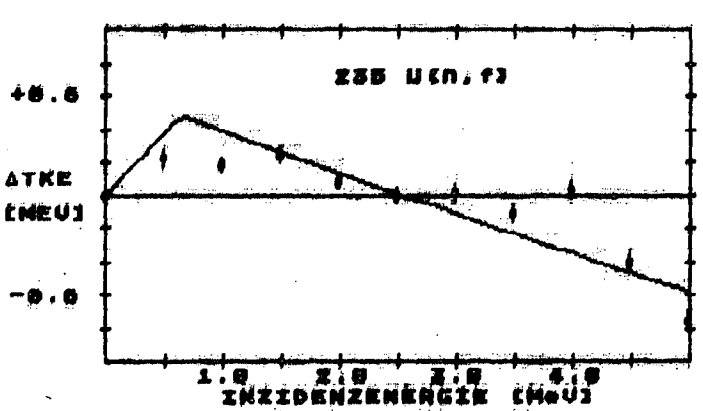

Fig. 3
Average TKE-difference with reference to thermal-neutron induced fission of 235-U as a function of incidence energy
line - TSM,
points - Straede et al. /6/

The average TKE-differences, shown in Figure 3, were deduced by folding the total kinetic energy with the fragment mass distribution. This average value is mostly determined by the region of the TKE-maximum. That leads to the increase above 1 MeV incidence energy. Below this energy, the excitation of the fissioning nucleus does not suffice for pair braiking. This leads to an increasing TKE.

3. Application to multiple chance fission

The high-energy induced fission reactions are characterized by the simultaneous existance of the (n,xnf) attendant reactions. In the framework of our model, multiple chance fission is evaluated by separate calculation of fragment energy distributions of the partial reactions and a summation, weighted up by the partial fission cross sections. In the following figure, the results of such calculations are shown for the 14.5 MeV neutron induced fission of 238-U. Yamamoto et al. /8/ found experimentally similar results.

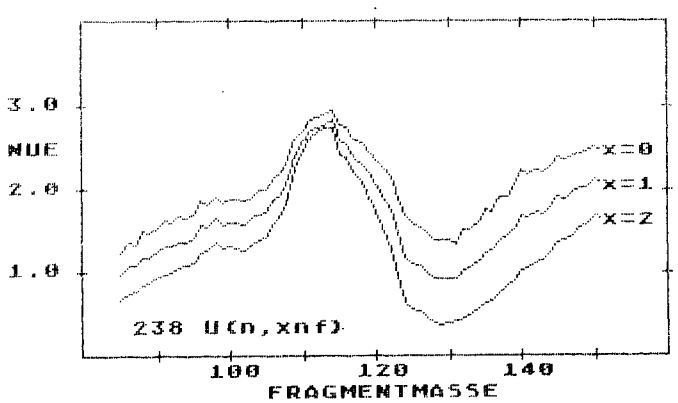

Fig. 4
Calculated average neutron multiplicities for the three partial reactions of the 14.5 MeV neutron induced fission of 238-U

4. Evaluation of neutron multiplicities

A further application of the TSM is the evaluation of experimentally received neutron multiplicities. The general energy balance fixes the sum of the neutron multiplicities of two complementary fragments. As the only free parameter remains the partition on the fragments. This allows the comparison of neutron multiplicities with the energy balance or the adaption to the energy balance. Because of the well-known total kinetic energies and the rather accurate calculation of the Q-value such adaptions are possible for many fission reactions.

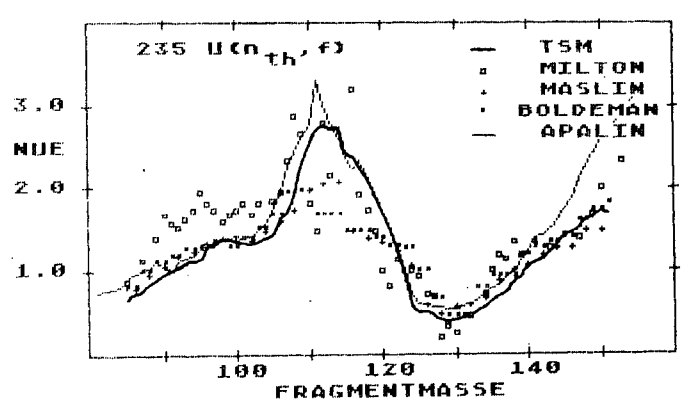

Fig. 5
Experimentally received /9/ and adapted (thick line) neutron multiplicities for 235 U (n,f)

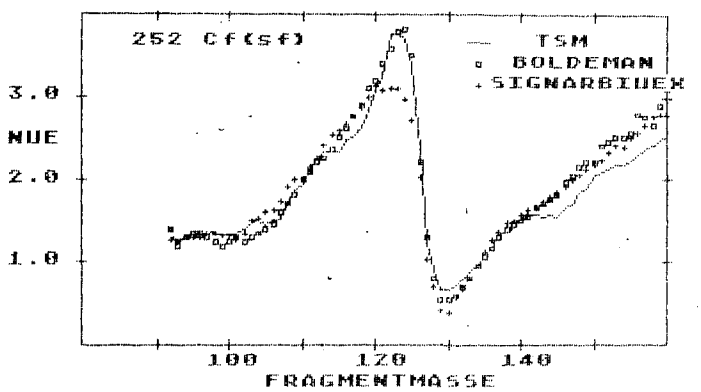

Fig. 6
Experimentally received and adapted (thin line) neutron multiplicities for 252 Cf(sf)

The last figures show the results for two fission reactions. In the case of uranium we get the thick line by adapting Apalins experimental values /10/ to the energy balance. For the spontaneous fission of californium we can approximately reproduce the newer results of Walsh and Boldeman /11/ by adapting the values from Signarbieux /12/.

5. Conclusion

The semi-empirical formalism used in the TSM allows the calculation and the analysis of fission energetics and prompt fission neutron emission in the range of fissioning nuclei between thorium and californium. The accuracy of the calculated energy partition is comparable with that of experimental results.

REFERENCES

/ 1/ H. Märten, A. Ruben, D. Seeliger; Proc. IAEA Advisory Group Meeting on Properties of Neutron Sources, Leningrad, 1986, IAEA-TECDOC-410 (1987) 153

/ 2/ J. Terrell; Proc. IAEA Symp. on Physics and Chem. of Fission, Salzburg 1965, IAEA, Vienna, 1965) Vol. II, 3

/ 3/ M. Kildir, N.K. Aras; Phys. Rev. C25 (1982) 365

/ 4/ F. Gönnenwein; All-Union Conf. on Nuclear Fission, Obninsk 1987, unpublished, c.f. contribution at this conference

/ 5/ A. Bohr, B.R. Mottelson; "Nucleare Structure" (Benjamin, New York 1975) Voll.II, 607

/ 6/ C.A. Straede et al.; "Neutron induced fission of 235-U", Thesis, CBNM Geel, Belgium, 1985

/ 7/ A.V. Ignatiuk et al.; Jad. Fiz, 42/3 (1985) 569

/ 8/ H. Yamamoto et al.; J. Nucl. Sci. and Technol. (Japan), Vol. 16/11 (1979) 779

/ 9/ H. Nifenecker et al.; IAEA-Symp. on Physics and Chem. of Fission, Rochester 1973, IAEA, Vienna, 1974) Vol. II, 117

/10/ V.F. Apalin et al., Nucl. Phys. 71 (1965) 553

/11/ R.L. Walsh, J.W. Boldeman, Nucl. Phys. A267 (1977) 189

/12/ C. Signarbieux et al.; Phys. Letters 39B (1972) 503

THE FISSION NEUTRON SPECTRUM OF ^{232}Th

H. Märten, D. Richter, A. Ruben, D. Seeliger
Technische Universität Dresden, GDR

G.N. Lorchikova, S.E. Sukhikh, A.M. Trufanov
Institute for Physics and Power Engineering, Obninsk, USSR

Abstract:

The fission neutron spectrum has been measured for neutron-induced fission of ^{232}Th at 7.3 MeV incidence energy using time-of-flight technique in conjunction with the efficient pulse shape discrimination of background γ-rays (three-dimensional spectroscopy of neutron time of flight, scintillator light output, and pulse shape amplitude) as well as sliding-bias method.

Systematic errors have been diminuished or excluded due to the spectrum analysis with reference to the $^{252}Cf(sf)$ neutron spectrum (nuclear standard) measured under identical experimental conditions.

The experimental post-fission neutron spectrum of ^{232}Th is compared with calculations performed in the framework of the generalized Madland-Nix model with account of multiple-chance fission.

1. Introduction

Nuclear data for thorium are of importance for reactor projects based on the ^{232}Th - ^{233}U fuel cycle. On the other hand, investigations of neutron nuclear reactions with fissionable nuclei are assumed to give clues for the further understanding of reaction mechanisms in conjunction with the development and/or check of fission neutron models.

Thorium as a light-actinide nucleus has a rather small fission cross section. Therefore, the measurement of the fission neutron spectrum by the use of a fission chamber (as required for high incidence energy) is difficult due to the relatively low foreground/background ratio. Previous experiments are only known for the incidence energies 1.5, 2, and 14 MeV /1,2,3,4/. Hitherto, the spectra havn't yet been described theoretically.

The present paper includes the results of the experimental as well as theoretical study of the prompt neutron spectrum from the 7.3 MeV neutron-induced fission of ^{232}Th, i.e. both (n,f) and (n,n'f) reaction chances are open. In this case, pre-fission neutrons arising from the (n,n'f) reaction have a maximum energy of about 1 MeV. However, the present work concerns the pure post-fission neutron spectrum above 1 MeV. The theoretical description based on the generalized Madland-Nix model /5,6/ in combination with a semi-empirical scission point model for the calculation of fragment energies (excitation energy, kinetic energy averages) as a function of mass asymmetry has to account for both fission chances (cf. /7/).

2. Experimental method and data analysis

The experiment has been carried out at the Rossendorf 10-MeV tandem accelerator. 7.3-MeV incidence neutrons have been produced by the use of a gaseous deuterium target via $D(d,n)^3He$ reaction at an average beam current of 2 μA. The multi-plate fission chamber /8/ with 40 hemisphere plates and 750 mg ^{232}Th (total) has been located at 18 cm distance from the neutron-producing gaseous target. A (5" x 1.5") NE 213 scintillator viewed by a XP 2040 photomultiplier was applied as neutron detector located within a heavy shielding and collimator system at 90° with reference to incidence neutron direction.

The time-of-flight measurement based on a 1.32-m flight path has been combined with the efficient pulse shape discrimination /9/ to reduce the background. The three-dimensional measurement of neutron time of flight (TOF), light output (LO), and pulse shape amplitude

(PSA) enables

(i) the off-line distinction between neutron and γ-rays (background) and, hence, a careful background suppression without efficiency losses,

(ii) the application of the sliding-bias method in spectrum analysis /10/ and, consequently, the reduction of uncertainties (optimum foreground/background ratio for a given neutron energy E depends on bias).

In addition, the ^{252}Cf(sf) neutron spectrum has been measured by the use of the same experimental arrangement (Cf fission chamber, $5 \cdot 10^5$ fissions/min) to analyse the measured Th spectrum with reference to the well-known standard /11/.

A typical two-dimensional (TOF, LO) spectrum deduced from the three-dimensional data (sequently stored on magnetic disc) by a sorting procedure with n/γ-discrimination (defined PSA ranges depending on LO) are shown in Fig. 1. This spectrum itselves provides one possibility to calibrate the LO co-ordinate by comparing the LO response functions at fixed neutron energies with the corresponding distributions calculated by the use of a Monte-Carlo code /12/.

In addition to the spectrum analysis on the basis of the calculated efficiency data depending on neutron energy E and LO bias (two-dimensional matrix for direct application of the sliding-bias method), the measured Th fission neutron spectrum has been analysed with reference Cf standard spectrum. In this way, uncertainties due to scattered-neutron background, resolution, calibration etc. are diminuished or excluded.

Both the Th and the Cf neutron spectra measured have been corrected for time resolution /10. The γ-peak FWHM of the present measurements are 1.8 ns and 3.8 ns for the Cf and the Th experiment, respectively. In the case of the Th multi-plate fission chamber whose 40 electrodes are combined to 4 sectors each yielding one output signal, the rather high capacity of the sectors is the most important restricting factor.

The measurement has been carried out in a 200h nm.

3. Results

The measured Th fission neutron spectrum at 7.3 MeV incidence-neutron energy has been fitted to a Maxwellian distribution yielding a "temperature" parameter T = (1.31 ± 0.03) MeV, i.e. $\bar{E}$ = 1.965 MeV. The data are represented in fig. 2 in comparison with the spectrum calculated in the framework of the generalized Madland-Nix model (GMNM). The fragment mass yield curves, the average kinetic energies and excitation energies of the fragments as a function of their mass number, and the fragment angular distributions have been deduced for the possible fission chances (n,xnf) separately. Using the GMNM the double-differential emission probability $G_x(E,\Psi)$ (norm 1.) (Ψ - neutron angle with reference to incidence beam direction) can be calculated for the possible chances (x = 0,1 in the present case). We obtain the total cross section of fission neutron emission by

$$\sigma(E,\Psi) = \sum_{x=0}^{x_{max}} \sigma_{f,x} \overline{\nu}_x \, G_x(E,\Psi)$$

($\sigma_{f,x}$ - partial fission cross section for chance x, $\overline{\nu}_x$ - average number of neutrons per fission in chance x). The total number of fission neutrons including pre-fission neutrons is given by

$$\overline{\nu}_{tot} = \sum_{x=0}^{x_{max}} \frac{\sigma_{f,x}}{\sigma_{f,tot}} (\overline{\nu}_x + x)$$

As shown in fig. 3, the average energy $\bar{E}$ of post-fission neutrons increases with increasing incidence energy, but is considerably influenced by the second-chance fission reaction at the (n,n'f) threshold. This effect has been often neglected in previous works.

Conclusions

The spectrum of neutrons from ^{232}Th fission induced by 7.3-MeB neutrons has been measured.

It can be fairly well reproduced by a Maxwellian distribution with T = (1.31 ± 0.03) MeV. The GMNM, whose free parameters have been adjusted in the case of the ^{252}Cf(sf) standard neutron spectrum, has been used for the calculation of the Th fission neutron spectra without any further adjustments.

The very good agreement between experimental and theoretical data is a confirmation of the theoretical scheme applied in the present work. Specifically, the possible fission chances at incidence energies higher than about 6 MeV have been considered separately. The present work shows the influence of multiple-chance fission on the spectrum shape (represented by the average emission energy) in the case of Th at incidence energies close to the (n,n'f) threshold.

References

/1/ S.E. Sukhikh et al., Yad.Const. 3 (1986) 34
/2/ N. Hirakawa et al., Radiation Effects 93 (1986) 229
/3/ Yu.S. Zamyatnin et al., At.En. 4 (1958) 337
/4/ O.A. Salnikov et al., Izv. Akad. Nauk 12 (1968) 653
/5/ H. Märten, D. Seeliger, Nucl.Sci.Eng. 93 (1986) 370
/6/ H. Märten et al., Proc. IAEA Advisory Group Meeting on the Properties of Neutron Sources, Leningrad, 1986, IAEA-TECDOC-410 (1987) 153
/7/ H. Märten et al., Proc.Int.Conf. on Neutron Physics, Kiev, 1987, in print
/8/ S.E. Skuhikh, PEI Obninsk, unpublished
/9/ H.G. Ortlepp, Proc.Int.Symp. on Nuclear Electronics, Dresden, 1980
/10/ H. Märten et al., INDC(GDR)-28/L (1984)
/11/ W. Mannhart, loc.cit. /6/, 194
/12/ N.R. Stanton, COO-1545-92 (1971)

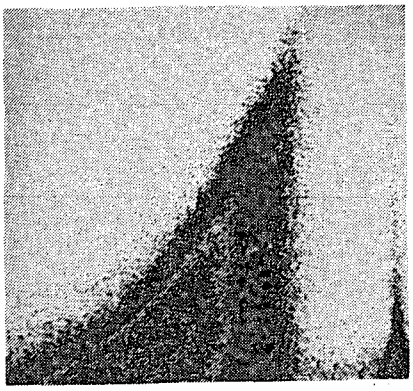

Fig. 1 Two-dimensional (TOF,LO) spectrum representing the broad neutron region as well as the position of the γ-peak

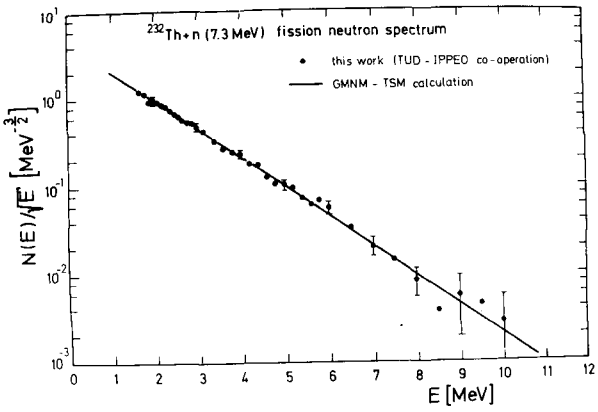

Fig. 2 The measured fission neutron spectrum for ^{232}Th + n (7.3 MeV) in comparison with the calculated distribution

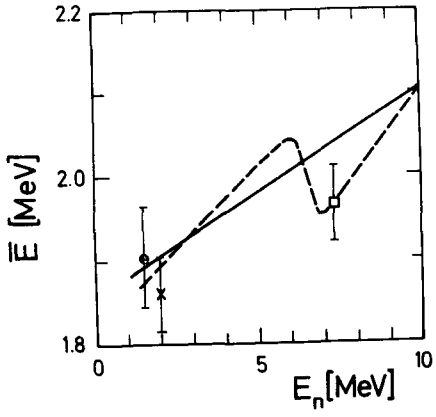

Fig. 3 Average LS emission energy of ^{232}Th post-fission neutrons as a function on neutron incidence energy
(● - /1/, x - /2/, □ - this work, straight line - ENDF/B-IV, dashed line - GMNM calculation)

ANGULAR DISTRIBUTIONS OF PROMPT GAMMA-RAYS IN THE BINARY AND TERNARY FISSION OF ^{252}Cf

W. Pilz, W. Neubert
Central Institute for Nuclear Research, Rossendorf, G.D.R.
K. Arnold, D. Lucas, H. Märten
Technical University of Dresden, G.D.R.

ABSTRACT

Double-differential emission probabilities $W(\theta,E_\gamma)$ of the prompt γ-rays accompanying the binary and ternary fission of 252-Cf were measured. An average angular momentum $\bar{L} \simeq 7\hbar$ has been derived for the binary fission mode. The gamma angular-distributions of the ternary fission mode show similar asymmetries but other shapes than the binary distributions.

1. INTRODUCTION

The analyse of preceding experiments, e.g./1,2/, has confirmed that the angular momentum of fission fragments after binary fission is aligned in a plane perpendicular to the axis defined by the two fragments like the angular momentum of compound nuclei relativ to the beam axis. The behaviour of the resulting angular distributions of the emitted prompt γ-rays was investigated in the theoretical work of Strutinsky /3/. Average angular momenta have been derived by fits of the measured double-differential angular distributions $W(\theta,E_\gamma)$ as shown by Skarsvåg /1/. Similar results for characteristic γ-transitions, produced in the s.f. of ^{252}Cf were published by Wolf and Cheifetz /2/. The hitherto existing measurements deal with the binary fission only. For the ternary fission mode there is only an estimate concerning ^{252}Cf for 0 deg/90 deg anisotropy by Ivanov /4/. He stated a ratio $R[0\text{ deg} / 90\text{ deg}] \approx 1$, but he has not measured this magnitude as a function of the γ-ray energy. Therefore, this measurement raises some questions. In this paper we present a first measurement of double-differential emission probabilities $W_\gamma(\theta,E_\gamma)$ of prompt γ-rays accompanying the ternary fission of ^{252}Cf.

2. EXPERIMENTAL SET-UP

Fig. 1 shows a sketch of the experimental set-up to study the angular distributions of prompt γ-rays from both the binary and ternary fission of ^{252}Cf. The fission fragments were registered position-dependently in coincidence with the γ-rays, detected by fixed detectors. We used two silicon detectors in order to increase the registration efficiency of the equatorial light charged particles (LCP) indicating the ternary fission mode. Each of these detectors (ø=23mm) covers an angular aperture of about 45 deg. Two γ-ray detectors were used: (i) a 2,0x2,0 inches NaJ(Tl) crystal which provides sufficient position-resolution for the measurement of the gamma angular distribution of the binary mode and (ii) two 5,0x6,5 inches NaJ(Tl) crystals in order to increase the registration efficiency (necessary for the ternary mode) and to check the forward-backward emission symmetry.

The ^{252}Cf-source on Ta-backing ($\sim 10^4$ fission acts per sec.), the transmission parallel plate avalanche counter (PPAC), the position sensitive PPAC and the silicon surface barrier detectors were mounted in a glass shade filled with 10 Torrs

of n-heptane. The position sensitive PPAC ($35x180mm^2$) covered an angular range from -3,5 deg to +92,4 deg with respect to the axis defined by the source and the centre of the forward NaJ(Tl) crystal. The transmission PPAC was mounted some mm's apart from the source and it delivered the start signal for both the TOF branch of the fission fragments (separation of the light and heavy groups) and the TOF of the γ-quanta.

Disturbing effects were eliminated by the following measures. The 6.12 MeV α-particles from the g.st. decay of ^{252}Cf were shielded by 36μm Al foils in front of the Si-detectors. A time window of 10ns around the prompt γ-peak eliminated nearly completely the prompt fission neutrons at the given flight path of 50cm. The arrangement with two large NaJ(Tl) crystals allowed also to estimate the level of multiple (two-fold) gamma rays and accidental coincidences which was found to be about 4% (ternary case) and 6% (binary case) of the true ones. The contamination of the detection system was found to be negligible (after the run of 1.5 months only 0.6% of coincidences came from the contamination). The influence of background contributions due to scattering in the surrounding materials was taken into account by measurements with lead shadow cones inserted between the glass shade and the NaJ(Tl) detectors. Sumarizing, the true coincidence counting rates for each γ-branch amounted to be 2500 per min., 360 per min. and 1.2 per min. for the binary fission configuration with the large and small NaJ(Tl) crystals and the ternary fission measurement, respectively. The experimental arrangement including the data acquisition system has been already described elsewhere /5/.

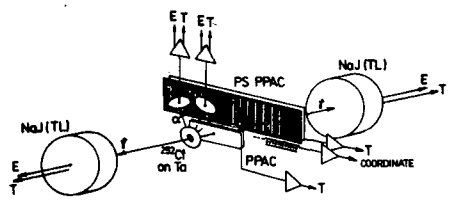

Fig.1 Detector arrangement

3. DATA EVALUATION AND MONTE-CARLO-SIMULATION

For each coincidence event three parameters were stored onto a magnetic disc: the fission fragment TOF, the coordinate of one fragment and the γ-ray response amplitude of each scintillation counter. The energy of the LCP was measured simultaneously with a multichannel analyser. The data evaluation starts with the generation of two-dimensional distributions, i.e. the fragment TOF vs. the coordinate. This procedure allowed a separation of events belonging to the light and the heavy fragment groups. By this it was possible to cover the angular range from 0 deg. to 180 deg. for the γ-rays with respect to the emission direction of the light fragments. The γ-response axes ($\geq$ 100 keV) were divided into 17 bins (binary case) or 10 bins (ternary case). The projections onto the position coordinate axis we generated within each bin. Then, a Gaussian deconvolution procedure was applied to the well resolved position spectra. Then the evaluated

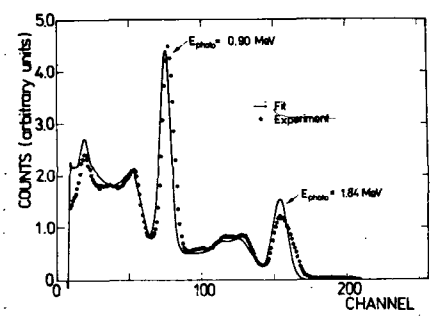

Fig.2 Example of a calibration spectrum ^{88}Y

distributions were normalized by geometrical "efficiencies" of the position sensitive PPAC. For this purpose, two-dimensional distributions of the fragment TOF and the coordinate were measured for the following conditions: (i) swich-off the coincidence with γ's and α's (binary "efficiency") and (ii) break of the coincidence with the γ's only (ternary "efficiency"). The resulting γ-ray distributions are represented with respect to the direction of the light fragment. The response functions of the used NaJ(Tl) crystals were measured with calibrated γ-ray sources and an improved procedure like that described in /6/ was used to fit these calibration spectra (Fig.2). The response matrix was evaluated from this set of data.

The double-differential emission probabilities $W_\gamma(\theta,E_\gamma)$ have been simulated by a Monte-Carlo-code which was applied up to now to reproduce the binary angular distributions only.

This code presupposes (1) the input of the fragment-mass yield distribution, (2) an average energy distribution of the emitted γ-rays, (3) the velocity distributions of the fragments including the stopping process in the Ta-backing, (4) the estimation of the moment of the γ-emission /7/, (5) the γ-multiplicity vs. fragment mass, (6) an energy-dependent ratio of the multipol orders E1 and E2, taken from /1/, (7) the c.m. angular distributions of E1 and E2 radiation according to Strutinsky's theory /3/, were we used a temperature of T=0.4 MeV and a moment of inertia $J=0.5\ J_{rigid}$, (8) an initial angular momentum distribution as described in /8/ and (9) our evaluated response functions of the NaJ(Tl) crystals. The Doppler effect was taken into account for each simulated event. After that, the emission angle and emission probability are transformat into lab.system. These calculated distributions were compared with the measured ones in order to determine the average angular momentum of the fragments. A satisfactory agreement with the experimental binary fission angular distributions was achieved for an average angular momentum of $\bar{L}\approx 7\ \hbar$ (Fig.3).

The angular distributions of the prompt γ-rays from the ternary fission mode are also given with respect to the direction of the emitted light fragment in order to compare these distributions with the binary ones. Fig.4 shows angular distributions of γ-rays associated with LCP and fission fragments for three selected energy intervals. The same data evaluation procedure was used as in the

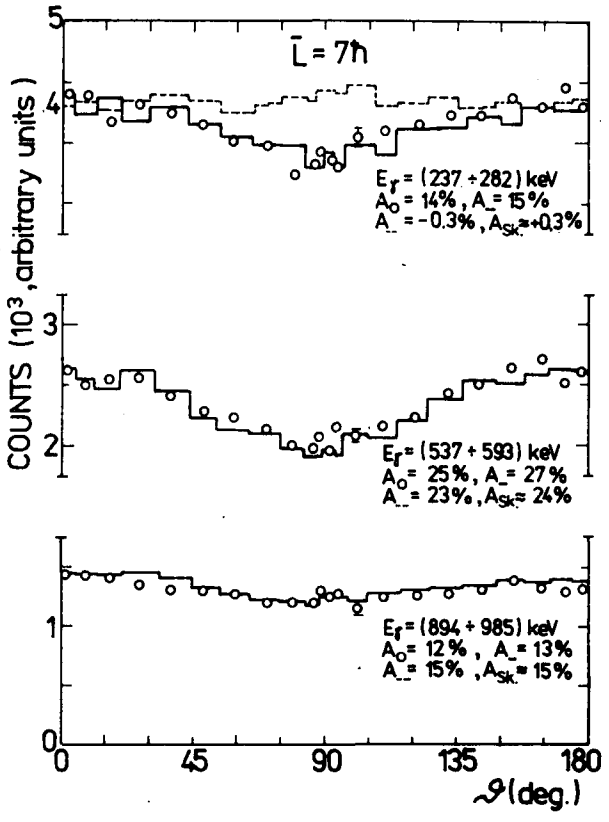

Fig.3 Measured and calculated binary angular distribution

case of the binary mode in order to represent the data points in the angular range from 0 deg to 180 deg. The intensities were normalized in each angular bin with the measured geometrical efficiency of the PS PPAC which takes into account registration probability of the LCP. For comparison, the angular distributions are given without and with regard of the response matrix of the large NaJ(Tl) crystals. On principle, the behaviour of the corrected distributions is similar to the direct experimental points in these energy bins.

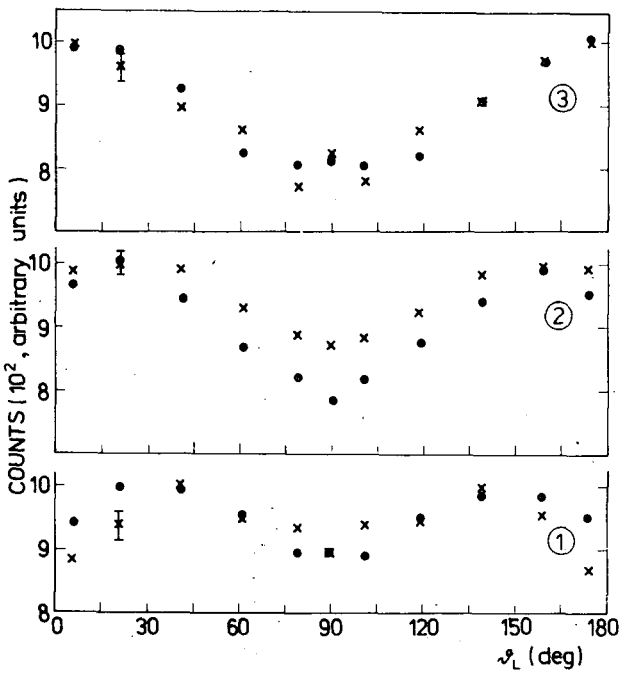

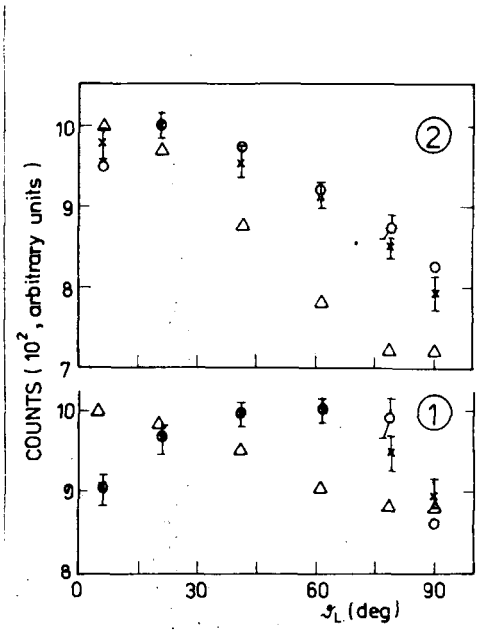

Fig.4 Measured ternary angular distributions
- x Measurement after normalization with the geometrical efficiencies
- • The "x"-distribution after multiplication with the inverse response matrix

① E_γ=(280-430)keV,
② E_γ=(540-820)keV,
③ E_γ=(820-1500)keV
(all distributions are normalized to maximum hight of 1000)

Fig.5 γ-angular distributions, if a light fragment was registered
- △ binary fission
- • ternary fission (backward NaJ-detector)
- x ternary fission (forward NaJ-detector)

① $E_{\gamma,response}$=(200-430)keV,
② $E_{\gamma,response}$=(430-1130)keV
(all distributions are normalized to a maximum hight of 1000)

The shapes of the angular distributions for both the binary and the ternary mode are compared in Fig.5 for the angular range from 0 deg. to 90 deg with respect to the direction of the light fragment. Only the direct experimental values (normalized by the geometrical efficiencies) are shown.

In conclusion we have found anisotropic angular distributions of prompt γ-rays in the ternary fission of ^{252}Cf contradictory to the result of ref./4/. In our opinion, the 0 deg / 90 deg ratio, R= 1.015, given in ref./4/, comprehends no further physical information. Our measurements show different shapes of the gamma angular distributions in the binary and the ternary fission mode of ^{252}Cf. This result challenges further theoretical investigations of the ternary fission process.

REFERENCES

/1/ K. Skarsvåg, Phys. Rev. C22 (1980) 638
/2/ A. Wolf, E. Cheifetz, Phys. Rev. C13 (1976) 1952
/3/ V.M. Strutinsky, Pisma ZhETF 3(9) (1959) 861
/4/ O.I. Ivanov, Yad. Fiz. 15 (1972) 1121
/5/ N.F. Bondar, W. Neubert, W. Pilz, Annual Report ZfK-621 (1986) 136
/6/ a) R.P. Gardner, Nucl. Instr. Meth. 138 (1976) 287
b) D. Lucas, H. Märten, W. Neubert, W. Pilz, Report ZfK-621 (1986) 134
/7/ K. Skarsvåg, Nucl. Phys. A253 (1975) 274
/8/ J.R. Huizenga, R. Vandenbosch, Phys. Rev. 120 (1960) 1305

APPLICATION OF BRAGG CURVE SPECTROSCOPY TO NUCLEAR FRAGMENTATION PROCESSES

L.N. Andronenko, A.A. Kotov, L.A. Vaishnene, A.I. Iljin
Leningrad Nuclear Physics Institute, Gatchina, U.S.S.R.
W. Neubert, W. Pilz
Central Institute for Nuclear Research, Rossendorf, G.D.R.

ABSTRACT

An axial ionization chamber for the determination of the energy and nuclear charge of fragments was constructed and has been tested with butane and pentane. Separated element distributions have been registered in low-energy heavy-ion reactions and in proton-nucleus collisions at 1 GeV incidence energy.

INTRODUCTION

Nuclear fragmentation induced by intermediate-energy projectiles is a current field of investigation. Relative light target-fragments are produced in the energy range from 1 MeV/u to 10 MeV/u in dependence on the target mass. This energy range enables us to test the methods of Bragg Curve Spectroscopy(BCS), ref.1), to resolve single nuclear charges of the emitted fragments.

PRINCIPLE OF BCS

This method is based on the generation of an ionization current signal in an axial ionization chamber characterized by the electric field parallel to the particle track. In this case, the anode signal represents the time reversal of the stopping process of the detected particle in the active chamber volume (Bragg curve). The height of the Bragg peak (BP) is directly related to the nuclear charge Z and,furthermore, the BP signal is independent on the energy of the registered particle. Therefore, a shaping time less than the duration of the current signal delivers the BP information. The measurement of the deposited energy requires a shaping time longer than the total collection time.

DETECTOR CONSTRUCTION AND OPERATION

The operation conditions were tested with a sample ionization chamber which has a distance of 11 cm between the cathode (Ni foil of 130μg/cm^{-2}, ϕ=20mm) and the anode (polished Cu plate). Ten equidistant guard rings between the cathode and the Frisch grid (separated by a distance of 2cm from the anode) maintain an electrical field nearly parallel to the incoming particles. Negative high voltage is supplied to the cathode and a divider chain determines the potentials of the field shaping rings and the Frisch grid. The ionization chamber was operated with a fixed ratio $(E/p)_{A-FG}/(E/p)_{FG-C}$=1.4 which was calculated from the screening inefficiency of the Frisch grid.
The gas pressure was adjusted to stop the incoming particle along the active chamber lenght. We tested three different gases: vapour of n-heptane, commercial butane and purified n-pentane. Heptane was refused because no regular pulse shape distributions were obtained. Perhaps, the electron recombination is too high in this gas.

Commercial butane with about 68vol.% of isobutane content was found to be a suitable chamber gas. We prefered butane in the experiments at the Tandem generator on account of its simple handling. But it has the drawback that the signal amplitude goes down without gas flow-through by about 2% per hour after a new filling. An enlarged ionization chamber was constructed based on the experience with the old one. The following improvements were introduced: 1) The entrance window was increased to 70 mm in the diameter and it serves as the cathode avoiding any dead gas layer. The entrance window is a Formvar foil of 60-70 μgcm^{-2} supported by a wire mesh of about 97% transparency. This window keeps the gas pressure up to 150 Torr in the ionization chamber. 2) The Frisch grid was grounded resulting in an improved h.f. trouble hardness. 3) Purified n-pentane (repeated freezing by means of liquid nitrogen and distillation into the evacuated ionization chamber) was used. The use of purified pentane resulted in a better long-term signal stability (linear amplitude loss of 0.5% per hour after new filling, established during 60 hours). The measured energy resolution amounts to be 55 keV FWHM for alpha particles of 5.15 MeV.

MEASUREMENTS AT THE ROSSENDORF TANDEM ACCELERATOR

The properties of the sample ionization chamber filled with butane were studied with "fragment-like" ^{12}C ions of 20 MeV scattered by a Au target (290μgcm^{-2}). The shaping times for the BP and E signals were chosen experimentally regarding the timing limitations of the available electronics. The total charge released by the ionization was measured with a pulse shaping of 2μs. Under this conditions, nearly full charge collection was attained for **E/p ≥ 2.0 V/Torr cm. The separation of different nuclear charges was tested with a target enriched in ^{10}B (mixed with ^{12}C)** which was bombarded by a 32 MeV ^{35}Cl beam. The incidence energy exceeds the Coulomb barrier (≈ 22 MeV) and the occurence of some transfer products is favoured by positive Q-values. Indeed, we observed pronounced branches of C,N, and O out of the products of elastic scattering. The ^{10}B and ^{12}C constituents of the target scatter the incoming ^{35}Cl ions elastically

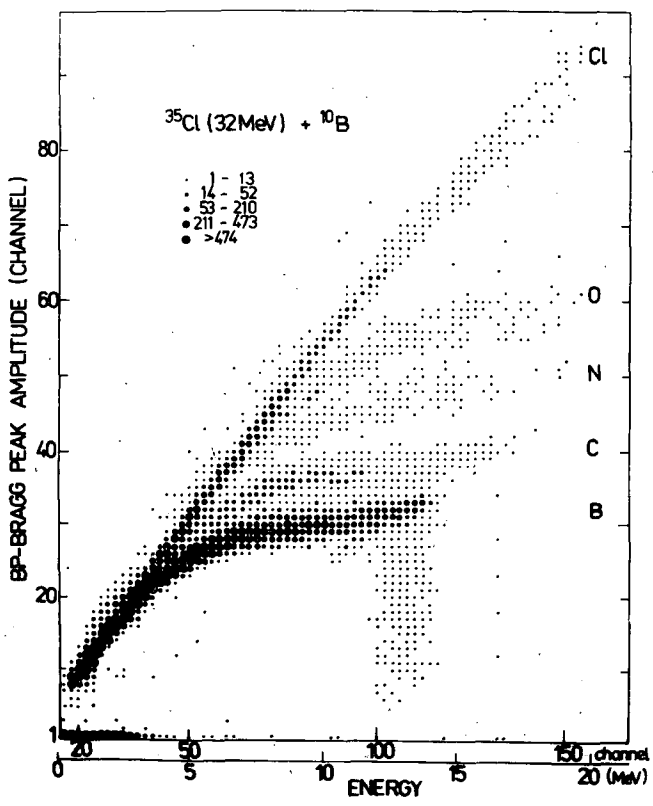

Fig.1 Bragg Peak amplitude (BP) vs. released energy (E) for products of the 35 Cl (32 MeV) → 10 B reaction, p=52.5 Torr of butane, τ(BP)=0.25μs, τ(E)=2μs.

into narrow cones which are not accepted by the ionization chamber mounted at 27.5 deg. with respect to the beam axis. This feature enables us to follow the low intensity branches of N and O down to about 8 MeV. Nevertheless, the upper branch in fig.1 belongs to the beam particles partially scattered from the Al target holder. The lower branch in fig.1 is formed by the $^{10}_{5}B$ target recoils. The range of these recoils ($\simeq$2.5 mgcm^{-2} in butane) exceeds somewhat the depht of the ionization chamber (1.85 mgcm^{-2}). The observed vertical fringe seems to be caused by no physical reasons.

Fig.2 shows the projection of the events (along the inclined isotopic branches) onto the BP-axis. In spite of the moderate energy resolution the nuclear charges from Z=5 to Z=8 are well separated. A linear relationship between the BP amplitude and the nuclear charge up to Z=17 was observed for butane.

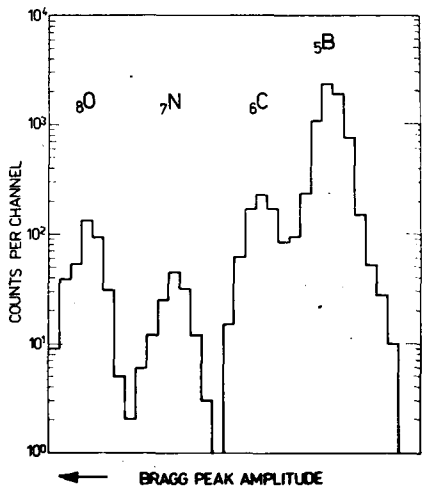

Fig.2 Distribution of nuclear charges obtained from fig.1

DETECTION OF FRAGMENTS IN RELATIVISTIC PROTON NUCLEUS COLLISIONS

The new improved axial ionization chamber was tested at the 1 GeV proton beam extracted from the Gatchina synchrocyclotron. The ionization chamber was mounted at a distance of 50 cm from a thin nickel target located in the centre of an evacuated reaction chamber. Fragments were detected at 144 deg. with respect to the beam axis. The ionization chamber was filled with purified n-pentane of 55 Torr and operated at a reduced field strenght of E/p=2.2 V/Torrcm in the cathode-anode volume. The BP signal was generated with a shaping time of 0.5μs. The CAMAC data acquisition system allows to accept an expanded range of shaping times for the E-signal.

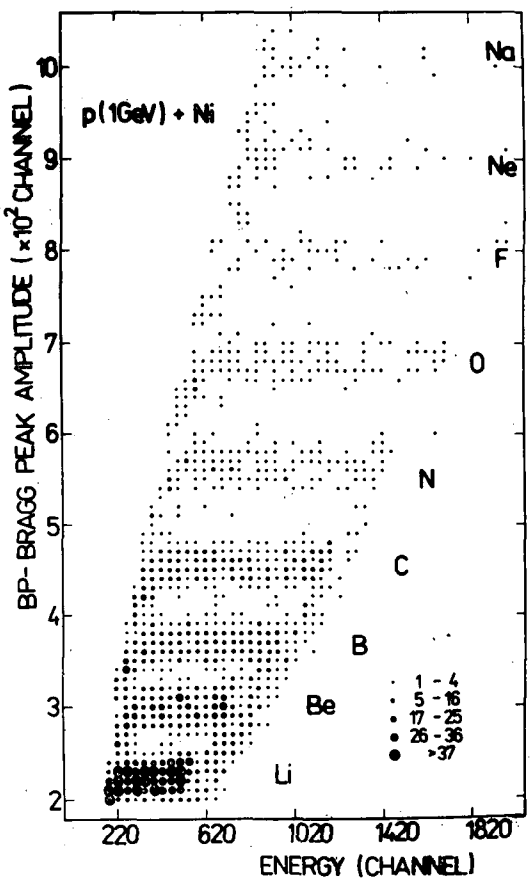

Fig.3 BP vs. E for the reaction p(1GeV)→Ni

The measurements were carried out with τ=4μs. A double-grid avalanche counter located near to the target served as fast trigger for the appearance of a fragment. Well separated isotopic branches from Z=2 to Z=11 were observed. As in the experiments with heavy ions we found an ascent of about 5% for the isotopic branches with increasing fragment energy. The plot shown in fig.3 is corrected for this effect. Therefore, events which belong to the same nuclear charge are located in branches parallel to the energy axis. As also seen in fig.3, the isotopic distributions correspond to a limited energy range of the registered fragments. For fixed Z, the distribution starts on the left where the BP amplitude becomes independent on the particle energy.

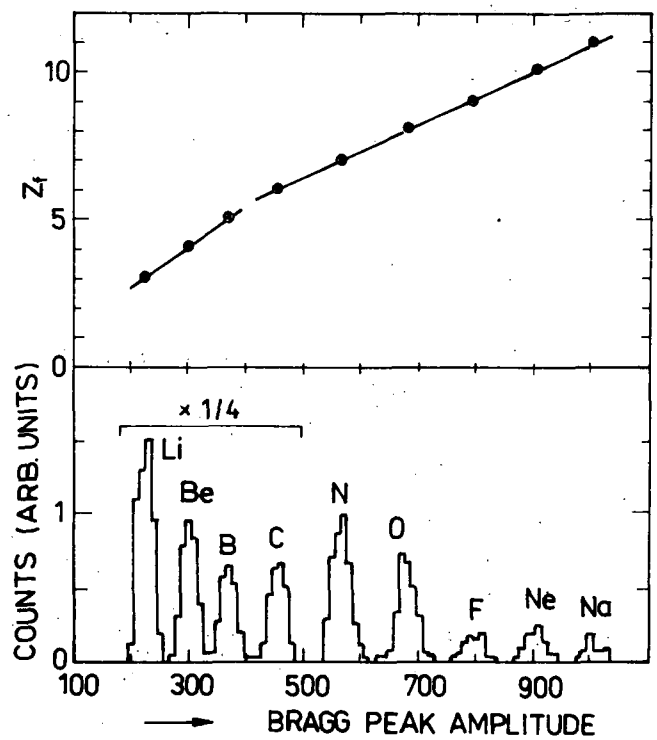

Fig.4 Distribution of nuclear charges in the target fragmentation of p+Ni (bottom) and relation between the fragment charge and BP amplitude (top)

The limit on the right is determined by the depht and the gas pressure of the ionization chamber, some of the produced fragments punch through the active chamber depht and, consequently, we see back-bending of some branches of equal nuclear charge. On account of the relative low pentane pressure, we observed only the low-energy part of the fragment distribution. Fig.4 shows the projection onto the BP axis. The resolution of adjacent nuclear charges amounts to be $Z/\Delta Z \approx 38...40$. This encouraging result opens a wide field for application of BCS in studies of nuclear fragmentation processes.

REFERENCES

1) C.R. Gruhn et al., Nucl. Instr. Methods 196 (1982) 33.

DYSON BOSON MAPPING THEORY AND NON-UNITARY REPRESENTATION OF THE SELFCONSISTENT COLLECTIVE-COORDINATE METHOD

K. Takada, Y.R. Shimizu and H. Thorn

Department of Physics, Kyushu University, Fukuoka 812, Japan

Abstract: The Dyson boson mapping theory for the multi-phonon collective subspace in the many-fermion Hilbert space is surveyed and the merit of this theory is emphasized. The Dyson-type reformulation of the selfconsistent collective-coordinate (SCC) method of Marumori, Maskawa, Sakata and Kuriyama is given and the relation between these two theories is discussed. Applying these theories to a simple SU(3) model and comparing the results with the exact solutions, we discuss the advantages of these theories.

1. Introduction

Various types of boson mapping theories, which transform the physics in the original collective subspace in the many-fermion Hilbert space into the physical boson subspace, have been proposed for the description of collective motions in the space of many-nucleon (or many-quasiparticle) states.

The most popular one is the Holstein-Primakoff-type mapping[1]. The merit of this type of boson mapping is that it is unitary and the hermiticity of the original fermion hamiltonian is conserved in the boson space. However, it has the demerit that the mapped operator is, in general, expanded in an infinite power series of boson operators. This causes serious discussions concerning the convergence of the expansion.

Another popular one is the Dyson-type boson mapping[2] whose merit is that the mapped operator is of a finite series of boson operator monomials. Therefore, we can avoid the problem coming from the infinite boson expansion as in the Holstein-Primakoff mapping. However, this type of mapping has an outward demerit; namely, the mapping is non-unitary and it does not conserve the hermiticity of the hamiltonian. It has therefore been thought that it is very difficult to calculate the B(E2) values in the Dyson boson mapping and to study the properties of the boson eigenstates.

Recently it has been clarified that complete information about the eigenstates in the hermitian boson theory (the Holstein-Primakoff boson mapping) can be obtained from the results of the Dyson boson theory[3]. Furthermore, it has been clarified that the non-hermitian eigenvalue problem in the Dyson boson theory is precisely converted into a hermitian eigenvalue problem equivalent to that in the Holstein-Primakoff theory in a very easy way[4]. Today, one can thus fully make a good use of the finiteness of the boson expansion in the Dyson boson mapping, since the difficulty of the non-unitarity of the Dyson boson mapping (or the non-hermiticity of the Dyson boson hamiltonian) has completely been solved[3,4].

When we intend to apply the boson mapping theories to realistic nuclei, we inevitably start from some truncated collective subspace in the full many-fermion Hilbert space and we map the subspace onto the corresponding boson space. One of the simplest truncations is the "phonon truncation" in which the space of many-fermion states is truncated to the multi-phonon subspace

$$\{ |i\rangle = X^{\dagger}_{2M_1} X^{\dagger}_{2M_2} \cdots X^{\dagger}_{2M_n} |0\rangle \; ; \; n = 0, 1, 2, \cdots \}, \tag{1.1}$$

where $X^{\dagger}_{2M}$ is the collective Tamm-Dancoff (TD) phonon with spin J=2 and the

algebra of the fermion-pair operators is forced to be closed within the above TD phonons. Under this truncation approximation, the Dyson mapping gives us a very simple but non-hermitian hamiltonian which consists of up to sixth-order boson operators. The eigenvalue problems for this non-hermitian boson hamiltonian are precisely converted into the hermitian eigenvalue problem equivalent to that in the Holstein-Primakoff mapping without being bothered by infinite boson expansions[4]. In this sense, the Dyson boson mapping theory is quite useful.

However, what we have to emphasize is that the contribution from the non-collective phonon degrees of freedom cannot be taken into account in the above collective subspace (1.1). It is however well-known that the anharmonicity effect due to the coupling between the collective and non-collective degrees of freedom plays an essential role in the transitional region of nuclei. In order to take the anharmonicity effect into account, we have to extend the subspace (1.1) to involve the non-collective phonons, but it is difficult since there are usually a great number of non-collective phonons.

Marumori, Maskawa, Sakata and Kuriyama[5] proposed a new method called the selfconsistent collective-coordinate (SCC) method to describe the large-amplitude collective motion within the framework of the time-dependent Hartree-Fock theory. This has made it possible to treat the above mode-mode coupling effect in a very systematic way. Recently, we have reformulated the SCC method in a Dyson-type non-unitary representation and we have clarified the relation to the generalized Dyson boson mapping[6].

In the present paper, we survey the main points of the Dyson boson mapping theory and the Dyson-type non-unitary representation of the SCC method. And we apply these theories to a simple SU(3) model. Comparing the results with the exact solutions, we will discuss the advantages of the Dyson boson mapping theory and the Dyson-type representation of the SCC method.

2. Dyson boson mapping

Let us define the quadrupole TD phonon $X^\dagger_{2M}$ in the multi-phonon subspace (1.1) by

$$X^\dagger_{2M} = \sum_{\alpha\beta} x(\alpha\beta)\, c^\dagger_\alpha c^\dagger_\beta . \tag{2.1}$$

Corresponding to the collective <u>fermion</u> subspace (1.1), we introduce the collective <u>boson</u> subspace

$$\{ |i) = (n!)^{-1/2}\, b^\dagger_{2M_1} b^\dagger_{2M_2} \cdots b^\dagger_{2M_n} |0) \}, \tag{2.2}$$

where $b^\dagger_{2M}$ is the quadrupole boson operator satisfying commutation relations

$$[\, b_{2M},\ b^\dagger_{2M'}] = \delta_{MM'},$$

$$[\, b_{2M},\ b_{2M'}] = [\, b^\dagger_{2M},\ b^\dagger_{2M'}] = 0. \tag{2.3}$$

In order to give the precise definition of the Dyson mapping, we have to introduce a set of orthonormalized basis vectors in the multi-phonon subspace

(1.1). To do this, we use a representation in which the norm matrix **N** whose matrix elements are defined by $N_{ij} = \langle i|j\rangle$ is diagonalized as

$$\sum_j (N_{ij} - n_a \delta_{ij}) u_a^j = 0. \tag{2.4}$$

It is easily seen that the eigenvalues are $n_a \geq 0$. Let us denote the zero-eigenvalue solution by $a = a_0$. One can assume the following orthonormality relations:

$$\sum_i u_a^{i*} u_b^i = \delta_{ab}. \tag{2.5}$$

Using these, we can define orthonormalized basis vectors of the multi-phonon subspace as

$$|a\rangle\!\rangle = n_a^{-1/2} \sum_i u_a^i |i\rangle, \qquad a \neq a_0 \tag{2.6}$$

which satisfy the orthonormality relation

The corresponding orthonormalized basis vectors in the boson space are given by

$$|a)\!) = \sum_i u_a^i |i).\tag{2.7}$$

Thus the physical subspace in the boson space is $\{|a)) ; a \neq a_0\}$, in which every state has its counterpart in the original fermion space, i.e. the multi-phonon subspace. Therefore the projection operator to the physical subspace in the boson space is defined by

$$\mathbf{P} = \sum_{a \neq a_0} |a)\!)(\!(a|. \tag{2.8}$$

Using the orthonormal basis vectors introduced above, we can define the Dyson mapping by the following transformation operators:

$$U_1 = \sum_{a \neq a_0} n_a^{1/2} |a)\!)\langle\!\langle a|, \tag{2.9a}$$

$$U_2 = \sum_{a \neq a_0} n_a^{-1/2} |a)\!)\langle\!\langle a|. \tag{2.9b}$$

In the Dyson mapping, we have two types of boson state vectors obtained by transforming a fermion state vector $|\Psi\rangle$; one is a <u>bra</u> $(\phi|$ and the other is a <u>ket</u> $|\psi)$ as

$$(\phi| = \langle\Psi| U_2^\dagger, \qquad |\psi) = U_1 |\Psi\rangle. \tag{2.10}$$

An arbitrary fermion operator O_F is transformed into O_D as

$$O_D = U_1 O_F U_2^\dagger = \sum_{a,b \neq a_0} \sum_{ij} |a)\!) u_a^{i*} \langle i|O_F|j\rangle u_b^j n_b^{-1} (\!(b|. \tag{2.11}$$

In order to calculate the matrix element of the original fermion operator O_F, $\langle i|O_F|j\rangle$, we use the phonon-truncation approximation explained before, in

which the following approximate commutation relation is assumed:

$$[X_{2M_1}, [X_{2M_2}, X^{\dagger}_{2M_3}]] = -2 \sum_{L=0,2,4} C_L \langle 2M_1 2M_2 | LM \rangle \langle 2M_3 2M_4 | LM \rangle X_{2M_4}, \quad (2.12)$$

where C_L is the structure constant determined by the amplitudes $x(\alpha\beta)$ appearing in the phonon operator (2.1). Then the matrix element of the original fermion operator O_F is written in the form of

$$\langle i | O_F | j \rangle = \sum_k f_{ik} \langle k | j \rangle. \quad (2.13)$$

Substituting this in (2.11), we have

$$O_D = \mathbf{P}(O_F)_D \mathbf{P} = (O_F)_D \mathbf{P}, \qquad (i|(O_F)_D|j) = f_{ij}. \quad (2.14)$$

What should be noticed here is that the norm matrix element $\langle i|j\rangle$ in (2.13) is cancelled by the inverse of the eigenvalue n_b in (2.11). This cancellation is the biggest merit of the Dyson mapping at the expense of losing unitarity of the transformation, because we have no more to treat the explicit form of matrix element $N_{ij} = \langle i|j\rangle$.

The quantity $f_{ij} = (O_F)_D$ can, in general, be expressed by matrix elements of simple boson operators; for example, if O_F is the collective phonon operator, then we have

$$(X^{\dagger}_{2M})_D = b^{\dagger}_{2M} - \sum_{L=0,2,4} C_L [[b^{\dagger}_2 b^{\dagger}_2]_L b_2]_{2M}, \quad (2.15a)$$

$$(X_{2M})_D = b_{2M}, \quad (2.15b)$$

where $[\ldots]_{LM}$ denotes an angular momentum coupling.

As discussed in the previous paper[3], as long as we do not make the maximum boson number extremely large in a practical case, we can consider $\mathbf{P} = 1$. Moreover, we proposed a method to verify whether $\mathbf{P} = 1$ is correct or not in a given boson space[4].

Although we have so far formulated a case of only one kind of retained phonon (the collective TD phonon) for simplicity, it should be noted that it is quite straightforward to generalize it to cases of more kinds of retained phonons.

3. Hermitian treatment of Dyson boson hamiltonian

In the hermitian boson theory we need to consider only the eigenket $|\Psi_\lambda)$ belonging to an eigenstate λ, while in the Dyson boson theory we have to consider both the eigenket $|\psi_\lambda)$ and the eigenbra $(\phi_\lambda|$. Expanding these eigenvectors as

$$|\Psi_\lambda) = \sum_i \alpha_i^{(\lambda)} |i), \quad |\psi_\lambda) = \sum_i \beta_i^{(\lambda)} |i), \quad (\phi_\lambda| = \sum_i \gamma_i^{(\lambda)*} (i|, \quad (3.1)$$

we have three types of eigenvalue equations,

$$\sum_j (h_{ij}^{HP} - E_\lambda \delta_{ij}) \alpha_i^{(\lambda)} = 0, \tag{3.2a}$$

$$\sum_j (h_{ij}^{D} - E_\lambda \delta_{ij}) \beta_i^{(\lambda)} = 0, \tag{3.2b}$$

$$\sum_i \gamma_i^{(\lambda)*} (h_{ij}^{D} - E_\lambda \delta_{ij}) = 0, \tag{3.2c}$$

where $h_{ij}^{HP} = (i|H_{HP}|j)$ and $h_{ij}^{D} = (i|H_D|j)$. The first equation of (3.2) is the eigenvalue equation in the Holstein-Primakoff boson theory and the second and the third are, respectively, the right- and left-hand-side eigenvalue equations in the Dyson boson theory.

The orthonormality conditions for the amplitudes α, β and γ are

$$\sum_i \alpha_i^{(\lambda)*} \alpha_i^{(\lambda')} = \delta_{\lambda\lambda'}, \qquad \sum_i \gamma_i^{(\lambda)*} \beta_i^{(\lambda')} = \delta_{\lambda\lambda'}. \tag{3.3a,b}$$

The second orthonormality (3.3b) is still not enough to determine the amplitudes β and γ, because $(\phi'_\lambda| = k_\lambda^{-1}(\phi_\lambda|$ and $|\psi'_\lambda) = k_\lambda|\psi_\lambda)$ also satisfy (3.3b), where k_λ is an arbitrary nonzero constant. Namely, there still remains an arbitrariness by a constant k_λ.

We can calculate the correct matrix element of an arbitrary Dyson operator without obtaining the explicit form of the correctly normalized eigenstates. Let $(\phi_\lambda|$ and $|\psi_\lambda)$ be eigenvectors which satisfy the orthonormality condition (3.3b) but are not necessarily correctly normalized. The corresponding correctly-normalized eigenvectors $(\bar{\phi}_\lambda|$ and $|\bar{\psi}_\lambda)$ are related to them through

$$(\bar{\phi}_\lambda| = k_\lambda^{-1}(\phi_\lambda|, \qquad |\bar{\psi}_\lambda) = k_\lambda|\psi_\lambda), \tag{3.4}$$

where one can assume without loss of generality that k_λ ia a real positive constant. Let O_D be the Dyson boson image of an arbitrary fermion operator O_F, and $\bar{O}_D$ be that of $O_F^\dagger$; notice that $\bar{O}_D = (O_F^\dagger)_D \neq (O_D)^\dagger$. For these operator, the relation

$$(\bar{\phi}_\lambda|O_D|\bar{\psi}_{\lambda'}) = (\bar{\phi}_{\lambda'}|O_D|\bar{\psi}_\lambda)^* \tag{3.5}$$

should hold. Putting (3.4) in (3.5), we have

$$(k_\lambda/k_{\lambda'})^2 = (\phi_\lambda|O_D|\psi_{\lambda'})/(\phi_{\lambda'}|\bar{O}_D|\psi_\lambda)^*. \tag{3.6}$$

Then the correct matrix element is given by

$$(\bar{\phi}_\lambda|O_D|\bar{\psi}_{\lambda'}) = (\phi_\lambda|O_D|\psi_{\lambda'}) \left[\frac{(\phi_{\lambda'}|\bar{O}_D|\psi_\lambda)^*}{(\phi_\lambda|O_D|\psi_{\lambda'})} \right]^{1/2} \tag{3.7}$$

We can generalize the above discussion. Let $|i)$ be a basis vector of the boson space and let $(\bar{i}|$ and $|\bar{i})$ be the corresponding correctly-normalized bra and ket vectors. Then we have the following correct matrix element between the boson basis states i and j:

$$(\bar{i}|O_D|\bar{j}) = (i|O_D|j)\left[\frac{(j|\bar{O}_D|i)^*}{(i|O_D|j)}\right]^{1/2}. \tag{3.8}$$

Assume that O_D and $\bar{O}_D$ in (3.8) are the Dyson boson Hamiltonian H_D. Then we have

$$(\bar{i}|H_D|\bar{j}) = (i|H_D|j)\left[\frac{(j|H_D|i)^*}{(i|H_D|j)}\right]^{1/2}. \tag{3.9}$$

This is hermitian. An eigenvalue problem consisting of the matrix elements (3.9) is equivalent to the eigenvalue problem for the hamiltonian H_{HP}. Thus we have got a method to exactly hermitize the non-hermitian Dyson boson hamiltonian.

4. Application of Dyson boson mapping to simple SU(3) model

Let us apply the Dyson boson mapping theory to a simple SU(3) model consisting of three single-particle levels, each of which has a same j value and then same degeneracy $2\Omega = 2j+1$. In this model, a single-particle state is specified by a set of quantum numbers (jm).

We consider the generators K_{ij} of the SU(3) Lie algebra:

$$K_{ij} = \sum_{m=1}^{2\Omega} c_{im}^{\dagger} c_{jm}, \qquad (i, j = 0, 1, 2). \tag{4.1}$$

We assume the following hamiltonian:

$$\begin{aligned} H_F = & \sum_{i=1}^{2} \varepsilon(i) K_{ii} + V_1 \sum_{ij=1}^{2} K_{i0} K_{0j} \\ & + \frac{1}{2} V_2 \sum_{ij=1}^{2} (K_{i0} K_{j0} + K_{0j} K_{0i}) \\ & + V_3 \sum_{ijk=1}^{2} (K_{i0} K_{jk} + K_{kj} K_{0i}). \end{aligned} \tag{4.2}$$

And we also assume that the lowest single-particle level (i = 0) is completely filled; so that we are considering 2Ω-particle system.

Now let us introduce the TD phonon operator by

$$X_{\lambda}^{\dagger} = \frac{1}{\sqrt{2\Omega}} \sum_{i} x_{\lambda}(i) K_{i0}. \tag{4.3}$$

In this model, we have two kinds of TD phonons (λ = 1, 2). We start from the following multi-phonon subspace containing both the phonons:

$$\{ |n_1, n_2\rangle = (n_1! n_2!)^{-1/2} (X_1^{\dagger})^{n_1} (X_2^{\dagger})^{n_2} |0\rangle ; \; 0 \leq n_1 + n_2 \leq 2\Omega \}. \tag{4.4}$$

Corresponding to the fermion subspace (4.4), we introduce the boson subspace

$$\{ |n_1, n_2) = (n_1! n_2!)^{-1/2} (b_1^{\dagger})^{n_1} (b_2^{\dagger})^{n_2} |0); \; 0 \leq n_1 + n_2 \leq 2\Omega \}. \tag{4.5}$$

where the boson operators satisfy

$$[b_\lambda, b^+_{\lambda'}] = \delta_{\lambda\lambda'}, \quad [b_\lambda, b_{\lambda'}] = [b^+_\lambda, b^+_{\lambda'}] = 0. \tag{4.6}$$

According to the procedure of the Dyson boson mapping shown in sect. 2, we have the Dyson boson images of the generators as follows:

$$(K_{i0})_D = \sqrt{2\Omega} \sum_{\lambda=1}^{2} x_\lambda(i)\, b^+_\lambda\, (1 - n/2\Omega), \quad (K_{0i})_D = \sqrt{2\Omega} \sum_{\lambda=1}^{2} x_\lambda(i)\, b_\lambda,$$

$$(K_{ij})_D = \sum_{\lambda\lambda'=1}^{2} x_\lambda(i)\, x_{\lambda'}(j)\, b^+_\lambda\, b_{\lambda'}, \tag{4.7}$$

where $\mathbf{n}$ is the boson number operator $\mathbf{n} = \sum_\lambda b^+_\lambda b_\lambda$. Using these, we have the Dyson boson hamiltonian

$$\begin{aligned} H_D &= \mathbf{P}\, \tilde{H}_D\, \mathbf{P} = \tilde{H}_D\, \mathbf{P}, \\ \tilde{H}_D &= \sum_{\lambda\lambda'} \varepsilon(\lambda, \lambda')\, b^+_\lambda\, b_{\lambda'} \\ &+ \sum_{\lambda\lambda'} V_X(\lambda, \lambda')\, b^+_\lambda\, (2\Omega - n)\, b_{\lambda'} \\ &+ \frac{1}{4\Omega} \sum_{\lambda\lambda'} V_V(\lambda, \lambda') \{ b^+_\lambda\, (2\Omega - n)\, b^+_{\lambda'}\, (2\Omega - n) + b_{\lambda'} b_\lambda \} \\ &+ \frac{1}{\sqrt{2\Omega}} \sum_{\lambda\lambda'} V_Y(\lambda, \lambda') \{ b^+_\lambda\, (2\Omega - n)\, b^+_{\lambda'}\, b_{\lambda''} + b^+_{\lambda''} b_{\lambda'} b_\lambda \}. \end{aligned} \tag{4.8}$$

Since there is a strict one-to-one correspondence between subspaces (4.4) and (4.5), $\mathbf{P} = 1$ holds exactly in the boson subspace (4.5). Therefore, diagonalizing the original hamiltonian H_F is exactly equal to diagonalizing the boson hamiltonian $\mathbf{H}_D = \tilde{\mathbf{H}}_D$ within the subspace (4.5).

Next let us consider the <u>collective</u> subspace in which only the collective phonon ($\lambda = 1$) is retained and <u>non-collective</u> one ($\lambda = 2$) is neglected. This just corresponds to the Dyson boson mapping for the collective subspace. The numerical results and the comparison with the exact solution are shown in Fig. 1.

5. The Dyson representation of the selfconsistent collective-coordinate method

In applying the Dyson boson mapping so far discussed, we start from some collective fermion subspace; usually, we take the multi-phonon subspace consisting of the collective TD phonon. However, this choice of subspace is not always good, when the coupling effects between collective and non-collective phonon degrees of freedom are large, for instance, in the so-called transitional nuclei. Marumori et al.[5] proposed the selfconsistent collective-coordinate (SCC) method to describe the large-amplitude collective motion within the framework of the TDHF theory. This has made it possible to treat the above coupling effects in a very systematic way.

We have recently reformulated the SCC method using a non-unitary representation[6]. Taking a special kind of representation in this reformulation, we

can obtain just the original version of the SCC method, but what we are most interseted in is the Dyson-type representation, which corresponds to the Dyson boson mapping whereas the original version of the SCC method corresponds to the Holstein-Primakoff boson mapping[7]. Let us explain this below.

A quantum state at a time t is described by a bra $\langle\Phi(t)|$ and a ket $|\Psi(t)\rangle$ whose time-development is determined by the variational principle

$$\delta \langle \Phi(t) | i\hbar \frac{\partial}{\partial t} - H | \Psi(t) \rangle = 0 . \tag{5.1}$$

We should assume that $\langle\Phi(t)|$ and $|\Psi(t)\rangle$ satisfy the normalization condition $\langle\Phi(t)|\Psi(t)\rangle = 1$.

Now we restrict our space under consideration to the time-dependent Hartree-Fock (TDHF) manifold; namely, every statevector is restricted within the space of states consisting of time-dependent single Slater determinants.

We also assume that the time dependence of $\langle\Phi(t)|$ and $|\Psi(t)\rangle$ is specified by two kinds of time-dependent parameters $\xi(t)$ and $\eta(t)$ which we call the collective coordinates. In the original version of the SCC method[5], the corresponding parameters are $\eta(t)$ and its complex conjugate $\eta^*(t)$. There exist infinite numbers of ways of parametrization with the use of the collective coordinates ξ and η . In order to specify the parametrization, we assume the canonical-variable conditions (CVC) introduced for the first time by Marumori et al.[5]; the CVC in the present case are

$$\langle \Phi(\xi,\eta) | \frac{\partial}{\partial \eta} | \Psi(\xi,\eta) \rangle = \frac{1}{2}\xi, \quad \langle \Phi(\xi,\eta) | \frac{\partial}{\partial \xi} | \Psi(\xi,\eta) \rangle = -\frac{1}{2}\eta. \tag{5.2}$$

Under the CVC, we get the following canonical equations of motion from the variational principle (5.1):

$$\dot{q} = \frac{\partial \mathcal{H}_D}{\partial p}, \qquad \dot{p} = -\frac{\partial \mathcal{H}_D}{\partial q}, \tag{5.3}$$

$$q = (\xi + \eta)/\sqrt{2}, \quad p = i(\xi - \eta)/\sqrt{2}, \quad \mathcal{H}_D = \langle \Phi | H | \Psi \rangle,$$

where the "collective hamiltonian" $\mathcal{H}_D(\xi, \eta)$ is not always real.

According to Thouless's theorem, we can express the statevectors as

$$|\Psi(\xi,\eta)\rangle = N_1(\xi,\eta)\, e^{\hat{G}_1} |\phi_0\rangle, \quad \langle\Phi(\xi,\eta)| = N_2(\xi,\eta) \langle\phi_0| e^{\hat{G}_2}, \tag{5.4}$$

where $|\phi_0\rangle$ is the stationary Hartree-Fock ground state and

$$\hat{G}_1 = \sum_{\mu i} g_1(i\mu)\, a_\mu^\dagger b_i^\dagger, \qquad \hat{G}_2 = \sum_{\mu i} g_2(\mu i)\, b_i a_\mu, \tag{5.5}$$

and $a_\mu^\dagger$ and $b_i^\dagger$ are the particle and hole creation operators, respectively, and g_1 and g_2 are functions of the parameters ξ and η . The normalization condition leads to

$$N_1(\xi,\eta) N_2(\xi,\eta) = N(\xi,\eta) = \langle\phi_0| e^{\hat{G}_2} e^{\hat{G}_1} |\phi_0\rangle^{-1}. \tag{5.6}$$

Now, let us assume

$$N_1(\xi,\eta) = \{N(\xi,\eta)\}^k e^{S(\xi,\eta)},\ N_2(\xi,\eta) = \{N(\xi,\eta)\}^{1-k} e^{-S(\xi,\eta)} \tag{5.7}$$

The explicit form of $S(\xi, \eta)$ will be given later. We can obtain

$$\langle \phi_0 | e^{\hat{G}_2} e^{\hat{G}_1} | \phi_0 \rangle = \exp\{\mathrm{Tr}[\log(1 + g_1 g_2)]\}, \tag{5.8}$$

where g_1 and g_2 are matrices consisting of the matrix elements $g_1(i\mu)$ and $g_2(\mu i)$. We introduce matrices **f** and **g** whose matrix elements are defined by

$$(f)_{i\mu} = ((1 + g_1 g_2)^{-1} g_1)_{i\mu}, \qquad (g)_{\mu i} = g_2(\mu i). \tag{5.9}$$

If we choose a special representation called the <u>Dyson-type</u> representation; namely we choose k = 1 and

$$S(\xi,\eta) = \tfrac{1}{2}\mathrm{Tr}[fg]. \tag{5.10}$$

Then we have a much simplified expression of the SCC method. The CVC are simply written

$$\mathrm{Tr}\left[f\frac{\partial g}{\partial \xi} - \frac{\partial f}{\partial \xi} g\right] = \eta, \qquad \mathrm{Tr}\left[f\frac{\partial g}{\partial \eta} - \frac{\partial f}{\partial \eta} g\right] = -\xi. \tag{5.11}$$

And the expectation values of the fermion operators are written as

$$\langle \Phi | a_\mu^\dagger b_i^\dagger | \Psi \rangle = (g - gfg)_{\mu i}, \quad \langle \Phi | b_i a_\mu | \Psi \rangle = (f)_{i\mu},$$

$$\langle \Phi | a_\mu^\dagger a_\nu | \Psi \rangle = (gf)_{\mu\nu}, \qquad \langle \Phi | b_i^\dagger b_j | \Psi \rangle = (fg)_{ji}. \tag{5.12}$$

So that the collective hamiltonian $\mathcal{H}_D(\xi, \eta)$ are also simply written in terms of **f** and **g**.

The functions **f** and **g** of the canonical variables ξ and η are, in principle, obtained by solving the CVC (5.11) and the variational equation (5.1). Expanding **f** and **g** in power series of ξ and η, we can get order by order solutions. However, since the expression is somewhat lengthy, we omit here. One can refer to ref. 6).

It should be noted that, if we take only the first order of the (ξ, η)-expansion of **f** and **g** and replace ξ and η by a boson creation operator $b^\dagger$ and an annihilation operator b, respectively, then the results correspond to the Dyson boson mapping within the collective multi-phonon subspace. Therefore, we can take into account the coupling effect between the collective and non-collective phonon by taking the higher-order terms than the first order.

In Fig. 1, the results of the application of the present theory to the simple SU(3) model are shown. We took up to the third-order terms in this calculation. Comparing them with the results of the Dyson boson mapping discussed in sect. 4 and the exact solution, one can see that the Dyson-type representation of the SCC method is quite useful.

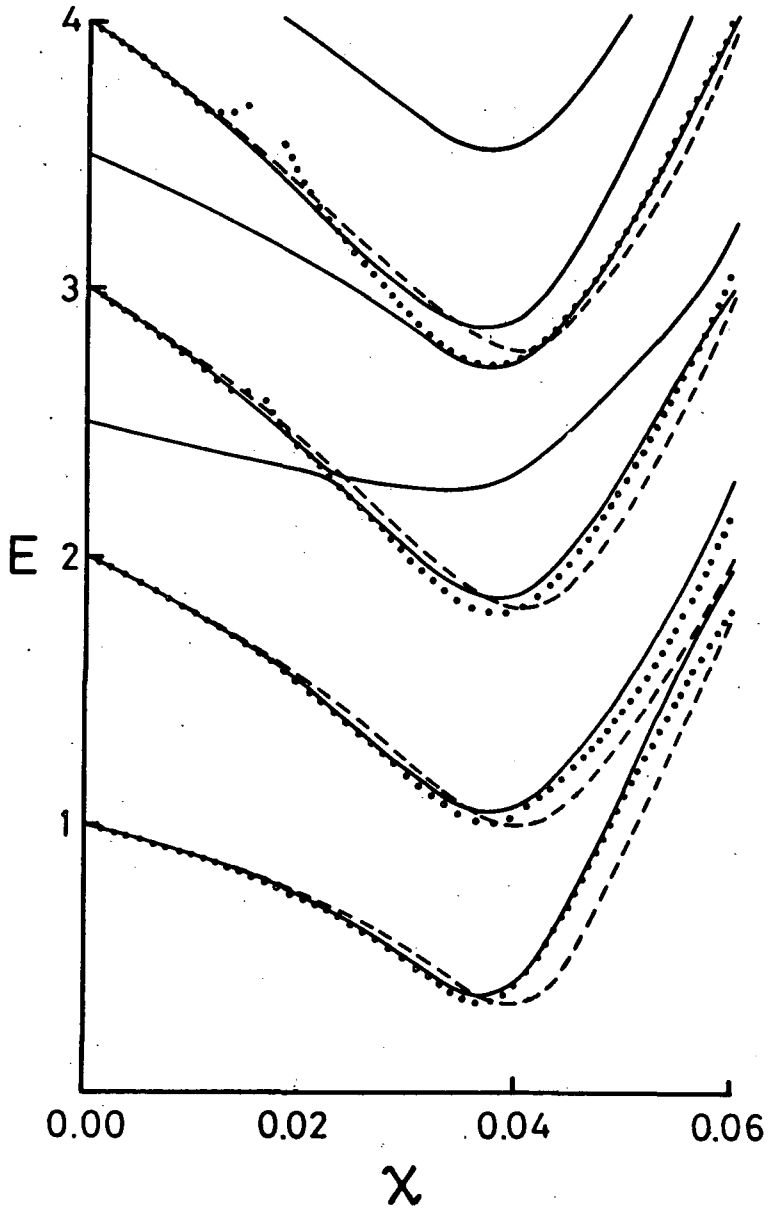

Fig. 1 Energy eigenvlaues of the SU(3) model. The abscissa denotes the interaction strength χ. The values of the parameters in the fermion hamiltonian (4.2) are taken as follows: $\varepsilon(1) = 1.0$, $\varepsilon(2) = 2.5$, $V_1 = V_2 = \chi$, and $V_3 = 0.5\chi$ The solid lines denote the exact eigenvalues of the hamiltonian. The dashed lines denote the results of the Dyson boson mapping retaining the collective TD phonons only. The dotted lines denote the results of the SCC method, in which the Dyson ordering is used in the quantization procedure and the Fock terms ($1/2\Omega$-terms) in the collective hamiltonian $\mathcal{H}_D(\xi, \eta)$ are neglected.

6. Summary

(1) The Dyson boson mapping method became very useful for the collective multi-phonon subspace, because there is no problem relating to the convergence of the boson expansion and the problem of non-hermiticity of the boson hamiltonian has completely been resolved.

(2) It has been clarified that the Dyson-type non-unitary representation of the SCC method is quite useful in order to take into account the coupling effect between the collective and non-collective phonon degrees of freedom.

References

1) T. Holstein and H. Primakoff, Phys. Rev. **58** (1940) 1098
2) F.J. Dyson, Phys. Rev. **102** (1956) 1217; **102** (1956) 1230
3) K. Takada, Nucl. Phys. **A439** (1985) 489
   K. Takada, T. Tamura and S. Tazaki, Phys. Rev. **C31** (1985) 1948
4) K. Takada, Phys. Rev. **C34** (1986) 750
5) T. Marumori, T. Maskawa, F. Sakata and A. Kuriyama, Prog. Theor. Phys. **64** (1980) 1294
6) K. Takada and Y.R. Shimizu, Nucl. Phys. **A468** (1987) 11
   Y.R. Shimizu and K. Takada, Prog. Theor. Phys. **77** (1987) 1192
7) A. Kuriyama and M. Yamamura, Prog. Theor. Phys. **66** (1981) 2130
   F. Sakata, T. Marumori, Y. Hashimoto and T. Une, Prog. Theor. Phys. **70** (1983) 424

PHONONS IN SOFT NUCLEI AND DYNAMICAL O(5)-SYMMETRY

O.K. Vorov, V.G. Zelevinsky
Institute of Nuclear Physics, 630090 Novosibirsk, USSR

The review of results obtained in the semimicroscopical theory of anharmonic nuclear vibrations is given. Main publications are the following:

O.K. Vorov, V.G. Zelevinsky, Yad. Fiz. 37 (1983) 1392
Nucl. Phys. A 439 (1985) 207
Proc. XXI LINP winter school, Leningrad (1986) 195

V.G. Zelevinsky, Sov. Phys. Izvestia, ser. fiz. 48 (1984) 79
Nuclear Structure, Dubna 1985, 173
Nuclear Structure, Reactions and Symmetries, Dubrovnik 1986.

The theory is based on the traditional picture of quadrupole phonons in superfluid nuclei. In soft nuclei the vibrational frequency is low and the vibrational amplitude is large giving rise to strong nonlinear effects. The microscopic consideration reveals the dominance of quartic anharmonicy and, as a consequence, O(5) symmetry of spectra. The resulting pattern of spectra and transition probabilities (E2 and M1) is found to be in good agreement with data for practically all spherical non-magic nuclei. The physical picture emerging is that of two boson condensates, nemely usual s-boson (Cooper pair) condensate and the new one, the d-boson pair O(3) - and O(5) - symmetrical condensate. Artificial IBM postulates (strict conservation of the boson number, out of collective bands and so on) become redundant and the data description is, as a rule, better than in the IBM using the parameter number less than that of various IBM versions.

Prospects of developing the full microscopic theory are discussed.

THE NEUTRON-RICH N=59 ISOTONES-TIES BETWEEN SPHERICAL AND STRONGLY DEFORMED NUCLEI

H. Ohm and K. Sistemich
Institut für Kernphysik, Kernforschungsanlage Jülich
Postfach 1913, D 5170 Jülich, F.R.Germany

G. Lhersonneau, B. Pfeiffer and K.-L. Kratz*
Institut für Kernchemie, Universität Mainz
Postfach 3980, D 6500 Mainz

Abstract: The neutron-rich N=59 isotones lie at the unusually rapid transition between spherical nuclei with N < 58 and well deformed isotopes with N > 60. In accordance with this unique position, evidence for shape coexistence has been observed which is reviewed here. At present there is no indication of a particular softness of these nuclei with respect to deformations.

1. Introduction

The study of products of nuclear fission has revealed the existence of a new region of deformed nuclei at A ~ 100. This has been a surprising finding since calculations in the frame of the spherical shell model predicted remarkable subshell closures at Z=38,40 and N=56 which indeed showed up in the properties of the nuclei around $^{96}_{40}Zr_{56}$. An even more surprising result was the fact that the transition from spherical to deformed nuclear shapes in this mass region is unusually sudden. It is by now well known that several nuclei with N>60 are strongly deformed while their close neighbours with N<58 have properties of spherical nuclei. This leaves the N=59 isotones as candidates for a "transitional region". Consequently one would expect softness or shape coexistence for these isotopes which makes their investigation very appealing. One important aspect in these studies is the relevance of the shapes and of a possible softness of the A ~ 100 nuclei for the calculations of the energy balance in the fission process. In this paper the presently available knowledge on the N=59 nuclei is discussed, after the evidence for the spherical nature of the lighter isotopes and for the deformations of the heavier ones have been outlined in sections 2 and 3.

2. The properties of the nuclei with N<58

Some of the experimental data which characterize the individual nuclei of the A ~ 100 region are compiled in Fig. 1. There is little doubt that the nuclei with N<58 are basically spherical at least in their ground states, as will be discussed in the following.

^{96}Sr: This nucleus 1) seems to have vibrational character where the 0_2^+ level at 1229 keV may be an intruder.

^{95}Sr: The ground state is based on the $\tilde{s}_{1/2}$ quasiparticle configuration 2) in accordance with the shell-model expectation for the 57th neutron, cf. Fig. 2. The 556 keV level is a good candidate for being the $\tilde{g}_{7/2}$ state while the interpretation of the 352 keV level as $\tilde{d}_{3/2}$ poses some difficulties 3).

* Support granted by the BMFT under contract 06MZ552

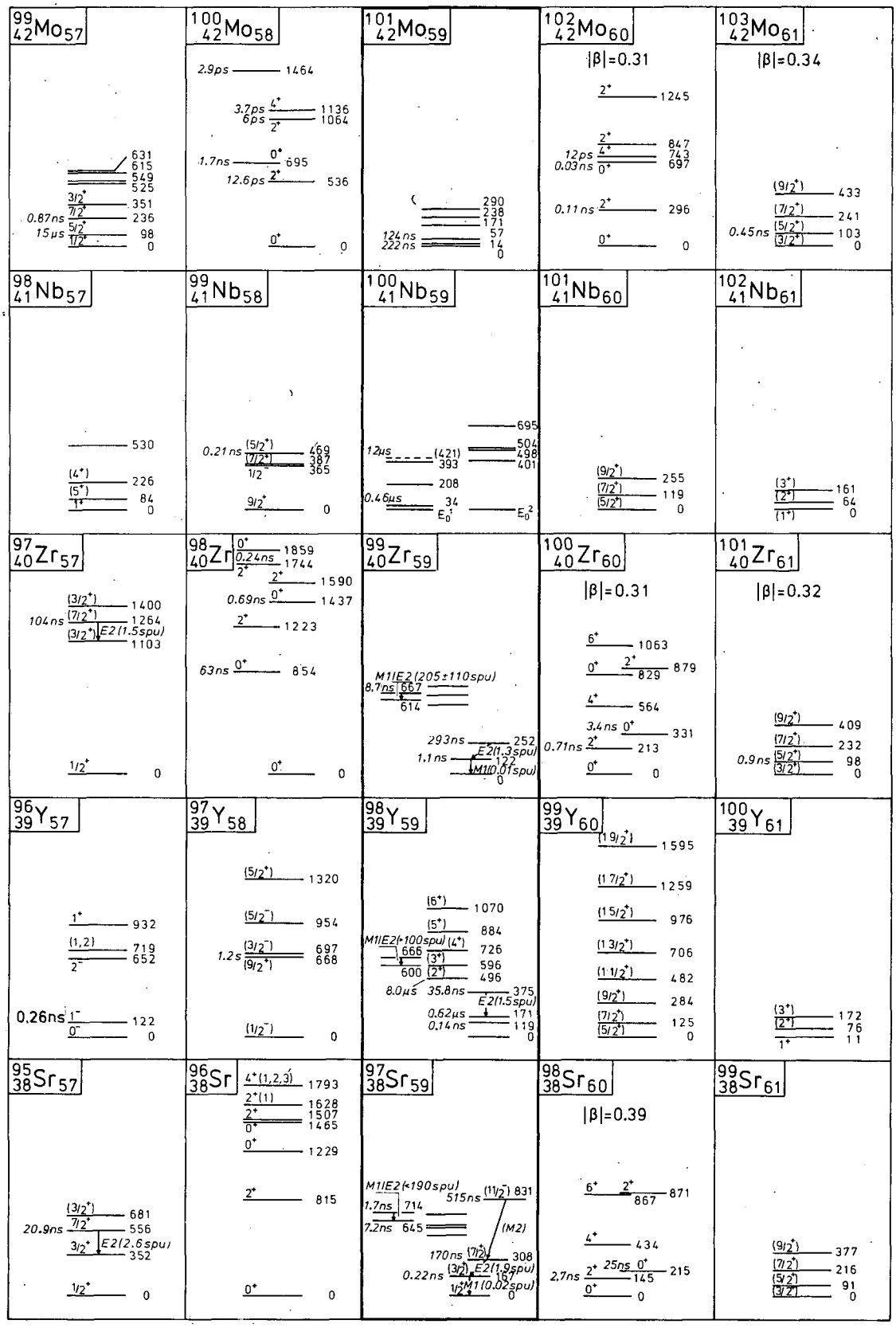

Fig. 1: Selected experimental information on the nuclei at the onset of deformation near A=100. The values of |β| have been deduced from the lifetimes of the first-excited states.

^{97}Y: As in the case of ^{95}Sr the lowest-lying states can be understood as quasi-particle configurations while the levels above 1 MeV are presently investigated in terms of particle-core coupling calculations 4). It is interesting to note that an isomer at 3523 keV with a half-life of 144 ms exists 5) which probably has $[\pi g_{9/2}, \nu(h_{11/2}, g_{7/2})]$ quasiparticle character. Hence, it is concluded that this nucleus shows single-particle nature even at high excitation energies.

^{96}Y: The experimental knowledge about the properties of the low-lying levels is especially extended for this isotope. Hence, calculations in terms of IBFFM could be performed 3) which provide a good interpretation of all known levels as being based on proton-neutron quasiparticle configurations including some coupling to the ^{94}Sr core.

^{98}Zr: The high-lying first excited states indicate the effect of shell closures both for protons and neutrons $[d^6_{5/2} + s^2_{1/2}?]$. The decay properties of the levels have led to a grouping into bands based on the ground and the first excited states 6). The fact that the 0^+_2 level is strongly populated in the (d,^{6}Li) reaction is interpreted as evidence for strong proton-pair neutron-pair correlations. The band which has been attributed to the 0^+_2 level exhibits a vibrational behaviour. (Here it should be mentioned that the 4^+ and 6^+ spin- and parity assignments for the levels at 1843 and 2491 keV, respectively, in this band are at variance with results of recent γ- γ angular correlation studies 7) at the fission-product separator JOSEF.

^{97}Zr: This nucleus has the highest lying first excited state of all the odd-mass nuclei in this region in accordance with the fact that it has just one valence neutron beyond the doubly submagic ^{96}Zr. The single-particle nature of the lowest levels has been tested in nuclear reaction studies 8) and through a measurement of the g factor of the 1264 keV level 9).

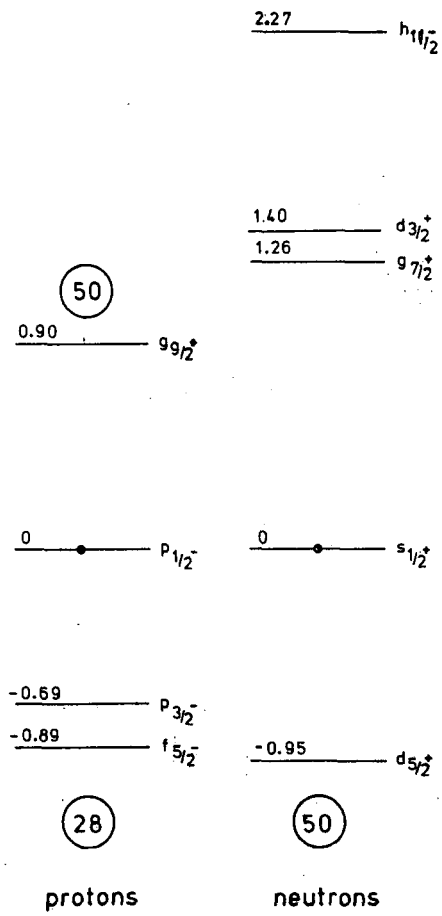

Fig. 2: Single particle levels near ^{96}Y (energies in MeV)

^{99}Nb: The low-energy spectrum contains proton-quasiparticle states 10). At energies around 500 keV core-coupled states may come into play 11).

^{98}Nb: The properties of this isotope are determined by a valence proton and a valence neutron beyond ^{96}Zr 12).

^{100}Mo: The structure has been reproduced in IBA calculations 13) where configuration mixing (N_π=1 and N_π=3) has been taken into consideration. The ground state is a mixture of about 60% of the "spherical" configuration (N_π=1) and 40% of the collective one (N_π=3), while the 0^+_2 level is orthogonal. The decay properties indicate 14) the band structure outlined in Fig. 1.

^{99}Mo: The low-lying states are also here interpreted as single neutron configurations 15).

Hence, the available knowledge on the levels shows that the nuclei with N<58 can well be described in terms of the spherical shell model. In the special case of ^{97}Y this is true even for high-lying states which indicates that the subshell closures in this region are remarkably efficient. In other cases like ^{98}Zr collective

structures seem to exist at higher excitation energies 6) although it is still to be studied to which extent these structures are connected with static deformations.

3. Rotational structures in the isotones with N>60.

Bands with rotational level-energy sequences have been observed in several nuclei with N >60. Information on the size of the deformation has been obtained in some cases through the determination of the lifetimes of the band members by β^--γ and γ-γ delayed coincidence measurements and of the isotope shifts by laser spectroscopy 16). Fig. 1 shows the lowest-lying ones of the observed bands.

^{98}Sr: A rotational ground-state band exists in this nucleus. The half-life 17) of the 2_1^+ level of 2.7 ns shows that the $2_1^+ \rightarrow 0_1^+$ transition is very collective (B(E2) = 98 single particle units). Under the assumption that the classical relationship between B(E2) and the deformation parameter β is valid, a value of $|\beta|$=0.39 results where the prolate shape is most probable. This value is remarkably large in view of the fact that the close neighbour ^{97}Y shows no evidence for any deformed structures and that an extremely low-lying 0^+ state exists 18) which indicates configuration mixing. According to configuration-mixing calculations 19), this 0_2^+ state belongs to a nuclear shape which is different from the one of the ground state. The best fit to the available data is found with $\beta(0_2^+)$ = -0.2.

^{99}Sr: A ground-state band is observed which has the pattern of a symmetric rotor 20,21). Only a few members of this band could be studied since these levels can be reached exclusively through the β^- decay of ^{99}Rb. No determination of the size of the deformation has been published as yet.

^{99}Y: The knowledge about rotational bands is unusually rich for this nucleus. Eight members of the ground-state band could be identified in the study of the γ radiation from an 8.7μs isomer with high spin. Several side bands have been observed which provide key information for the determination of the Nilsson parameters for this new region of deformed nuclei 22-24). The size of the deformation has not yet been determined. But the properties of the bands and, in particular, the probable Nilsson configurations of the band heads indicate a prolate deformation of a similar size as in the neighbours. It is interesting to note that basically all observed levels have been assigned to bands. Thus there is no evidence known for a coexistence in this isotope in contrast to the situation in both even-even N=60 neighbours ^{98}Sr and ^{100}Zr.

^{100}Y: A band based on the 11 keV level has been identified 25) which is characterized by a moment of inertia of about 90% of the rigid-rotor value - a result which is typical for the odd-odd nuclei of the A ~ 100 region.

^{100}Zr: A rotational ground-state band coexists with a low-lying 0_2^+ state. There is a striking similarity between ^{100}Zr and ^{98}Sr with the exception that the 0_2^+ state in ^{100}Zr may belong to a spherical structure 19).

^{101}Zr: The existence of a ground-state deformation is well established 20,26). The knowledge on higher-lying levels is still scarce and it cannot be said whether different shapes coexist.

^{101}Nb and ^{102}Nb: In both cases the energy sequences of the low-lying levels indicate deformation the size of which still has to be determined.

^{102}Mo: The lifetime of the 2_1^+ level shows that the $2_1^+ \rightarrow 0_1^+$ transition is collective but the energies of the levels (E_{4^+}/E_{2^+} = 2.52) do not correspond to those of the band for a good rotor. Similar to the case of ^{100}Mo, this nucleus is well described through the IBA calculations 13) with coexisting N_π=1 and N_π=3 configurations.

^{103}Mo: In contrast to the situation in ^{102}Mo, a rotational ground-state band has been identified 27). In spite of the fact that only a few members could be observed in the study of the γ radiation accompanying the β^- decay of the ground-state of ^{103}Nb with the probable spin and parity $5/2^+$, the band characterizes ^{103}Mo as a good rotor 27).

Thus all the nuclei with N=60 (except maybe for ^{102}Mo) shown in Fig. 1 are probably strongly deformed in their ground states with prolate (and symmetric?) shapes. (It should be mentioned that evidence for deformations has also been observed for N>60 nuclei with smaller and larger Z than discussed here.) An interesting fact is that the odd-mass nuclei seem to be "better" rotors than their even-even neighbours as can be concluded from the comparison between ^{99}Y and ^{98}Sr, ^{100}Zr and between ^{103}Mo and ^{102}Mo. A second remarkable fact is that according to the present knowledge the deformation of ^{98}Sr is at least as large as the one 28) of ^{100}Sr which is considered to bé one of the best rotors of the A ~ 100 region (E_4+/E_2+ = 3.23).

4. The structure of the N=59 nuclei.

The comparison between the properties of the isotopes with N<58 outlined in section 2 with those that have N>60 (section 3) shows that really an unusually drastic transition occurs for the isotopic chains with Z < 42. This is particularly obvious for Y and Sr: ^{97}Y has single-particle nature even at high excitation energies while ^{99}Y shows all properties of a symmetric rotor, and ^{96}Sr has a vibrational level pattern while the deformation has already gained its full size at ^{98}Sr. In fact, the deformation decreases rather than increases from ^{98}Sr to ^{100}Sr 17).

Thus the "transitional region" at A ~ 100 is basically confined to the N=59 nuclei for which therefore either softness with respect to shape changes or shape coexistence would be expected. And, indeed, there is strong evidence for shape coexistence.

^{98}Y: The best example is ^{98}Y 29) where a band of levels with a rotational energy sequence built upon the 496 keV level has already been discovered at the same time when information on ground-state bands in the even-even nuclei was found. This band is very regular with very little staggering and indicates a well pronounced deformation of ^{98}Y in this excited state.

In contrast, the levels below the 496 keV state show no rotational pattern. Recent studies 30) of the absolute γ-ray intensities in the A=98 β^- decay chain suggest that the ground state of ^{98}Y has negative parity (in contrast 29) to earlier conclusions); the spin is probably 0 or 1. These configurations can be reproduced well with the available shell model orbitals (e.g. $\pi p_{1/2}$ and $\nu s_{1/2}$). The strength of the β^- decay is interpreted as evidence for the single particle character of the ground state of ^{98}Y. Moreover, if a rotational band with a similar deformation as the one of the 496 keV level would be built on the ground state, then some feeding from the higher spin members of the known band above 496 keV would be expected.

Thus it is probable that ^{98}Y is spherical (or only weakly deformed) in its ground state. The unusually many isomeric states also point to shape coexistence in this nucleus since part of them can hardly be due to large differences of the spins of the involved levels 29). Additional rotational structures may well exist in ^{98}Y, and the 600 and 666 keV levels are candidates for being the first two members of an additional band: The γ transition between the 666 and 600 keV levels seems to contain a highly collective E2 component with B(E2) > 100 single particle units (deduced from α_T (66 keV) = 1.5(7) and $t_{1/2}$(666 keV level) < 0.8 ns). The 600 keV level is strongly fed (logft= 4.4) through the β^- decay of the deformed ground state of ^{98}Sr. The results of the RPA calculations with the code of 31) predict strongly fed deformed 1^+ levels at about 600 keV excitation energy. It is interesting to note that the energy difference of the discussed levels is the same as in the rotational bands of the odd-odd neighbours like ^{100}Y and ^{102}Nb 32).

^{97}Sr and ^{99}Zr: The isotones ^{97}Sr and ^{99}Zr seem to be very similar nuclei 33,34) - in analogy to the properties of the neighbours ^{98}Sr and ^{100}Zr. Recently, it has been shown 2,16) that properties of the ground-state of ^{97}Sr are compatible with its interpretation as the $\tilde{s}_{1/2}$ level. Hence it is reasonable to assume that the lowest levels of ^{97}Sr have quasiparticle nature. The isomer at 307 keV may well be based on the $\tilde{g}_{7/2}$ configuration. It is then remarkable how strongly the $\tilde{s}_{1/2}$ - $\tilde{g}_{7/2}$ gap has decreased with respect to the situation in ^{97}Zr. This trend can already be observed in a comparison of ^{97}Zr and ^{95}Sr, cf. section 2. It cannot be said whether the 167 keV level has $\tilde{d}_{3/2}$ character since the position of this quasiparticle state at A ~ 100 is still unclear 3).

The nature of the ground state of ^{99}Zr has not been determined experimentally. But the similarity with ^{97}Sr renders the assumption of $I^{\pi}=1/2^{+}$ reasonable. This has been the original suggestion which has later been revised 35) to $3/2^{+}$ from the analogy to heavier odd-mass N=59 isotones. In any case, the lowest levels of ^{99}Zr do not form a rotational band as the energies of the first and second excited state might suggest. The half-life of the 252 keV level rules out its interpretation as a band member. On the other hand, if the 121 keV level would belong to a ground-state band then further members should have been observed in the study of the β^{-} decay of the $5/2^{+}$ ground state of ^{99}Y.

Candidates for being members a rotational band in ^{99}Zr are the 614 and 667 keV levels (in close analogy to ^{98}Y). It is now known that the 667 keV level has a half-life 36) of 8.7(5) ns. The conversion coefficient of the 53 keV transition between the two levels has been determined to α_K=2.0(7). Thus this transition must have an enhanced E2 component with B(E2) ~ 200(100) spu. A similar pair of states with possibly an enhanced E2 transition between them are the 645 and 714 keV levels in ^{97}Sr. Hence although there is no definite proof, it is probable that there are co-existing shapes in ^{97}Sr and ^{99}Nb.

^{100}Nb: The available data are too scarce to draw any conclusions on the structure. It is remarkable that two completely independent sets of levels have been observed 37) in the study of the β^{-} decay of ^{100}Zr (right-hand side of the scheme of this nucleus in Fig. 1) and in the depopulation of a μs isomer in ^{100}Nb. One of these sets is expected to be built upon the ground state (probably the one from the β^{-} decay) while the other may be based on the 3-s isomer in ^{100}Nb.

^{101}Mo: The level structure, transfer data and the transition probabilities have well been reproduced through IBFM/PTQM calculations where ^{100}Mo has been taken as a transitional core 4). Similar calculations have successfully been applied to the heavier odd-mass N=59 isotones ^{103}Ru and ^{105}Pd 38,39).

In conclusion, it can be stated that the rapid transition into the new region of deformed nuclei at A ~ 100 brings about a very attractive class of N=59 nuclei. There is strong evidence for shape coexistence in ^{98}Y, whereas there is no hint at a particular softness with respect to deformations. For ^{97}Sr and ^{99}Zr there are indications of a similar structure but more detailed studies, in particular on level lifetimes, are needed to check the conjectures on the rotational patterns above 600 keV. The N=59 isotones with higher Z seem to have a more classical transitional nature in accordance with the fact that the shape transition is less sudden in the Mo chain and beyond than in the lighter elements. For calculations of the energy balance in the fission process it can be assumed that the nuclei with N>58 will be produced in a deformed shape while those with N<58 might prefer spherical configurations even at high excitation energies (e.g. ^{97}Y). It would be of interest to search for evidence of the rapid structure transition at N=59 in the kinetik-energy vs mass distribution in fission.

References:

1) G. Jung, B. Pfeiffer, L.J. Alquist, H. Wollnik, P. Hungerford, M.S. Scott and W.D. Hamilton: Phys. Rev. C22 (1980) 252
2) F. Buchinger, E.B. Ramsay, R.E. Silverans, P. Lievens, E. Arnold, W. Neu, R. Neugart, K. Wendt, G. Ulm, and the ISOLDE Collaboration: Z. Phys. A-Atoms and Nuclei 327 (1987) 361
3) S. Brant, G. Lhersonneau, M.L. Stolzenwald, K. Sistemich and V. Paar: "Proton-Neutron Multiplets in ^{96}Y", to be published.
4) S. Brant, University of Zagreb, Yugoslavia, and KFA Jülich, priv. communication
5) G. Lhersonneau, D. Weiler, P. Kohl, H. Ohm, K. Sistemich and R.A. Meyer: Z. Phys. A-Atoms and Nuclei 323 (1986) 59
6) R.A. Meyer, E.A. Henry, L.G. Mann and K. Heyde: Phys. Lett. 177B (1986) 271.
7) M.L. Stolzenwald, IKP, Kernforschungsanlage Jülich, private communication.
8) B. Haesner and P. Luksch: Nuclear Data Sheets 46 (1985) 607 and references therein
9) Z. Berant, R.L. Gill, M.H. Rafailovich, R.E. Chrien, J.C. Hill, F.K. Wohn, R.F. Petry, C. Chung, G. Peasley and H. Mahsen: Phys. Lett. 156 B (1985) 159.
10) E.R. Flynn, R.E. Brown, F. Ajzenberg-Selove and J.A. Cizewski: Phys. Rev. C.28 (1983) 575
11) G. Battistuzzi, K. Kawade, H. Lawin, K. Shizuma and K. Sistemich: Z. Phys. A-Atoms and Nuclei 306 (1982) 113
12) L.R. Medsker and H.T. Fortune: Phys. Lett. 5813 (1975) 297
13) M. Sambataro and G. Molnár: Nucl. Phys. A376 (1982) 201
14) G. Menzen, K. Sistemich, G. Lhersonneau and H. Gietz: Z. Phys. A-Atoms and Nuclei 327 (1987) 119
15) B. Barman Roy and D.C. Chondhury: Phys. Rev. C12 (1975) 323
16) F. Buchinger, E.B. Ramsay, R.E. Silverans, P. Lievens, E. Arnold, W. Neu, R. Neugart, G. Ulm, K. Wendt, D. Berdichevsky, R. Fleming and D.W.L. Sprung: Contrib. to the 5th Int. Conf. on Nuclei far from Stability, Sept. 14-19,1987, Rosseau Lake, Ontario, Canada, in press
17) H. Ohm, G. Lhersonneau, K. Sistemich, B. Pfeiffer and K.-L. Kratz: Z. Phys. A-Atoms and Nuclei 327 (1987) 483
18) F. Schussler, J.A. Pinston, E. Monnand, A. Moussa, G. Jung, E. Koglin, B. Pfeiffer, R.V.F. Janssens and J. van Klinken: Nucl. Phys. A339 (1980) 415
19) F.K. Wohn, J.C. Hill, C.B. Howard, K. Sistemich, R.F. Petry, R.L. Gill, H. Mach and A. Piotrowski: Phys. Rev. C33 (1986) 677
20) F.K. Wohn, J.C. Hill, R.F. Petry, H. Dejbakhsh, Z. Berant and R.L. Gill: Phys. Rev. Letters 51 (1983) 873
21) B. Pfeiffer, E. Monnand, J.A. Pinston, J. Münzel, P. Möller, J. Krumlinde, W. Ziegert and K.-L. Kratz, Z. Phys. A-Atoms and Nuclei: 317 (1984) 123
22) R.A. Meyer, E. Monnand, J.A. Pinston, F. Schussler, I. Ragnarsson, B. Pfeiffer, H. Lawin, G. Lhersonneau, T. Seo and K. Sistemich: Nucl. Phys. A439 (1985) 510
23) R.F. Petry, H. Dejbakhsh, J.C. Hill, F.K. Wohn, M. Schmid and R.L Gill: Phys. Rev. C31 (1985) 621
24) B. Pfeiffer, S. Brant, K.-L. Kratz, R.A. Meyer and V. Paar: Z. Phys. A-Atoms and Nuclei 325 (1986) 427
25) F.K. Wohn, J.C. Hill, J.A. Winger, R.F. Petry, J.D. Goulden, R.L. Gill, A. Piotrowski and H. Mach: Phys. Rev. C36 (1987) 1118
26) H. Ohm, G. Lhersonneau, U. Paffrath, K. Shizuma and K. Sistemich: Z. Phys. A-Atoms and Nuclei 326 (1987) 233
27) T. Seo, H. Lawin, G. Lhersonneau, R.A. Meyer, G. Menzen and K. Sistemich: Z. Phys. A-Atoms and Nuclei 320 (1985) 393
28) R.E. Azuma, G.L. Borchert, L.C. Carraz, P.G. Hansen, B. Johnson, S. Mattsson, O.B. Nielsen, G. Nyman, I. Ragnarsson, and H.L. Ravn, Phys. Lett. 86B (1979) 5
29) G. Lhersonneau, R.A. Meyer, K. Sistemich, H.P. Kohl, H. Lawin, G. Menzen, H. Ohm, T. Seo and D. Weiler: Conf. to the ACS Meeting on Nuclei off the Line of Stability, Sept. 8 - 13, 1985 Chicago, USA, ACS Symp. Series 324, p. 202, R.A. Meyer and D.S. Brenner eds.
30) H. Mach, R.L. Gill, G. Molnár, R.F. Casten, A. Wolf and J.A. Winger: Contrib. to the 5th Int. Conf. on Nuclei far from Stability, Sept. 14-19, 1987, Rosseau Lake, Ontario, Canada, in press.
31) J. Krumlinde and P. Möller: Nucl. Phys. A417 (1984) 419
32) H. Ohm, A.-M. Schmitt, K. Shizuma, R.W. Hoff, R.A. Meyer, H. Ahrens, J.P. Bocquet, N. Kaffrell, H. Lawin, G. Lhersonneau, K. Sistemich, N. Trautmann: Ann. Report 1984 of the IKP, KFA Jülich, F.R.Germany, Report Jül-Spez-305 (1985) p.93
33) H.A. Selič, G. Sadler, T.A. Khan, W.-D. Lauppe, H. Lawin, K. Sistemich, E. Monnand, J. Blachot, J.P. Boquet and F. Schussler: Z. Phys. A289 (1979) 197
34) K.-L. Kratz, H. Ohm, A. Schröder, H. Gabelmann, W. Ziegert, B. Pfeiffer, G. Jung, E. Monnand, J.A. Pinston, F. Schussler, G.I. Crawford, S.G. Prussin and Z.M. de Oliveira: Z. Phys. A-Atoms and Nuclei 312 (1983) 43
35) R.A. Meyer: Hyperfine Interactions 22 (1985) 385
36) K. Kawade, G. Lhersonneau, H. Ohm, K. Sistemich and R.A. Meyer: Ann. Report 1986 of the IKP, KFA Jülich, F.R. Germany, Report Jül-Spez-403 (1986) p.21
37) G. Lhersonneau and K. Sistemich: Ann. Report 1985 of the IKP, KFA Jülich, F.R. Germany, Report Jül-Spez-344, p. 29, and references cited therein
38) H. Seyfarth, A.M. Hassan, W. Delang, P. Göttel, B. Kardon, K. Schreckenbach, R.A. Meyer, S. Brant and V. Paar: "The Level Structure of ^{103}Ru", to be published.
39) R.A. Meyer, S.V. Jackson, S. Brant and V. Paar: "The Levels of ^{105}Pd Populated in the Decay of ^{105}Ag $^{m+g}$", to be published

CHAOS AND ORDER IN ATOMIC NUCLEI

I. Rotter
Zentralinstitut für Kernforschung Rossendorf, Dresden, 8051, GDR

Abstract

The transition from the resonance reaction mechanism at low level density to the direct reaction mechanism at high level density is investigated by means of numerical results obtained from microscopic calculations for nucleon induced reactions. The transition takes place rather sharply at $\bar{\Gamma} \approx \bar{D}$. Here, two types of motion of the nucleons exist simultaneously: a motion in long-living states which are near equilibrium and a motion in short-living states which are far from equilibrium. A formation of new order far from equlibrium takes place only in the open quantum mechanical nuclear system. It is caused by the quantum fluctuations via the continuum.

1. Introduction

The formation of order out of chaos is one of the most interesting problems in present time[1]. Although it is a general problem it should be discussed carefully in some special cases which are proved experimentally in detail. Such a case might be the atomic nucleus the properties of which are investigated for more than fifty years.

The nucleus is a physical system consisting of particles which are all of the same type. They move in an average central field which is created by the particles themselves. Every nucleus appears in different states which can be excited and investigated by means of different nuclear reactions. Two types of nuclear reactions induced by, e.g., low-energy nucleons are very well known for a long time: the fast direct reaction process and the slow resonance reaction process. While in the first case, information on the target nucleus can be obtained, the resonance process contains information on the compound nucleus. For both processes, mathematical methods are worked out the results of which are in good agreement with the experimental data. Although the methods used in both cases are completely different from each other, a regular motion of the nucleons inside the nucleus is proposed in both cases. Nevertheless, nuclear physicists hold often the idea that nucleons in nuclei move chaotically[2,3].

It is the aim of the present paper to discuss this problem on the basis of numerical results obtained from microscopic calculations.

2. Bound and isolated nuclear states

The basis of the microscopic nuclear structure calculations is the shell model in which a regular motion of the nucleons is assumed to take place in a conservative field of force. The basic equation is the Schrödinger equation in a function space (Q space) in which all nucleons occupy bound and quasibound single-particle states,

$$(H_{QQ} - E_R^{SM})\,\phi_R^{SM} = 0 \qquad (1)$$

with the Hamilton operator

$$H = H_0 + V \qquad (2)$$

and $H_{QQ} \equiv QHQ$. Here, Q is the projection operator onto the Q space which is the total function space in nuclear structure calculations (Q = 1). The wavefunctions of the many-particle nuclear states are identified with the eigenfunctions ϕ_R^{SM} while the real eigenvalues E_R^{SM} are assumed to be the energies of the states. The Hamilton operator is proposed to be Hermitean since the system is considered to be enclosed fully into the Q space. Collective effects additionally to the creation of the average field are enclosed in the residual interaction V_{QQ}. The wavefunctions

$$\Phi_R^{SM} = \sum_i a_{Ri}\, \varphi_i \tag{3}$$

are mixed in the basic wavefunctions φ_i, the energies E_R^{SM} are real.

The results of the microscopic nuclear structure calculations describe successfully the low-lying bound nuclear states as well as the states at higher excitation energy which are isolated due to their small decay widths or (and) their large distance from other states with the same spin and parity. The results of the nuclear structure calculations represent the real nuclear theory proved by many experimental data, sometimes in a "revolutionary" manner[4] as, e.g., by the discovery of isobaric analogue resonances and of Gamow-Teller resonances. It must be concluded, therefore, that the nucleons move inside the nucleus with some regularity which is, obviously, dictated by the Pauli exclusion principle. The main cooperative effect is the formation of the central potential.

It is, however, very well known that the wavefunctions Φ_R^{SM} of the nuclear structure calculations do not have the true asymptotic behaviour and that the finite lifetime of the nuclear states cannot be calculated within the model. The point is that the nucleus is treated as a closed system (Q = 1) in nuclear structure calculations although most of the nuclear states can decay by particle emission since they lie above particle decay thresholds. The system, included in the Q space, is, in reality, coupled to the continuum (P space) and must be treated as an open system: The nuclear states are "quasibound states embedded in the continuum" (QBSEC)[5]:

Recently, a method has been worked out[5,6] for treating the nucleus as an open quantum mechanical system. The basic Schrödinger equation $H\psi = E\psi$ is linear in the whole P + Q function space (P + Q = 1), but nonlinear for the system confined in the Q space:

$$(H_{QQ} - E)\psi = -H_{QP}\psi \tag{4a}$$

or[5,6]

$$(H_{QQ} - E)\,\Phi_R^{SM} = -\,H_{QP}\, G_P^{(+)}\, H_{PQ}\, \Phi_R^{SM} \tag{4b}$$

As a consequence, correction terms to the Hamilton operator

$$H_{QQ}^{eff} = H_{QQ} + H_{QP}\, G_P^{(+)}\, H_{PQ} \tag{5}$$

as well as to the wavefunction

$$\tilde{\Omega}_R = (1 + G_P^{(+)}\, H_{PQ})\, \tilde{\Phi}_R \tag{6}$$

appear by which the coupling of the Q subspace to the P subspace is taken into account. The wavefunctions

$$\tilde{\Phi}_R = \sum_{R'} b_{RR'}\, \Phi_{R'}^{SM} \tag{7}$$

are expanded in terms of the shell model wavefunctions Φ_R^{SM}. The wavefunction $\tilde{\Omega}_R$ has the true asymptotic behaviour[5,6]. The Hamilton operator H_{QQ}^{eff} is non-Hermitean. Its eigenvalues are complex,

$$H_{QQ}^{eff}\, \tilde{\Phi}_R = (\tilde{E}_R - \tfrac{1}{2}\, \tilde{\Gamma}_R)\, \tilde{\Phi}_R \tag{8}$$

describing the positions $\tilde{E}_R$ as well as the widths $\tilde{\Gamma}_R$ of the nuclear states. The widths $\tilde{\Gamma}_R$ are inverse proportional to the lifetimes $\tilde{T}_R$ of the resonance states.

It has been shown[6,7] on the basis of this model that the spectroscopic properties of the different nuclear states can be described by the standard nuclear structure methods to a good approximation as long as the nuclear states are either bound or well isolated. In such a case, the additional forces via the continuum (feedback), which appear in the open system, are small. As a consequence, the nuclear states may be considered as conservative structures, to a good approximation. The coefficients $b_{RR'}$ in the expansion (7) fulfill approximately the

condition $b_{RR'} \approx \delta_{RR'}$. The energy shifts $E_R^{SM} - \tilde{E}_R$ are small but nonvanishing even for bound states. The finite lifetime $\tilde{T}_R$ of the resonance states follows immediately from the non-Hermitean part $H_{QQ}^{eff} - H_{QQ}$ of the Hamilton operator.

The equations of the open quantum mechanical nuclear system in the Q space are nonlinear, eqs. (4). Further, strong cooperative effects are known for a long time[2] to exist in the nuclear system. Self-organisation is expected therefore, from a mathematical point of view, to take place in the nuclear system.

The regular motion of the nucleons supposed in all nuclear structure calculations can be, indeed, understood[8] as a consequence of the strong cooperative effects existing between the individual nucleons. The formation of the common potential H_0 by the nucleons themselves is a genuine cooperative effect. The residual interaction V_{ik} between the nucleons is relatively small. The different many-particle states of a nucleus differ by the different occupation of the single-particle states with nucleons in the common potential. Only in the ground state, all the nucleons occupy the lowest single-particle states. In the excited states, some of the nucleons occupy higher-lying single-particle states, which are still bound, by leaving holes in the low single-particle states. If these states of the many-particle system lie above particle decay thresholds, they have a finite lifetime against decay into the open channels.

Thus, the regular motion of the nucleons in bound and isolated nuclear states is not in contradiction to the existence of strong cooperative effects between the nucleons, as proposed in ref.[2], but is caused by them. The description of the nuclear structure by restricting to the Q space is a good approximation according to the slaving principle which is universal in synergetics[9]. Further, the different nuclear states should be considered as dissipative structures formed by self-organisation far from equilibrium in accordance with the definition of dissipative structures in open systems[1,10].

3. Calculations for isolated and overlapping resonance states

In contrast to the success of nuclear structure calculations at low level density, the experimental results at higher level density are not described satisfactorily. They raise a number of questions which are on the interface of reaction theory and nuclear structure and force us to rethink our assumptions in dealing with nuclear reactions on serveral points.

In standard nuclear reaction theory, the motion of the nucleons is assumed to be a chaotic one[3]. The nuclear states are proposed to be statistically independent although this assumption could not be proven experimentally, e.g.[11], and all the nuclear structure studies point to strong cooperative effects. The existence of the central potential represents the basis not only of all nuclear structure studies but also of the standard nuclear reaction theories since the proposed statistical independence of the nuclear states makes sense only if nuclear states in a central potential exist.

In order to clarify this problem, microscopic calculations in an open nuclear system have been performed in dependence on the degree of coupling between the system (Q subspace) and the environment (P subspace). The method used is the Rossendorf continuum shell model (CSM) sketched by eqs. (1) to (8), for details see refs[5,6]. The degree of coupling between the two subspaces has been varied by hand. The calculations are performed in the following manner.

(i) The shell model problem (1) is solved for the compound nucleus ^{16}O with basic wavefunctions φ_i out of the configuration space $(1p_{3/2},1p_{1/2})_2^{-1}(2s_{1/2},1d_{5/2})^1$ and $(1s_{1/2})^{-1}(1p_{3/2},1p_{1/2})^{-1}(2s_{1/2},1d_{5/2})^2$. The 76 states with $J^\pi = 1^-$ (mixed isospin) are mixed in the basic states φ_i, eq. (3), six of which are of (1p-1h) type and the remaining ones are of (2p-2h) type. The potential used is of Woods-Saxon type with standard parameters[12].

(ii) The shell model problem (1) is solved for the residual nuclei ^{15}N and ^{15}O within the configuration space $(1p_{3/2})^{-1}$ and $(1p_{1/2})^{-1}$ by using the same parameters as for ^{16}O.

(iii) The Schrödinger equation (8) with the non-Hermitean operator (5) is solved in an energy region where the $d_{3/2}$ single-particle resonance is not important, with 29 or 30 out of the 76 resonance states which are used as basic states in the coupled channel calculations (8). The 29 resonance states have small components of the basic 1p-1h configurations. In some calculations, another resonance state has been added to the 29 ones with the main component $\varphi_i = (1p_{3/2})^{-1}\, 1d_{5/2}$, either T = 0 or T = 1. The number of channels taken into account in the calculations is 1 (corresponding to the ground state $1/2^-$ of ^{15}N), 2 (corresponding to the two states $1/2^-$ and $3/2^-$ of ^{15}N) or 4 (corresponding to the two states $1/2^-$ and $3/2^-$ in both nuclei ^{15}N and ^{15}O).

In figs. 1 and 2, the dependence of the inelastic cross section and of the widths $\tilde{\Gamma}_R$ on the degree of overlapping $\langle\Gamma\rangle/\langle D\rangle$ of the resonance states (where $\langle\Gamma\rangle \equiv \bar{\Gamma}$ is the mean width and $\langle D\rangle \equiv \bar{D}$ the mean distance) is shown. The overlapping has been varied by solving eq. (8) with input values E_R^{SM} obtained as solutions of eq. (1) as well as with other values $E_R^{'SM}$ changed by hand in such a manner that the differences ΔE_R^{SM} between the energies of the different shell model states are reduced. The wavefunctions ϕ_R^{SM} of the shell model states used as input in eq. (8) thereby remain unchanged. Such a procedure to vary the degree of overlapping is justified because the eigenfunctions $\tilde{\phi}_R$ and eigenvalues $\tilde{E}_R - \frac{i}{2}\tilde{\Gamma}$ of the operator (5) depend only weakly on energy. The parameters of the Woods-Saxon potential and of the residual interaction remain unchanged in this procedure (for details see ref.[13]).

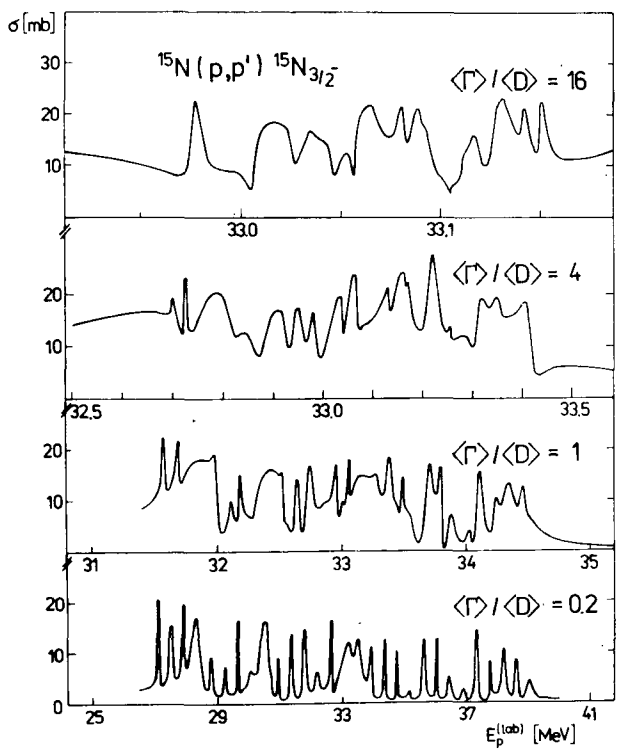

Fig. 1
The inelastic cross section $^{15}N(p,p')$ in dependence on the degree of overlapping $\langle\Gamma\rangle/\langle D\rangle$. The calculation has been performed with two channels and with 30 resonance states, 29 of which have dominant 2p-2h nuclear structure (corresponding to Fig. 1 in ref.[13]) and 1 state has dominant 1p-1h nuclear structure and T ≈ 1.

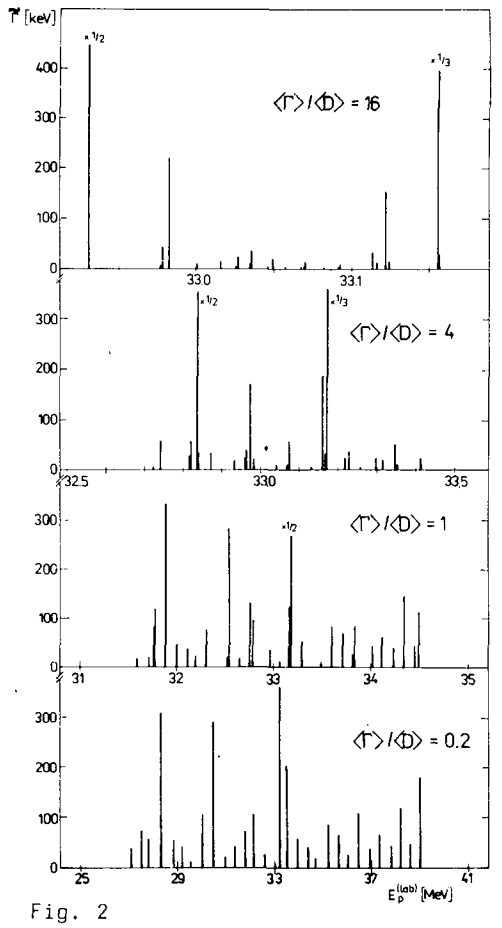

Fig. 2
The widths $\tilde{\Gamma}_R$ of the individual resonance states R in dependence on the degree of overlapping $\langle\Gamma\rangle/\langle D\rangle$. The calculation has been performed with two channels and with the same 30 resonance states as in Fig. 1.

In Fig. 3, the dependence of $\sum_{R=1}^{m} \tilde{\Gamma}_R$ on the degree of overlapping $\bar{\Gamma}/\bar{D}$ of the resonance states is shown. The sum runs over those m resonance states the widths of which are the largest ones, i.e. $\tilde{\Gamma}_1 \geq \tilde{\Gamma}_2 \geq \tilde{\Gamma}_3 \geq \tilde{\Gamma}_4 \geq \ldots$. It holds[6]

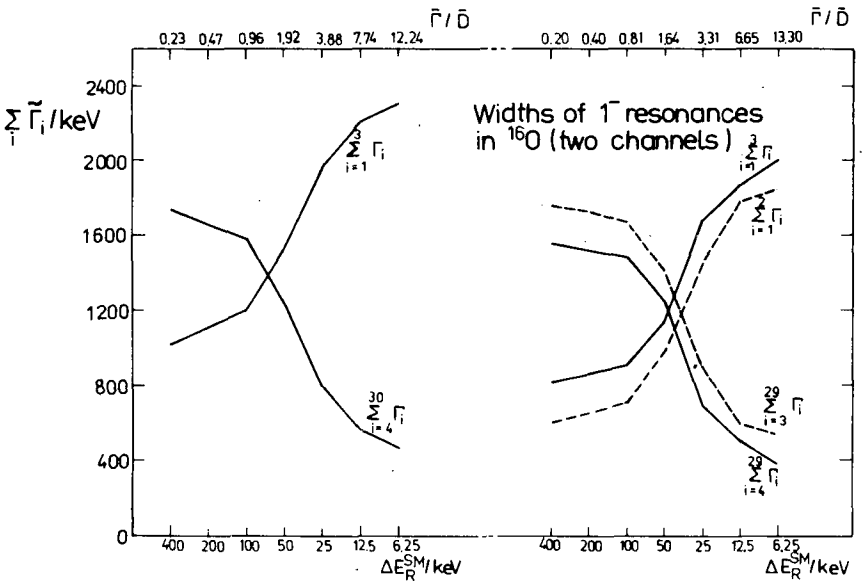

Fig. 3

The sum of the two and three, resp., largest widths and the sum of the remaining widths for the 30 resonance states shown in Figs. 1 and 2 and for the 29 resonance states shown in Figs. 1 and 2 of ref.[13] in dependence on the degree of overlapping /D.

$$\sum_{R=1}^{N} \tilde{\Gamma}_R = \sum_{R=1}^{N} \Gamma_R \qquad (9)$$

where $\tilde{\Gamma}_R$ are the widths of the resonance states R by taking into account the external mixing (eigenvalues of H_{QQ}^{eff} according eq. (8)) and Γ_R are their widths calculated by neglecting the external mixing (diagonal matrix elements of H_{QQ}^{eff}). Due to the condition (9) it follows

$$\sum_{R=1}^{N} \tilde{\Gamma}_R = \text{const} \qquad (10)$$

and

$$\sum_{R=m+1}^{N} \tilde{\Gamma}_R = \text{const} - \sum_{R=1}^{m} \tilde{\Gamma}_R \qquad (11)$$

at a certain excitation energy E where N is the total number of resonances. The widths shown in Fig. 3 are calculated at the positions $\tilde{E}_R$ of the resonance states.

The degree of overlapping $\tilde{\Gamma}/\bar{D}$ of the resonances corresponds to the strength of external mixing, involved in eqs. (7) and (8), which is given by the non-diagonal matrix elements

$$\langle \Phi_R^{SM} | H_{QQ}^{eff} - H_{QQ} | \Phi_{R'}^{SM} \rangle = \langle \Phi_R^{SM} | H_{QP}\, G_P^{(+)}\, H_{PQ} | \Phi_{R'}^{SM} \rangle \quad . \qquad (12)$$

The more the resonances overlap, the larger are the matrix elements (12). The results shown in figs. 1 to 3 illustrate therefore the behaviour of the nuclear system in dependence on the degree of external mixing of the resonance states via the continuum .

4. The transition from isolated to overlapping resonance states

The eigenfunctions Φ_R^{SM} of H_{QQ}, eq. (3), as well as the eigenfunctions $\tilde{\Phi}_R$ of H_{QQ}^{eff}, eq. (7), are the more mixed in the corresponding basic functions φ_i and Φ_R^{SM} the stronger the residual interaction V is in the first case and the non-diagonal matrix elements (12) at fixed residual interaction V in the second case. Strong internal mixing corresponds to large coefficients a_{Ri} with $R \neq i$ in the expansion (3) in the same manner as strong external mixing leads to large coefficients $b_{RR'}$ with $R \neq R'$ in the expansion (7). The coefficients a_{Ri} are real while the coefficients $b_{RR'}$ are complex since the operator H_{QQ} is Hermitean and the operator (5) is non-Hermitean.

The basic wavefunctions φ_i of the shell model problem (1) describe a regular motion of the nucleons in the central potential which is dictated by the Pauli principle. If the eigenfunctions Φ_R^{SM} are mixed strongly in the φ_i, i.e. no main component in the expansion (3) can be found, then the motion of the nucleons is usually considered to be a chaotic one. Another representation, e.g. by taking into account the collective aspects in the interplay between

the constituent particles from the very beginning, is more adequate in this case. This fact is very well known from the numerous nuclear structure calculations for heavy nuclei.

The motion of the nucleons in the nucleus cannot be characterized by a simple time dependent description as in the classical case. The concept chaos used here is therefore more complicated than that used for classical systems. In the model, applied in this paper, time is not fixed and the motion cannot be characterized by its time behaviour. All the dynamics involved in the model is caused by the finite lifetime of the resonance states calculated from the energies by means of the uncertainty relation between energy and time. According to the energy representation used in the model the quantum chaos is defined in this paper by means of the spectroscopic properties of the A nucleon system: the quantum chaos is characterized by a strong mixing of the wavefunctions (eigenfunctions) of the A nucleon system in the basic wavefunctions as well as by an information loss on its spectroscopic properties. The mixing of the eigenfunctions is model dependent: a strong mixing in relation to a certain basis may often be transformed into a small mixing in relation to another basis, e.g. by choosing another shape of the central potential. Therefore, it is necessary to consider also the information aspect. As long as spectroscopic information on the A nucleon system can be obtained from the experimental data (e.g. from the reaction or scattering cross sections), the motion of all A nucleons should be considered as a regular one. Otherwise, it is chaotic and the different nuclear states manifest themselves in the cross section not by isolated resonances but by fluctuations around an average value. The widths of the resonance states are, in such a case, small with small differences in absolute value. This information aspect in connection with the chaos will be discussed in the following on the basis of numerical results obtained (figs. 1 to 3).

It is worth mentioning that a definition of the quantum chaos from a spectroscopic point of view is used also in problems of atomic physics and quantum chemistry.

In a closed system, a chaotic motion of the nucleons (from the one-body point of view) corresponds to the formation of an equlibrium state: the different basic states are excited with a probability which is about the same for all φ_i, and the lifetime of the nuclear state is infinite by definition. An equilibrium state of the system will be reached therefore if the system is closed and if the residual interaction is not too small.

In the open system, the external mixing creates also an excitation of the basic states ϕ_R^{SM} which is more or less the same for all ϕ_R^{SM} if the external mixing is not too small. But in contrast to a closed system, the open system has to organise itself in such a manner that the lifetime of the states reached is as long as possible. Otherwise, the state reached cannot be considered as an equilibrium state.

The results shown in fig. 3 illustrate this behaviour of the open nuclear system. Instead of the lifetime of the resonance states, their widths are considered. As long as the resonance states do not overlap, it holds $b_{RR'} \approx \delta_{RR'}$. The motion of the nucleons in the eigenstates of H_{QQ}^{eff} is therefore of the same regularity as in the corresponding eigenstates of H_{QQ}. As soon as the resonance states begin to overlap, the system tends to reach an equilibrium state by means of the external mixing: The expansion (7) contains many terms the weights $b_{RR'}$ of which are of almost the same magnitude. Additionally, the widths of most resonance states are reduced, i.e. their lifetimes are enlarged. This reduction of the widths must, however, be compensated in the open system due to the condition[6] (10). The numerical results show that the compensation takes place by an enlargement of the widths of a small number of states. The stronger the external mixing, the larger is the difference between the widths of the many long-living states and those of the few short-living states. The redistribution of the widths starts rather suddenly at $\bar{\Gamma} \approx \bar{D}$.

The matrix elements $\langle \phi_R^{SM} | H | \xi_E^c \rangle$ of the operator H_{QP} between the wavefunctions ϕ_R^{SM} of the Q space and the scattering wavefunctions ξ_E^c of the P space are involved in both expressions the width $\tilde{\Gamma}_R$ as well as the excitation probability of the resonance state R in nucleon induced reactions. A long lifetime $\tilde{T}_R$, corresponding to a small width $\tilde{\Gamma}_R$, is correlated

therefore with a small excitation probability[8]. Consequently, the equilibrium states with a long lifetime are excited with a small probability in nucleon induced reactions.

The few other states of the system which appear due to the condition (10) in an open system together with the many "equilibrium" states, are far from equilibrium. These states have a large width, corresponding to a short lifetime, and will be excited in nucleon induced reactions with a large probability. They can therefore be simulated by single-particle resonances in relation to the target nucleus, i.e. by changing the central potential. In this representation, the short-living resonance states consist of one unbound nucleon in relative motion to the target nucleus which consists of A - 1 bound nucleons. The motion of these A - 1 nucleons is a regular one in the central potential created by the A - 1 nucleons themselves.

In an open system the equilibrium state with a chaotic motion of the nucleons can, therefore, not be reached immediately. On the way to the equilibrium, another state far from equilibrium appears which becomes soon the overwhelming one due to its large and fast probability of excitation. This state can be represented by a regular (and not chaotic) motion of all but one nucleon.

The two extreme cases of reaction mechanism at low and high level density are very well known in nuclear reaction theory. While information on the nuclear structure of the resonances in the A nucleon system can be obtained at low level density, this information is lost at high level density. According to the chaotic motion of the nucleons, the resonance states can be seen at high level density as fluctuations around an average value only[13,14]. This average value is determined by the fast direct process which contains the information on the environment (motion of a nucleon relative to the target nucleus). The correlation between the system (Q space) and the continuum (P space) is so strong at high level density that the consideration of the nucleus as an open system (in the Q space) looses its meaning. The properties of the system at high level density are determined mainly by the P space in which the motion of only A - 1 nucleons is a regular one.

It is worthy of note that irreversibility on a microscopic level[8] exists still at high level density in the long-living states, but is hidden partly by the fast direct scattering process which is reversible as a whole in the P + Q space. The scattering process is described by a Hamilton operator which is Hermitean in the closed P + Q space.

It can be seen from fig. 3 (see also ref.[16]) that the transition from the resonant process to the direct one takes place at $\bar{\Gamma} \approx \bar{D}$, independently of the nuclear structure of the resonance states and of the number of channels taken into account in the calculation. The addition of a resonance state with mainly 1p-1h nuclear structure and with isospin $T \approx 0$ or $T \approx 1$ does not change the final result discussed above. The resonance state with mainly 1p-1h nuclear structure can be identified in the cross section at low level density but not at high level density[14]. The number of channels taken into account in the numerical calculation is correlated with the number of short-living resonance states at high level density as it is to be expected from calculations in a schematic model[15]. The general picture of the transition from one type of regular motion to another one is, however, independent of the number of channels. It is, obviously, the sharper, the larger the continuum is, i.e. the larger the number of channels is (ref.[16]).

5. Summary

The transition from the resonance reaction mechanism at low level density to the direct reaction mechanism at high level density has been investigated in this paper by means of numerical results obtained from microscopic calculations for nucleon induced reactions. In the resonance reaction mechanism, a compound nucleus is formed the properties of which can be described by standard nuclear structure calculations. The nucleons move in an average potential in a regular manner. The second part of the Hamilton operator (5) is small in comparison with the first part. In the direct reaction mechanism, the nucleon is scattered in the field of the target nucleus as a whole. All but one nucleon move in an average potential in a regular

manner. The second part of the Hamilton operator (5) plays an important role.

The numerical calculations give the following results

(i) The transition from resonant to direct reaction mechanism takes place rather sharply at $\bar{\Gamma} \approx \bar{D}$. The transition is the sharper the larger the continuum is, i.e. the more channels are taken into account in the calculation (ref.[16]).

(ii) The second part of the Hamilton operator (5) creates both an information loss on the nuclear structure of the compound nucleus and an information gain on the nuclear structure of the open channels, i.e. on the nuclear structure of the target and residual nuclei.

(iii) At high level density, two types of motion of the nucleons exist simultaneously: a motion in long-living states which are near equilibrium, and a motion in short-living states which are far from equilibrium. The long-living states are excited in nucleon induced reactions with a small probability while the short-living ones are excited with a high probability. Furthermore, the reaction via the short-living states is very fast. Due to their large widths, these states overlap the long-living states, and the nucleus behaves more or less as a whole.

(iv) From the point of view of the compound nucleus, the nucleons move chaotically in long-living states at high level density. These states appear in the cross section as fluctuations around an average value.

(v) From the point of view of the target and residual nuclei, the motion of the nucleons at high level density of the compound nucleus is represented by a regular motion of all but one nucleon in the average field of the target and residual nuclei, respectively. The average value of the cross section is determined by the scattering of a nucleon in the field of the target nucleus as a whole.

(vi) The numerical results show that order out of chaos takes place only in the open quantum mechanical nuclear system. In a closed system, there are no forces to introduce a new order. If the equilibrium state is reached in a closed system, it can exist a long time without any distortion.

(vii) There exists a strong correlation between the finite lifetime of the states near equilibrium in an open system and the formation of states far from equilibrium. In the states far from equilibrium, the target nucleus behaves as a whole, i.e. the many-body aspects play a subordinate role in the P + Q space.

(viii) The finite lifetime of the nuclear states creates an irreversibility on a microscopic level. This irreversibility continues to exist at high level density although the main process (scattering of a nucleon on a target nucleus) is, of course, reversible.

Although most of the discussed results are very well known in nuclear physics for a long time, a direct experimental test has yet to come (for a detailed discussion see ref[8]). The most direct way is to investigate the lifetime of the compound nucleus states in dependence on the excitation energy and the correlations between the resonance amplitudes. In both cases, deviations from the assumptions of standard nuclear reaction theory result if the nucleus is considered as an open system, i.e. if the feedback of the final state (consisting of the final nucleus and a nucleon) on the decaying state (in the compound nucleus) is considered.

In this paper, only nucleon channels have been considered. The results hold, however, in an analogous manner also for, e.g., alpha particle channels and for the coupling to the electromagnetic field.

References

1. I. Prigogine, I. Stengers, Order out of chaos (London 1984 and Moscow 1986)

2. N. Bohr, Nature 137 (1936) 344

3. H.A. Weidenmüller, Comments on Nuclear and Particle Physics 16 (1986) 199; Nuclear Structure 1985, ed. by R. Broglia et al. (North-Holland 1985), p. 213; and references therein

4. E. Vogt, Intern. Conf. on Spin Excitations in Nuclei, Telluride, Colorado, 1982, TRI-PP-83-17 (TRIUMF 1983)

5. H.W. Barz, I. Rotter and J. Höhn, Phys. Letters 37B (1971) 4; Nucl. Phys. A275 (1977) 111

6. I. Rotter, Fiz. Elem. Chastits At. Yadra 15 (1984) 762 (translation 15 (1984) 341 and ZfK-508 (1983))

7. I. Rotter, Phys. Rev. C27 (1983) 2261; C29 (1984) 1119; H.R. Kissener, I. Rotter and N.G. Goncharova, Fortschritte der Physik (1987)

8. I. Rotter, J. Phys. G12 (1986) 1407; Fiz. Elem. Chastits At. Yadra (in press; translation ZfK-598 (1986)

9. H. Haken, Synergetics (Springer 1978); Advanced Synergetics (Springer 1983)

10. I. Prigogine, From Being to Becoming (San Francisco 1979 and Moscow 1985)

11. E.P. Kanter et al., Nucl. Phys. A299 (1978) 230; B.H. Chou et al., Phys. Rev. Letters 45 (1980) 1235; W.K. Wells et al., Z. Phys. A297 (1980) 215; J.F.Jr. Shriner et al., Z. Phys. A305 (1982) 307

12. P. Kleinwächter and I. Rotter, Nucl. Phys. A391 (1982) 137

13. P. Kleinwächter and I. Rotter, Phys. Rev. C32 (1985) 1742

14. P. Kleinwächter and I. Rotter, to be published

15. V.V. Sokolov and V.G. Zelevinsky, private communication

16. I. Rotter, to be published

STATISTICAL PROPERTIES OF DECAYING STATES

V.V. Sokolov, V.G. Zelevinsky
Institute of Nuclear Physics, 630090 Novosibirsk, USSR

Using the general phenomenological description of resonance reactions in terms of the nonhermitian Hamiltonian $\hat{\mathcal{H}} = \hat{H} - \frac{i}{2}\hat{\Gamma}$, the statistical properties of decaying states are analyzed as a generalization of Wigner-Dyson statistical spectroscopy. The hermitian part $\hat{H}$ is assumed to belong to GOE of N x N orthogonal random matrices. Statistical properties of $\hat{\Gamma}$ having matrix elements $\Gamma_{mn} = \sum_a A_m^a A_n^a$ are determined through Gaussian independent random amplitudes A_m^a for open channels $a = 1,\ldots,k$; $\langle A_m^a A_n^b \rangle = \delta^{ab}\delta_{mn}\gamma^a/N$. Due to the algebraic structure of $\hat{\Gamma}$, for $k < N$ there exist only k nonzero eigenvalues of $\hat{\Gamma}$.

The distribution function for complex energies $\mathcal{E}_n = E_n - \frac{i}{2}\Gamma_n$ (*eigenvalues of* $\hat{\mathcal{H}}$) is found. It reveals the quadratic repulsion $\sim|\mathcal{E}_n - \mathcal{E}_m|^2$ at small distances in accordance to the T-noninvariance of decaying systems. Linear repulsion of level energies E_n at spacings less then the widths is removed.

In the case of strongly overlapped resonances algebraic properties of $\hat{\Gamma}$ become decisive generating k "collective" rapidly decaying states ($k < N$) which absorb the total width $\mathrm{Tr}\,\Gamma$. Similar picture has been observed in numerical calculations by I. Rotter. The complex level density $\rho(E,\Gamma)$ and the average S-matrix are obtained.

The conclusion is that the level statistics of unstable systems differs significantly from that of stable systems at $\Gamma/D \sim 1$ the phase transition takes place and the system gets into the strong overlap regime with quite different collective behaviour.

First results are published in Proccedings of Kiev Conference on Neutron Physics (September 1987), and submitted for publication to Phys. Lett. B.

STATES WITH FIXED EXCITON NUMBER AND PARITY IN ODD - A NUCLEI

W. Augustyniak
Institute for Nuclear Studies, Nuclear Reactions Department, Warsaw, Poland

Abstract

The densities of states of doubly even nuclei at high excitation energy are very well described within frame of BCS theory with finite temperature. A possibility to include into the calculations a realistic set of simple particle states makes the results more credible /2,3,4/. The results are very sensitive to sequences and energies at single particle states as well as to the pairing forces; as opposite to quadrupole - quadrupole forces /5/. The quadrupole - quadrupole forces do not alter significantly the results; thus the free quasi - particles model seems to describe properly the density of states at high excitation energy. Application of BCS theory with finite temperature and the Monte - Carlo method has allowed to predict the parity and exciton number distributions /6/. For the odd - A nuclei the level density has been successfully reproduced by means of introducing of a proper shift of the excitation energy to the level density of neighbouring doubly even nuclei /4,7/. The fact that the level density in odd - A nuclei is well reproduced by shift of the excitation energy scale is rather a good prescription than transformation of properties of doubly even systems into odd ones. Here the blocking method given in ref. /3/ has been used to describe the properties of odd - A nuclei. Additionally, the Pauli principle has been taken into consideration.

References

1. H. Sano, S. Yamasaki: Progr. Theor. Phys., 29, 277 /1963/
2. P. Decowski, W. Grochulski, A. Marcinkowski, K. Siwek, Z. Wilhelmi, Nucl. Phys. A110, 129 /1968/
3. W. Augustyniak: Nuovo Cimento A79, 457 /1984/
4. A.N. Bekhami, J.R. Huizenga, Nucl. Phys. A217 /1973/
5. V.G. Soloviev, CH. Stayanov, A.I. Volovin, Nucl. Phys. A224, 411 /1974/
6. W. Augustyniak, Z. Phys. A 317, 225 /1984/
7. M. Hillman, J.R. Grover, Phys. Rev. 185, 1303 /1969/.

NOTIZEN